1997

Heat transfer evaluation of HFC-236ea and HFC-236fa in evaporation and condensation

Shin-Miin Tzuoo
Iowa State University

INFORMATION TO USERS

This manuscript has been reproduced from the microfilm master. UMI films the text directly from the original or copy submitted. Thus, some thesis and dissertation copies are in typewriter face, while others may be from any type of computer printer.

The quality of this reproduction is dependent upon the quality of the copy submitted. Broken or indistinct print, colored or poor quality illustrations and photographs, print bleedthrough, substandard margins, and improper alignment can adversely affect reproduction.

In the unlikely event that the author did not send UMI a complete manuscript and there are missing pages, these will be noted. Also, if unauthorized copyright material had to be removed, a note will indicate the deletion.

Oversize materials (e.g., maps, drawings, charts) are reproduced by sectioning the original, beginning at the upper left-hand corner and continuing from left to right in equal sections with small overlaps. Each original is also photographed in one exposure and is included in reduced form at the back of the book.

Photographs included in the original manuscript have been reproduced xerographically in this copy. Higher quality 6" x 9" black and white photographic prints are available for any photographs or illustrations appearing in this copy for an additional charge. Contact UMI directly to order.

UMI

A Bell & Howell Information Company
300 North Zeeb Road, Ann Arbor MI 48106-1346 USA
313/761-4700 800/521-0600

Heat transfer evaluation of HFC-236ea and HFC-236fa in evaporation and condensation

by

Shin-Miin Tzuoo

A dissertation submitted to the graduate faculty

in partial fulfillment of the requirements for the degree of

DOCTOR OF PHILOSOPHY

Major: Mechanical Engineering

Major Professor: Michael B. Pate

Iowa State University

Ames, Iowa

1997

Graduate College
Iowa State University

This is to certify that the Doctoral dissertation of

Shin-Miin Tzuoo

has met the dissertation requirements of Iowa State University

Signature was redacted for privacy.

Committee Member

Signature was redacted for privacy.

Committee Member

Signature was redacted for privacy.

Committee Member

Signature was redacted for privacy.

Committee Member

Signature was redacted for privacy.

Major Professor

Signature was redacted for privacy.

For the Major Program

Signature was redacted for privacy.

For the Graduate College

TABLE OF CONTENTS

LIST OF TABLES

LIST OF FIGURES

NOMENCLATURE

Abbreviations

A	surface area (m^2)
Ar	Achimedes number
Bo	Bond number
Cp	specific heat at constant pressure (J/kg·K)
D	diameter (m)
f	frequency (1/s)
fpi	fins per inch
fpm	fins per meter
g	gravity (m/s^2)
h	heat transfer coefficient ($W/m^2 \cdot K$)
i	enthalpy (J/kg)
i_{fg}	enthalpy of vaporization (J/kg)
Ja	Jakob number
k	thermal conductivity (W/m·K)
L	length (m)
$LMTD$	logarithmic mean temperature difference (°C)
$\dot{m}$	mass flow rate (kg/s)
N	number of tube rows measured from top row
NR	row number counted from top row
Nu	Nusselt number
N/A	not available
ODP	ozone depleting potential
P	pressure (N/m^2)
Pr	Prandtl number
q	heat transfer rate (W)

R	thermal resistance (K/W)
r	radius (m)
Re	Reynolds number
RR	recirculation rate
STC	Sieder-Tate coefficient
s	Coordinate distance along curved condensing profile (m)
T	temperature (°C)
ΔT	temperature difference between the tube wall and the saturated refrigerant (°C)
U_o	overall heat transfer coefficient based on the outer surface area of a tube ($W/m^2 \cdot K$)
UN	uncertainty in heat trasnsfer coefficient (± %)
v	specific volume (m^3/kg)
We	Weber number
y	the fraction of the total refrigerant flow existing the test section as vapor in spray evaporation

Symbols

Γ	liquid mass flow rate per unit tube length (kg/m·s)
γ	bubble contact angle (radians)
π	pi, 3.14159
ρ	density (kg/m^3)
σ	surface tension (N/m)
η	fin efficiency
μ	dynamic viscosity ($N \cdot s/m^2$)
ζ	film thickness (m)

Subscripts

av	average
B	boiling
b	bubble
C	convection
c	critical

f	fin
i	tube-side (in-tube); inside
in	inlet
l	liquid
N	row number counted from the top row
nb	normal boiling point
nonb	nonboiling
o	shell-side; outside
out	outlet
r	root
sat	saturated refrigerant
spr	spray evaporation
t	fin tip
ts	test section
v	vapor
w	tube wall
x	local
*	reduced

Superscripts

''	area basis ($1/m^2$)

ACKNOWLEDGMENTS

This dissertation is dedicated to my late mother, Duan Zang, I would also like to express my sincere gratitude to my family for their unending love and support.

In addition, I wish to thank my major professor, Dr. Michael Pate, for his technical instruction and assistance throughout the study. Members of my committee, Drs. Howard Shapiro, Ron Nelson, Bruce Munson, and John Stufken, are also appreciated. Special thanks also go to Ms. Kerri Peterson, my colleagues in Beul and Heat Transfer Lab, and the support of Department of Mechanical Engineering.

Special thanks are extended to the Wolverine tube Inc. for providing the tubes (1024-fpm, 1575-fpm, Turbo-CII, Turbo-B, and Turbo-BII), and the Trane Co. for supplying the spring-type turbulators.

This research was supported by the Environmental Protection Agency (EPA) in cooperation with the United States Navy Contract #CR820755-01-4 and # 5D2520NAEX. Funding for this work was provided by the Department of Defense's Strategic Environmental Research and Development Program through the EPA, and this sponsor is acknowledged.

CHAPTER 1 INTRODUCTION

Background

Shell-and-tube heat exchangers in Navy shipboard chillers presently use integral-fin (748-fpm and 1024-fpm) tubes and CFC-114 as the working refrigerant. Shell-side heat transfer coefficients indicate the heat transfer performance of shell-and-tube heat exchangers where refrigerant is employed on the shell side. As such, this research evaluates the heat transfer coefficients of two environmentally safe refrigerants (HFC-236ea and HFC-236fa) on the outside of a single horizontal tube with a nominal outer diameter of 19.1 mm (3/4 inch).

CFC-114 has been used in Navy shipboard chillers because of its favorable characteristics such as moderate pressure and lowest toxicity. The refrigerant pressure is a major factor determining the weight and size of components in refrigeration systems, which are critical parameters to naval applications. In addition, toxicity of refrigerant is also extremely important in the confined quarters on board ships and submarines.

However, the depletion of stratospheric ozone by chlorofluorocarbons (CFCs) was suspected in the 1970s and resulted in the impending phase-out requirement of CFCs by the 1987 Montreal Protocol and its subsequent amendments. CFC-114 was forced to phase out at the end of 1995 in the United States due to its relatively high ozone depleting potential (ODP= 0.8). Alternative refrigerants, such as the non-toxic and non-flammable hydrofluorocarbon (HFC)-based substances, were considered to replace CFCs that have been used in refrigeration applications for decades.

The two refrigerants of interest here, HFC-236ea and HFC-236fa, do not reduce stratospheric ozone and are considered to be potential substitutes for CFC-114 which is harmful to the ozone layer. Both the refrigerants have a molecular weight of 152 and are non-flammable as CFC-114. The basic physical properties of these two refrigerants and CFC-114 at the operating temperatures of 2°C (35.6°F) and 40°C (104°F) are presented in Table A.1. The properties were taken from REFPROP [57].

Three successive stages of investigation (Phase I, Phase II, and Phase III) were supported by the EPA (Environmental Protection Agency) in cooperation with the U. S. Navy to determine the heat

transfer coefficients of the two ozone-friendly alternatives (HFC-236ea and HFC-236fa) for CFC-114. Each of these three phases has its separate issues and different objectives. This Ph.D. program covers the work in both Phase II and Phase III. The scope for the three phases is summarized in Table 1.1.

The feasibility of the HFC-236ea system replacing the existing CFC-114 system was assessed in Phase I [38], a study in the comparative heat transfer coefficients of CFC-114 and HFC-236ea during shell-side pool boiling and shell-side condensation for a plain tube and two types of low integral-fin (1024-fpm and 1575-fpm) tubes.

The investigation in the heat transfer coefficients of HFC-236ea was extended from the Phase I study of the integral-fin tubes during shell-side condensation and pool boiling to the current study (covered in the Phase II study) of high performance enhanced (Turbo-CII, Turbo-B, and Turbo-BII) tubes during pool boiling, spray evaporation, and shell-side condensation.

The heat transfer coefficients of HFC-236fa during condensation and pool boiling were also measured in this research (covered in the Phase III study) for both the two integral-fin tubes previously evaluated in Phase I [38] and the high performance enhanced tubes evaluated in Phase II.

The hermetically sealed compressors in vapor compression refrigeration systems require lubricant to protect moving components. However, a small amount of the lubricant is entrained with refrigerant leaving the compressor and circulates through the whole system. The oil carried with refrigerant might significantly affect the performance of evaporators since the oil concentration in the liquid mixtures increases when the volatile refrigerant is evaporated and the non-volatile oil is left in evaporators. The effects of additional oil on pool boiling were investigated for CFC-114 (Phase I), HFC-236ea (Phase I), and HFC-236fa (Phase III). Results are discussed in Chapter 6.

Both HFC-236ea and HFC-236fa were compared with CFC-114 in heat transfer coefficients in order to help the U. S. Navy or industries to make intelligent selection of a proper substitute for CFC-114. Additionally, comparison of the integral-fin tubes and high performance enhanced tubes was made for these two alternative refrigerants in order to assess the applicability of the high performance enhanced tubes relative to integral-fin tubes in shell-side heat exchangers and find the optimum tubes for pool boiling, spray evaporation, and shell-side condensation heat transfer.

High performance enhanced tubes with improved heat transfer characteristics and with complex fin profiles are widely used in heat exchangers for refrigeration and air-conditioning applications, and, therefore, are potential replacements for the integral-fin tubes presently used in Navy shipboard chillers.

Table 1.1 Scope for Phase I, Phase II, and Phase III

Heat transfer form	Fluid type	Tupe type				
		1024-fpm	1575-fpm	Turbo-B	Turbo-BII	Turbo-CII
Pool boiling	HFC-236fa	Yes (Phase III)	Yes (Phase III)	Yes (Phase III)	Yes (Phase III)	No
	HFC-236ea	Yes (Phase I)	Yes (Phase I)	Yes (Phase II)	Yes (Phase II)	No
	CFC-114	Yes (Phase I)	Yes (Phase I)	No	No	No
	HFC-236fa/oil	Yes (Phase III)	Yes (Phase III)	Yes (Phase III)	Yes (Phase III)	No
	HFC-236ea/oil	Yes (Phase I)	Yes (Phase I)	No	No	No
	CFC-114/oil	Yes (Phase I)	Yes (Phase I)	No	No	No
Spray evaporation	HFC-236ea	No	Yes (Phase II)	Yes (Phase II)	No	Yes (Phase II)
Condensation	HFC-236fa	Yes (Phase III)	Yes (Phase III)	No	No	Yes (Phase III)
	HFC-236ea	Yes (Phase I)	Yes (Phase I)	No	No	Yes (Phase II)
	CFC-114	Yes (Phase I)	Yes (Phase I)	No	No	No

Enhanced heat transfer is an important subject here, because the surface area of a heat exchanger required to effect a specific heat transfer rate is usually smaller for the heat exchanger producing a higher heat transfer coeffcient. Enhanced tubes might provide higher heat transfer coeffcients compared with plain tubes and integral-fin tubes, and thus reduce the weight and size of heat exchangers.

Since no general correlations exist to predict heat transfer coefficients as a function of either refrigerant type, tube surface geometry, or lubricant addition, experiments are the most reliable means to determine the heat transfer coefficients for specific applications. The effects of refrigerant type, tube surface geometry, and lubricant addition on heat transfer performance were investigated in this research. Selecting proper alternative refrigerant and tube types are fundamental to improve the heat transfer performance of heat exchangers. A broad review of the research in the two-phase heat transfer to new alternative refrigerants is given by Stephan [68] and Thome [72].

Research program

Objectives

This research not only determined the shell-side heat transfer coefficients of two environmentally safe alternatives (HFC-236ea and HFC-236fa) for various tubes but also compared the heat transfer coefficients of HFC-236fa, HFC-236ea and CFC-114, where the two HFC refrigerants are proposed as alternative refrigerants for CFC-114.

In addition, research on shell-side heat transfer enhancements for nucleate pool boiling, spray evaporation, and condensation on various surface geometries was also an important objective. The heat transfer performance of the tubes (1024-fpm, 1575-fpm, Turbo-CII, Turbo-B, and Turbo-BII) tested was compared for each refrigerant.

This research provided the heat transfer coefficient data for retrofitting the existing CFC-114 system as well as for redesign and optimization of new chillers employing the alternatives (HFC-236ea and HFC-236fa).

Scope

Using mainly the same test facility which allows analysis of three different heat transfer forms (pool boiling, spray evaporation, and condensation), measurements were conducted on a single-tube configuration at a saturation temperature of 2°C for pool boiling as well as spray evaporation and at 40°C for condensation. The testing range of heat fluxes was from 15 kW/m^2 to 40 kW/m^2 for both

condensation and pool boiling, and 10 kW/m^2 to 30 kW/m^2 for spray evaporation.

Three types of high performance enhanced tubes (Turbo-CII, Turbo-B, and Turbo-BII) were tested for both HFC-236ea and HFC-236fa in this research. In addition, two types of integral-fin tubes (1024-fpm and 1575-fpm) were also tested with HFC-236fa, and previously with HFC-236ea in the Phase I study [38].

The two integral-fin tubes were tested with HFC-236fa during both pool boiling and shell-side condensation. The enhanced condensation Turbo-CII tube was evaluated during shell-side condensation for not only HFC-236fa but also HFC-236ea, while the two enhanced boiling tubes (Turbo-B and Turbo-BII tubes) were evaluated in pool boiling for both HFC-236ea and HFC-236fa. Besides, the Turbo-B and Turbo-CII tubes as well as the 1575-fpm tube were tested for HFC-236ea in spray evaporation.

The heat transfer coefficients for the integral-fin tubes were used as a baseline for comparing the heat transfer performance of the high performance enhanced tubes. All tubes had an equivalent tube diameter of 19.1 mm (3/4 inch) and were compared based on the outside surface area of a corresponding smooth tube. That is, calculation of heat flux was based on the envelope area of the tube where a diameter to the fin tips was measured. The boiling coefficient is commonly defined in terms of the projected surface area to take into account the area enhancement and fin efficiency for the enhanced tubes tested.

The heat transfer coefficients of the three refrigerants (HFC-236fa, HFC-236ea, and CFC-114) were compared for each individual tube tested during pool boiling and condensation. The optimum tube for heat transfer may differ when it is tested with different refrigerants for specific applications.

The comparative heat transfer performance of spray evaporation with pool boiling for HFC-236ea was also made by using the Turbo-B tube and 1575-fpm tubes (covered in the Phase II study). Since a smaller refrigerant volume is required for performing spray evaporation relative to pool boiling, a spray evaporator rather than a flooded evaporator might potentially reduce the initial cost for building a vapor-compression system.

In addition, saturated pool boiling was investigated for HFC-236fa/oil mixtures with the oil concentrations of 1% and 3% by weight in order to assess the effects of the oil presence on the boiling heat transfer performance. The oil used (Castrol Icematic SW-68) is a synthetic polyol-ester lubricant with a viscosity of 340 SUS at 37.8°C (100°F).

The data taken in this study were obtained using the same test facility as previously used in Phase I [38]. Data were taken with increasing heat loads during condensation and with decreasing heat loads during pool boiling. Each tube type for spray evaporation was tested with increasing and decreasing

heat flux. Repeat runs were performed on different days for all the tubes tested in these three heat transfer forms in order to test the accuracy and repeatability of the system.

Data are mainly presented in the form of heat transfer coefficient versus heat flux, since the heat transfer coefficient during evaporation and condensation depends on the heat load. The heat transfer coefficient related to the temperature difference between the saturated refrigerant and the tube wall is also illustrated with figures.

CHAPTER 2 LITERATURE REVIEW OF POOL BOILING

Overview

Boiling is defined as vaporization of liquid that occurs at the interface of a solid surface and a liquid when the temperature of the heated surface exceeds the saturation temperature of the liquid. Pool boiling is boiling from a heated surface immersed in a pool of stationary liquid whose motion near the surface is due to free convection and to the agitation of bubble generation.

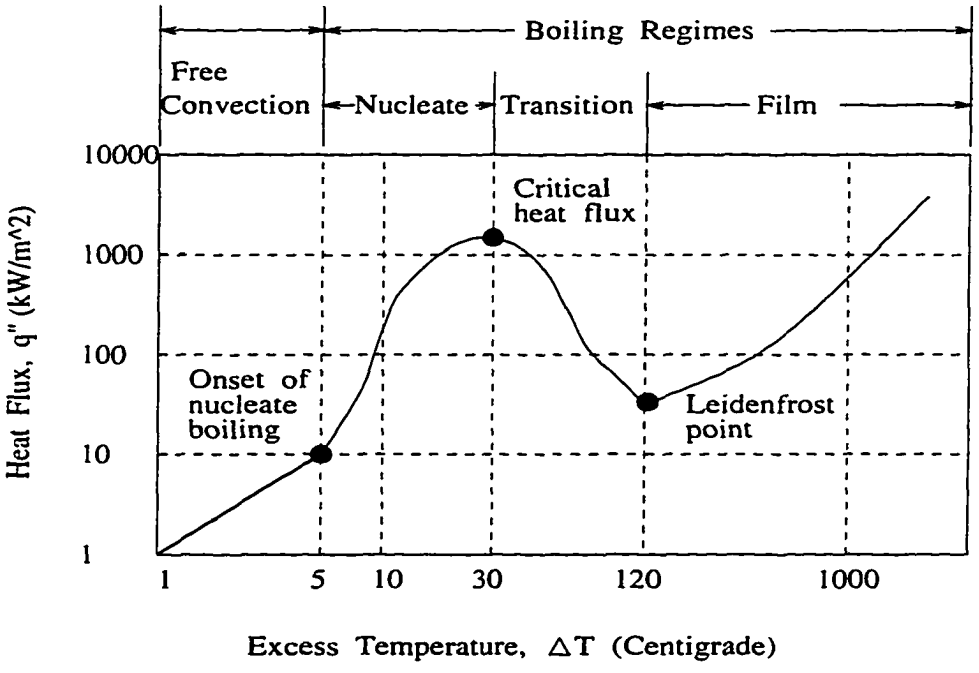

Figure 2.1 Typical boiling curve for water at one atmosphere

The pool boiling curve plotted in terms of surface heat flux against wall superheat (excess temperature) is usually used to delineate the whole pool boiling heat transfer process varying with the wall superheat. The curve is composed of four main regimes— free convection, nucleate boiling, transition boiling, and film boiling, in ascending order of wall superheat. The four distinct regimes are sketched

in the boiling curve of Figure 2.1 for water [39].

The pool boiling investigated here is saturated pool boiling where the temperature through most of the bulk liquid remains at or slightly above saturation temperature (i.e., boiling point) and is nucleate boiling where a small amount of wall superheat causes vapor nucleation from the imperfections of a heating surface.

Nucleate pool boiling is characterized by a high heat transfer rate associated with a relatively small wall superheat. Its favorable effects on boiling is shown in Figure 2.1, where the nucleate boiling curve exhibits the steepest slope (i.e. highest heat transfer coefficient). Although Figure 2.1 was sketched for water, other fluids show similar trends. None of the plentiful theoretical models developed or phenomena observed can explain satisfactorily the great improvement in heat transfer in this region. Hsu and Graham [34] suggested that the process of nucleate pool boiling combines the heat transfer mechanisms of bubble agitation, thermal boundary layer stripping, and evaporation.

Because the shell-side boiling mechanism consists of both nucleate boiling and forced convection vaporization (convective evaporation), the heat transfer coefficient for nucleate pool boiling is required for prediction of chiller performance. However, knowledge of the mechanisms associated with nucleate boiling as well as convective evaporation on enhanced surfaces is limited.

Experimental evidence indicates that the configuration of the heated surface for boiling has definite effects on the heat transfer mechanisms for either pure refrigerant or refrigerant-oil mixtures. The surface with high density of re-entrant cavities can act as effective and stable nucleation sites and, thus, requires lower wall superheat to initiate and sustain boiling. Nevertheless, the advantage of numerous re-entrant cavities may diminish during boiling in the presence of oil since these cavities can be blocked by immiscible lubricants.

Surface geometries were shown by the investigators to significantly affect boiling heat transfer. A number of papers concerning boiling mechanisms on different surface geometries have been published. The evolution of enhanced surface geometries for nucleate boiling was surveyed by Webb [78]. A detailed discussion on enhanced boiling surfaces was provided by Thome [73]. Later, a comprehensive literature survey of 61 references concerning pool boiling on enhanced surfaces was published by Pais and Webb [62]. Pais and Webb concluded that the enhanced surfaces in the existing data for refrigerants provided 2 to 4 times greater heat transfer coefficients than the conventional integral-fin tubes.

Other parameters that can affect pool boiling, such as gravitational field and liquid subcooling, were reported to be negligible for nucleate pool boiling [39].

Theoretical analysis

Superheat requirement for vapor nucleation

During nucleate pool boiling, surface heat is carried away with bubble motion while bubbles periodically grow and release from the pits, cracks, or cavities (i.e., nucleation sites) in the heated surface. The necessary energy for sustaining cyclical bubble growth (i.e., nucleate boiling) at a nucleate site is provided by the surrounding superheated liquid.

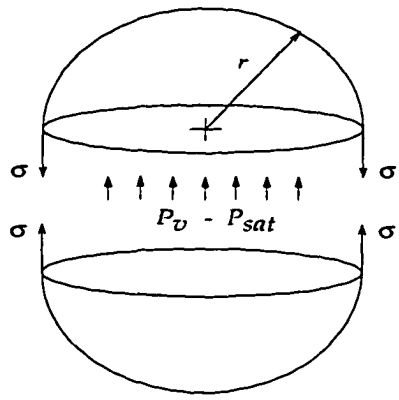

Figure 2.2 Schematic of a bubble in mechanical equilibrium

As shown in Figure 2.2 for a spherical bubble of radius r to exist stably in a liquid at temperature of T_l, the net pressure force between the inside and the outside of a bubble, $(P_v - P_l)\pi r^2$, must be balanced by the surface tension force, $2\pi r\sigma$, at the liquid-vapor interface. This mechanical equilibrium leads to

$$P_v - P_l = \frac{2\sigma}{r} \tag{2.1}$$

The pressure inside the bubble (P_v) is frequently assumed to be equal to the saturation pressure of the ambient liquid (P_{sat}). Accordingly, Equation 2.1 becomes

$$P_{sat} - P_l = \frac{2\sigma}{r} \tag{2.2}$$

Using the Clasius-Clapeyron equation together with the perfect gas approximation under the condition of $v_g \gg v_f$, the liquid superheat $(T_l - T_{sat})$ corresponding to the pressure difference $(P_{sat} - P_l)$ in Equation 2.2 can be calculated to give

$$T_l - T_{sat} = \frac{2\sigma}{(dP/dT)_{sat} \cdot r} \tag{2.3}$$

where $(dP/dT)_{sat}$ is the slope of the saturation curve of P_{sat} versus T_{sat}.

Equation 2.3 shows that the surrounding liquid temperature (T_l) must be greater than its saturation temperature (T_{sat}) for the vapor bubble of radius r to exist in thermal equilibrium. This liquid superheat ($T_l - T_{sat}$) is provided by the heated wall. The wall superheat ($T_w - T_{sat}$) between the heated surface and bulk saturated liquid is related to the liquid superheat ($T_l - T_{sat}$), and their relationship can be seen by writting the wall superheat as the sum of the temperature drop across the thin evaporating liquid and the liquid superheat.

$$T_w - T_{sat} = [T_w - T_l] + [T_l - T_{sat}] \tag{2.4}$$

Boiling will not begin until a certain amount of surface superheat as shown in Equation 2.4 is attained. In view of this, this research tested various tubes and compared their heat transfer performance in order to seek proper enhanced surfaces that can transfer tremendous heat at a small boiling temperature difference (i.e. wall superheat $T_w - T_{sat}$) and thus reduce the energy-related costs.

Fundamental boiling mechanism

Hsu and Graham [34] summarized the possible mechanisms responsible for the large heat transfer improvement during nucleate pool boiling on plain, smooth surfaces. As illustrated in Figure 2.3, the authors concluded that the principal mechanisms for nucleate boiling relative to single-phase natural convection on the same surfaces as follows:

1. *Bubble agitation (Figure 2.3a)*

   The growth and departure of bubbles on a heated surface induce turbulence (forced convection) to transport sensible heat in the form of superheated liquid into the bulk of the liquid.

2. *Vapor-Liquid exchange, thermal boundary layer stripping (Figure 2.3b)*

   Heat is transported as sensible heat in the hot liquid rising from the surface with the departing bubbles, a fresh cooler liquid then rushes in and takes heat from the wall before being transported

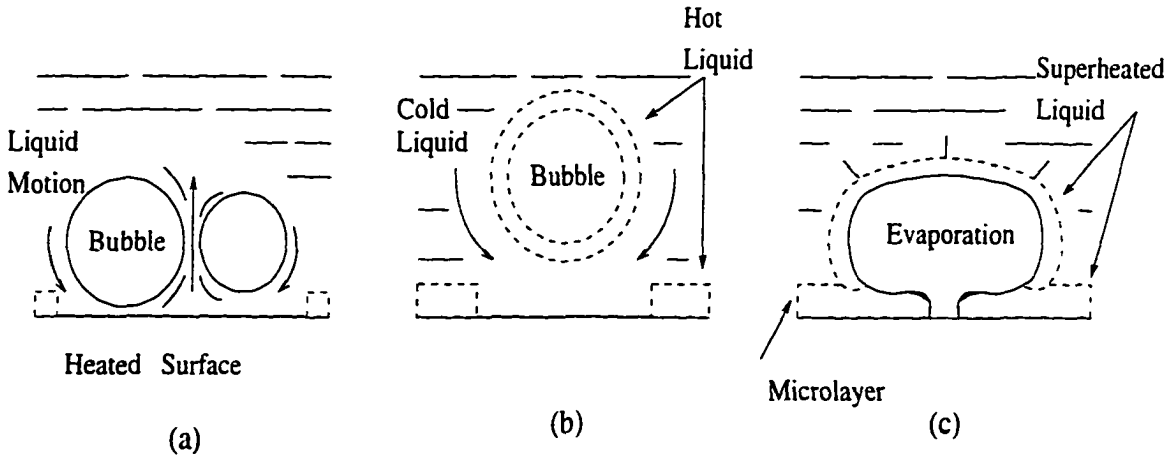

Figure 2.3 Nucleate pool boiling mechanisms on a plain, smooth surface

away into the bulk liquid. In other words, the periodically departing bubbles cyclically strip the thermal boundary layer formed by transient heat conduction into the liquid adjacent to the heated wall and thus remove heat.

3. *Evaporation (Figure 2.3c)*

   Vapor bubbles grow by virtue of evaporative fluxes (latent heat) from the liquid interfaces, i.e., by vaporization of superheated liquid surrounding the bubbles and by thin-film evaporation in the microlayer of superheated liquid trapped underneath the bubbles.

Although usually only one of these three mechanisms was considered to be dominant in the heat transfer coefficient correlations developed, the real boiling process is composed of these mechanisms. It is not yet clear on which mechanisms are predominant and to what extent in the boiling process.

Incropera and DeWitt [39] interpreted the fundamental heat transfer mechanisms from the dimensionless parameters related to the dependent variables of heat transfer coefficient. The authors concluded that the heat transfer coefficient (h) for both pool boiling and condensation depends on the following 9 parameters:

$$h = h[\Delta T, i_{fg}, \sigma, g(\rho_l - \rho_v), L, \rho, Cp, k, \mu] \tag{2.5}$$

where ΔT, i_{fg}, σ, $g(\rho_l - \rho_v)$, and L are the temperature difference between the saturated fluid and the surface, latent heat, surface tension, body force resulted from the density difference of liquid and vapor,

and characteristic length. The other terms in Equation 2.5 (ρ, Cp, k, and μ) are the thermophysical properties of the liquid or vapor.

By using Buckingham pi theorem, Incropera and DeWitt grouped the ten variables in Equation 2.5 into 5 pi-groups as

$$\frac{hL}{k} = f\left[\frac{Cp \cdot \mu}{k}, \frac{g(\rho_l - \rho_v)L^2}{\sigma}, \frac{Cp \cdot \Delta T}{i_{fg}}, \frac{g(\rho_l - \rho_v)L^3}{\mu^2}\right] \tag{2.6}$$

Equation 2.7 gives the other expression for Equation 2.6 related to the dimensionless groups

$$Nu_L = f\left[Pr, Bo, Ja, \frac{g(\rho_l - \rho_v)L^3}{\mu^2}\right] \tag{2.7}$$

Equations 2.5 and 2.6 give the clues to the factors that affect the two-phase heat transfer mechanisms. In addition, the fundamental heat transfer mechanisms might be described by the physical interpretations of the dimensionless parameters in Equation 2.7.

Boiling mechanism on enhanced surfaces

Surface roughness has been known to improve nucleate boiling performance for more than 60 years. Numerous experimental and theoretical studies that deal with boiling on rough surfaces or enhanced surfaces with artificially nucleation sites have been reported. The studies on understanding the character of nucleation sites and the cavity shape necessary to form stable vapor traps were described and discussed by Webb [88]. Webb [80] also gave equations for the relationship between the liquid-vapor interface radius and five cavity geometries.

The favorable artificially formed cavities on enhanced surfaces must allow boiling to occur at a lower wall superheat than the natually nucleation sites on smooth surfaces. The shape and the opening width of a surface cavity seem to be crucial parameters in enhancement since they have a significant influence on the liquid superheat required for nucleation within the cavity. These geometric parameters can be optimized to suit a particular fluid.

Since enhanced surfaces provide artificially formed nucleate sites, heat transfer to the liquid can occur on both the exterior and interior of an enhanced boiling surface by evaporation and convection. Thome [73] suggested that the following four possible heat transfer mechanisms are employed on enhanced boiling surfaces to attain high performance:

1. Surface heat is transported as sensible heat in the superheated liquid flowing over the exterior surface.

2. Surface heat is transported as sensible heat in the superheated liquid drawn into and driven out of the enhancement by the pumping action of the bubbles.

3. Surface heat is transferred as latent heat in bubbles growing on the exterior surface and emerging from the subsurface.

4. Surface heat is transferred as latent heat in vapor formed within the subsurface.

Predictive methods

The correlations of earlier work derived to predict the heat transfer coefficients for pool boiling were concentrated on smooth surfaces [20], [46], [64]. Some recent analytical models have been developed specifically for enhanced tubes [25], [90]. Correlations for enhanced pool boiling have been reviewed in [73] [88]. A number of correlations are also available to predict the heat transfer coefficients for mixtures of refrigerant and oil [13], [40], [41].

Not much theoretical research has been done for the heat transfer mechanisms of nucleate boiling on enhanced tubes. Most of the equations were developed for normal engineering surfaces, that is, plain surfaces without enhancement surfaces, such as extended surfaces or sintered metallic coatings.

Even though the main research topics addressed here are on finned and structured surfaces, correlations on plain surfaces are briefly reviewed as reference in order to provide the fundamental understanding on pool boiling heat transfer mechanisms.

Plain surfaces

Some reseachers attempted to derive nucleate boiling correlations in the following expression commonly used for the single-phase turbulent convection,

$$Nu = C \cdot Re^x \cdot Pr^y \tag{2.8}$$

For the convection-based correlations, it is assumed that the highly turbulent liquid promoted by the motion of bubbles transports heat into the bulk of the liquid. That is, the bubble agitation mechanism (Figure 2.3a) proposed by Hsu and Graham [34] is assumed to dominate the boiling heat transfer

process. The earliest correlation developed for nucleate boiling by Rohsenow [64] was based on this convection mechanism. The Rohsenow correlation is

$$Nu_d = \frac{1}{C_{sf}} \cdot Re^{2/3} \cdot Pr^{-0.7} \tag{2.9}$$

The dimensionless parameters in Equation 2.9 are defined as

$$Nu = \frac{q'' \cdot D_b}{(T_w - T_{sat}) \cdot k_l} \tag{2.10}$$

$$Re = \frac{q'' \cdot D_b}{i_{fg} \cdot \mu_l} \tag{2.11}$$

$$Pr = \frac{Cp_l \cdot \mu_l}{k_l} \tag{2.12}$$

where the characteristic length used to form the Nusselt and Reynolds numbers is the bubble diameter at departure (D_b) from the surface

$$D_b = \left[\frac{\sigma}{g(\rho_l - \rho_v)}\right]^{1/2} \tag{2.13}$$

Substituting Equations 2.10 through 2.12 into Equation 2.9 gives the other expression related to the wall superheat ($T_w - T_{sat}$):

$$\left[\frac{Cp_l \cdot (T_w - T_{sat})}{i_{fg}}\right] = C_{sf}\left[\frac{q''}{\mu_l \cdot i_{fg}} \cdot \left(\frac{\sigma}{g(\rho_l - \rho_v)}\right)^{1/2}\right]^{1/3} \cdot \left[\frac{Cp_l \cdot \mu_l}{k_l}\right]^{1.7} \tag{2.14}$$

The fluid properties in the above equations are caluculated at the saturation temperature corresponding to the local pressure and the coefficient C_{sf} in Equations 2.9 and 2.14 depends on the combinations of fluid and surfaces. Values of C_{sf} for different surface-fluid combinations are given in [64] and [75]. Rohsenow suggested for water only the exponent of Prandtl number in Equation 2.9 be changed to zero, that is, the exponent of the last term to the right in Equation 2.14 be changed to one.

In another convection-based correlation proposed by Cornwell and Houston [20], the tube diameter instead of the departure bubble diameter was used as the characteristic length in forming the Reynolds number

$$Re = \frac{\dot{m}_v D}{\mu_l \cdot A} = \frac{q'' \cdot D}{i_{fg} \cdot \mu_l} \tag{2.15}$$

By comparison with boiling heat transfer data published and assuming that the convection in boiling is driven by the vapor bubble flow and, hence, is directly related to the boiling Reynolds number, the correlation is expressed as:

$$Nu = A \cdot F(P) \cdot Re^{0.67} \cdot Pr^{0.4} \tag{2.16}$$

Where the pressure dependence of boiling was incorporated in the $F(P)$ term. The $F(P)$ equation derived based on the law corresponding states by Mostinski [58] is a function of the reduced pressure ($P_* = P/P_c$) and used in the Cornwell-Houston correlation.

$$F(P) = 1.8 \cdot P_*^{0.17} + 4 \cdot P_*^{1.2} + 10 \cdot P_*^{10} \tag{2.17}$$

The coefficient A in Equation 2.16 was determined by the best fit of the available experimental data, and is a function of the critical pressure (P_c) of fluids.

$$A = 9.7 \cdot P_c^{0.5} \tag{2.18}$$

The Cornwell and Houston correlation was derived for fully developed nucleate boiling on horizontal tubes of 8 $\sim$ 50 mm in diameter using prescribed fluids (water, refrigerants, and organics) from

experimental data. Fourty references including the experimental data for 16 fluids were used in the develepement of this correlation. The generality of this correlation is in doubt. since there were insufficient fluids with a wide range of database to make a precise analysis.

In addition to the Rohsenow model [64], Stephan and Abdelsalam [69] proposed another physical property based model. The major deficiency of the physical property based model is that it is complicated to evaluate because it requires accurate thermophysical properties. The heat transfer coefficient of a new refrigerant can not be predicted from this correlation when the relevant refrigerant properties are unknown.

Other empirical correlations developed as a function of reduced pressure were given by Cooper [19] and Gorenflo et al. [24]. Examination of these two correlations, together with the one derived by Cornwell and Houston [20] and reviewed here, shows that the heat transfer coefficient increases with increasing reduced pressure.

Finned surfaces

Hahne et al. [25] developed a theory for finned tubes based on the model of Mikic and Rohsenow [51] for boiling on plain surfaces. In the model of Mikic and Rohsenow, the total transferred heat flux is assumed to be the sum of a latent heat flux transferred from the bubble influence area due to nucleate boiling ($q_B^{"}$) and a single-phase heat flux transferred from the remaining surface due to convection ($q_C^{"}$).

According to the Mikic-Rohsenow model which assumed that heat is transferred through transient conduction to the superheated liquid layer attached to the heating surface, the heat flux ($q_B^{"}$) and the heat transfer coefficient (h_B) due to nucleate boiling are in the following forms:

$$q_B^{"} = h_B \cdot (T_w - T_{sat}) \cdot \frac{A_B}{A} \tag{2.19}$$

and

$$h_B = 2 \cdot \pi^{1/2} \cdot (k_l \cdot \rho_l \cdot Cp_l)^{1/2} \cdot f^{1/2} \tag{2.20}$$

Figure 2.4 shows the cross section of finned tubes modeled by Hahne et al. The authors modified the model of Mikic and Rohsenow to account for the influence area of a bubble on finned tubes as a band with the width of twice the bubble departure diameter (D_b) and influential length (L_i) reaching across both the fin base and fin flank. The influence area of N bubbles over the heating surface on finned tubes (A_B/A) in Equation 2.19 is defined as

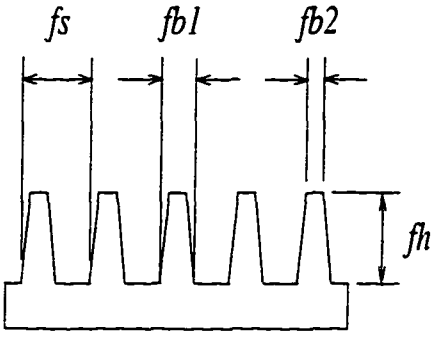

Figure 2.4 Schematic of the fin geometry modeled by Hahne et al.

$$\frac{A_B}{A} = \frac{N}{A} \cdot (2D_b) \cdot L_i \tag{2.21}$$

where the bubble departure diameter (D_b) is related to the fluid properties (σ, ρ_l, and ρ_v) and the bubble contact angle (γ)

$$D_b = 0.851 \cdot \gamma \left[\frac{2\sigma}{g(\rho_l - \rho_v)}\right]^{1/2} \tag{2.22}$$

and the influential length (L_i) is

$$L_i = 2\left[\frac{(fb1 - fb2)^2}{4} + fh^2\right]^{1/2} + fs - fb1 \tag{2.23}$$

The nucleation site density (N/A) was derived as a function of the critical radius of a bubble. Equation for calculation of the nucleation site density (N/A), which requires three empirical coefficients, was given by the authors [25].

The liquid exchange frequency (f) in Equation 2.20 is determined as

$$f = \begin{cases} f_b & \text{for } \frac{A_B}{A} \leq 1 - \frac{A_{fl}}{A}, \\ f_b \cdot \frac{A_B}{A} & \text{otherwise} \end{cases} \tag{2.24}$$

where the bubble frequency (f_b) is estimated from the relationship presented by Zuber [91]

$$f_b \cdot D_b = 0.59 \left[\frac{\sigma g(\rho_l - \rho_v)}{\rho_l^2}\right]^{1/4} \tag{2.25}$$

and A_{ft} is the total area of the fin tips. The other symbols in Equations 2.19 through 2.25 are introduced in the Nomenclature.

The data of Hahne et al. for both types of finned tubes (748-fpm and 1024-fpm tubes) were predicted within an average value of 4.4% by the model, which includes three empirical constants obtained from their data for the single finned tubes.

Structured surfaces

Xin and Chao [90] developed a heat transfer model to predict boiling on a planar Gewa-T type surface. The T-shaped cross section of fins modeled by the authors is illustrated in Figure 2.5. As shown in the figure, the adjacent fin tips for the Gewa-T type surface were deformed to construct the channels with rectangular cross-section. Xin and Chao assumed the liquid continuously flows

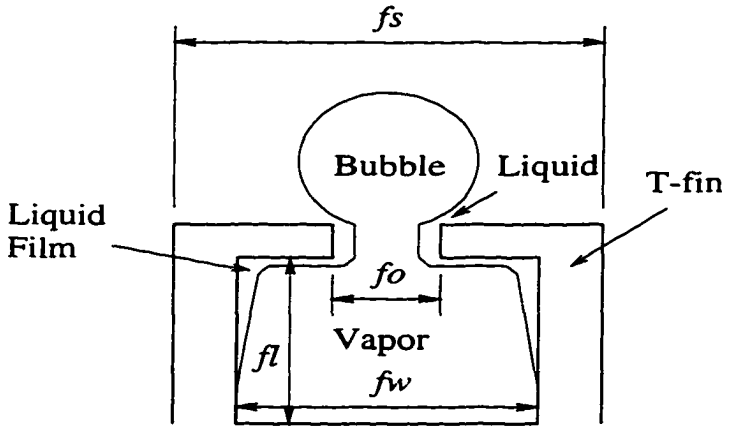

Figure 2.5 Schematic of the surface geometries modeled by Xin and Chao

through the gap at the top of the channel and along the fin wall into the channel, while the vapor escapes simultaneously out of the channel through the center of the gap's opening. Heat was assumed to be transferred as latent heat (evaporation) from inside the channel in addition to the sensible heat (convection) from the external surface to the liquid pool.

The model was developed for a planar T-finned surface with rectangular channels in cross-section but was assumed to be applicable to the actual Gewa-T tubes with nearly circular channels. The equation for the Xin-Chao model is

$$Nu = 3.76 \cdot \frac{2fl + fw}{2fo} \cdot Ar^{1/3} \cdot Re^{-0.15} \cdot We^{0.29} \cdot Pr^{0.76} \quad (2.26)$$

Their data were predicted within ± 30% by the model, which includes eight empirical constants. The readers can refer to the original paper [90] for the definitions of the dimensionless parameters, Nusselt number (Nu), Achimedes number (Ar), Reynolds number (Re), Weber number (We), and Prandtl number (Pr), in Equation 2.26.

Both the surface area and the thickness of the evaporating liquid film were considered in this model, while nucleation site density or bubble dynamics, however, were not. In addition, the assumption that vapor and liquid flow reversely and simultaneously through the openings at the top of the channel is physically unrealistic, since the bubble evolution process is cyclic rather than steady.

Thome [73] examined the Xin and Chao [90] correlation by the experimental data for Gewa-T tubes from five selected references and found that this correlation performed most accurately for non-refrigerants, within the error of approximately −25%.

Turbo-B and other surfaces

The Turbo-B and porous surfaces are also basic enhancement geometries in addition to the enhanced surfaces discussed here. The fundamental studies and phenomena on the porous surfaces have been reviewed and described completely by Thome [73] and Webb [88]. However, mathematical models for the Turbo-B and Turbo-BII tubes have not been developed, which may be attributed to the difficultly defined dimensions of their complex enhancement geometries and the interaction within interconnected cavities.

The only existing correlation for the Turbo-B tube was derived from the experimental data reported by Webb and coworkers for five pure refrigerants (HFC-134a, HCFC-123, CFC-12, CFC-11, and HCFC-22) boiling on a horizontal tube including plain, 1024-fpm, Turbo-B, Gewa-SE, and Gewa-TX tubes. Webb and Pais [86] correlated these data in the form of $h = b \times (q")^m$. The values of the coefficient (b) and the exponent (m) for the 1024-fpm and Turbo-B tubes tested at 4.4°C are shown in Table 2.1.

Table 2.1 Coefficient b and exponent m in Webb and Pais model

Tube	Refrigerant	b	m
1024-fpm	CFC-11	2.300E0	7.26E-1
	CFC-12	4.170E1	5.19E-1
	HCFC-22	5.972E1	5.09E-1
	HCFC-123	2.870E0	7.06E-1
	HFC-134a	6.043E1	4.89E-1
Turbo-B	CFC-11	8.305E2	2.98E-1
	CFC-12	2.060E2	4.29E-1
	HCFC-22	2.966E2	3.97E-1
	HCFC-123	1.702E2	4.02E-1
	HFC-134a	3.044E2	3.89E-1

Refrigerant and oil mixtures

While a number of experimental studies that deal with lubricating oil's effects on nucleate boiling coefficients have been done (see next section and Table 2.2), the phenomena observed on boiling of oil and refrigerant mixtures have yet to be understood completely and explained satisfactorily.

The thermophysical properties of the pool liquid during boiling (e.g., surface tension, viscosity, and vapor pressure) change due to the addition of oil to pure refrigerant. Specifically, the bubble point temperature for mixtures of refrigerant and oil is higher than pure refrigerant and it increases with increasing oil concentration, while the saturation temperature of pure refrigerant is the bubble point temperature of bulk liquid. Therefore, the wall superheat necessary to initiate vapor bubbles, the size of bubbles, the frequency of bubbles departure from the heating surface, and the heat transfer rate change as these properties change.

Boiling of refrigerant and oil mixtures is dominated by the combined processes of heat and mass transfer. The mixtures of oil and refrigerant are binary mixtures. Binary mixtures usually have lower evaporation rates than single-component cases because of their low interfacial mass transfer rates. The viscous oil-rich film built up at the vapor-liquid interface reduces bubble growth rate and contributes to the decreased heat transfer performance.

Some experiments [76], [87], [89] confirmed that the additional oil decreases heat transfer. However, a number of studies indicated that heat transfer coefficients increased when refrigerant mixed with a small amount of oil, which were attributed by some researchers to the foaming activity occurring at the phase interface [38], [50].

Modeling the heat transfer behavior of refrigerant/oil mixtures to account for the effect of fluid properties and surface geometry becomes extremely difficult for lack of accurate mixture properties and has yet to be developed. Jabardo and da Silva [40] have tried to predict the mixture heat transfer coefficients by using the mixture properties with the correlation developed for pure refrigerant. The poor agreement between the experimental and predicted values indicates that not only the physical properties but also the boiling mechanisms are changed when refrigerant is mixed with oil.

Chongrungreong and Sauer [13], Jabardo and da Silva [40], and Jensen and Jackman [41] correlated selected refrigerant/oil mixture data in simple forms including empirical coefficients for each refrigerant-oil concentration combination. The heat transfer coefficients predicted by Chongrungreong and Sauer [13] and Jensen and Jackman [41] decrease monotonically with increasing oil concentration, while the experimental data correlated by Jabardo and da Silva [40] show one-percent oil effects on the increased heat transfer coefficients.

Experimental results

Table 2.2 compiles the recent publication on nucleate pool boiling. As shown in Table 2.2, most of the studies included tests on complex enhanced tubes in addition to smooth and low integral-fin tubes. The subjects of alternative refrigerants were concerned with HCFC-123 and HFC-134a, which are proposed substitutes for the respective refrigerants CFC-11 and CFC-12 commonly used in industry. The research on CFC-114 and its alternatives (HCFC-124, HFC-227, HFC-236ea, HFC-236fa) was also important. Besides, the lubricant effect on boiling performance is drawing attention, too.

The effects of oil on the heat transfer coefficients of CFC-114 with up to 10% oil (by mass) during pool boiling on a porous-coated (High-Flux) tube and on a smooth tube were investigated at $-2.2°C$ and $6.7°C$ by Wanniarachchi et al. [76]. The porous-coated tube performed ten times better than the smooth tube in pure CFC-114 and seven times better than it in CFC-114 with up to 10% oil over the heat flux range of 10 kW/m^2 to 40 kW/m^2. They reported that the presence of up to 3% oil caused about a 35% reduction in the heat transfer performance of the porous-coated tube over the heat flux range of 0.5 kW/m^2 to 95 kW/m^2, and the presence of oil equal to or greater than 6% degraded the boiling performance dramatically beyond the heat flux of 30 kW/m^2. The effects of the two boiling temperatures tested were found insignificant.

Wanniarachchi et al. also plotted the ratio of the heat transfer coefficients with and without oil versus oil percentage for different heat fluxes to show the oil effects clearly. The ratio of mixture to oil-free boiling coefficients for the smooth tube exhibited an inexplicable wavy pattern, while for the

Table 2.2 Recent studies on nucleate boiling of refrigerants

Work	Fluid	Tube geometry	T_{sat} or P_{sat}	Oil (%)
Wanniarachchi et al. [76]	CFC-114	Plain & High-Flux	−2.2 & 6.7°C	0~10%
Webb & Pais [85]	HFC-134a HCFC-123 HCFC-22 CFC-12 CFC-11	1024-fpm Turbo-B Gewa-SE	26.7°C	0
Gorenflo & Sokol [24]	HFC-134a	Plain & Gewa-TX	1.4~36.5 bar	0
	HFC-227	Plain & Gewa-TX	1.0~26.4 bar	0
Webb & Pais [86]	HFC-134a HCFC-123 HCFC-22 CFC-12 CFC-11	Plain Gewa-TX 1024-fpm Turbo-B Gewa-SE	4.4 & 26.7°C	0
Memory &Marto [49]	CFC-114	Plain, 1024-fpm, Gewa-T Gewa-YX, Turbo-B High-Flux, Thermoexcel-E	2.2°C	0~10%
Memory et al. [50]	HCFC-124	Plain, 728-fpm, 1024-fpm Turbo-B, High-Flux	2.2°C	0~10%
Webb & McQuade [87]	HCFC-123 CFC-11	Plain, Turbo-B, Gewa-SE	4.4°C	0~5%
Huebsch & Pate [38]	CFC-114 HFC-236ea	Plain, 1024-fpm, 1575-fpm	2.0°C	0~3%
Webb et al. [89]	HCFC-123	Plain, Turbo-B Gewa-SE, High-Flux	4.4°C	0~10%

porous-coated tube it always decreased as the oil percentage increased.

Pool boiling of five pure refrigerants (HFC-134a, HCFC-123, CFC-12, CFC-11, and HCFC-22) on a 1024-fpm, a Gewa-SE, and a Turbo-B tube was evaluated at 26.7°C by Webb and Pais [85]. Subsequently, the same five refrigerants boiling on plain and Gewa-TX tubes as well as on these three tubes were tested at 26.7°C and 4.4°C by the same authors [86].

In both studies of Webb and Pais [85] [86], the boiling heat transfer coefficients of HCFC-123 and HFC-134a were found to be similar to the respective values of CFC-11 and CFC-12 for most of the tubes tested, the deviation was within 10%. The boiling coefficient ratio of HCFC-123 to CFC-11 for the Turbo-B tube was 60% at both the saturation temperatures (26.7°C and 4.4°C) and it was 80% for the Gewa-SE tube tested at 26.7°C. The boiling coefficient data for the high pressure refrigerants (HFC-134a, CFC-12, and HCFC-22) were higher than those for the low pressure refrigerants (CFC-

11 and HCFC-123), and the heat transfer coefficient increased with increasing saturation temperature (i.e. with increasing reduced presure). The optimum tube may differ for different refrigerants from the fact that the Turbo-B tube was the best tube for HCFC-123 while the Gewa-SE tube was superior in HFC-134a.

Pool boiling of HFC-134a and HFC-227, which are proposed substitutes for the respective refrigerants CFC-12 and CFC-114, was evaluated by Gorenflo et al. [24] for a plain tube and a Gewa TX tube. The boiling coefficients for the plain tube tested in HFC-134a and HFC-227 were approximately equal to the values measured in CFC-12 and CFC-114, respectively. While the performance of the Gewa-TX tube with HFC-134a and HFC-227 was better than that with the corresponding CFC-12 and CFC-114.

Three low integral-fin tubes (1024-fpm, Gewa-T, and Gewa-YX) and three structured-surface tubes (Thermoexcel-E, Turbo-B, and High-Flux) were tested by Memory and Marto [49] in their study of the oil effects on boiling hysteresis of CFC-114 at 2.2°C. The mineral oil used generally decreased the heat transfer performance of all the tubes tested except that a small oil concentration of 3% caused a small increase in the heat transfer performance of all integral-fin tubes.

Pool boiling of HCFC-124 mixed with an alkylbenzene oil up to 10% was tested by Memory et al. [50] for a smooth tube and four enhanced tubes (748-fpm, 1024-fpm, Turbo-B, and High-Flux) at 2.2°C. Comparison with the previous results for CFC-114 was also made in order to determine the viability using HCFC-124 as a replacement for the CFC refrigerant. The smooth and finned tubes tested in HCFC-124 performed much better than those in CFC-114 for all heat fluxes over the whole oil concentration range (0% ~ 10%), the superiority was more than 50%. The boiling heat transfer coefficients of these two fluids were similar for the Turbo-B and High-Flux tubes with the oil concentration up to 3%.

Generally, the results of Memory et al. show that the heat transfer performance of the smooth and finned tubes increased with increased oil concentration up to 6% and decreased with further oil addition. The heat transfer increase at 6% oil was by up to 22% and 16% for the smooth tube and the 748-fpm tube, respectively. The authors attributed this increase to the foaming that occurred. The presence of oil had a negligible effect on the heat transfer performance of the 1024-fpm tube over the whole oil concentration range tested. The performance of the High-Flux and Turbo-B tubes decreased with any increase in oil concentration and dropped by 18% and 35% at 10% oil, respectively. Even though, the Turbo-B and High-Flux tubes had the highest heat transfer coefficients at practical design heat fluxes (10 to 30 kW/m^2) and oil concentration (3%). These two tubes also performed best with the pure refrigerant for all heat fluxes.

Pool boiling of CFC-11 and HCFC-123 with the oil concentration varying from 0% to 5% on a plain

tube and two enhanced tubes (Gewa-SE and Turbo-B tubes) was investigated at 4.4°C by Webb and McQuade [87]. The oil-free boiling coefficients for the two refrigerants were withing 5% for the plain and Turbo-B tubes, and 10% for the Gewa-SE tube. The Turbo-B tube performed best in the tests of both pure CFC-11 and HCFC-123.

The data of Webb and McQuade show that the boiling coefficients for all the geometries tested decreased with increased content of the mineral oil, and a larger performance degradation occurred on the enhanced tubes than on the plain tube. For 5% oil, the heat transfer performance of the plain tube, the Gewa-SE tube, and the Turbo-B tube decreased by 15%, 24%, and 28%, respectively. Furthermore, the oil decreased the boiling coefficients of CFC-11 more than that of HCFC-123. At 2% oil, the performance degradation for the enhanced tubes was found to be 10% for HCFC-123 and 20% for CFC-11. As also reported by Memory et al. [50], the Turbo-B tube exhibited the largest adverse effect of oil.

Measurements of heat transfer coefficients during pool boiling of CFC-114 and HFC-236ea with oil concentrations of 0%, 1%, and 3% were conducted on a plain, a 1024-fpm, and a 1575-fpm tube by Huebsch and Pate [38]. The oil used was a mineral oil for CFC-114 and a polyol-ester oil for HFC-236ea. The tubes tested with HFC-236ea gave equal or higher heat transfer coefficients relative to those with CFC-114 for all testing parameters. Maximum heat transfer increases for HFC-236ea of 39% and 34% compared with pure CFC-114 were obtained by the 1024-fpm tube and the 1575-fpm tube, respectively. Moreover, the 1024-fpm tube outperformed the 1575-fpm tube by 18% and the plain tube by 41% for HFC-236ea. The plain tube performed worse than the two finned tubes in all tests.

With the presence of oil in the refrigerant, Huebsch and Pate concluded a general improvement in the heat transfer coefficients of CFC-114 in contrast to the coefficients of HFC-236ea. The addition of oil increased the CFC-114 coefficients up to 30% and decreased the HFC-236ea coefficients up to 17%.

The results of Huebsch and Pate show that the heat transfer performance in pool boiling depended on not only the types of refrigerants, tubes, and oils but also the oil quantity added. The heat transfer performance of the two finned tubes was similar in the CFC-114/oil mixtures, and it improved by around 30% with respect to the pure CFC-114. In the case of HFC-236ea, the 1% and 3% oil concentrations decreased the heat transfer coefficients for the 1024-fpm tube by 6% and 17%, respectively. While the 1575-fpm tube showed negligible oil effects on heat transfer performance at the 1% oil concentration, the presence of oil produced a 10% degradation from the pure HFC-236ea results at the 3% oil concentration.

Webb et al. [89] tested HCFC-123 with a mineral oil for GEWA-SE, Turbo-B, porous surface, and plain tubes at 4.4°C. The test range for oil concentration was from 0% to 10%. The present data for

the oil-free refrigerant agree very closely with those of Webb and Pais [85] for HCFC-123 on the same tubes tested (i.e., plain, Turbo-B, and GEWA-SE). The best heat transfer coefficients were given by the Turbo-B and porous tubes, followed by the Gewa-SE and plain tube.

With oil concentrations lower than 2%, Webb et al. found that the heat transfer coefficients for all tubes decreased but not significantly at any heat flux tested and concluded that effects of the small amount of oil can be neglected for all the tubes tested. In addition, they also reported that the mineral oil used with HCFC-123 decreased the heat transfer performance of the GEWA-SE and Turbo-B tubes greater than that of the plain and porous surface tubes.

Applicability of single-tube data to the design of a flooded evaporator

The effects of finned tube pitch on the pool-boiling heat transfer of CFC-11 were investigated by Hahne et al. [25]. Two tube types, namely a single tube and twin tubes, were tested at a saturation pressure of 1 bar. The tube pitch was observed to have no effect on the heat transfer coefficients once fully developed boiling had been reached, while larger tube pitches produced higher heat transfer coefficients when boiling was not fully developed.

An experimental study was conducted by Hahne and Müller [26] to measure heat transfer coefficients of CFC-11 for a single tube, twin tubes, and a bundle in flooded evaporators operated at a saturation state of 1 bar and 23.3°C. The bundle tubes were in an aligned-tube arrangement with a square tube pitch which is twice the root diameter of the tubes, while the twin tubes were arranged vertically and had the same tube pitch as the bundle. Heat transfer coefficients for the finned tubes in the bundle were found to be in agreement with those in the twin-tube arrangement.

In general, the boiling coefficients for the bottom tubes of a bundle are comparable to those predicted by a single-row tube, while the two-phase fluid circulating up through a bundle enhances the boiling coefficients for the upper tubes substantially. Heat transfer coefficients for a single tube may coincide with those for a tube bundle if nucleate boiling rather than forced convection dominates the heat transfer process. Webb [78] reported that a tube bundle had approximately the same boiling coefficients as a single tube when enhanced tubes were used to enhance nucleate boiling, but had substantially higher boiling coefficients when plain or standard finned tubes in bundles were tested.

Since boiling coefficients vary over the bundle depth, the amount of refrigerant charge in a realistic flooded evaporator should be determined by experimental tests to give the highest evaporator performance. Overcharge will invoke a hydrostatic head penalty across the rows, while insufficient charge will cause dry-out phenomena occurring on the upper tubes.

No published data regarding nucleate boiling of HFC-236ea on tube bundles were available for comparison.

CHAPTER 3 LITERATURE REVIEW OF SPRAY EVAPORATION

Overview

Falling-film evaporators using water or ammonia as the working fluid are commonly employed in the wine and poultry industries for processing, distillation, and desalination. However, the use of hydrocarbon-type refrigerants has been restricted to this type of evaporators.

In a falling-film evaporator, the fluid liquid is distributed onto the hotter tube surface, droplets that miss hitting the tube(s), together with those that are not evaporated on the tube surface before falling due to gravitational and aerodynamic drag forces, return to the pump. The liquid is then recirculated from the pump to the distribution systems.

Eight different distribution systems previously used to introduce liquid onto the tube(s) for testing falling-film evaporation (i.e., spray evaporation) were summarized by Chyu et al. [17]. Fujita and Tsutsui [22] [23] investigated the influence of the liquid feeding systems and methods on falling-film evaporation of CFC-11 by testing six liquid feeding systems. Although spray nozzles have been used by few investigators [44] [52] [70], most of the falling-film evaporation tests were done with liquid dripped by gravitational force from a distributor (or distributors) located above the tube(s).

The heat transfer rate through falling-film evaporation from a heated surface wetted by a liquid film has the potential to be higher than that through pool boiling from a heated surface immersed in a liquid pool, since the thermal boundary layer built within a liquid film is thinner than that within a liquid pool. In addition, the quantity of refrigerant needed in spray evaporators is much smaller than in flooded evaporators. This is particularly valuable for the systems using expensive alternative refrigerants. Another advantage of falling-film evaporation is that the head loss over the bundle depth commonly found in liquid pool is eliminated.

Theoretical analysis

Recirculation rate

The recirculation rate (RR) of refrigerant in the test section is defined as the mass flow rate of refrigerant distributed to the test section ($\dot{m}_{spr}$, kg/s) divided by the mass flow rate of refrigerant vapor leaving the test section ($\dot{m}_v$, kg/s). The mass and energy rate balances across the test section were used to obtain this parameter since the facility in this study was not able to measure the mass flow rates of refrigerant existing the test section as liquid ($\dot{m}_l$, kg/s) and as vapor ($\dot{m}_v$, kg/s).

Under steady state conditions, the mass rate balance across the test section is formulated as,

$$\dot{m}_{spr} = \dot{m}_l + \dot{m}_v \tag{3.1}$$

and the energy rate balance across the test section is given as,

$$q + \dot{m}_{spr} \cdot i_{spr} = \dot{m}_l \cdot i_l + \dot{m}_v \cdot i_v \tag{3.2}$$

where the heat transfer rate (q, W) was obtained from Equation 5.2; the total spray rate ($\dot{m}_{spr}$, kg/s) was measured; the enthalpies (J/kg), i_{spr}, i_l, and i_v, were calculated based on the measured temperatures of the manifold, the liquid outlet of the test section, and the vapor outlets of the test section, respectively.

The fraction of the total refrigerant flow leaving the test section as vapor (y) was calculated by substituting its definition given by Equation 3.3 into Equations 3.1 and 3.2 and solving the two equations. With the fraction of the total refrigerant flow leaving the test section as vapor, y, defined as

$$y \equiv \frac{\dot{m}_v}{\dot{m}_{spr}} \tag{3.3}$$

Equation 3.1 becomes

$$\dot{m}_{spr} = \dot{m}_l + y \cdot \dot{m}_{spr} \tag{3.4}$$

and Equation 3.2 becomes

$$q + \dot{m}_{spr} \cdot i_{spr} = \dot{m}_l \cdot i_l + y \cdot \dot{m}_{spr} \cdot i_v \tag{3.5}$$

The y was calculated by solving Equations 3.4 and 3.5.

The recirculation rate (RR), the ratio of the total feed rate to the rate evaporated, was then determined by simply inverting y,

$$RR \equiv \frac{\dot{m}_{spr}}{\dot{m}_v} = \frac{1}{y} \tag{3.6}$$

Heat transfer mechanism

When liquid drops impinge on the tube surface during spray evaporation testing, the intensive droplets integrate together and form a thin film on the surface. Heat is transferred through evaporation occurring at the liquid-vapor interface and through nucleation boiling occurring within the thin liquid film. Therefore, the process of spray evaporation generally combines the heat transfer mechanisms of nucleate boiling and convective evaporation.

The relative heat transfer contribution of nucleation boiling to spray evaporation performance depends on heat transfer surface geometry and heat flux density. Nucleate boiling has been shown to play a predominant role during spray evaporation on enhanced boiling surfaces, while it does not even occur in the case of low heat flux density. The forced convection boiling model proposed by Chen [10] can be used to represent the shell-side heat transfer mechanism of spray evaporation. The overall shell-side heat transfer coefficient ($h_{overall}$) in the Chen model combines heat transfer contributions from nucleate boiling ($S \cdot h$) and forced convection vaporization ($F \cdot h_l$). The equation for the Chen model is given as

$$h_{overall} = S \cdot h + F \cdot h_l \tag{3.7}$$

where the parameters S, h (W/m^2-K), F, and h_l (W/m^2-K) in Equation 3.7 are suppression factor, heat transfer coefficient for nucleate boiling on a single tube, forced convection multiplier, and single-phase (liquid) forced convection coefficient. The parameters S and F are two-phase flow parameters.

The distinguishing difference between nucleate boiling and forced convection vaporization is that the boiling heat transfer coefficent (h) is a strong function of heat flux density while the forced convection coefficient (h_l) strongly depends on fluid velocity. A detailed discussion in the heat transfer mechanisms of nucleate boiling has been given in Chapter 2. As shown in Equation 3.7, the forced convection vaporization ($F \cdot h_l$) is represented as single-phase forced convection (h_l) multiplied by a multiplier (F) which is related to the two-phase friction pressure gradient. The relationship between the single-phase forced convection coefficient (h_l) and fuild velocity (V_l) can be seen from the simple empirical correlation derived for a circular cylinder in cross flow by Hilpert and introduced by Incropera and DeWitt [39]. The Hilpert correlation is expressed as

$$\frac{\bar{h}_l D}{k_l} = C \cdot \left(\frac{\rho_l V_l D}{\mu_l}\right)^m \cdot Pr_l^{1/3} \tag{3.8}$$

where the coefficient C varies from 0.989 to 0.027 and the exponent m varies from 0.330 to 0.805 with the change of Reynolds number from 0.4 to 400000. Equation 3.8 indicates that forced convection coefficient increases with increasing fuild velocity.

Falling-film evaporation heat transfer is similar to film condensation heat transfer in that the liquid on the tube yields a thermal resistance to heat transfer between the vapor and the surface. Therefore, for both the heat transfer forms a higher heat transfer rate is obtained through a thinner liquid film. However, an evaporating thin liquid film tends to rupture and thus results in a loss of performance. Film evaporation requires a mechanism to spread a thin film on the heat transfer surface and maintain the surface fully wet.

The heat transfer performance of falling-film evaporation is related to the film thickness on the tube, which is susceptible to the distribution systems and methods. Falling-film heat transfer coefficients measured from different feeders were reported to be different [63]. A reliable relationship between heat transfer and film-flow conditions has yet to be developed.

Predictive methods

Liquid distribution on tubes

Nonuniform liquid distribution along the tubes degrades the overall performance of spray evaporators. The portions of tube surface subjected to insufficient liquid dry out, while the portions with a dense spray are exposed to a thick liquid layer.

Zeng et al. [92] developed a predictive method for optimal design of a spray system using round, full-cone nozzles. As shown in Figure 3.1, in order to reduce the pumping power, the surrounding portion of a tube bundle in the spray zone (A1) and the overlapped area between two neighboring spray cones (A2) should be minimized. Based on this criterion for minimizing the amount of spray missing the tubes in a bundle of width (bw), the optimal distance (OL) between two neighboring nozzles is $1.41 \times bw$, and the corresponding height (d) of nozzles above tubes is $0.866 \times bw \times \cot(\beta/2)$, where β is the angle of a spray cone.

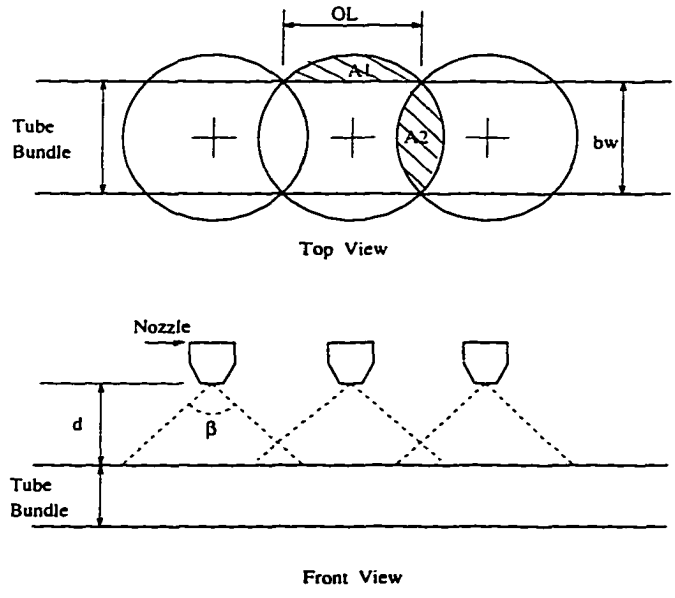

Figure 3.1 Schematic of nozzle spray system design

It should be noticed that the optimal dimensions of a spray system vary with the spray flow rate. The angle of a spray cone (β) varies with the spray flow rate, and thus, the optimal height (d) varies with the spray flow rate. Also, the overlapped cone area (A2) tends to be greater than the minimum value mentioned above in order to prevent dry-out of the tube surface.

Further prediction for the local spray flow rate distributed on individual tubes of a bundle was given in a later publication of Chyu et al. [17].

Heat transfer correlations

It is much more difficult to derive a general correlation of heat transfer coefficents for falling-film evaporation than pool boiling, because more parameters were thought to affect the heat transfer coefficient for falling-film evaporation. The falling-film heat transfer performance is dependent of the liquid film thickness (i.e., the boundary layer thickness) on tube surface, which is affected by tube diameter, feed flow rate, tube surface geometry, heat flux, feed flow rate, system pressure, and configuration of distribution system. The relative contribution of these factors to the performance is not yet clear.

Heat transfer through falling-film evaporation and boiling on horizontal plain tubes was investigated by Parken et al. [63] for boiling and nonboiling conditions over the heat flux range of 30 kW/m^2 to 80 kW/m^2. The shell-side water with the feedwater temperatures ranged from 49°C to 127°C and the feed flow rates ranged from 0.135 to 0.366 kg/s-m was introduced through a thin-slot distribution system onto the tube. The tubes tested were of 25.4 mm and 50.8 mm in diameter. Correlations of average heat transfer coefficients for boiling and nonboiling conditions were also developed for each tube diameter.

Parken et al. concluded that the average nonboiling heat transfer coefficient (h_{nonb}) increased with increasing flow rate and feedwater temperature, but were independent of heat flux. The authors assumed that the water flow rate can be represented by the Reynolds number (Re_l=4Γ/μ_l) and water temperature can be represented by the Prandtl number (Pr_l=$\mu_l \cdot Cp_l/k_l$), two nonboiling correlations (one for each tube diameter) in the following form were derived for their data.

$$h_{nonb}\left(\frac{\mu_l^2}{\rho_l^2 \cdot g \cdot k_l^3}\right)^{1/3} = a1 \cdot Re_l^{a2} \cdot Pr_l^{a3} \tag{3.9}$$

Since the average boiling heat transfer coefficient (h) was observed to increase with increasing wall heat flux in addition to flow rate and feedwater temperature, the effects of wall heat flux (q'') were incorporated into the two boiling correlations formulated as:

$$h\left(\frac{\mu_l^2}{\rho_l^2 \cdot g \cdot k_l^3}\right)^{1/3} = b1 \cdot Re_l^{b2} \cdot Pr_l^{b3} \cdot q''^{b4} \tag{3.10}$$

where $a1$, $a2$, $a3$, $b1$, $b2$, $b3$, and $b4$ in Equations 3.9 and 3.10 are empirical constants obtained for a given working fluid (water) and distribution system. The liquid water properties (μ_l, ρ_l, k_l, and Cp_l)

are defined in the Nomenclature. Γ is water mass flow rate per unit tube length (kg/s-m) and g is gravity (m/s^2).

Parken et al. found that their heat transfer coefficients measured for the 50.8-mm-diameter tube with a thin-slot water distribution system were around 20% lower than those obtained in an earlier study using a perforated-plate distribution system at similar conditions. These results of comparison indicate that the falling-film heat transfer coefficients are dependent on the feeding systems and methods.

Moeykens [52] developed two correlations for his falling-film evaporation data of HFC-134a and HCFC-123 by using regression analysis to account for the changes in the dependent variable (heat transfer coefficent). The bundle overfeed ratio and bundle heat flux were the two independent variables in both correlations, ten empirical constants were required in one correlation while sixteen constants were needed in the other one correlation which incorporated one more independent variable, oil concentration, for the tests of refrigerant/oil mixtures. Thirteen sets of the empirical constants were specified for each particular condition with a given refrigerant, tube surface, tube bundle, and lubricant. The author has tried but failed to use the traditional dimensionless parameter approach or power law formula to correlate his data.

Fujita and Tsutsui [22] proposed analytical correlations for heat transfer performance of falling film evaporating on a horizontal tube. Correlations of Nusselt number were developed for laminar and turbulent film conditions assuming that the effects of liquid feeding systems were negligible.

For laminar conditions, the average Nusselt number was composed of contributions in the developing, transition, developed regions of the thermal boundary layer along the tube periphery and it was derived as a function of film Reynolds number ($Re_l=4\Gamma/\mu_l$), Prandtl number ($Pr_l=\mu_l \cdot Cp_l/k_l$), and the dimensionless tube radius ($r/(\mu_l^2/\rho_l^2 g)^{1/3}$). For turbulent film conditions, the Nusselt number was derived using the eddy viscosity model, and it was derived as a function of film Reynolds number and Prandtl number.

It can be noted from the correlations present that both correlations were derived for nonboiling conditions without taking into account the effects of heat flux on heat transfer performance. Their experimental data of CFC-11 were under estimated 15% to 25% by their correlations.

Experimental results

Most of the previous falling-film evaporation studies have been done with water [15] [16] [63] or ammonia [45] [93] as the working fluid, moreover, liquid distributors rather than nozzles were used in the distribution systems.

Table 3.1 compiles recent publication on falling-film evaporation. Most of the works were conducted by Moeykens and co-workers in their series studies of HFC-134a, HCFC-22, and HCFC-123 [53] [54] [55] [56]. Specifically, the authors used nozzles to spray refrigerants over the tube(s). On the top of their test section, there were 5 nozzles spaced axially every 0.0762 m (3 inch) for the single tube tests and 7 nozzles spaced every 0.0889 m (3.5 inch) in a line for the tube bundle tests.

Table 3.1 Recent studies on falling-film evaporation of refrigerants

Work	Fluid	Test tube geometry	Liquid feed rate (kg/min)	Tube number	P_{sat} (kPa)
Moeykens and Pate [53]	HFC-134a	PL	2.3 ~ 3.0	1 & 2	314.5
Moeykens and Pate [54]	HFC-134a	26F, 40F, TCII SC, TB, SE, PL	2.8	1	314.5
Moeykens and Pate [55]	HCFC-22	TB, PL	15	5×4	531.3
	HFC-134a	TB, PL, SC, 40F	15 & 35	5×4	314.5
Moeykens et al. [56]	HCFC-123	TB, TCII, PL	25 & 35	5×4	35.7
Fujita and Tsutsui [23]	CFC-11	PL	0.008 ~ 1.4	1	200.0
PL: Plain, 26F: 26-fpi, 40F: 40-fpi, TCII: Turbo-CII, SC: Gewa-SC, TB: Turbo-B, SE: Gewa-SE					

The characteristics for sprayed fluid flowing through a tube bundle were studied by Zeng et al. [92]. The local performance of water distribution on the tubes affected by the tube surface geometry and tube bundle pattern was investigated in their study. Among the three tube types tested, the grooved tube performed similar to the plain tube, while the 1575-fpm tube performed worst because the longitudinal liquid movement was restricted by the fins. A bundle with tubes arranged in a square pitch (3×3) was found to require a lower feed flow rate in order to prevent the tubes from overheating than that in a triangular pitch (3–2–3), since the lower rows of the square-pitch bundle were irrigated with more intercolumnar drizzles than those of the triangular-pitch bundle.

In 1976, Danilova et al. [21] measured the heat transfer coefficients of HCFC-22, CFC-12, and CFC-113 in evaporation and boiling. A tube-in-tube distributor located above a horizontal tube bundle was used to drip liquid on the stainless tubes of 18 mm in diameter.

In the nonboiling (evaporation) region, the falling-film heat transfer coefficient was observed to increase with increasing liquid flow rate but almost not depend on heat flux. While in the developed boiling region, the observed heat transfer coefficient increased with increasing heat flux and was not significantly affected by the irrigation density.

Danilova et al. also found that the heat transfer coefficients for spray evaporation at the low heat fluxes ranged from 1 kW/m^2 to 6 kW/m^2 (i.e., the nonboiling region) were 2 to 5 times higher than

those for pool boiling.

Tests of falling-film evaporation, along with the comparative tests of pool boiling on plain tubes, were conducted by Moeykens and Pate [53]. The effects of nozzle types (high pressure drop and low pressure drop), tube diameters (12.7 mm and 19.1 mm), and liquid feed rates (2.3 kg/min ~ 3.0 kg/min) on spray-film heat transfer coefficients of HFC-134a were evaluated.

The results of Moeykens and Pate show that both nozzles producing higher pressure drop and tubes with a smaller diameter yielded higher heat transfer coefficients. The heat transfer coefficients were strongly dependent on the feed flow rates at high heat fluxes where dry-out phenomena became dominant, but were only weakly affected by the flow rates at low heat fluxes.

When the tube surface was not fully wetted, a loss of heat transfer performance existed and the performance was improved with increasing feed rate. The critical wall heat flux where the dry-out began to occur was around 25 kW/m^2 for both tubes tested. At this heat flux, an increase of 12% was observed for the 12.7-mm-diameter tube with a raise in spray mass flow rate from 2.3 kg/min to 2.8 kg/min. While for the 19.1-mm-diameter tube, a raise in spray mass flow rate from 2.8 kg/min to 3.9 kg/min resulted in a considerable increase of 25% at the high heat flux of 40 kW/m^2.

For the range of liquid feed rates evaluated, the heat transfer performance in spray evaporation was greater than that in pool boiling only at the heat fluxes less than 22.5 kW/m^2.

Collector tests were also performed at the total spray rate of 2.8 kg/min by Moeykens and Pate [53] in order to estimate the percentage of the spray flow rates acturally reaching the tube surface. The fraction of liquid hitting the tube surface was calculated through the tests of a collector which was put under the tube and had a width at its top equal to the tube diameter and a length equal to the heated length of tube. The collector test fraction, defined as the fraction of refrigerant supplied to the test section that reaches the tube, was 0.193 for the 19.1-mm-diameter tube and 0.143 for the 12.7-mm-diameter tube.

The effects of enhanced surface and lubricant on the single-tube performance during spray evaporation of HFC-134a at 2°C were reported in another paper of Moeykens and Pate [54]. Their data show that the two enhanced condensation (Turbo-CII and W-SC) tubes outperformed the two enhanced boiling (Turbo-B and Gewa-SE) tubes and the two low integral-fin (1024-fpm and 1575-fpm) tubes.

As will be noted in the discussion of condensation heat transfer, the tube which is effective for condensation tend to break the liquid film on its surface. The spray evaporation heat transfer performance has been shown to decrease when the tube surface is not fully wetted. Hence, it is unlikely that the enhanced condensation tubes would perform best in spray evaporation.

In the study of Moeykens and Pate [54], the heat transfer coefficients of HFC-134a increased with a small amount ($\leq$ 5%) of polyol-easter oil for the two tubes (1575-fpm Turbo-CII) tested at two different oil viscosities (32 and 68 Centistoke). The authors attributed this increase to the presence of foaming on the tube surface.

Moeykens and Pate [55] also evaluated the lubricant effects on the heat transfer performance of tube bundles for spray evaporation of HFC-134a and HCFC-22. Similarly as those reported previously [54] for HFC-134a, the small amount ($\leq$ 2.5%) of polyol-easter oil used with HFC-134a and the small amount ($\leq$ 1%) of alkyl-benzene oil with HCFC-22 increased the heat transfer coefficients for all the tubes tested. The heat transfer performance was found to be more dependent on lubricant concentration than film-feed supply rate for the testing conditions evaluated.

Different from the previous results [54], Moeykens et al. [56] found that the enhanced boiling (Turbo-B) tube performed better than either the enhanced condensation (Turbo-CII) tube or the plain tube in their study of HCFC-123 heat transfer coefficients for spray evaporation on tube bundles.

The lubricant effects on the heat transfer coefficients of HCFC-123 were also assessed [56]. However, the results are not like those previously reported for HFC-134a [54] [55] and for HCFC-22 [55], a small amount ($\leq$ 2.5%) of naphthenic mineral oil mixed with HCFC-123 improved the heat transfer performance of both the Turbo-CII tube and plain tube but degraded that of the Turbo-B tube. The degradation was up to 37%.

In this study, it was found that the cavities of the Turbo-B tube are easily blocked with oil and difficult to clean. Brand-new Turbo-B tubes should be used for different oil tests. Moreover, even brand-new tubes should be cleaned using a solvent before testing, since tubes are usually contaminated with some lubricant while they are being made. This observation might explain the inconsistent heat transfer performance of the Turbo-B tube reported by Moeykens and coworkers [54] and Webb and Pais [86]. Webb and Pais reported that the Turbo-B tube gave anomaly high heat transfer coefficients of CFC-11.

Fujita and Tsutsui [23] investigated the influence of the feeder types and feeding methods on falling-film evaporation of CFC-11 by using six different feeding systems, which included three feeder types (a porous sintered tube, a feeding tube with upward-facing holes, and with downward-facing holes) and two feeding methods (direct and indirect). The experiments were conducted at low operating heat fluxes of 0.5 $\sim$ 2.5 kW/m^2 to measure heat transfer coefficients from laminar flow at film Reynolds number of 10 to turbulent flow at Re = 2000. The independence of the measured heat transfer coefficients from heat fluxes indicates that dry-out phenomena and nucleate boiling did not occur during the tests. Their

data were under predicted by their analytical model previously derived [22]. The error was 15% to 25% under prediction.

Fujita and Tsutsui classified the feeding methods as direct and indirect methods. For a direct method, liquid is directly introduced onto a tube by a feeder, while for an indirect method, dummy tube(s) was (were) put between the feeder and tube and used as flow rectifier(s) to prevent maldistribution of the supplied films. All the feeding systems tested were found to produce similar falling-film heat transfer coefficients in the heat flux range tested, with a maximum deviation of 20%.

Applicability of single-tube data to the design of a spray evaporator

The applicability of single-tube data to the design of large-scale evaporators was investigated by Lorenz and Yung [45]. Below the critical Reynolds number of 300, the single tube was found to have higher heat transfer coefficients than the tube bundle where dry-out spots occurred on its tubes. Beyond the critical Reynolds number of 300, the average heat transfer coefficients of the bundle were equal to that of the single tube when the Reynolds number was large enough so that all the tubes were fully wetted. Nevertheless, these results were based on the low operating heat flux of $4 \sim 8$ kW/m^2 in tests with ammonia. The critical Reynolds number might be raised under the higher heat flux conditions.

No published data regarding spray evaporation of HFC-236ea on tube bundles were available for comparison.

CHAPTER 4 LITERATURE REVIEW OF SHELL-SIDE CONDENSATION

Overview

Condensation is defined as the removal of latent heat from a system in such a way that vapor is transformed into liquid. When refrigerant vapor contacts cooler tubes below the vapor's saturation temperature, condensate is formed on the tube surface as a liquid film or droplets and the liquid acts as a resistance to heat transfer on the tube surface. Then the accumulated condensate falls from the bottom of horizontal tubes as droplets, columns, or sheets due to drainage forces (e.g., gravity, surface tension, suction, and centrifugal force). The drainage patterns in horizontal bundles of different tube types were observed by Webb and Murawski [84] in their study of the row effects due to condensate loading.

Condensation heat transfer on a horizontal tube with rough surfaces is mainly subject to the combined effects of surface tension, gravitational force, and tube surface geometry. While surface tension has been found to play the predominant role during condensation of stagnant vapor on commercial finned tubes [79], the effects of vapor shear stress at the phase interface may dominate the falling mode of condensate in the presence of a large vapor velocity. The interfacial shear stress in the direction of gravity will reduce the condensate film and thus enhance condensation heat transfer. Condensation involving large vapor velocity is classified as forced convection condensation.

This research focuses on evaluating film condensation of stagnant vapor. Although dropwise condensation is superior to film-wise condensation because heat is transferred through droplets having the diameters much less than common film thickness, the non-wetted heat transfer surface where dropwise liquid usually occurs is difficult to maintain due to aging.

The existing theories and correlations for condensation are more greatly developed than for boiling. However, the theoretical models developed were restricted to condensation on low integral-fin tubes which have been found to enhance condensation of fluids with low surface tension such as refrigerants.

The models developed usually considered the effects of gravity, surface tension, and fin efficiency [1] [28] [81] on condensation of stagnant vapor, while some recent experiments were conducted on variety of finned tubes to assess the effects on condensation heat transfer of vapor shear stress at the liquid-vapor interface [5] [8] [14].

The geometrical characteristics of tube surfaces are closely related to the removal mechanism of condensate. Numerous studies that investigated the effects of fin density and geometry on the condensation heat transfer performance of horizontal finned tubes have been reported [7] [32] [71]. Sukhatme et al. [71] shows that the condensing coefficient increased with increasing fin height for the four 1417-fpm tubes having fin heights between 0.46 and 1.22 mm in their studies on film condensation of CFC-11 for nine integral-fin tubes, which have 945, 1417, 1890, and 2205 fins per meter.

Other parameters, such as the influence of noncondensable gases in the condensing vapor, were studied by Ullmann and Letan [74]. The noncondensable gases accumulating at the liquid-vapor interface will yield a thermal resistance to heat transfer between the vapor and the surface and decrease condensation heat transfer.

Theoretical analysis

Fundamental condensation mechanism

An earliest analytical model derived by Nusselt [61] in 1916 for laminar film condensation on plain vertical and inclined plates as well as on horizontal tubes provides the fundamental understanding of film condensation, although it was developed with assumptions of no interfacial shear stress and no surface tension drainage. (The Nusselt theory is introduced in heat transfer textbooks, e.g., Incropera and DeWitt [39]).

Nusselt assumed that the energy is transferred across the condensate film only by conduction, the surface heat flux can be expressed as

$$\begin{aligned} q'' &= h_x \cdot (T_{sat} - T_w) \\ &= \frac{k_l \cdot (T_{sat} - T_w)}{\zeta_x} \end{aligned} \tag{4.1}$$

Re-arrange Equation 4.1 to give the local convection coefficient (h_x) as

$$h_x = \frac{k_l}{\zeta_x} \tag{4.2}$$

where the film thickness (ζ_x) at a distance (x) from the top of the vertical plate was determined by applying the momentum equation with an energy balance to a differential element in the condensate film, as shown in Figure 4.1.

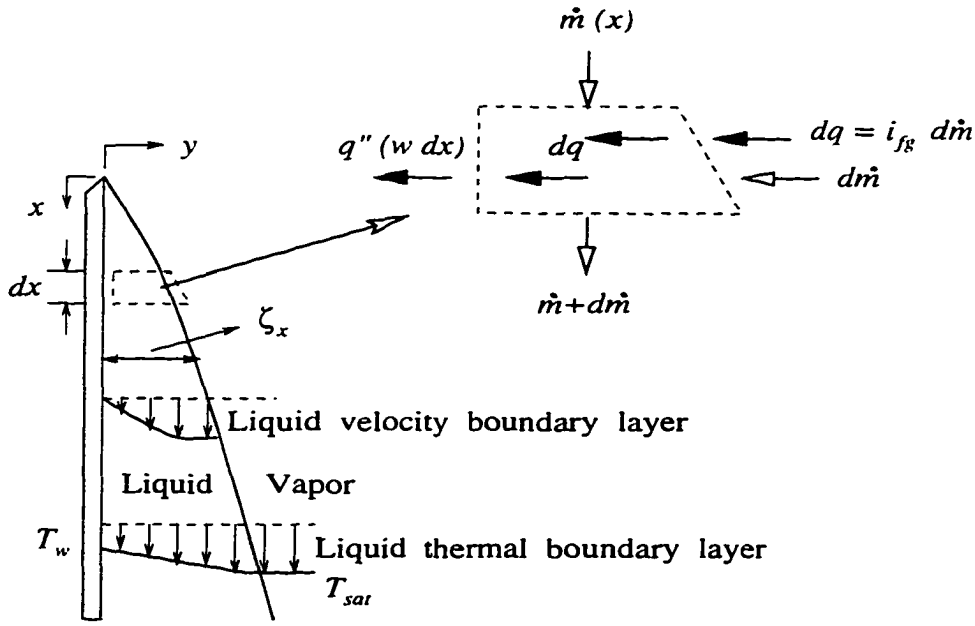

Figure 4.1 Boundary layer conditions related to Nusselt's analysis [61] for a vertical plate of width w

$$\zeta_x = \left[\frac{4k_l \cdot \mu_l \cdot x \cdot (T_{sat} - T_w)}{g \cdot \rho_l \cdot (\rho_l - \rho_v) \cdot i_{fg}}\right]^{1/4} \tag{4.3}$$

Substituting Equation 4.3 into Equation 4.2 and integrating Equation 4.2 over the plate length (L) gives the average film coefficient ($\bar{h}$) on a vertical plate as

$$\bar{h} = 0.943\left[\frac{g \cdot \rho_l \cdot (\rho_l - \rho_v) \cdot k_l^3 \cdot i_{fg}}{\mu_l \cdot (T_{sat} - T_w) \cdot L}\right]^{1/4} \tag{4.4}$$

The ζ_r in Equation 4.3 was derived for vertical plates, it is also applicable for inclined plates and horizontal tubes if g in Equation 4.3 is replaced with $g \sin\theta$, where θ is the plate angle from the vertical.

Similar to the development of Equation 4.4, the average film coefficient on a horizontal smooth tube was obtained by integrating Equation 4.2 over $0 \leq \theta \leq \pi$.

$$\bar{h} = 0.725 \left[\frac{g \cdot \rho_l \cdot (\rho_l - \rho_v) \cdot k_l^3 \cdot i_{fg}}{\mu_l \cdot (T_{sat} - T_w) \cdot D} \right]^{1/4} \tag{4.5}$$

From the Nusselt analysis (Equation 4.2), it can be noted that the film condensation heat transfer coefficient is related to the condensate film thickness and it increases with decreasing film thickness. The film coefficient can be calculated once the film thickness is determined and can be improved by reducing the film thickness. Hence, film condensation requires a mechanism to remove the condensate from the heat transfer surface and reduce the film thickness.

While industry has been finding new enhanced condensation surface that is effective to remove the accumulated condensate and reduce film thickness, theoretical studies have followed to explain enhancement mechanisms and predict the local film thickness on the new developed surface geometry.

Examination of Equations 4.4 and 4.5 in the Nusselt analysis shows that the condensing coefficient is inversely proportional to the saturation temperature of fluid. In contrast to pool boiling, the fluid tested at higher saturation temperature yields lower condensing coefficient.

Condensation mechanism on enhanced surfaces

Enhanced tubes provide considerable performance improvement over plain tubes. The heat transfer performance of enhanced tubes increases substantially more than the surface area enhancement provided the fins. That is, heat transfer is enhanced not only due to the additional heat transfer surface area but also due to the improved heat transfer mechanism.

Surface tension force dominates the enhancement mechanism on rough and extended surfaces in natural convection condensation. Surface tension in the presence of a liquid-vapor interface that has a changing curvature establishes the pressure gradient in the liquid film, which influences the motion of the condensate film. The pressure gradient pulls the condensate from the fins into the fin roots and thus reduces the film thickness on the fin surface.

Now use a simple two-dimensional fin as illustrated in Figure 4.2 to clarify the improved heat transfer mechanism on enhanced surfaces. Similar to the development of the mechanical equilibrium

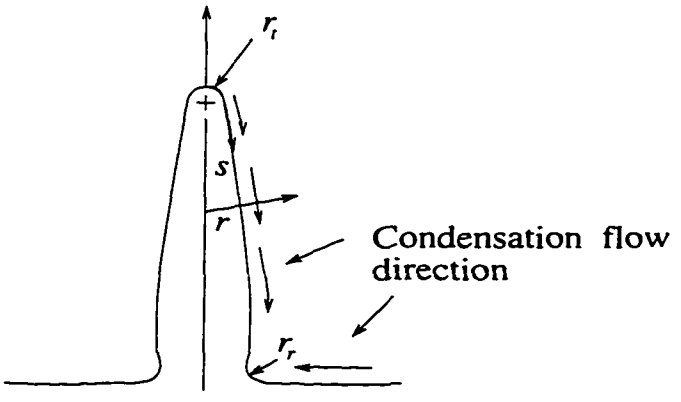

Figure 4.2 Film condensation on a fin

for a spherical liquid drop, the force balance for a convex liquid profile, such as the semicircular fin tip of radius r_t, is

$$P_l - P_v = \frac{\sigma}{r_t} \tag{4.6}$$

Equation 4.6 indicates that a maximum liquid pressure occurs on the fin tip having the smallest radius and the liquid pressure (P_l) decreases in the direction of increasing radius (r). Hence, condensate formed on the fin would be drained from the fin tip toward the fin base because that the local radius increases with increasing distance from the fin tip due to continuous condensation at the liquid-vapor interface. Equation 4.6 also shows that the pressure difference across the interface is related to surface tension.

Similar to the development of the mechanical equilibrium for a spherical vapor bubble, the force balance for a concave liquid film that exists at the fin base is expressed as:

$$P_l - P_v = -\frac{\sigma}{r} \tag{4.7}$$

Equation 4.7 indicates that a minimum liquid pressure occurs at the fin base where the condensate interface radius approaches to infinity and the liquid pressure (P_l) for a concave liquid film decreases with decreasing radius (r). Hence, condensate in the interfin region would be pulled into the corner of fin base because of the relative large condensate interface radius at the centerline between the fins compared to the corner radius r_r at the fin root.

The pressure gradient on the film curvature can be obtained by differentiating Equations 4.6 and 4.7 along the curved condensing profile (i.e., dP/ds). This term can be applied to a momentum equation along the condensing profile for calculation of local film thickness. The pressure gradient induced by surface tension on enhanced tubes draws the condensate from the convex surface to the concave surface.

It should be noted that the surface tension force drains the condensate from the fins, however, it retains condensate within the interfin region of finned tubes, which decreases the condensation heat transfer. The condensate retention angle, i.e., the flooded angle from the bottom of tubes, was shown to increase with increasing surface tension and fin density [67].

Predictive methods

Beatty and Katz [4] proposed the first analytical model for horizontal integral-fin tubes. The condensing coefficient was calculated as the area-weighted average of the coefficients for the finned surface and for the tube surface between fins by using the Nusselt [61] equations for condensation on vertical plates (Equation 4.4) and on horizontal tubes (Equation 4.5), respectively. The final results for the average condensing coefficient ($\bar{h}$) were given as follows:

$$\bar{h} = 0.689 \left[\frac{k_l^3 \cdot \rho_l^2 \cdot g \cdot i_{fg}}{\mu_l \cdot (T_{sat} - T_w) \cdot D_{eq}} \right]^{1/4} \tag{4.8}$$

where the equivalent diameter (D_{eq}) was given by

$$\left[\frac{1}{D_{eq}} \right]^{1/4} = 1.30 \cdot \eta_f \cdot \frac{A_f}{A_{ef}} \cdot \frac{1}{L^{1/4}} + \frac{A_r}{A_{ef}} \cdot \frac{1}{L^{1/4}} \tag{4.9}$$

The characteristic length (L) needed in Equation 4.4 or Equation 4.9 was assumed to be

$$L = \frac{\pi(D_o^2 - D_r^2)}{4D_o} \tag{4.10}$$

and the total effective heat transfer surface area (A_{ef}) was composed of contributions due to the fin and base (unfinned) surfaces.

$$A_{ef} = A_r + \eta_f \cdot A_f \tag{4.11}$$

The fin efficiency (η_f) in Equations 4.9 and 4.11 aprroaches one for low-finned copper tubes.

Although the agreement between their predicted heat transfer coefficents and experimental data including 6 low surface tension fluids and 7 integral-fin tubes was within ± 10%. this model is physically unrealistic because condensate drainage was assumed to be controlled by gravity force instead of surface tension force and it did not account for condensate retention. Therefore, the Beatty and Katz correlation is acceptable only for low surface tension fluids condensing on tube fins of wide fin spacing.

Later work by Karkhu and Borovkov [42] considered surface tension on the fin surface in the unflooded region but neglected heat transfer in the flooded region. Their experimental data were predicted within ± 5% using their surface tension drainage model.

The effects of surface tension drainage and condensate retention on film condensation were first incorporated in the model developed by Webb et al. [81]. This model assumed that surface tension force drains the condensate from the fins while gravity force dominates the condensate drainage on the tube surface between the fins.

The condensing coefficient in the model of Webb et al. is composed of condensation contributions on the fins and on the unflooded as well as on the flooded surface of the root tube. The film coefficient for the fin surface was predicted using the condensate film thickness developed by Adamek. The condensing coefficient for the unflooded area between the fins was calculated from the Nusselt [61] equation for horizontal tubes, while for the flooded area between the fins the heat transfer was treated as two dimensional conduction. Surface tension drainage in the fin root region and condensation on the fin tip were neglected in this model. The heat transfer values predicted by the model of Webb et al. were within ± 20% of their experimental data for CFC-11 condensing on 748, 1024, and 1378-fpm tubes.

A more precise but complex model proposed by Honda and Nozu [28] incorporated the effects of surface tension drainage in the fin root region and accounted for the nonuniform distribution of wall temperature and pressure gradient on the fin surface. Thus, the model is applicable to realistic fins having a trapezoidal cross section with different local condensate film thickness.

The condensing coefficient was predicted for unflooded and flooded regions, where heat transfer for the fin tip, the corner of the fin tip, and the upper and lower regions of the fin side was considered in the flooded region while a two-region model was used for the unflooded region. An iterative solution

was required for solving the wall temperatures in both unflooded and flooded regions. The readers can refer to the original paper [28] for the details of the predictions. This comprehensive model can predict most of the available experimental data including 11 different fluids and 22 integral-fin tubes within ± 20%.

In another advanced model proposed by Adamek and Webb [1], the fin was divided into several regions subjected to surface tension drainage and gravity drainage. The local film thickness derived in another study [2] was used to calculate the local film coefficient. The analysis was simplified by assuming a uniform pressure gradient along the fin flank. The data including 7 fluids for 80 different integral-fin tubes were predicted within ± 15% by this model.

The available analytical correlations for prediction of condensing coefficients and current understanding of condensation mechanisms are limited to integral fins. No analytical models have been specifically developed to predict the condensing coefficient of complex fin geometries such as the Turbo-CII tube.

All the analytical heat transfer models including surface tension effects on film condensation have been done based on a two-dimensional approach. The existing analytical equations developed for film condensation can only predict the heat transfer performance of tube fins with rectangular or trapezoidal cross section. Webb and Murawski [84] derived an empirical equation using their condensation data of CFC-11 for four enhanced (Turbo-C, Gewa-SC, Tred-D, and Modified Turbo-C) tubes in addition to an integral-fin (1024-fpm) tube.

The row heat transfer coefficients for a vertical rank of five horizontal tubes were measured. Webb and Murawski correlated the average heat transfer coefficient for the Nth tube row ($\bar{h}_{NR}$, W/m^2-K) as a function of the condensate Reynolds number leaving the Nth tube row (Re_{NR}) only,

$$\bar{h}_{NR} = c \cdot Re_{NR}^{-n} \tag{4.12}$$

where the Reynolds number (Re) for film condensation on tubes was defined as,

$$Re = \frac{4 \cdot \Gamma}{\mu_l} \tag{4.13}$$

Equation 4.12 indicates that the row condensing coefficient decreases as the Reynolds number is increased with row number N. The average condensing coefficient ($\bar{h}_N$, W/m^2-K) over a bundle of N tube rows was obtained by integrating Equation 4.12 from the first row to the Nth row.

$$\bar{h}_N = \frac{c \cdot (Re_{NR})^{-n} - (Re_1)^{-n}}{(1-n) \cdot (Re_{NR} - Re_1)} \tag{4.14}$$

The parameters Re_1, Re_{NR}, Γ, and μ_l are the condensate Reynolds number leaving the first row, leaving the Nth row, condensate mass flow rate per unit tube length (kg/s-m), and dynamic viscosity of condensate (kg/m-s), respectively. Table 4.1 provides the values of the constants c and n in Equations 4.12 and 4.14, which were obtained by curve fits of the experimental data of CFC-11.

Table 4.1 Constant c and exponent n in Webb and Murawski correlation

Tube	c (W/m^2-K)	n
1024-fpm	13900.0	0.000
Turbo-C	257800.0	0.507
Gewa-SC	54140.0	0.220
Tred-D	269900.0	0.576
Modified Turbo-C	113300.0	0.446

Experimental results

Since a detailed literature review on the subjects of film condensation has been prepared by many researchers [37] [47] [88], specifically, Huber [37] provided a chronological survey of the existing condensation data from 1916 to 1992, this study attempts to review recent literature on alternative refrigerants only. Table 4.2 compiles the recent publication on shell-side condensation of new refrigerants. A number of recent experimental data are still available for ozone-depleting refrigerants [6] [12] [60].

The surveys given [37] [47] [88] show that the majority of the previous experimental studies have been performed on low integral-fin tubes, while Table 4.2 indicates that recent studies included tests on complex enhanced tubes in addition to low integral-fin tubes. Moreover, the subjects of alternative refrigerants were mainly concerned with HCFC-123 and HFC-134a which are intended to replace the respective refrigerants CFC-11 and CFC-12 commonly used in industry.

Cheng and Wang [11] investigated the row effects for HFC-134a condensing on a vertical rank of three horizontal tubes. The tube types tested included a plain tube, three low integral-fin tubes (1024-, 1260-, and 1614-fpm), and three complex finned tubes. The authors did not give commercial names for the complex finned tubes.

Table 4.2 Recent studies on shell-side condensation of new refrigerants

Work	Fluid	Test tube Geometry	Configuration	T_{sat} or P_{sat}
Cheng and Wang [11]	HFC-134a	Plain 1024-fpm, 1260-fpm, 1614-fpm Tube A, Tube B, Tube C	1×3	963 kPa
Huebsch & Pate [38]	CFC-114 HFC-236ea	Plain, 1024-fpm, 1575-fpm	Single tube	40°C
Huber et al. [35]	HFC-134a	1024-fpm, 1575-fpm	5×5	35°C
Huber et al. [36]	HFC-134a	Turbo-CII, Gewa-SC	5×5	35°C
Honda et al. [31]	HCFC-123	Four finned tubes 1041, 1922, 1999, 1999-fpm	3×15	35°C
Chang et al. [9]	HFC-134a	1024-fpm, 1575-fpm Gewa-TWX, Gewa-C	Single tube	40.6~45°C
Honda et al. [32]	HCFC-123	Four finned tubes 1041, 1922, 1999, 1999-fpm	3×15	35°C

Cheng and Wang concluded that the low integral-fin (i.e., two-dimensional-fin) tubes had negligible row effects on the heat transfer coefficients of HFC-134a. In turn, the tube having complex fins (i.e., three-dimensional fins) showed a faster decrease in the heat transfer with increasing row number than that having low integral fins. For plain tube, they reported that the relationship between the average heat transfer coefficients for the N tube rows ($\bar{h}_N$) and for the top tube ($\bar{h}_1$) is

$$\bar{h}_N/\bar{h}_1 = N^{-0.2} \tag{4.15}$$

The finned tube data of Cheng and Wang were under predicted by the Beatty and Katz correlation, the error was 17% to 54% under prediction.

Huebsch & Pate [38] measured heat transfer coefficients for shell-side condensation of CFC-114 and HFC-236ea on a plain, a 1024-fpm, and a 1575-fpm tube. The two refrigerants were found to have similar performance characteristics on the two integral-fin tubes, which yielded heat transfer coefficients approximately four times those produced from the plain tube. Their data for the plain tube were predicted within ± 10% by the Nusselt correlation, while for the finned tubes their results were predicted within 21% by the Beatty and Katz correlation.

Huber et al. [35] [36] studied HFC-134a condensing over a staggered tube bundle for two low

integral-fin (1024-fpm and 1575-fpm) tubes and two complex finned tubes (Turbo-CII and Gewa-SC), respectively. The highest heat transfer coefficients were provided by the Turbo-CII tube, while the lowest were given by the 1024-fpm tube. The Turbo-CII tube produced average coefficients approximately two to three times larger than the finned tubes. The Gewa-SC tube only performed better than the 1024-fpm tube, with an increase in the average coefficients around 15%. The 1575-fpm tube outperformed the 1024-fpm tube by 20% in the average bundle heat transfer coefficients.

In addition, the Turbo-CII tube exhibited a faster decrease in average bundle heat transfer coefficients with increasing heat flux than the other three tubes and it also produced the largest uncertainty. Therefore, their results should be reviewed with care. The maximum experimental uncertainty for the Turbo-CII tube was up to ± 36% for the average bundle heat transfer coefficie and ± 53% for the average row heat transfer coefficients.

Using the same experimental apparatus as that previously used for testing condensation of CFC-113 in bundles of horizontal finned tubes [29] [30], Honda et al. [31] [32] tested condensation of CFC-11 and HCFC-123 for four finned tubes having flat-sided annular fins (i.e., two-dimensional fins).

The finned tubes tested include two conventional low-fin tubes with fin pitches of 0.96 mm and 0.52 mm and two high performance finned tubes with the same fin pitch of 0.50 mm. One of the high performance finned tubes having a monotonically increasing radius of curvature near the fin tip and a constant thickness near the fin root yielded the highest heat transfer coefficients of HCFC-123 and outperformed the conventional 1041-fpm tube by 85% under the lower vapor velocity conditions.

For condensation over a in-line tube bundle of conventional 1041-fpm tubes. The results of Honda et al. showed that the heat transfer coefficients of HCFC-123 were around 10% lower than the CFC-11 values.

Honda et al. also investigated the effects of inundation on both in-line and staggered bundles. The decrease in heat transfer performance due to condensate inundation was more significant for the in-line tube bundle and for the tube with smallest fin spacing and fin height. The theoretical predictions developed previously [28] compared well with their experimental data at a low vapor velocity ($\approx$ 2 m/s) and low-to-medium condensate inundation.

Chang et al. [9] measured heat transfer coefficients of HFC-134a condensing on a horizontal tube at two saturation temperatures of 40.6 and 45°C. The tubes tested were 1024-fpm, 1575-fpm, Gewa-TWX, and Gewa-C tubes. Their results show that the Gewa-C tube with the smallest fin pitch performed best and the four different tubes had the order of ascending heat transfer performance being: 1024-fpm, 1575-fpm, Gewa-TWX, and Gewa-C. The boiling performance ratio of the Gewa-C tube to the 1024-

fpm tube was around 1.6 to 1.9. The condensing coefficients for the two finned tubes were compared with the Beatty-Katz model [4] and Rudy-Webb model [66]. In general, their data were under predicted within 32% by the Beatty-Katz model and over predicted within 10% by the Rudy-Webb model.

Applicability of single-tube data to the design of a shell-side condenser

Row heat transfer coefficients were tested by Cheng and Wang [11], Honda et al. [30], and Webb and Murawski [84] for CFC-11, CFC-113, and HFC-134a, respectively. Their results show that the row effects on the condensation heat transfer coefficients were negligible for the two-dimensional, low-fin tubes, but more significant for the three-dimensional finned tubes. The heat transfer coefficients for the 3-D, enhanced tubes were found to decline noticeably at the lower rows in a bundle where the tubes were arranged vertically with flow entering at the top.

Nguyen and Orozco [60] condensed CFC-113 on a vertical tier of four horizontal tube rows and investigated the effects of the row spacing between the enhanced (Gewa-SC, Gewa-TW, and Gewa-TWX) tubes on the average heat transfer coefficients. The condensation heat transfer coefficients for the tubes tested were found to be inversely proportional to the spacing between tube rows.

Condensation on a tube bundle in vertically downward flow is different from condensation on a single tube, because the heat transfer coefficients decrease at the lower tubes in a vertical bundle due to the increase in the film thickness for each successive tube. In general, the coefficients for the top tubes (first tube row) of a bundle are comparable to those predicted for a single-row tube, while the condensate falling through a bundle increases the film thickness for each successive tube and reduces the condensing coefficients for the lower-row tubes substantially. If the coefficient for the top tube row of a bundle ($\bar{h}_1$) is known, the average condensing coefficient ($\bar{h}_N$) for a bundle of N tube rows can be then determined from the relationship, such as the Webb-Murawski correlation mentioned earlier, derived for the heat transfer coefficients between tube rows.

In addition to the Webb-Murawski correlation, a well-known relationship between the average heat transfer coefficients for a vertical rank of N horizontal tube rows ($\bar{h}_N$, W/m^2-K) and a single horizontal tube (h_1, W/m^2-K) was proposed by Nusselt [61]. The equation is given by

$$\bar{h}_N/\bar{h}_1 = N^m \tag{4.16}$$

Equation 4.16 was derived based on an assumption of a constant wall temperature and laminar

film condensing on plain tubes. The value of the exponent m in Equation 4.16 was given as -0.25 by Nusselt, it differs according to several references [11] [43].

The average heat transfer coefficient for the Nth tube row ($\bar{h}_{NR}$, W/m^2-K) can also be related to that for a single tube ($\bar{h}_1$, W/m^2-K) by manipulating Equation 4.16. Webb and Murawski [84] provided the details of the derivation. The result is

$$\bar{h}_{NR}/\bar{h}_1 = N^{1-m} - (N-1)^{1-m} \tag{4.17}$$

No published data regarding condensation of HFC-236ea on tube bundles were available for comparison.

CHAPTER 5 EXPERIMENTAL DESCRIPTION

Experimental apparatus

Even though the same test rig was used in all the experiments, a different experimental arrangement was required for testing pool boiling, spray evaporation, and condensation. The schematics of the experimental arrangements for testing these three heat transfer forms are shown in Figures 5.1 through 5.3, respectively. The main components of the test facilities include the test section, test tubes, closed water loop, closed refrigerant loop, glycol/water chiller, and data acquisition system.

The heat transfer experiments were performed in a cylindrical, stainless steel chamber equipped with sightglasses in the front and the rear wall for allowing observation of heat transfer phenomena. This stainless steel chamber was referred to as the test section. On the top of the test section were two ports, which were passageways for vapor, and the five other threaded ports where spray nozzles could be installed with compression fittings for testing spray evaporation. The test section also had two other ports on the bottom to serve as liquid paths. Two tube sheets with threaded ports were attached to both ends of the cylindrical chamber so that the tube could be changed by adjusting the compression fittings. The test section is sketched in Figure 5.4.

The tubes tested, 1024-fpm, 1575-fpm, Turbo-CII, Turbo-B, and Turbo-BII tubes, were copper alloy and had a 19.1-mm (3/4-inch) nominal outer diameter. The inner tube surface of the high performance enhanced tubes (Turbo-CII, Turbo-B, and Turbo-BII tubes) was grooved by the manufacturer for increasing the in-tube heat transfer coefficient. In addition, a spring-type turbulator was inserted inside each tube tested to promote continuous turbulence and thus balance the thermal resistance on both sides of the tube. The turbulator was provided by the Trane Company located in La Crosse, Wisconsin and made of a wire coil with such a diameter that can be held at the inner tube surface by the friction fit between the stretched spring and the tube wall. The geometric specifications of the tubes tested are given in Table B.1 in SI units and Table B.2 in English units. In addition, the tube geometries are illustrated in Figures 5.5 and 5.6 for the two finned tubes and Figures 5.7 through 5.9 for the three enhanced tubes. All tubes were supplied by Wolverine Tube, Inc., Decatur, Alabama.

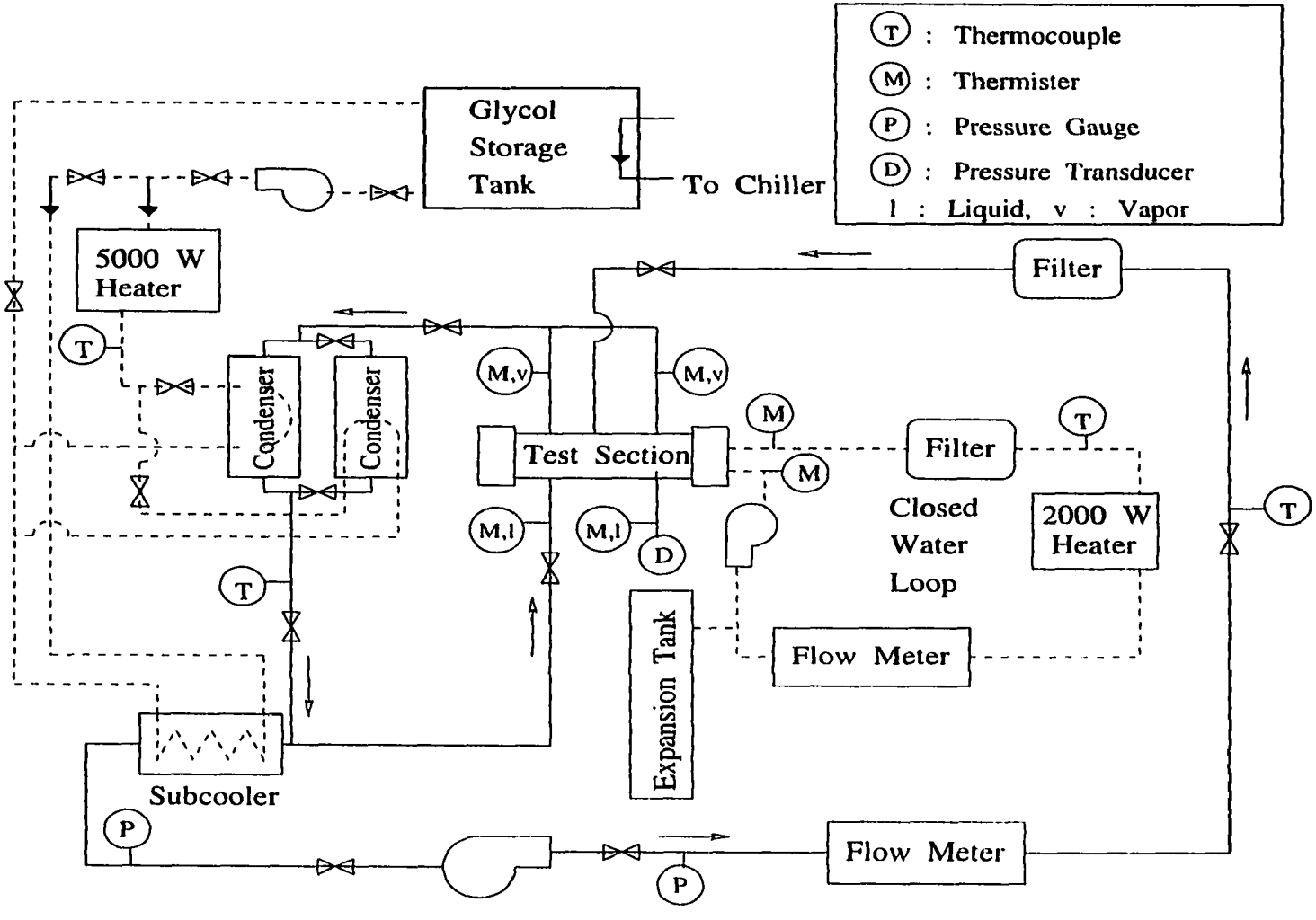

Figure 5.1 Schematic of test facility for pool boiling tests

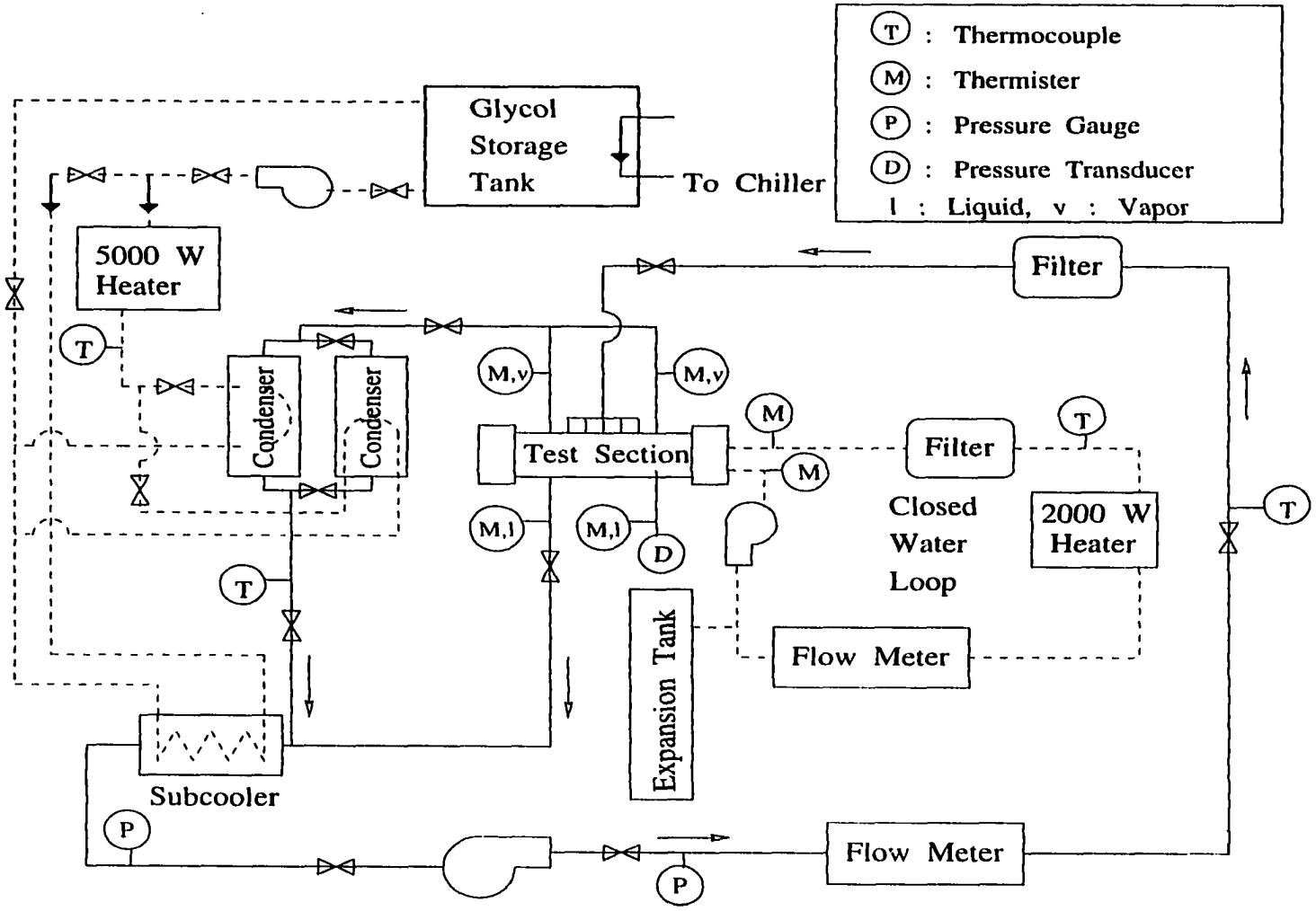

Figure 5.2 Schematic of test facility for spray evaporation tests

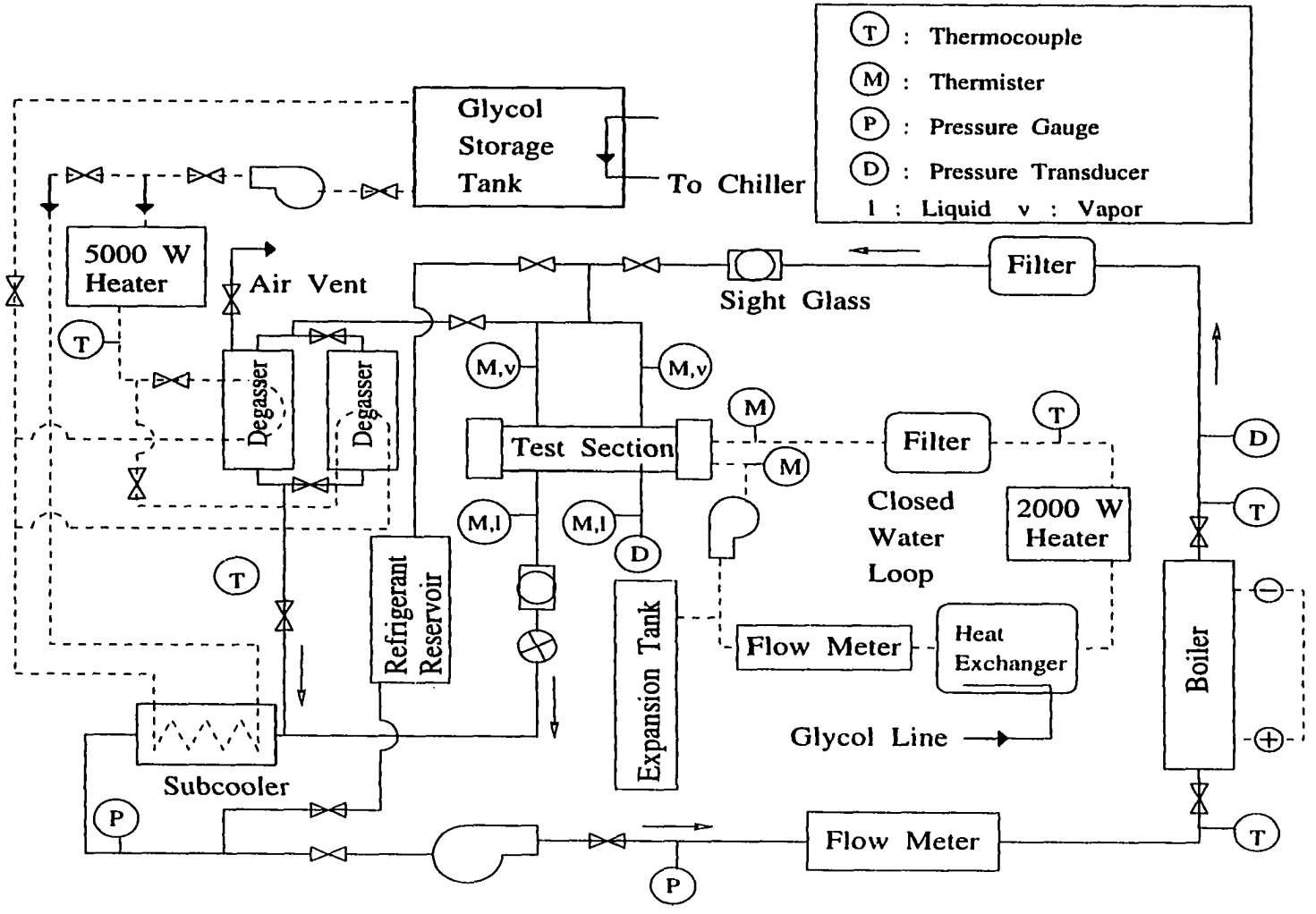

Figure 5.3 Schematic of test facility for condensation tests

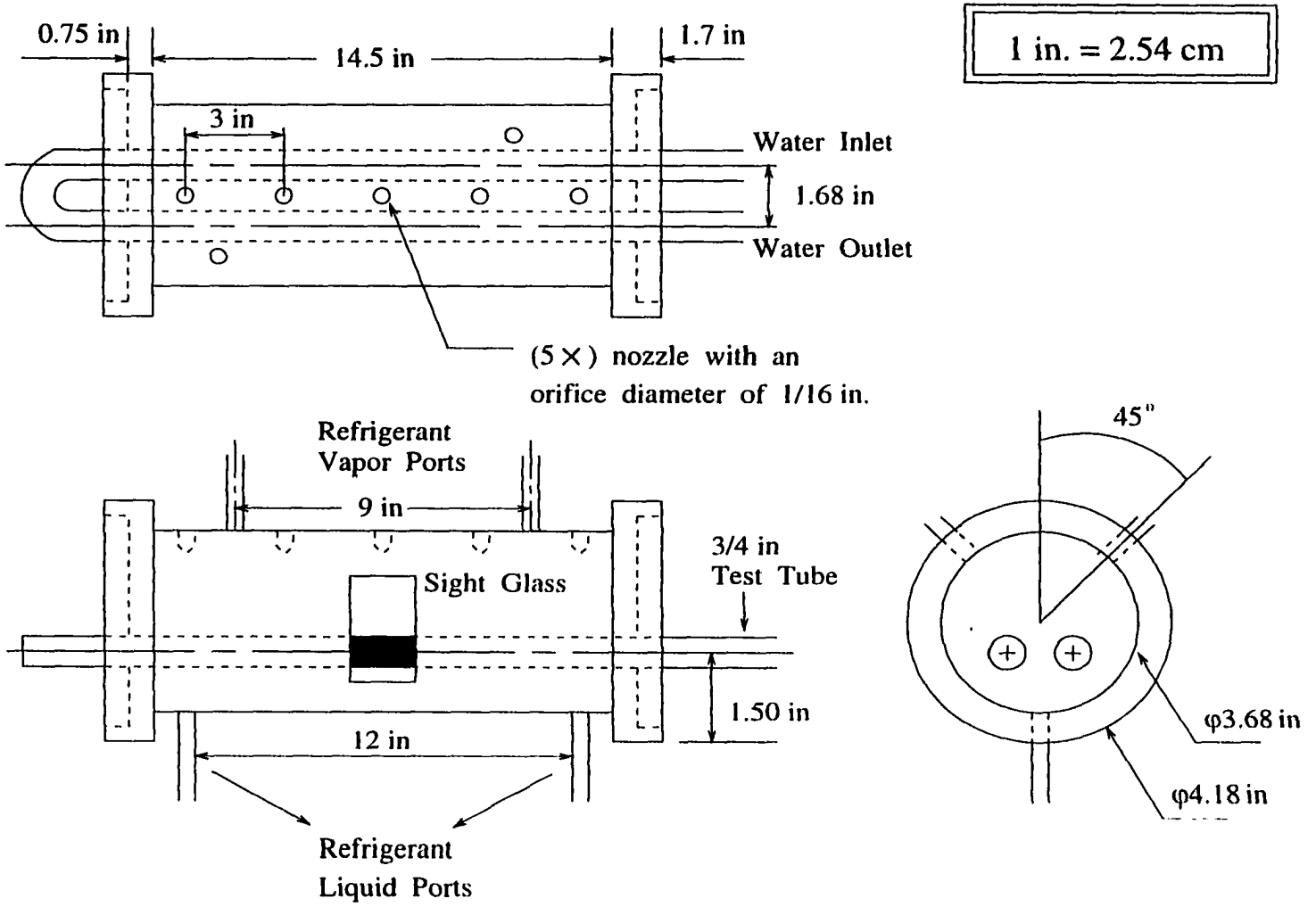

Figure 5.4 Schematic of test section

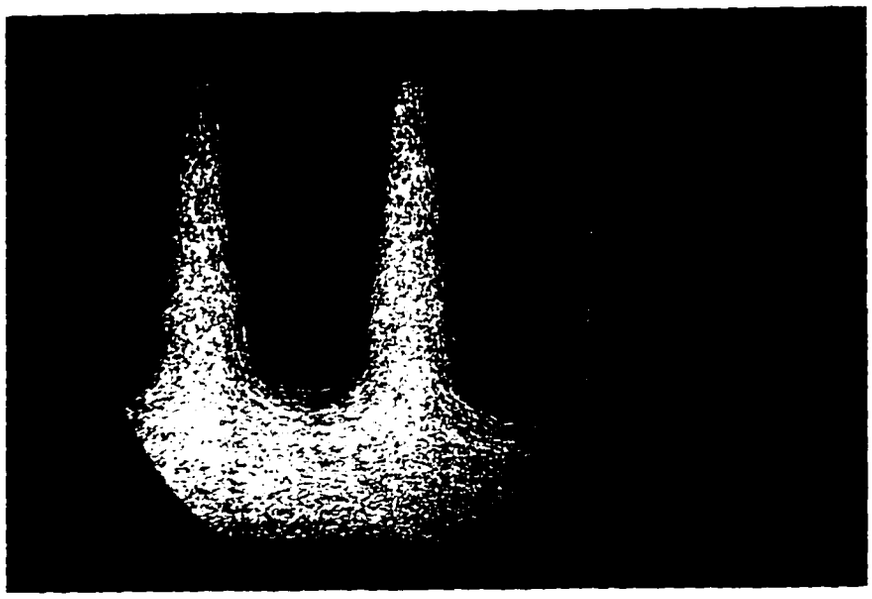

Figure 5.5 Fin profile of a 1024-fpm tube

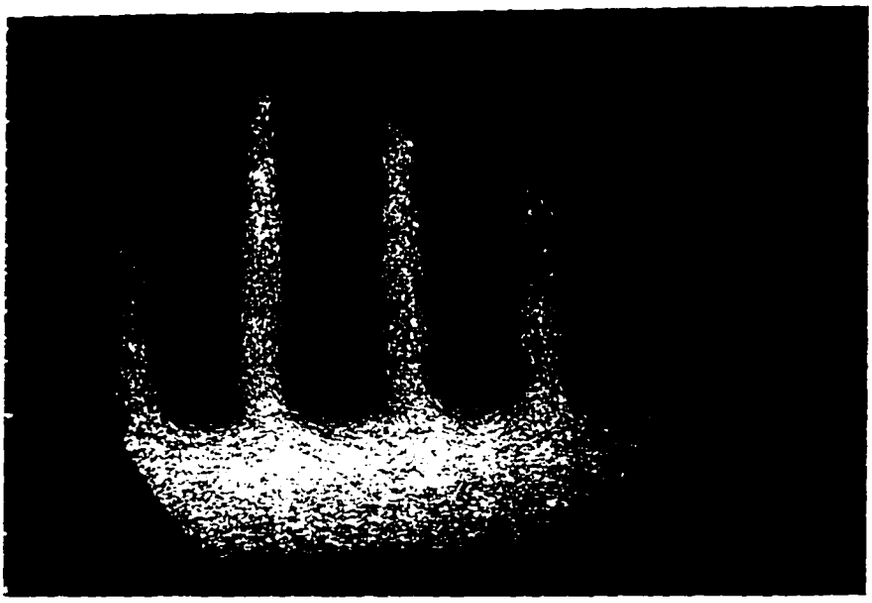

Figure 5.6 Fin profile of a 1575-fpm tube

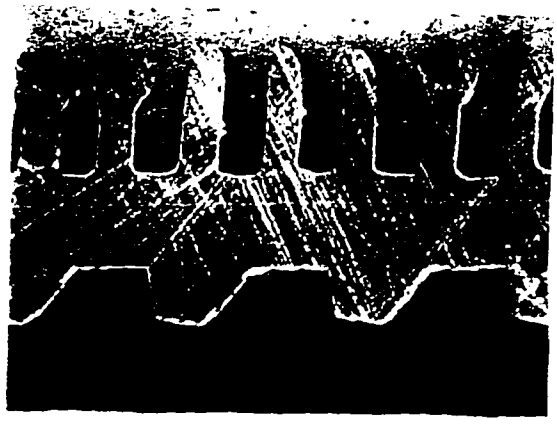

Figure 5.7 Fin profile of a Turbo-CII tube

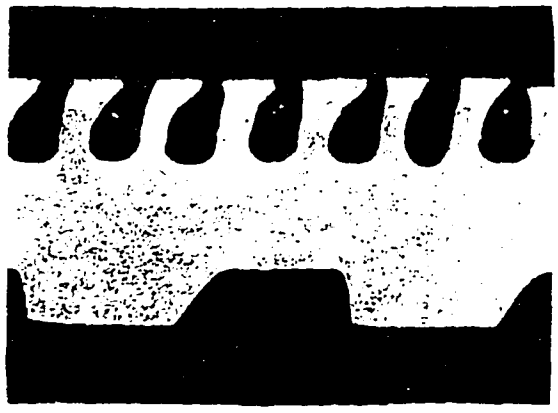

Figure 5.8 Fin profile of a Turbo-B tube

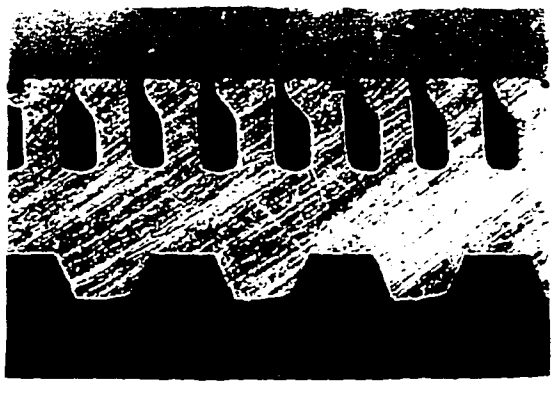

Figure 5.9 Fin profile of a Turbo-BII tube

All the tubes tested have external enhanced surface geometries. Both the 1024-fpm and 1575-fpm tubes are low integral-fin tubes having fin profiles of nearly trapezoidal cross section. The 1024-fpm tube has a fin density of 26 fins per inch and the 1575-fpm tube has 40 fins-per-inch. Furthermore, the fine height of the 1024-fpm tube is about 70% greater than the 1575-fpm tube. Basically, all the high performance enhanced tubes evaluated here are made by deforming or modifying integral-fin tubes and have complex, outward enhanced surface geometries. The Turbo-CII tube has short roughened fins, and the Turbo-B and Turbo-BII tubes are characterized by reservoir-type (or re-entrant) cavities with narrow openings constructed by the compressed, doubly cut knurl.

The design of the Turbo-B tube is based on a 1575-fpm tube, whereas the Turbo-BII tube is based on a 1969-fpm (50-fpi) tube. The higher fin density of the Turbo-BII tube provides a higher density of nucleation sites. In addition, the boiling sites of the Turbo-BII tube are shape-optimized for specific types of refrigerants, while those of the Turbo-B tube are not. The Turbo-CII tube is effective for shell-side condensation, while the Turbo-B and Turbo-BII tubes are designed to improve nucleate boiling. Researchers usually classify low integral-fin tubes (e.g., 1024-fpm and 1575-fpm) as two-dimensional finned tubes and complex finned tubes (e.g., Turbo-CII, Turbo-B, and Turbo-BII) as three-dimensional finned tubes.

The closed water loop consists mainly of a storage tank, two triplex diaphragm pumps, a flow meter, an immersion heater, and a dual-tube heat exchanger. The heater and heat exchanger were used to control the water temperature.

The glycol/water mixture was pumped through a chiller of 105-kW (30-ton) cooling capacity and could be supplied through manifolds to a dual-tube heat exchanger, two condensers, and a subcooler.

While water was circulated in the tube tested, refrigerant was delievered by a triplex diaphragm pump to the test section through several routes with different auxiliary facilities for different purposes. During condensation tests, a stainless steel boiler was used to vaporize refrigerant before it reached the test section. For evaporation tests, a subcooler and two condensers were utilized to condense refrigerant after it was boiled in the test section. A reservoir was set for adjusting the refrigerant quantity required for the tests.

Instrumentation and calibration

The temperature necessary for calculating the shell-side heat transfer coefficient was measured by thermisters and compared with the saturation temperature corresponding to the measured pressure. The acceptable difference in these two temperatures was within 0.2°C for condensation tests, and 0.1°C

for evaporation tests.

Due to the low pressures of HFC-236fa and the low operating temperatures for the evaporation tests (see Table A.1), the strain-gauge pressure transducer which has been used to measure the saturation pressure of the test section was sent to the Setra Company and calibrated professionally instead of being calibrated by a simple dead-weight tester. The thermisters were also re-calibrated by using a constant temperature bath. No scatter found in the calibration results indicates that the accuracy of the calibration.

The instrumentation accuracy is ± 0.05°C for the thermisters. ± 0.1% of the full scale for the pressure transducer, and ± 0.20% of the full scale for the water mass flow meter.

Experimental procedures

Figure 5.10 compares the refrigerant state in the test section for testing pool boiling, spray evaporation, and shell-side condensation. The detailed procedures for testing these three heat transfer forms are discussed in the following sections.

Procedures for testing pool boiling and spray evaporation

The pool of liquid refrigerant was boiled by the circulating warm water in the test section and condensed in the condensers where the glycol/water mixture (coolant) was circulated and then returned to the pump. The refrigerant temperature was maintained at a steady state value of 2°C by controlling the flow rates and temperatures of the water and coolant. The circulating water was heated by a heater, and the water temperature change through the tube tested was controlled at 2°C. In addition, the two condensers were adjusted to work independently or in parallel for the different heat load requirements.

The flow rates and temperatures of the water and coolant to meet the different heat transfer rate requirements were adjusted to provide the whole range of heat fluxes.

For pool boiling testing of refrigerant/oil mixtures, a small amount of oil was injected at the pump discharge line. The system was circulated for a few hours before a sample of refrigerant/oil mixtures was drawn from the test section to ensure that the circulating oil completely migrated to the test section. Oil was separated from refrigerant by virtue of the different volatility of the two components. The mass fraction of oil in the mixtures was able to be calculated when the volatile refrigerant was evaporated and the non-volatile oil was left in the sample cylinder.

Spray evaporation was operated in the similar way as pool boiling except the refrigerant was evenly distributed to the test section through a set of nozzles, and the tube was not immersed in a liquid pool.

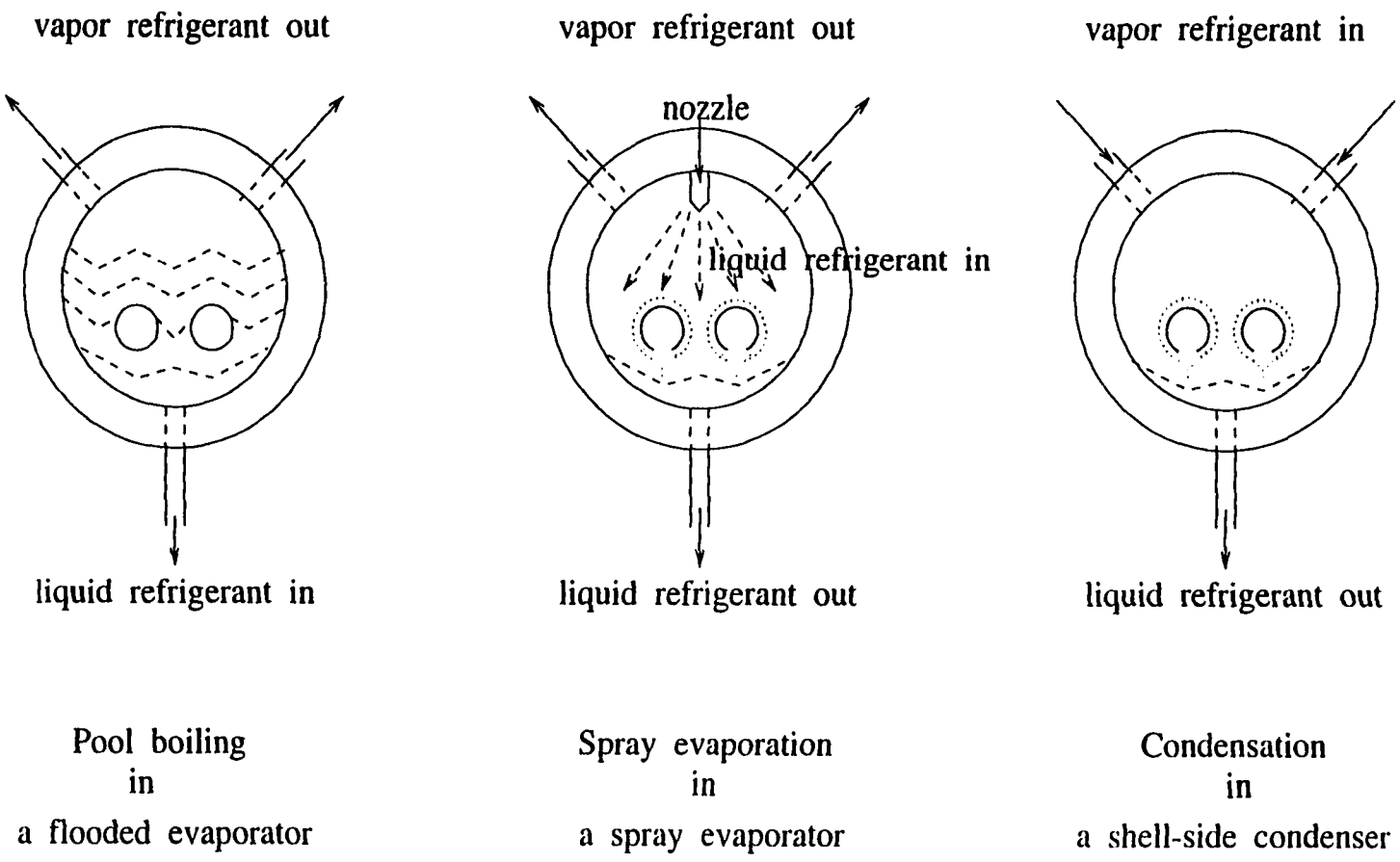

Figure 5.10 Comparison of the refrigerant state in a flooded evaporator, a spray evaporator, and a shell-side condenser

Procedures for condensation testing

After the system was verified to be leak-free, it was evacuated by a vacuum pump for 8 hours. Subsequently, the refrigerant was charged into the system. The noncondensible gas in the system was purged through the vent valves on the top of degassers (condensers), while the refrigerant was boiling in the test section. This degassing procedure was repeated until the temperatures registered by the thermisters compared with the saturation temperature corresponding to the pressure transducer reading were within 0.2°C. The condensers were isolated once the purging had been done.

The liquid refrigerant delivered from the pump was converted to vapor in a boiler and then condensed by the cooler water flowing through the tube tested. The refrigerant condensed in the test section flowed back to the pump and was recirculated. With flows established, the water and refrigerant flow rates along with the temperatures of the refrigerant in the boiler and water were adjusted to meet the required energy rate balance and maintain the refrigerant saturation temperature of 40°C in the test section. Meanwhile, the temperature change of water through the test section was maintained at 2°C. Temperatures of water flowing inside the tube tested were controlled by a heater and a heat exchanger where the glycol/water mixture (coolant) was circulated through it.

The flow rates of the two fluids (water and refrigerant) and the temperatures of the refrigerant in the boiler and water were adjusted to meet the different heat transfer rate requirements over the whole range of heat fluxes tested.

Data reduction

The average shell-side heat transfer coefficient (h) for a single-row tube with two passes arranged side by side was determined using the heat transfer rate balance between the two fluids (refrigerant and water), where a logarithmic mean temperature difference ($LMTD$) method was applied. The measured parameters for calculating shell-side heat transfer coefficients were the temperatures of water entering and leaving the test section, the saturation temperature and pressure of the test section, and the flow rates of water and refrigerant.

The heat flux applied to or taken from the refrigerant was controlled throughout the experiments to obtain the average shell-side heat transfer coefficient. The testing range of heat fluxes was from 15 kW/m^2 to 40 kW/m^2 for both condensation and pool boiling, and 10 kW/m^2 to 30 kW/m^2 for spray evaporation.

A modified Wilson plot method was used to determine the in-tube heat transfer coefficient (h_i,

W/m^2-K), and then the average shell-side heat transfer coefficient (h, W/m^2-K) was calculated from the UA-value by applying the $LMTD$ approach. Under steady state conditions, the heat transfer rate (q, W) between the refrigerant and the water is formulated as,

$$q = U_o \cdot A_o \cdot LMTD \tag{5.1}$$

where the heat transfer rate (q, W) was calculated from the measured inlet and outlet temperatures of water ($T_{i,in}$ and $T_{i,out}$, °C), water flow rate ($\dot{m}_i$, kg/s), and the known specific heat of water (Cp_i, J/kg-K).

$$q = \dot{m}_i \cdot Cp_i \cdot (T_{i,out} - T_{i,in}) \tag{5.2}$$

The logarithmic mean temperature difference ($LMTD$, °C) in Equation 5.1, defined by Equation 5.3, was known from the measured refrigerant saturation temperature in the test section (T_{sat}, °C) and water temperatures entering and leaving the test section ($T_{i,in}$ and $T_{i,out}$, °C).

$$LMTD = \frac{(T_{i,out} - T_{i,in})}{ln\frac{(T_{sat} - T_{i,in})}{(T_{sat} - T_{i,out})}} \tag{5.3}$$

The overall heat transfer coefficient (U_o, W/m^2-K) based on the outside tube surface area (A_o, m^2) in Equation 5.1 was calculated by obtaining q from Equation 5.2 and $LMTD$ from Equation 5.3.

$$U_o = \frac{q}{A_o \cdot LMTD} \tag{5.4}$$

The shell-side heat transfer coefficient (h, W/m^2-K) was then determined from the overall heat transfer coefficient by subtracting the tube-wall thermal conductance (R_w, K/W) and the forced convective heat transfer coefficient (h_i, W/m^2-K) on the water side,

$$h = \frac{1}{\frac{1}{U_o} - \frac{A_o}{A_i}\frac{1}{h_i} - A_o R_w} \tag{5.5}$$

The tube-wall thermal resistance (R_w, K/W) in Equation 5.5 is given by

$$R_w = \frac{ln(D_o/D_i)}{2\pi k_w L} \tag{5.6}$$

and the in-tube heat transfer coefficient (h_i) was calculated by the Sieder-Tate equation listed below and deduced by a modified Wilson plot technique.

$$h_i = STC \cdot \frac{k_i}{D_i} Re_i^{0.8} Pr_i^{0.33} \left(\frac{\mu_i}{\mu_w}\right)^{0.14} \tag{5.7}$$

The thermal conductivity of tube wall (k_w, W/m-K) in Equation 5.6 and the viscosity of water (μ_w, N·s/m^2) in Equation 5.7 were calculated using the tube wall temperature (T_w= (T_{sat}+$T_{i,bulk}$)/2, °C). While the calculation of Reynolds number (Re_i), Prandtl number (Pr_i), thermal conductivity (k_i, W/m K), dynamic viscosity (μ_i, N·s/m^2) in Equation 5.7 was based on the average bulk temperature ($T_{i,bulk}$ = ($T_{i,in}$+$T_{i,out}$)/2, °C) and properties of water. The remaining parameters in the equations above: L (m), D_i (m), D_o (m), and A_i (m^2) are the tube length, inside tube diameter, outside tube diameter, and inner surface area of the tube, respectively.

Based on the modified Wilson plot technique, the constant STC (Sieder-Tate coefficient) required in Equation 5.7 was determined by boiling refrigerant at a constant heat load of 1.5 kW and maintaining a constant saturation temperature of 2°C on the outside of the tube tested while varing the in-tube water flow rate (i.e., Re_i).

The following equation was generalized by substituting the Sieder-Tate equation (Equation 5.7) into the equation of thermal resistance (Equation 5.5),

$$Y = \frac{1}{STC} \cdot X + \frac{1}{h} \tag{5.8}$$

where

$$Y = \frac{1}{U_o} - A_o R_w$$

$$X = \frac{A_o/A_i}{\frac{k_i}{D_i} Re_i^{0.8} Pr_i^{0.33} \left(\frac{\mu_i}{\mu_w}\right)^{0.14}}$$

The range of the Reynolds number tested for water was from 2800 to 19000 for the finned tubes [38] and from 2800 to 18000 for the high performance enhanced tubes. Corresponding to the different water flow rates, the X values versus Y values required in Equation 5.8 were plotted in Figure 5.11 for the Turbo-CII, Turbo-B, and Turbo-BII tubes. The X and Y values for the 1024-fpm and 1575-fpm tubes were reported in the Phase I study [38].

As indicated in Equation 5.8, the STC is the inverse of the slope of the X-Y line. The STC value was found to be 0.0471 [38] for the 1024-fpm tube, 0.0514 [38] for the 1575-fpm tube, 0.131 for the Turbo-B tube, 0.108 for the Turbo-BII tube, and 0.1138 for the Turbo-CII tube.

The numerical values for all the data obtained in this study are tabulated in Appendix C for HFC-236ea and Appendix D for HFC-236fa.

Experimental uncertainty of data

The estimate of the uncertainty in the calculated heat transfer coefficients is listed in Table 5.1 for pool boiling data, Table 5.2 for spray evaporation data, and Table 5.3 for condensation data. Appendix E presents the derivation of uncertainty analysis equations for the calculated shell-side heat transfer coefficients.

Table 5.1 Uncertainty in the pool boiling heat transfer coefficients

Tube type	Refrigerant type	Heat flux		
		15 kW/m^2	30 kW/m^2	40 kW/m^2
1024-fpm	HFC-236fa	± 10%	± 8%	± 7%
1575-fpm	HFC-236fa	± 8%	± 7%	± 6%
Turbo-B	HFC-236fa	± 11%	± 9%	± 7%
Turbo-BII	HFC-236fa	± 19%	± 11%	± 9%
Turbo-B	HFC-236ea	± 9%	± 7%	± 7%
Turbo-BII	HFC-236ea	± 14%	± 9%	± 8%

It is important to balance the thermal resistance on both sides of a tube. The uncertainty of the shell-side heat transfer coefficients was found to be smaller when the tube side had a denser turbulator inserted because it enabled a higher heat transfer coefficient with water flowing inside the tube, and thus properly equalized the heat transfer coefficients for the two fluids.

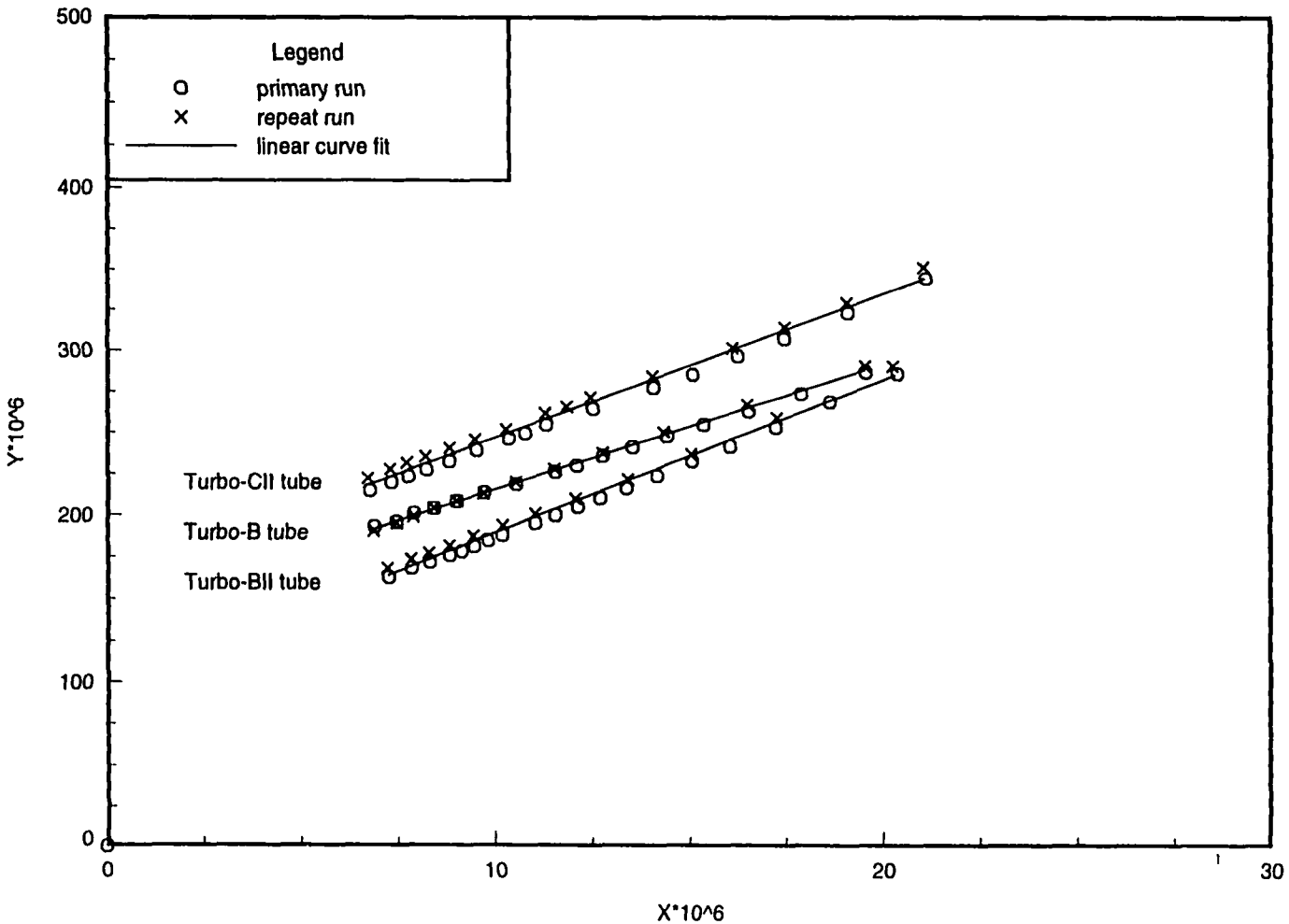

Figure 5.11 Wilson plot data for the Turbo-CII, Turbo-B, and Turbo-BII tubes (D= 19.1 mm) with turbulators installed

Table 5.2 Uncertainty in the spray evaporation heat transfer coefficients of HFC-236ea

Tube type	Spray rate ($\dot{m}_{spr}$, kg/min)	Heat flux		
		10 kW/m^2	20 kW/m^2	30 kW/m^2
Turbo-B	2.6	± 25%	± 13%	± 6%
	2.8	± 27%	± 14%	± 7%
	3.0	~	± 14%	± 8%
	3.2	± 29%	± 14%	± 8%
Turbo-CII	2.6	± 25%	± 11%	± 6%
	2.8	± 24%	± 12%	± 7%
	3.0	± 24%	± 12%	± 7%
	3.2	~	± 13%	± 8%
1575-fpm	2.6	± 16%	± 9%	± 6%
	2.8	± 17%	± 10%	± 6%
	3.0	± 17%	± 11%	± 7%
	3.2	± 17%	± 11%	± 7%

Table 5.3 Uncertainty in the shell-side condensation heat transfer coefficients

Tube type	Refrigerant type	Heat flux		
		15 kW/m^2	30 kW/m^2	40 kW/m^2
1024-fpm	HFC-236fa	± 9%	± 6%	± 6%
1575-fpm	HFC-236fa	± 8%	± 6%	± 6%
Turbo-CII	HFC-236fa	± 7%	± 6%	± 5%
Turbo-CII	HFC-236ea	± 8%	± 6%	± 6%

The Turbo-CII tube was tested twice for HFC-236ea during spray evaporation and condensation. Results for the first test show that the Turbo-CII tube produced relatively high shell-side heat transfer coefficients at low heat loads, and the overall heat transfer coefficients were dominated by the tube-side resistance. In other words, the relatively low thermal resistance on the shell side caused a large uncertainty in the shell-side heat transfer coefficients.

The large uncertainty produced by the Turbo-CII tube for condensation at low heat loads is in accordance with that reported by Huber et al. [36] who found that the maximum experimental uncertainty was up to ± 36% for the average bundle heat transfer coefficients and ± 53% for the average row heat transfer coefficients. The large uncertainty was caused by the imbalance of the thermal resistances between both sides of a tube.

In order to reduce the uncertainty in shell-side heat transfer coefficients, the Wilson data plot was generated again for the tube, this time with a denser turbulator inserted to create greater turbulence in the tube. The Sieder-Tate coefficient for the Turbo-CII tube was substantially increased from 0.0484 to 0.1138. As shown in Equation 5.7, the STC is in direct proportion to the in-tube heat transfer coefficient (h_i), a large STC value hence means a large h_i value.

It was also found that a linear curve could fit the data for a Wilson plot better when the tube side had a denser turbulator inserted. In addition to the Turbo-CII tube, the Turbo-B tube was also re-tested by installing a denser in-tube turbulator in order to reduce the uncertainty in the shell-side heat transfer coefficients. The Sieder-Tate coefficient for the Turbo-B tube was substantially increased from 0.067 to 0.131.

Another reason for a re-test of these tube types is that the tubes were found to be contaminated with oil, which might have been due to the lubricant applied to the tubes when they were made. The tubes were cleaned before they were tested by using a solvent, CFC-113.

Results of the spray-evaporation tests show that a larger uncertainty occurred at low heat fluxes. This larger uncertainty was attributed to the low operating temperatures of water, which resulted in small $LMTD$ values.

CHAPTER 6 POOL BOILING RESULTS

Measurements of heat transfer coefficients were conducted on two integral-fin (1024-fpm and 1575-fpm) tubes and two high performance enhanced (Turbo-B and Turbo-BII) tubes for pure HFC-236fa and HFC-236fa with oil, and on the two finned tubes for HFC-236ea in this research.

The heat transfer performance of the tubes tested was compared with each other for HFC-236ea, HFC-236fa, and HFC-236fa with oil. Comparison of the heat transfer coefficients of the three refrigerants (HFC-236fa, HFC-236ea, and CFC-114) tested in the same test facility was also made for each individual tube. The CFC-114 data for the 1024-fpm and 1575-fpm tubes and the HFC-236ea data for the Turbo-B and Turbo-BII tubes were tested previously [38]. Data were not taken for CFC-114 with the Turbo-B and Turbo-BII tubes.

All the pool boiling tests in this study were carried out in a single-tube apparatus at a saturation temperature of 2°C with decreasing heat flux from 40 kW/m^2 to 15 kW/m^2. The data are tabulated numerically in Appendixes C and D and illustrated in the figures of this chapter, where the repeatability of the experiments can be seen.

In the previous researches [3] [25] [50], the hysteresis effects were avoided by running all the experiments in order of decreasing heat loads. Accordingly, all the experiments performed here for pool boiling were in order of decreasing heat flux.

Pool boiling coefficients of HFC-236ea

Pool boiling performance of a Turbo-B and a Turbo-BII tube

The heat transfer coefficients shown in Figure 6.1 for the Turbo-B and Turbo-BII tubes indicate a direct relationship to heat flux and they increased as the heat flux increased. More bubbles were created as the active nucleation sites increased with increasing heat flux, and hence resulted in the increase of the heat transfer coefficients.

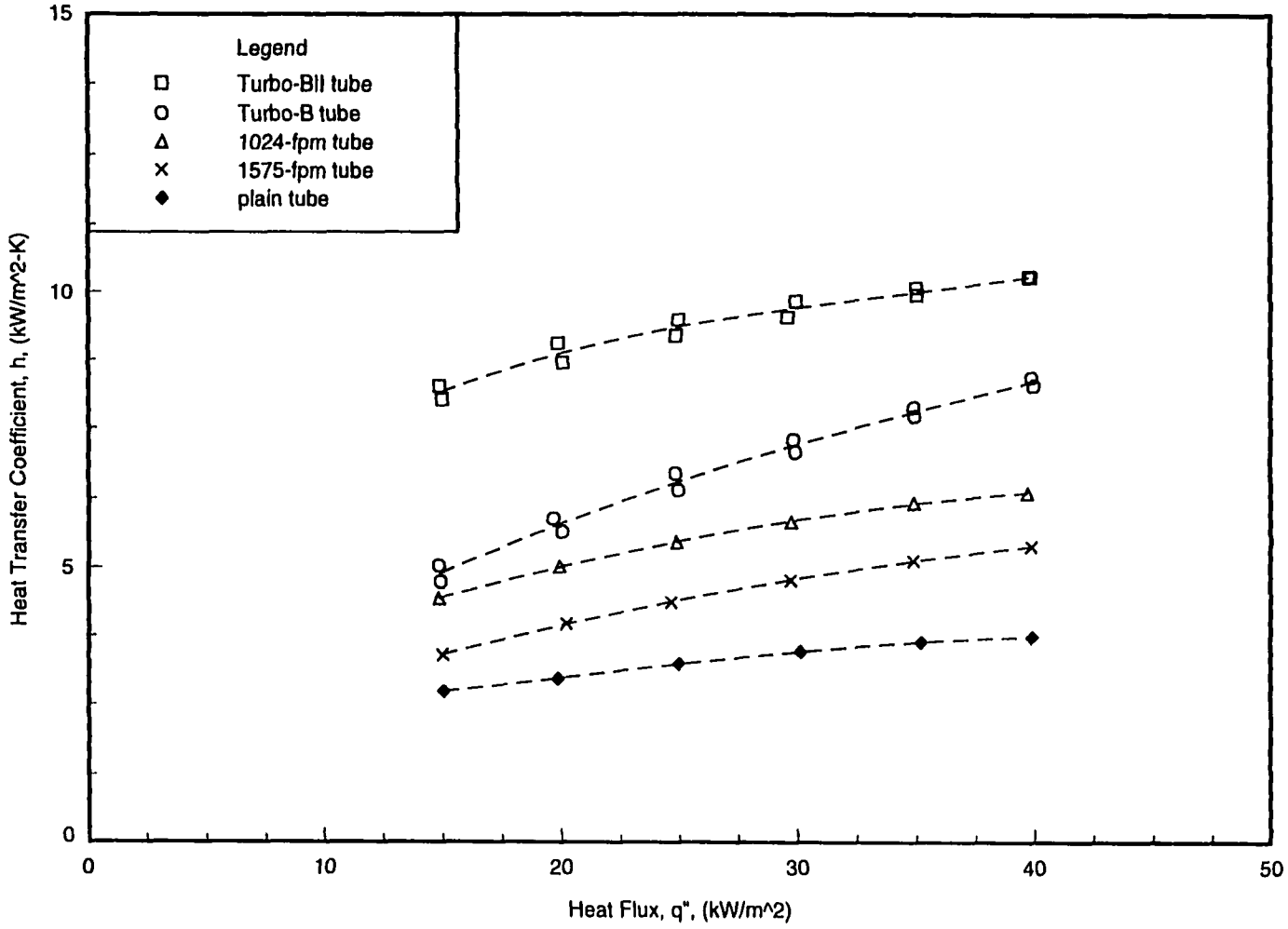

Figure 6.1 Pool boiling heat transfer coefficients of HFC-236ea for the Turbo-BII, Turbo-B, 1024-fpm, 1575-fpm and plain tubes (D= 19.1 mm) at T_{sat}= 2°C

On the other hand, Barthau [3] developed a simple optical method for counting active nucleation sites on a horizontal plain tube using CFC-114 as the testing fluid. Even though the active nucleate site density was observed to be directly proportional to the heat flux, the heat transfer contribution of an individual active site was found to decrease strongly with increasing heat flux, based on his experimental results and theoretical assumptions.

After almost all the nucleation sites were activated, that is, when nucleation was fully developed, the increase in heat transfer coefficients slowed down even though the heat flux increased. Figure 6.1 indicates that most of the h-q" curves tend to flatten out at higher heat fluxes.

The Turbo-BII tube was found to provide heat transfer coefficients around 120% to 170% of those for the Turbo-B tube. As mentioned in Chapter 5, the Turbo-BII tube is made based on a tube of higher fin density that provides higher density of nucleation sites relative to the Turbo-B tube and, therefore, the Turbo-BII tube is expected to perform better than the Turbo-B tube.

Comparison of the Turbo-B and Turbo-BII tubes with 1024-fpm and 1575-fpm tubes

The pool boiling heat transfer coefficients of HFC-236ea measured in this study for the Turbo-B and Turbo-BII tubes were compared with those measured previously for the 1024-fpm, 1575-fpm, and plain tubes in Figures 6.1 and 6.2. Results were plotted in terms of heat transfer coefficient versus heat flux and versus excess temperature, respectively.

The comparison shows that the two high performance enhanced tubes were able to promote heat transfer processes better than the plain tube, and especially better than the two integral-fin tubes. Higher heat transfer rate can be achieved with an alternative design that uses the high performance enhanced tubes instead of finned or plain ones.

Figure 6.1 shows that the effects of tube types on the boiling heat transfer coefficients of HFC-236ea over the heat flux range of 10 kW/m^2 to 40 kW/m^2. The Turbo-B tube yielded approximately 10% to 30% higher heat transfer coefficients than the 1024-fpm tube, 40% to 50% higher values than the 1575-fpm tube, and 80% to 120% higher values than the plain tube. While the Turbo-BII tube outperformed the other tubes tested and produced heat transfer coefficients approximatedly 1.6 to 1.8, 1.9 to 2.4, 2.8 to 3.0, and 1.2 to 1.7 times as large as the values given by the 1024-fpm tube, 1575-fpm tube, plain tube, and Turbo-B tube, respectively. Webb and Pais [85] presented single-tube data for pool boiling on three tube types. The Turbo-B tube was found to outperform the 1024-fpm tube by 35% for HCFC-123 and 30% for HFC-134a.

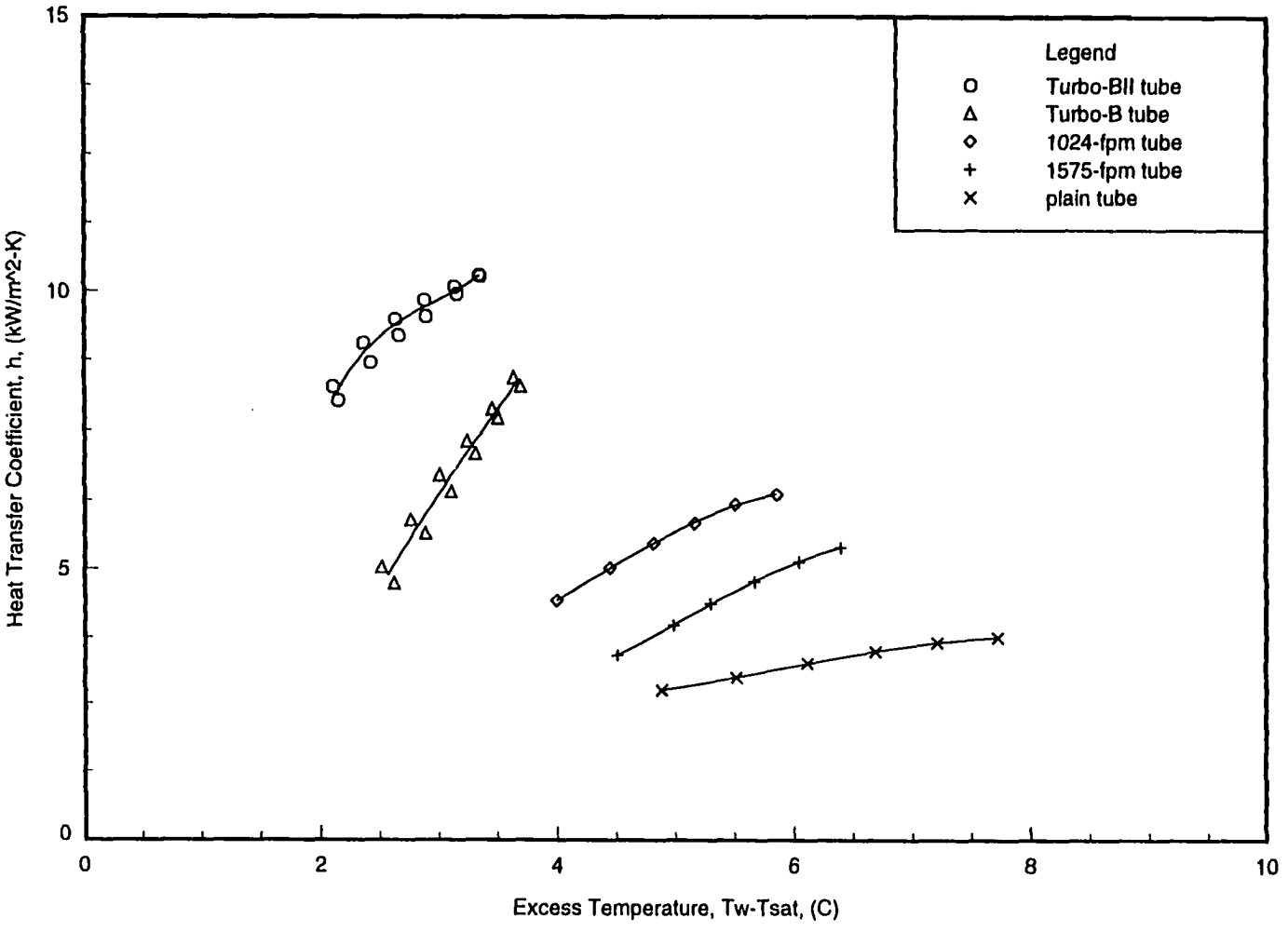

Figure 6.2 Temperature difference effects on the pool boiling heat transfer coefficients of HFC-236ea at T_{sat}= 2°C

Figure 6.2 shows that the heat transfer coefficients for all the tubes tested depended on the temperature difference between the heated surface and the saturated refrigerant (i.e.. excess temperature or wall superheat), and they increased as the excess temperature increased for the high performance enhanced tubes as well as for the conventional finned tubes and plain tube. The specified heat transfer rate was accomplished with a smaller temperature difference by using the high performance enhanced tubes rather than the conventional finned tubes or plain tube. Specifically, the Turbo-BII tube required the smallest wall superheat to obtain the same heat transfer rate. In other words, the Turbo-BII tube resulted in the largest heat transfer rate at the same wall superheat.

It stands to reason that the Turbo-B tube and the Turbo-BII tube. which are especially designed for the enhancement of nucleate boiling, performed better than the traditional integral-fin tubes in pool boiling. However, these high performance enhanced tube types could not be concluded to produce higher overall heat transfer coefficients because the overall shell-side heat transfer performance is affected by both nucleate boiling and forced convection mechanisms as mentioned earlier. The results compared here only indicate that the high performance enhanced tubes performed better during nucleate boiling than the finned tubes. Webb et al. [83] reported that forced convection tended to dominate the process of forced convection boiling (i.e., overall shell-side heat transfer) when standard integral-fin tubes were used.

Pool boiling coefficients of HFC-236fa for a Turbo-B, a Turbo-BII, a 1024-fpm, and a 1575-fpm tube

The heat transfer performance of the 1024-fpm, 1575-fpm, Turbo-B, and Turbo-BII tubes was tested with HFC-236fa during pool boiling and compared with each other in the form of heat transfer coefficient versus heat flux in Figure 6.3 and versus excess temperature in Figure 6.4.

Figure 6.3 shows that the heat transfer coefficient increased as the heat flux increased for any tube tested. With increasing heat flux, the more violent fluid motion in the pool is induced by numerous vapor bubbles which are generated at the increased active nucleation sites, and thus results in increased heat transfer. Figure 6.3 also shows that the two high performance enhanced tubes produced higher heat transfer coefficients at a specified heat flux than the two finned tubes.

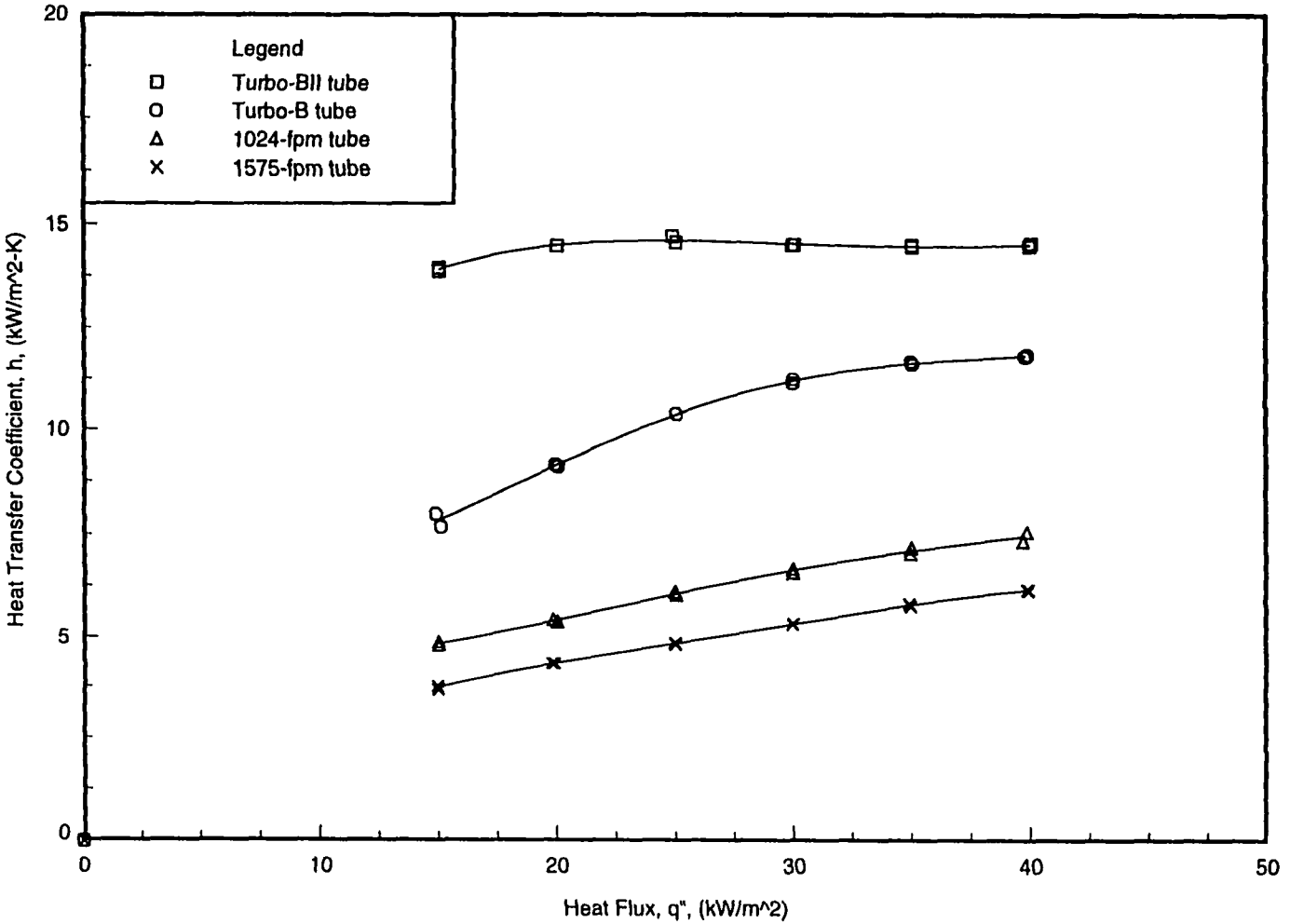

Figure 6.3 Pool boiling heat transfer coefficients of HFC-236fa for the Turbo-BII, Turbo-B, 1024-fpm, and 1575-fpm tubes (D= 19.1 mm) at T_{sat}= 2°C

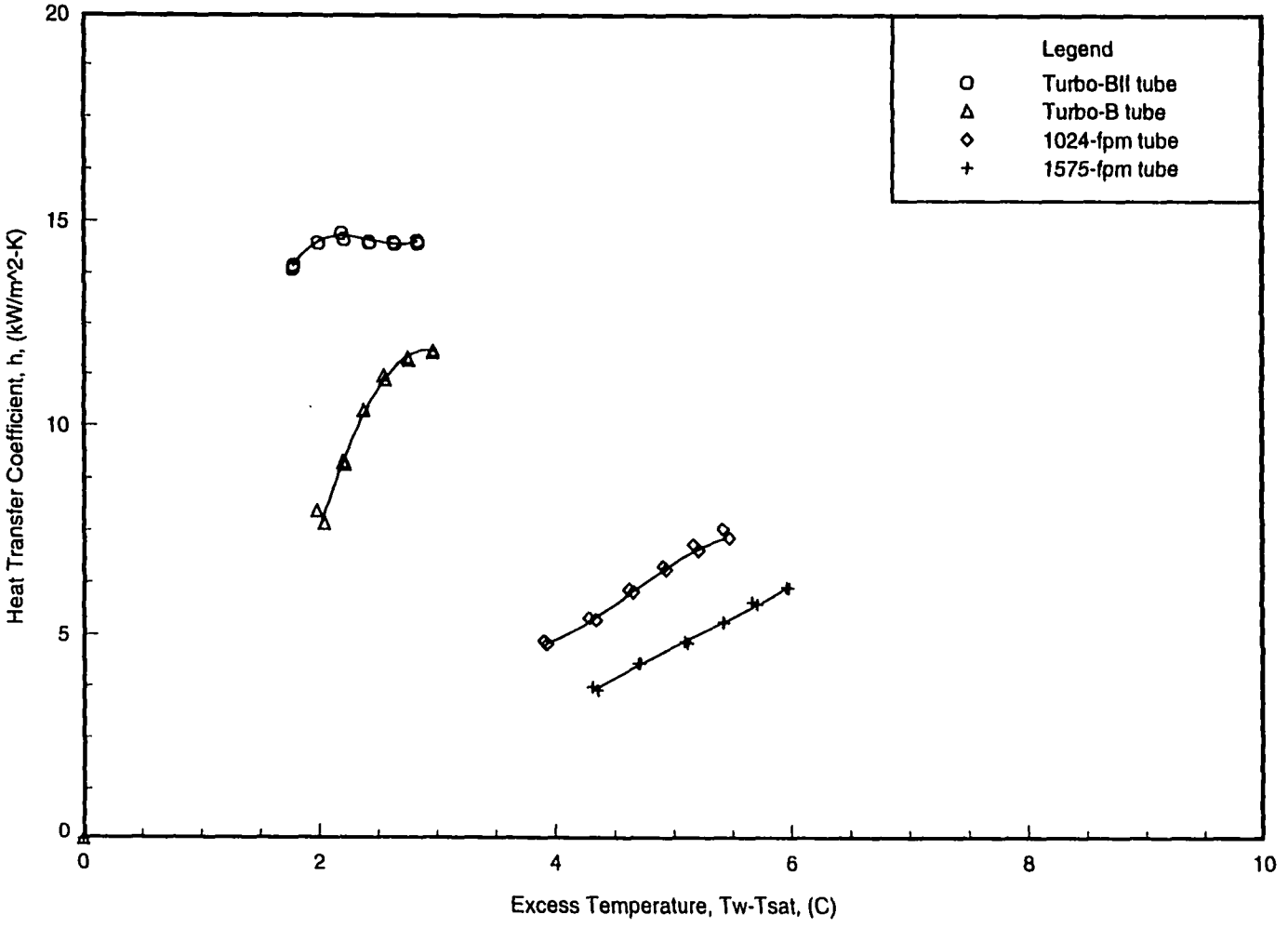

Figure 6.4 Temperature difference effects on the pool boiling heat transfer coefficients of HFC-236fa at T_{sat}= 2°C

Figure 6.4 shows the variation of the heat transfer coefficient versus wall superheat for all the tubes tested. The heat transfer coefficient for all the tubes increased as the excess temperature increased. The two high performance enhanced tubes required a relatively smaller wall superheat for a specific heat transfer rate than the two integral-fin tubes.

The Turbo-B tube yielded approximately 60% to 70% higher heat transfer coefficients than the 1024-fpm tube and 90% to 120% higher values than the 1575-fpm tube. The heat transfer performance produced by the Turbo-BII tube was around 2.0 to 2.9, 2.4 to 3.8, and 1.2 to 1.8 times as large as the values given by the 1024-fpm tube, 1575-fpm tube, and Turbo-B tube, respectively.

Similar to the tests with HFC-236ea, The enhanced boiling surfaces (Turbo-B and Turbo-BII) tested with HFC-236fa improved the heat transfer performance in nucleate boiling when compared to both plain and low integral-fin surfaces. These trends are in accordance with the numerous experimental results reported [38] [50] [85].

Pool boiling coefficients of HFC-236fa/oil mixtures for a Turbo-B, a Turbo-BII, a 1024-fpm, and a 1575-fpm tube

Saturated pool boiling of HFC-236fa in the presence of oil was investigated. A miscible polyol-ester oil was added to HFC-236fa with the oil concentrations of 1% and 3% by weight, in order to assess the effects of the oil contamination on the boiling performance. The polyol-ester oil used in this study has a viscosity of 340 SUS [1] at 37.8°C (100°F) and a trade name of Castrol Icematic SW-68.

Calculation of the boiling coefficient was based on the measured temperature of bulk mixtures. The difference between the measured temperatures and the saturation temperature of the mixtures was found to be within 0.2°C in the tests refrigerant/oil mixtures performed here.

Figures 6.5 through 6.8 show that the variation of the heat transfer coefficient with heat flux at three oil concentrations (0%, 1%, and 3%) for the 1024-fpm tube, 1575-fpm tube, Turbo-B tube, and Turbo-BII tube, respectively. As can be seen in these figures, the boiling heat transfer coefficient depended on the oil concentration as well as the heat flux.

The effects of tube types on heat transfer coefficients were clarified in Figure 6.9 for pool boiling of HFC-236fa with 1% oil and in Figure 6.10 for the 3% oil case. Figures 6.9 and 6.10 as well as Figure 6.3 which compared the tube performance for oil-free HFC-236fa in the previous section show that the four tubes had similar trends with the order of descending heat transfer coefficients being: Turbo-BII tube, Turbo-B tube, 1024-fpm tube, and 1575-fpm tube.

[1] = Saybolt Universal Seconds

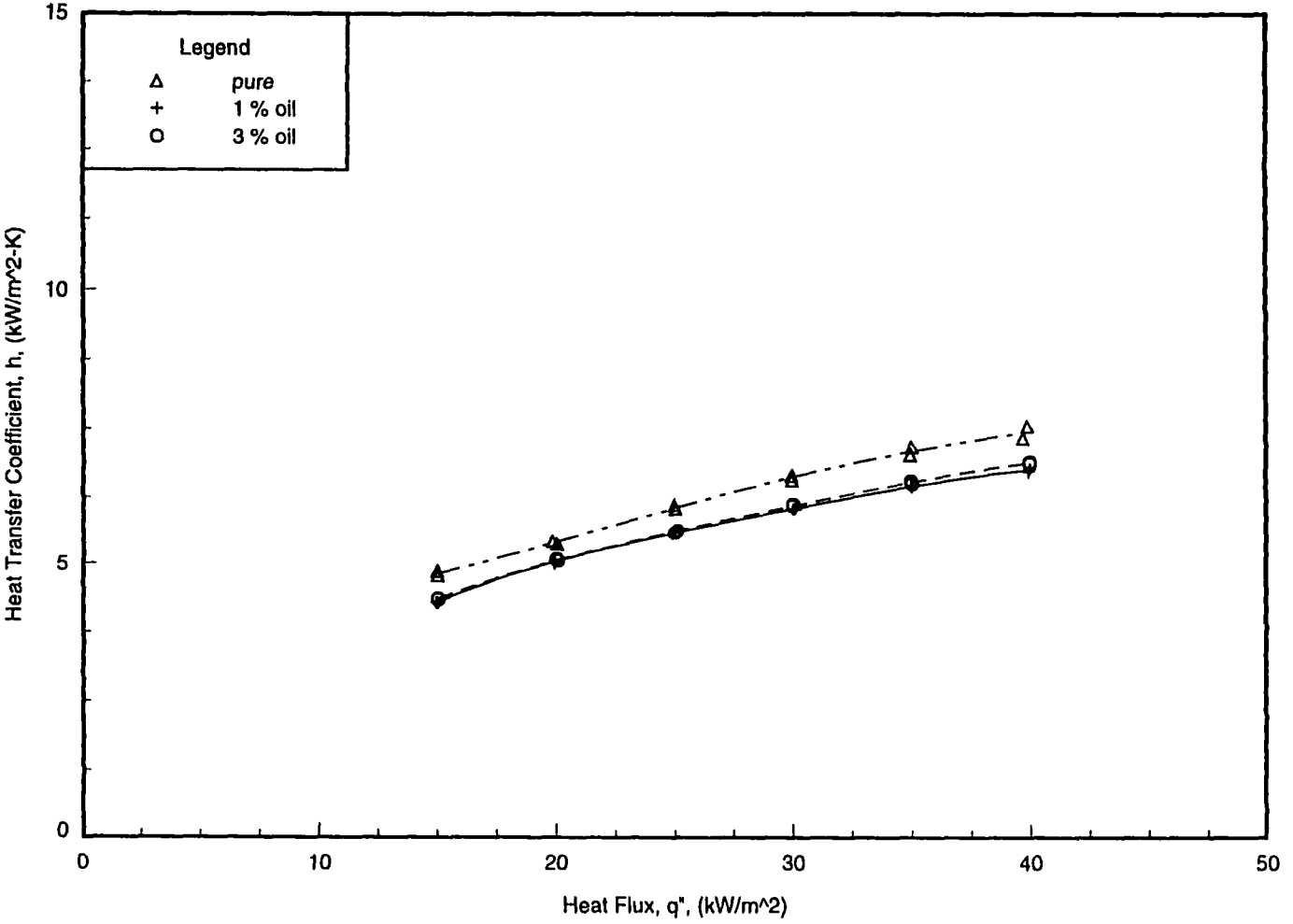

Figure 6.5 Oil effects on the pool boiling heat transfer coefficients of HFC-236fa for the 1024-fpm tube (D= 19.1 mm) at T_{sat}= 2°C

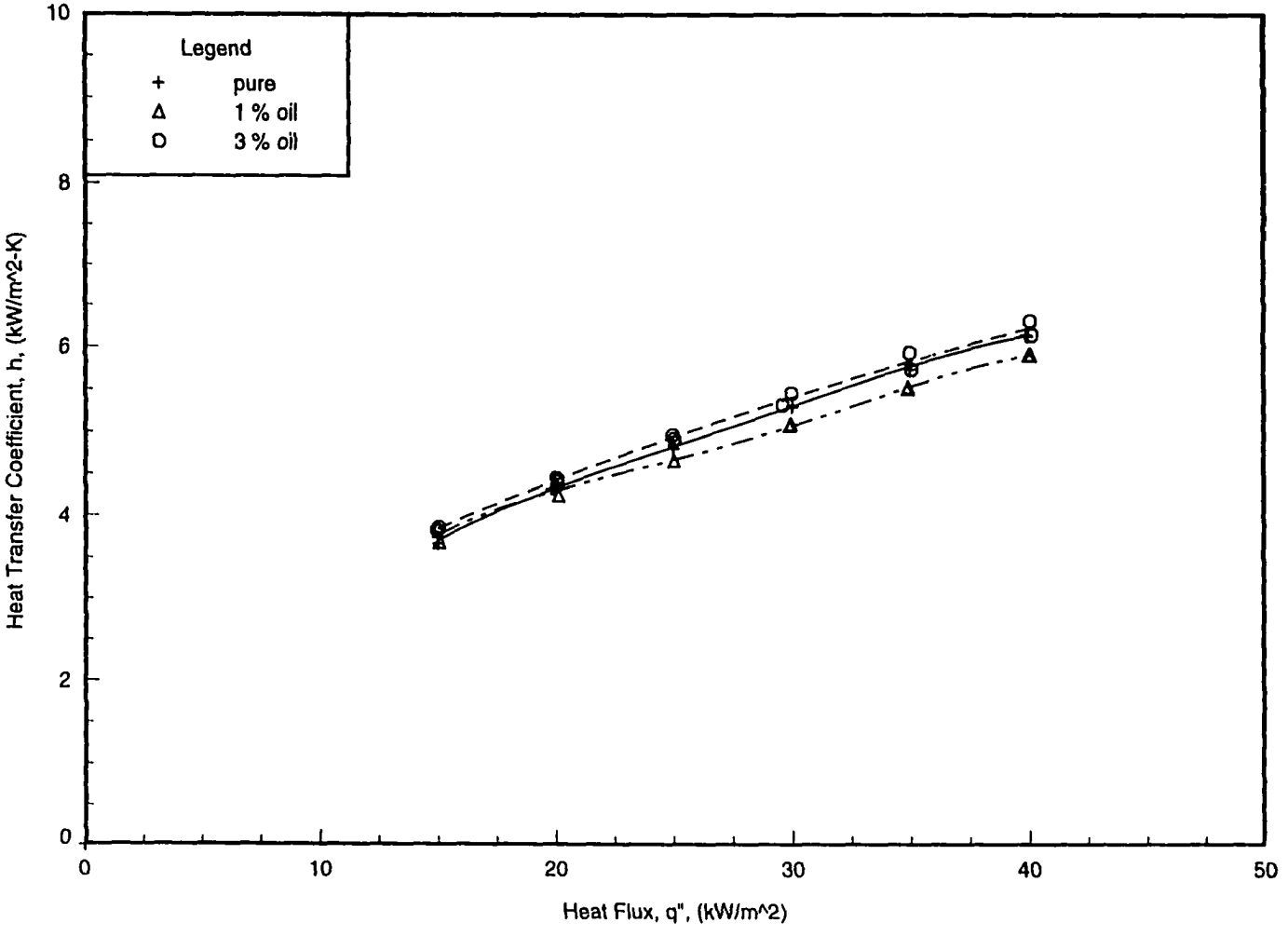

Figure 6.6 Oil effects on the pool boiling heat transfer coefficients of HFC-236fa for the 1575-fpm tube (D= 19.1 mm) at T_{sat}= 2°C

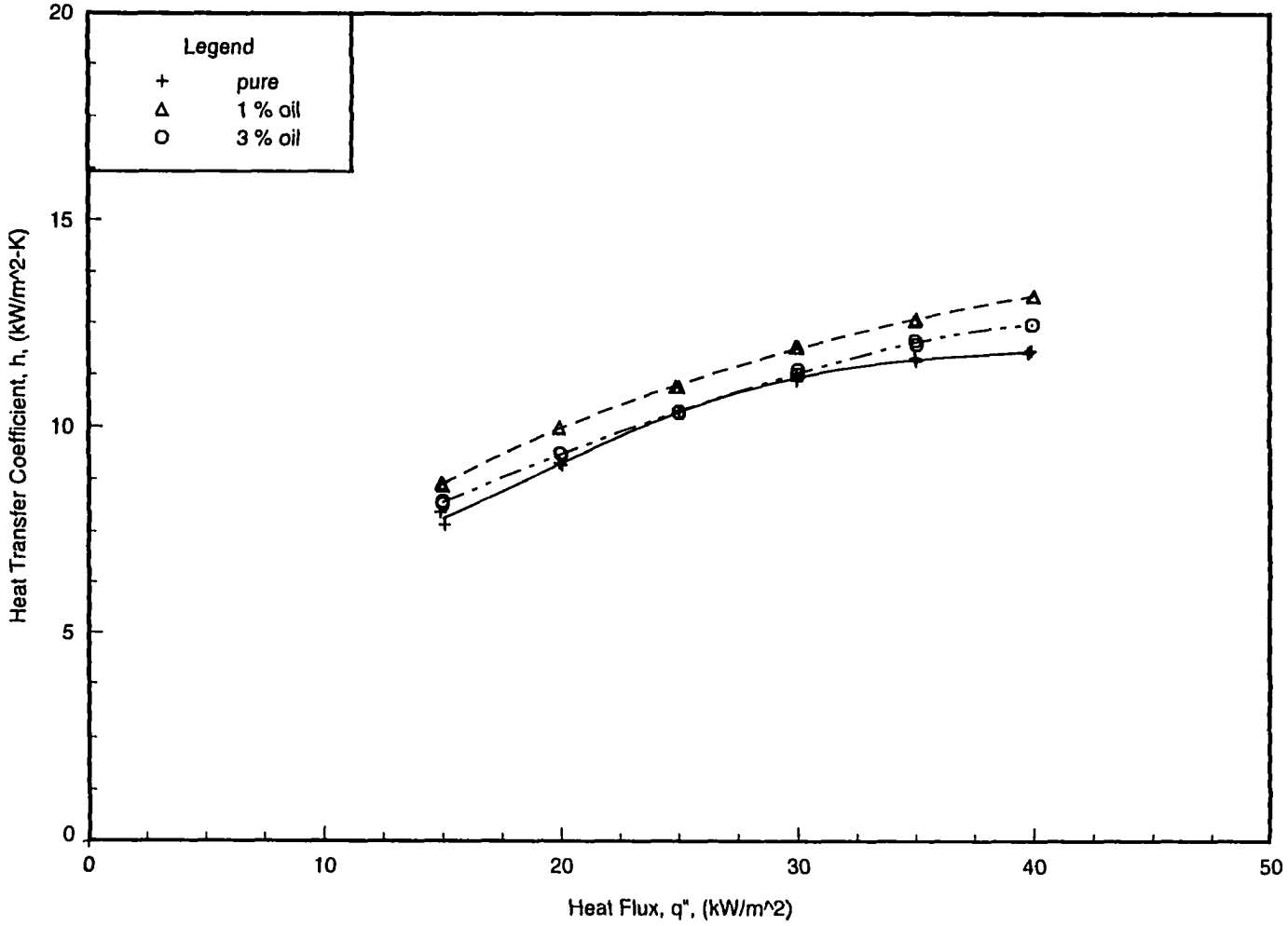

Figure 6.7 Oil effects on the pool boiling heat transfer coefficients of HFC-236fa for the Turbo-B tube (D= 19.1 mm) at T_{sat}= 2°C

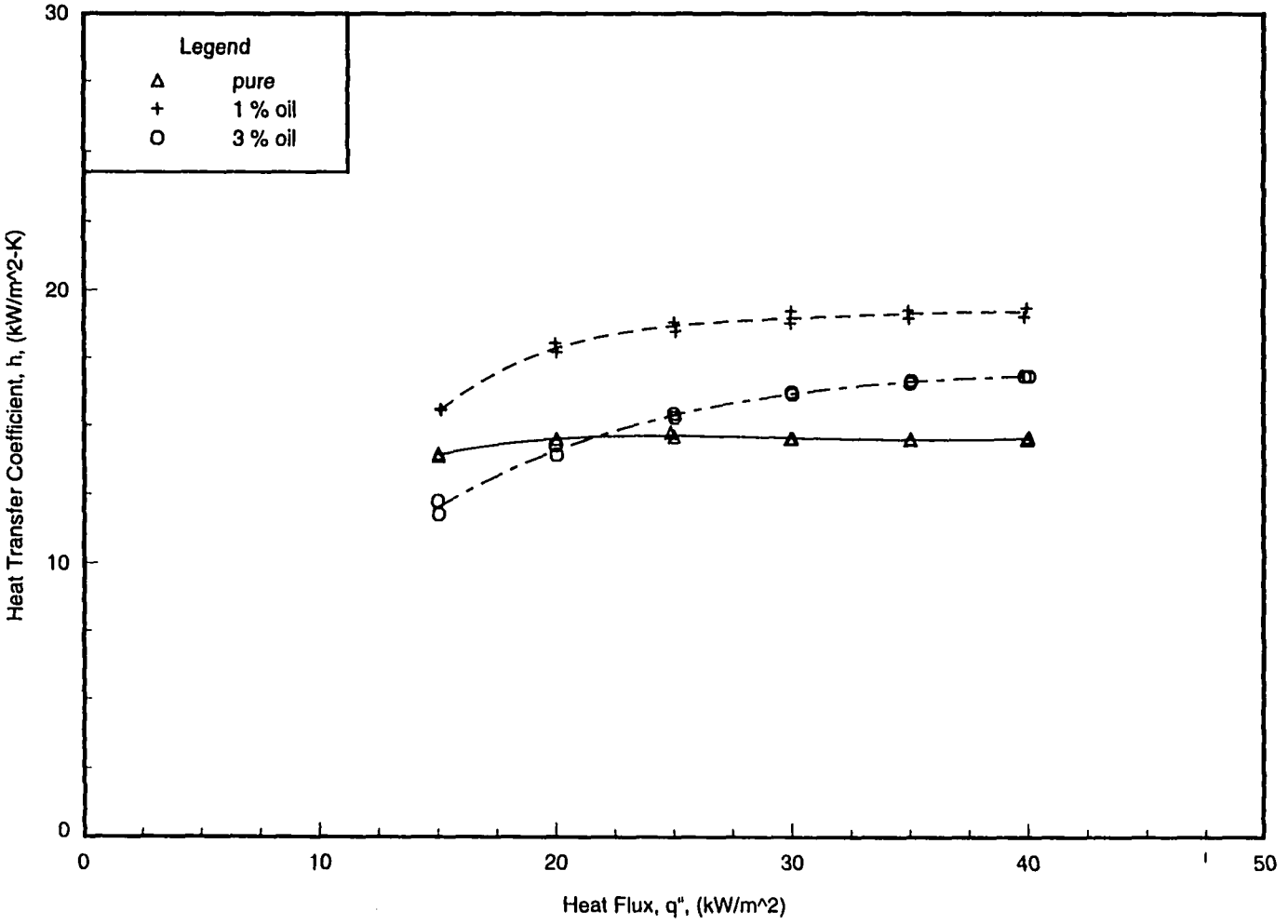

Figure 6.8 Oil effects on the pool boiling heat transfer coefficients of HFC-236fa for the Turbo-BII tube (D= 19.1 mm) at T_{sat}= 2°C

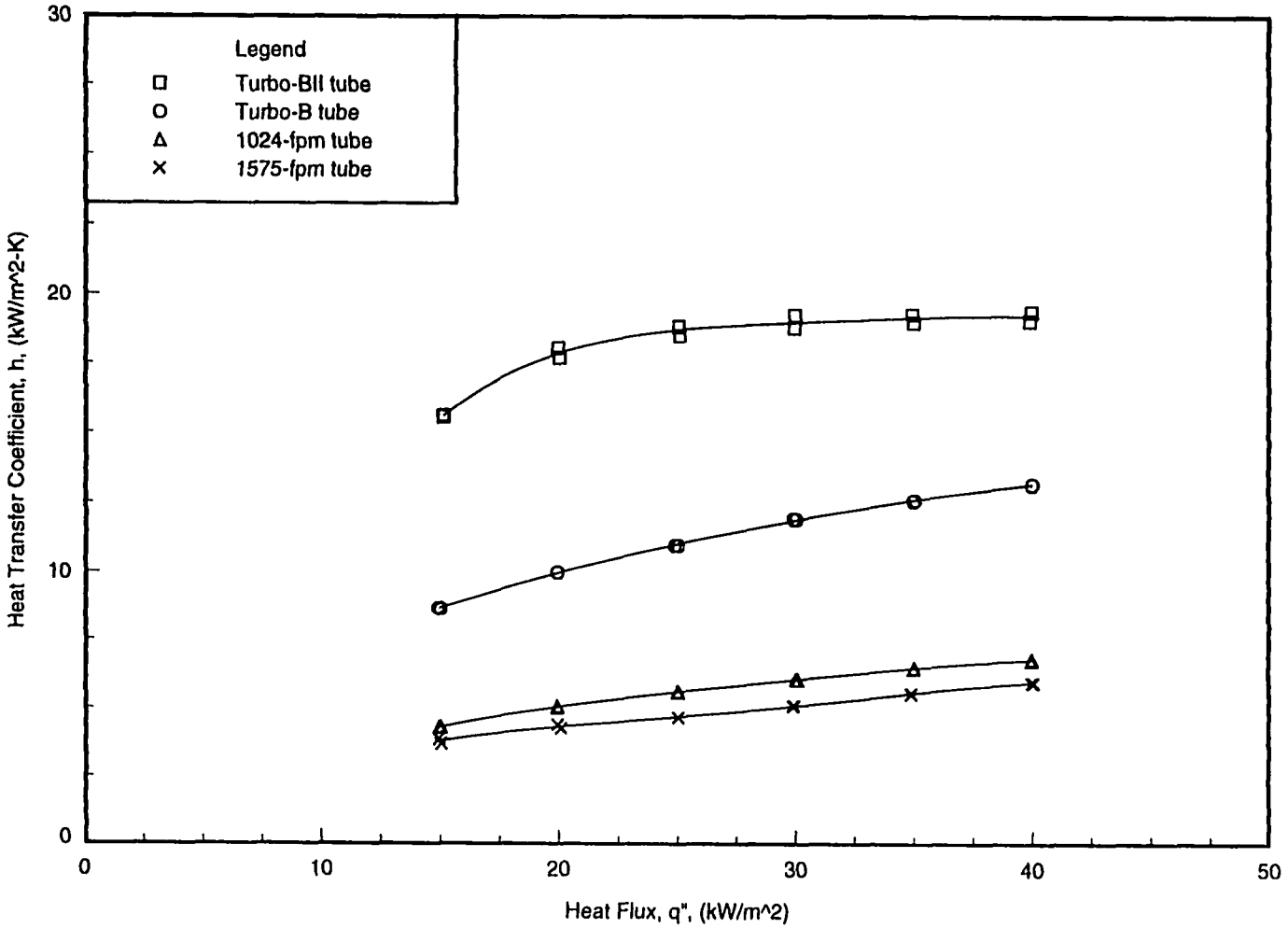

Figure 6.9 Comparison of the Turbo-BII, Turbo-B, 1024-fpm, and 1575-fpm tubes (D= 19.1 mm) in pool boiling of HFC-236fa with 1% oil at T_{sat}= 2°C

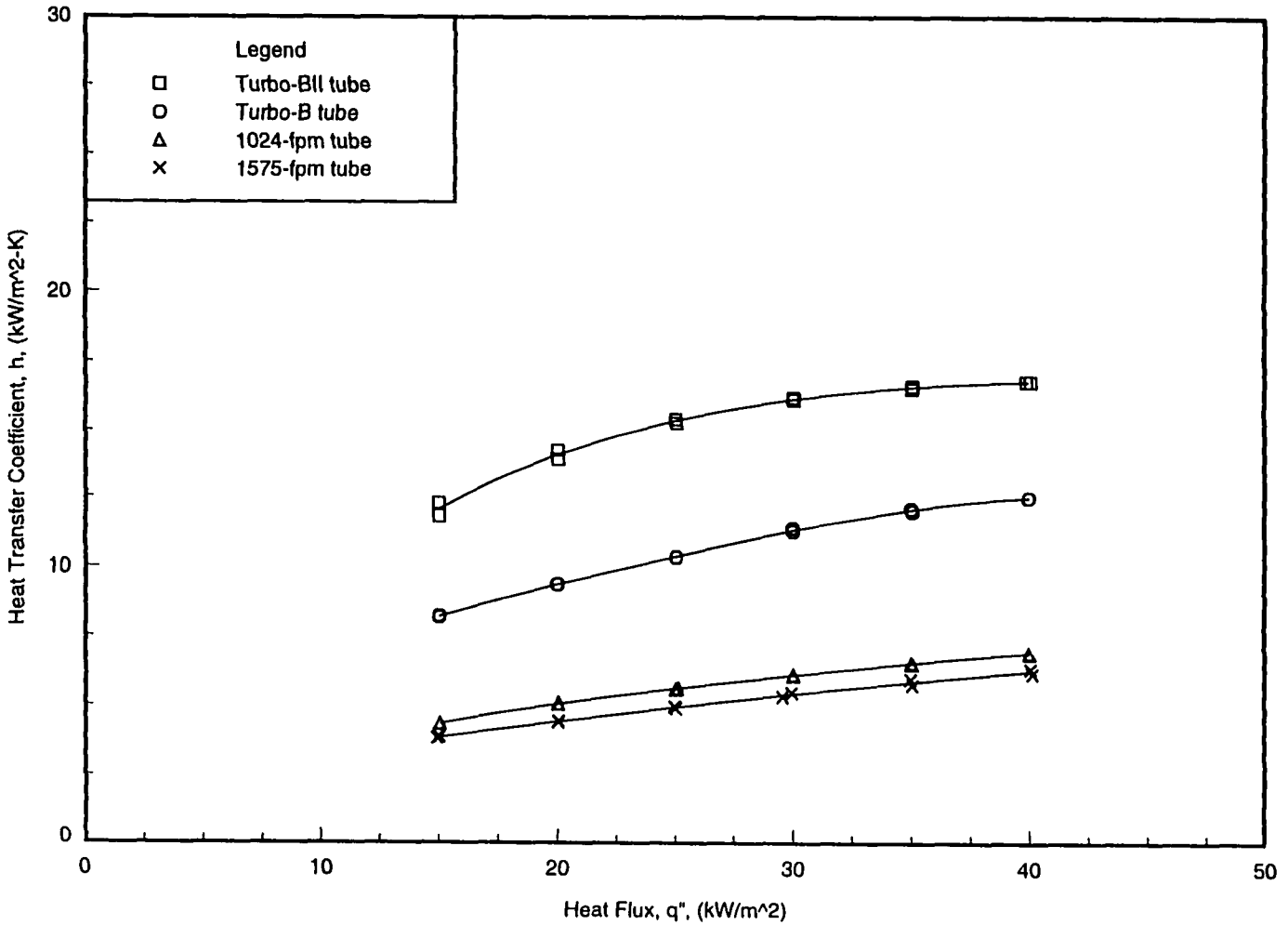

Figure 6.10 Comparison of the Turbo-BII, Turbo-B, 1024-fpm, and 1575-fpm tubes (D= 19.1 mm) in pool boiling of HFC-236fa with 3% oil at T_{sat}= 2°C

The two high performance enhanced tubes provided the best heat transfer coefficients for pool boiling of HFC-236fa with oil concentrations of 3% or less, this conclusion is in general agreement with the results of Memory et al. [50].

It is difficult to summarize a systematic dependence of each tube on the oil concentration for the tests performed here since the polyol-ester oil used with HFC-236fa caused insignificant change in the heat transfer performance of most tubes, and most of the change was within the experimental uncertainty. The small amount of oil, up to 3% concentration, present during pool boiling was found to affect the heat transfer performance by less than 10% compared with the pure HFC-236fa for all but one of the tubes tested. The exception was the Turbo-BII tube. As noted, the Turbo-BII tube showed the largest increase in heat transfer performance with a 30% increase at 1% oil and a 15% enhancement at 3% oil over the pure refrigerant value.

In general, the heat transfer coefficients for HFC-236fa with 1% oil relative to those for pure HFC-236fa decreased for the two finned tubes, but increased for the two high performance enhanced tubes. In comparison with the 1% oil case, the heat transfer coefficients with 3% oil concentration increased for the two finned tubes, but decreased for the two high performance enhanced tubes.

As shown in Figure 6.5, the addition of oil in HFC-236fa decreased the heat transfer coefficients for the 1024-fpm tube up to 10% at both the concentrations tested relative to the oil-free refrigerant, the 1024-fpm tube exhibited almost identical performance at the two oil concentrations.

Figure 6.6 shows that the small amount of oil (1% and 3%) in HFC-236fa caused the boiling coefficients for the 1575-fpm tube to differ by less than 5% from the pure refrigerant's boiling coefficients. Since the small deviation in the heat transfer coefficients caused by the addition of oil was within the experimental errors of measurements, the presence of oil in refrigerant almost had no effect on heat transfer. While Memory et al. [50] reported the presence of alkylbenzene oil in HCFC-124 had a negligible effect on the boiling performance of the 1024-fpm tube over the whole oil concentration range tested (0% $\sim$ 10%) in their tests of 748-fpm, 1024-fpm, Turbo-B, and High-Flux tubes.

Compared with pure HFC-236fa, the heat transfer performance of the Turbo-B tube shown in Figure 6.7 was improved by up to 10% at the 1% oil concentration but only up to 5% at the 3% oil concentration.

As shown in Figure 6.8, the heat transfer coeffcients of HFC-236fa with a 1% oil concentration for the Turbo-BII tube were 10% to 30% higher than those of the pure HFC-236fa. With a 3% oil concentration, they fell below those of pure HFC-236fa over about the lowest third of heat fluxes, but were greater than the pure coefficients over the remaining range of higher heat fluxes. Specifically, the

heat transfer coeffcients in the case of 3% oil were 10% lower compared with pure HFC-236fa at the lowest heat flux of 15 kW/m^2, but gradually increased and finally were 15% greater at the highest heat flux of 40 kW/m^2. The reason for the degradation with 3% oil at lower heat fluxes may be due to the clogging of surface cavities with oil associated with the less vigorous boiling where the thermal diffusion of the heavier oil component is slow.

The difference in the surface geometries between finned tubes and high performance enhanced tubes can result in different heat transfer behaviors between them in the HFC-236fa/oil mixtures. For example, the effects of oil can be more pronounced on a high performance enhanced surface than on a finned surface, since the numerous re-entrant cavities provided on the boiling surface of the high performance enhanced tubes tend to trap more oil locally than in the bulk mixtures. Webb and McQuade [87] reported that the enhanced tubes yielded larger performance degradation compared with the plain tube in the mixtures of refrigerant and oil.

A small amount of oil present was found to cause monotonic heat transfer degradation [76] [87] [89] or both heat transfer degradation and enhancement [38] [50], depending on the combined effects of tubes and refrigerant-oil mixtures. Overall, the published studies revealed that there were no significant effects of oil addition to the refrigerant on the boiling heat transfer performance for oil concentrations typically lower than 3%. No significant change in the heat transfer performance due to oil concentrations up to 3% was also observed in this research, which agrees with the general consensus among the previous studies.

Pool boiling coefficients of HFC-236fa, HFC-236ea, and CFC-114

Comparison of pure HFC-236fa, HFC-236ea, and CFC-114

Figures 6.11 through 6.14 clarify the effects of refrigerant types (HFC-236fa, HFC-236ea, and CFC-114) on pool boiling heat transfer performance for a 1024-fpm, a 1575-fpm, a Turbo-B, and a Turbo-BII tube, respectively. The heat transfer results for all the tubes tested show that the three different refrigerants had similar trends with the order of descending heat transfer coefficients being: HFC-236fa, HFC-236ea, and CFC-114. Data were not taken for CFC-114 with the Turbo-B and Turbo-BII tubes.

The increase in heat transfer coefficients of HFC-236fa compared with those of CFC-114 was around 50% to 80% for the 1024-fpm tube and 40% to 70% for the 1575-fpm tube. When compared with the HFC-236ea data, the HFC-236fa performance was about 10% to 20% higher for the 1024-fpm tube, 10% for the 1575-fpm tube, 40% to 60% for the Turbo-B tube, and 40% to 70% for the Turbo-BII tube.

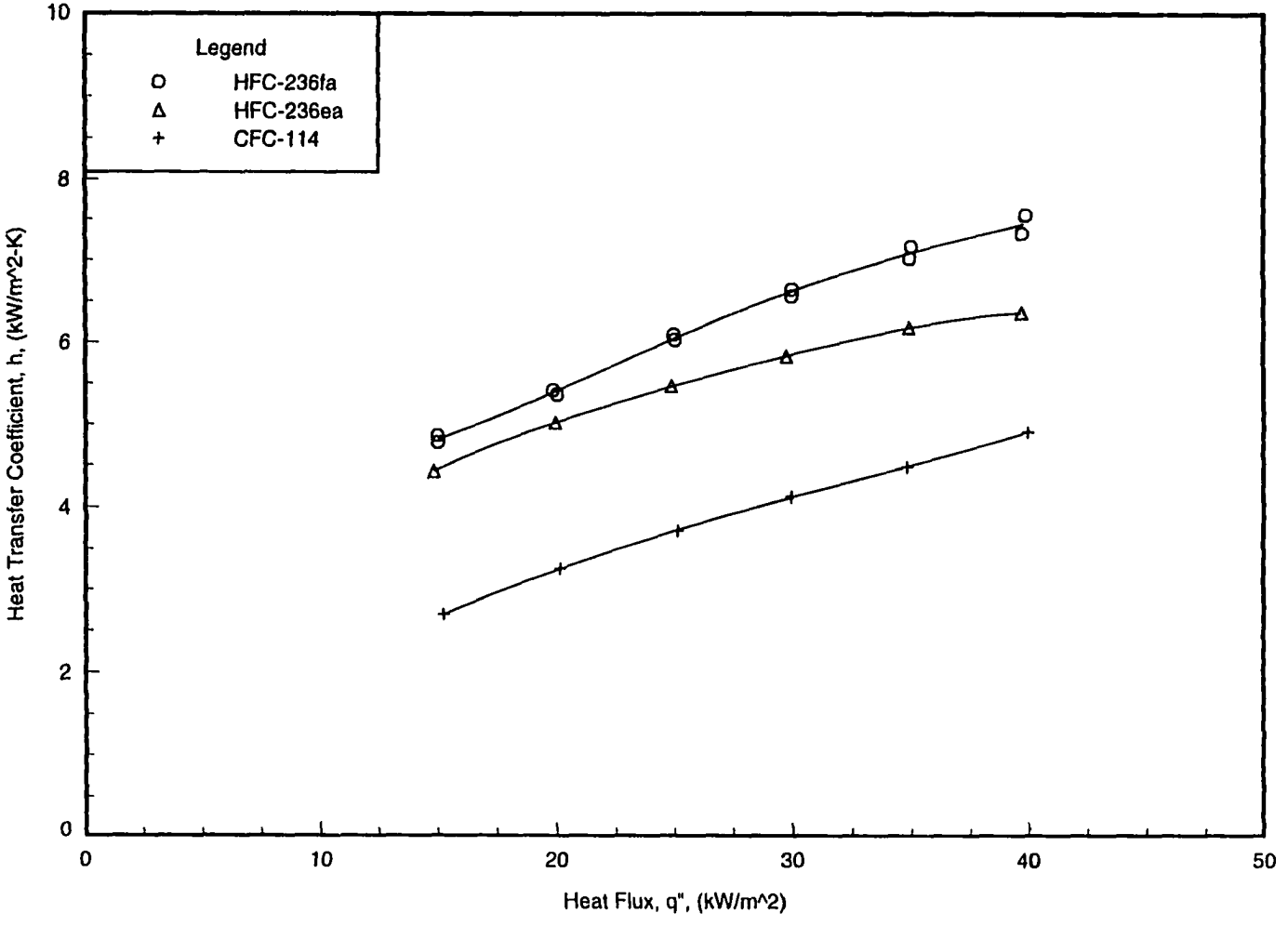

Figure 6.11 Pool boiling coefficients of HFC-236fa, HFC-236ea, and CFC-114 for the 1024-fpm tube (D= 19.1 mm) at T_{sat}= 2°C

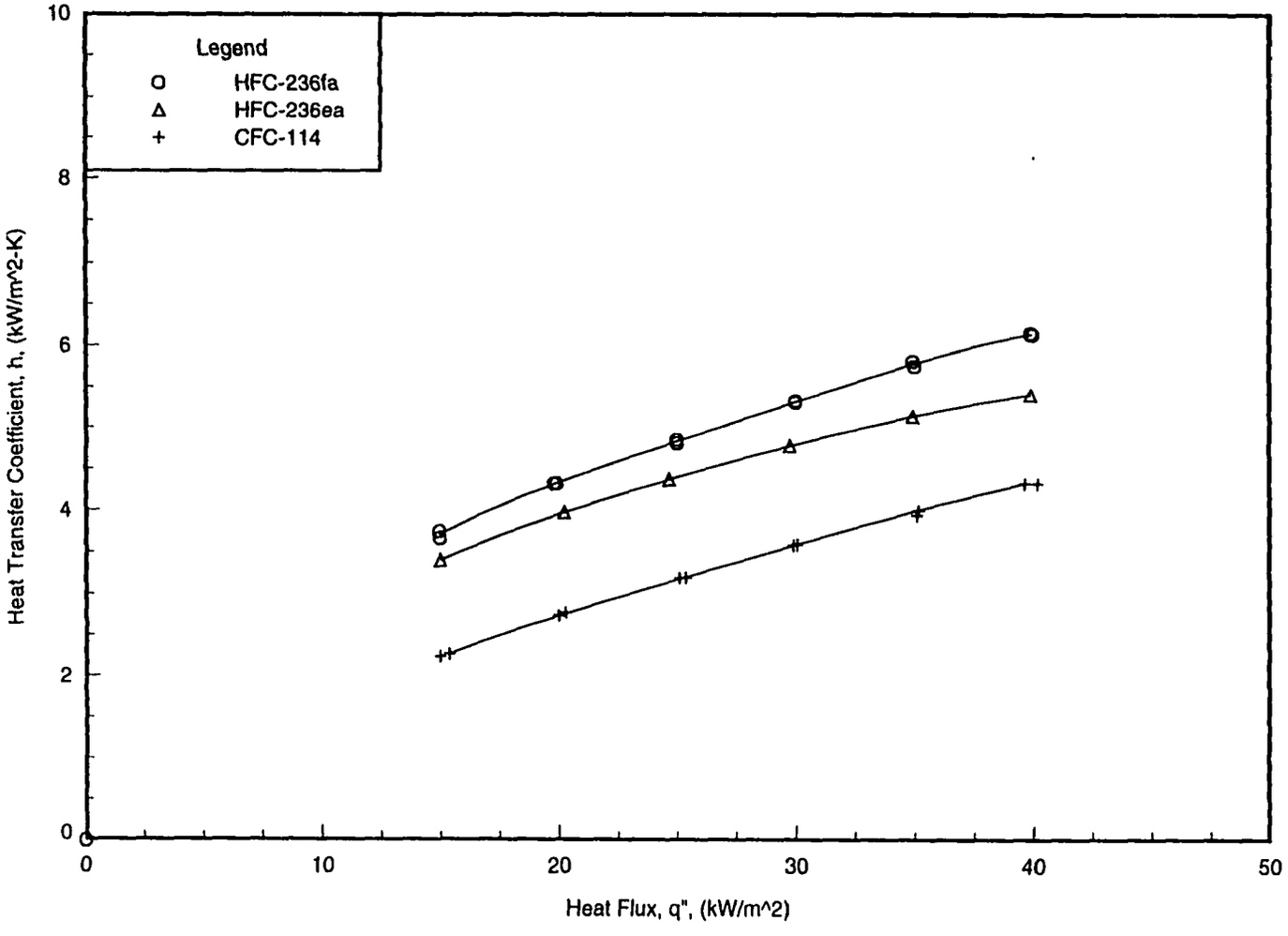

Figure 6.12 Pool boiling coefficients of HFC-236fa, HFC-236ea, and CFC-114 for the 1575-fpm tube (D= 19.1 mm) at T_{sat}= 2°C

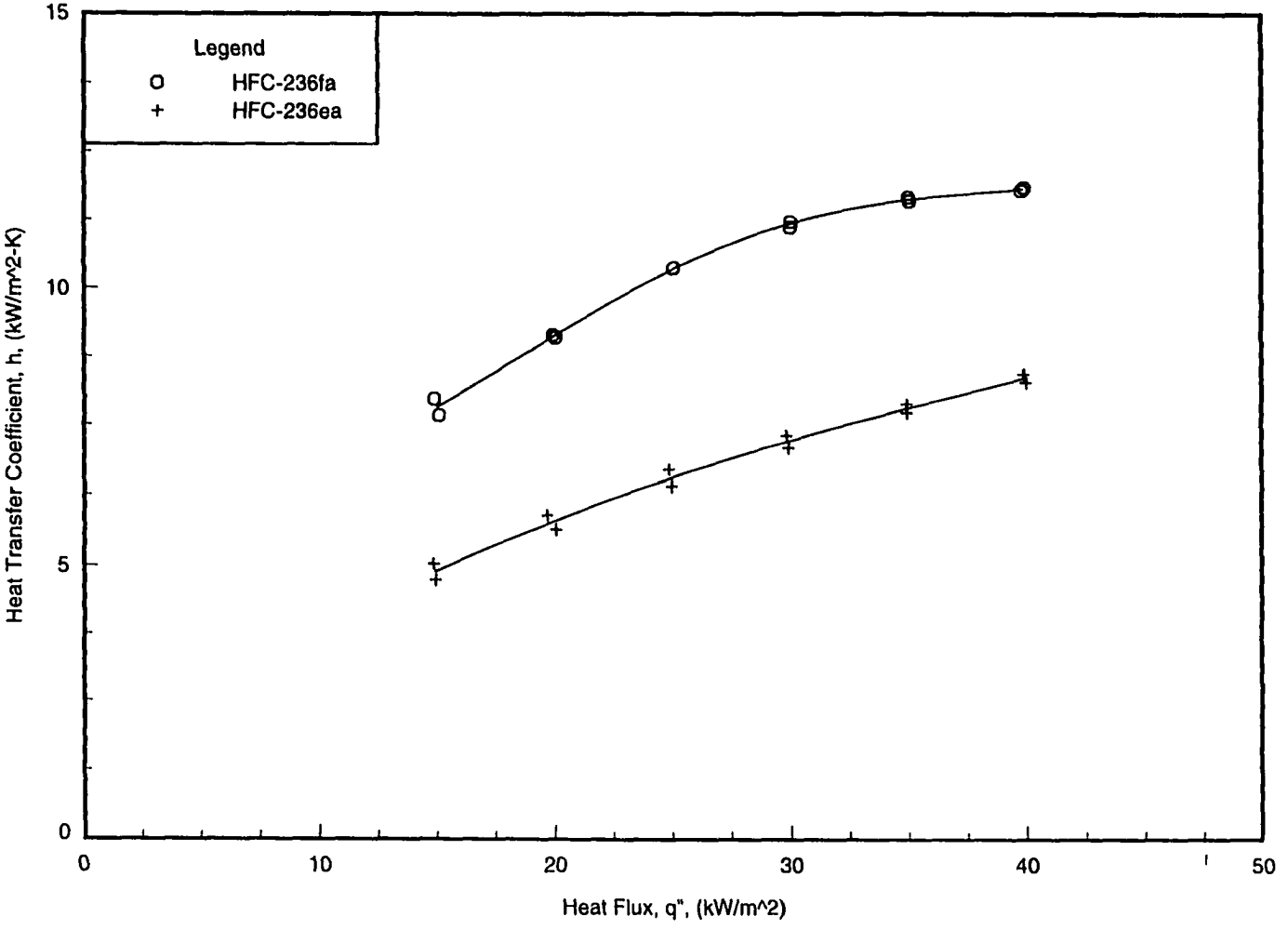

Figure 6.13 Pool boiling coefficients of HFC-236fa and HFC-236ea for the Turbo-B tube (D= 19.1 mm) at T_{sat}= 2°C

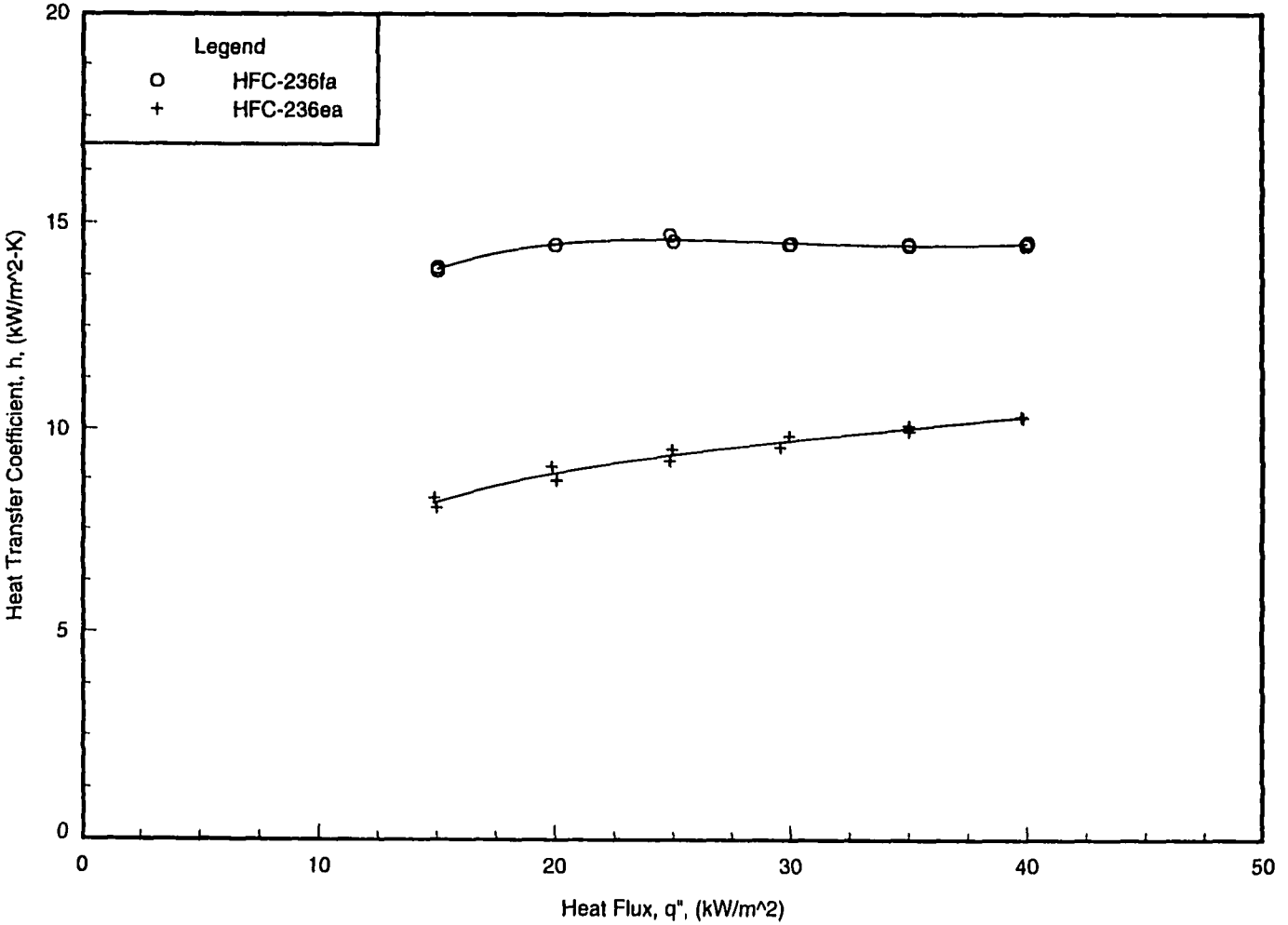

Figure 6.14 Pool boiling coefficients of HFC-236fa and HFC-236ea for the Turbo-BII tube (D= 19.1 mm) at T_{sat}= 2°C

Comparison of CFC-114/oil and HFC-236fa/oil

Comparison of HFC-236fa and CFC-114 with oil concentrations of 0, 1, 3% was made for the 1024-fpm tube in Figures 6.15 and for the 1575-fpm tube in Figures 6.16. The CFC-114 data at each oil concentration are shown as a series of dotted curves for distinguishable comparison with the HFC-236fa data points.

A larger difference between these two refrigerants exists only in their oil-free performance. Both the finned tubes generally showed improvement with HFC-236fa. When compared with pure CFC-114 as reported in the previous section, pure HFC-236fa showed an increase of up to 80% with the use of the 1024-fpm tube and 70% with the 1575-fpm tube.

The addition of oil reduced the difference in the heat transfer coefficients of HFC-236fa and CFC-114. At the two oil concentrations tested, the boiling coefficients of the two refrigerants for the two tubes were within 10%. The performance of the two finned tubes with HFC-236fa was similar to that with CFC-114 when a small amount of oil was present (i.e., 1% and 3%).

Comparison of data with published results

The pool boiling data for the 1024-fpm and Turbo-B tubes evaluated at T_{sat}= 2°C in this study were compared with those collected at T_{sat}= 4.4°C by Webb and Pais [86] in Figure 6.17 and Figure 6.18, respectively. The tubes compared had almost the same tube diameter and configuration.

Webb and Pais [86] correlated the data of five pure refrigerants for plain, 1024-fpm, Turbo-B, Gewa-SE, and Gewa-TX tubes in the form of $h = b \times (q")^m$. The values of the coefficient (b) and the exponent (m) for the 1024-fpm and Turbo-B tubes tested at 4.4°C are shown in Table 2.1.

Experimental results show that the heat transfer coefficients for high pressure refrigerants were higher than those for low pressure refrigerants [50] [85]. The correlations developed [19] [20] [24] also reveal that the heat transfer coefficient of a fluid is in direct proportion to the fluid's reduced pressure. A high pressure fluid usually has a high reduced pressure since the fluid's reduced pressure is defined as the ratio of its saturation prssure to its critical pressure.

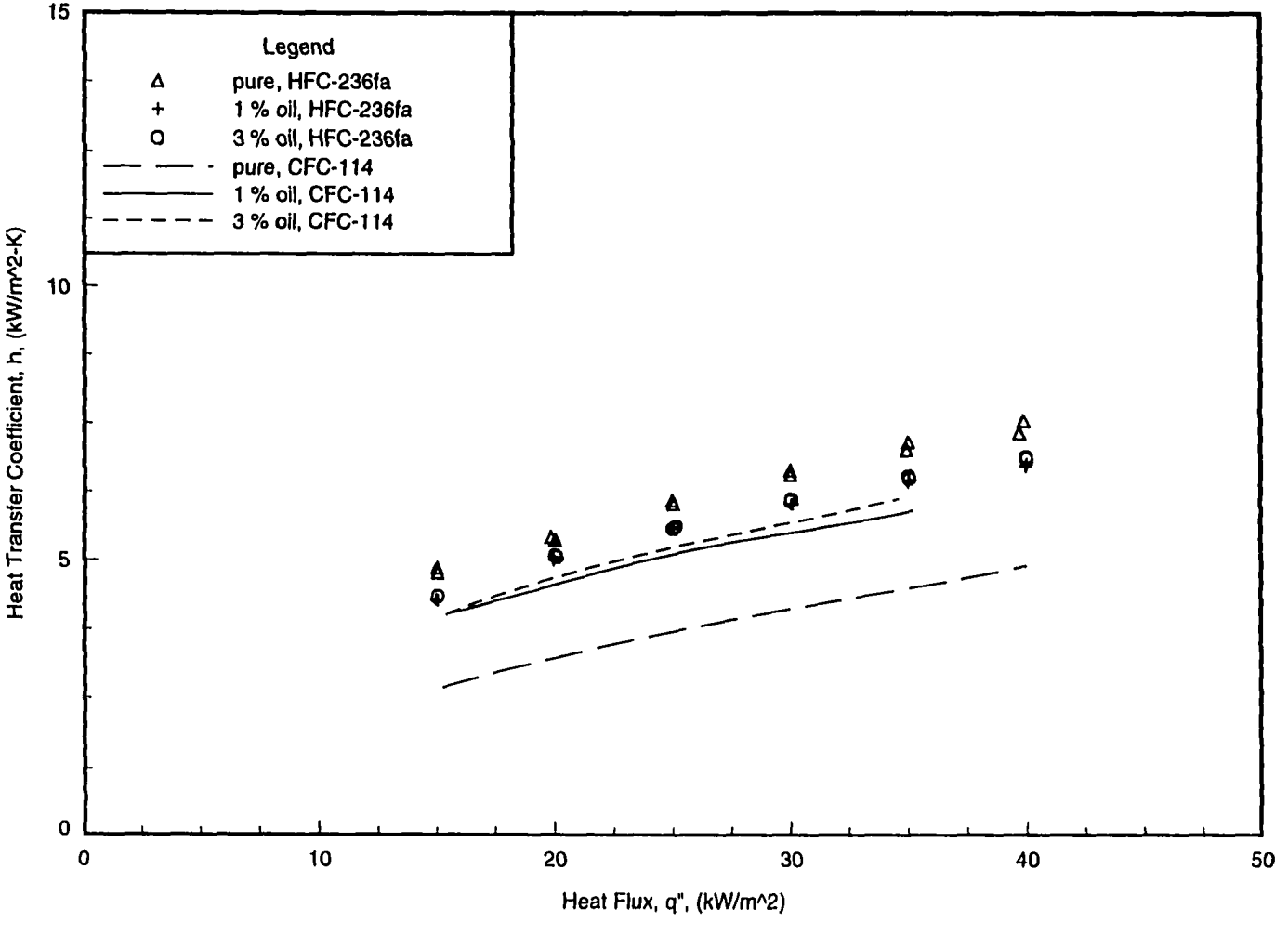

Figure 6.15 Pool boiling of HFC-236fa and CFC-114 for the 1024-fpm tube (D= 19.1 mm) at oil concentrations of 0, 1, and 3% and T_{sat}= 2°C

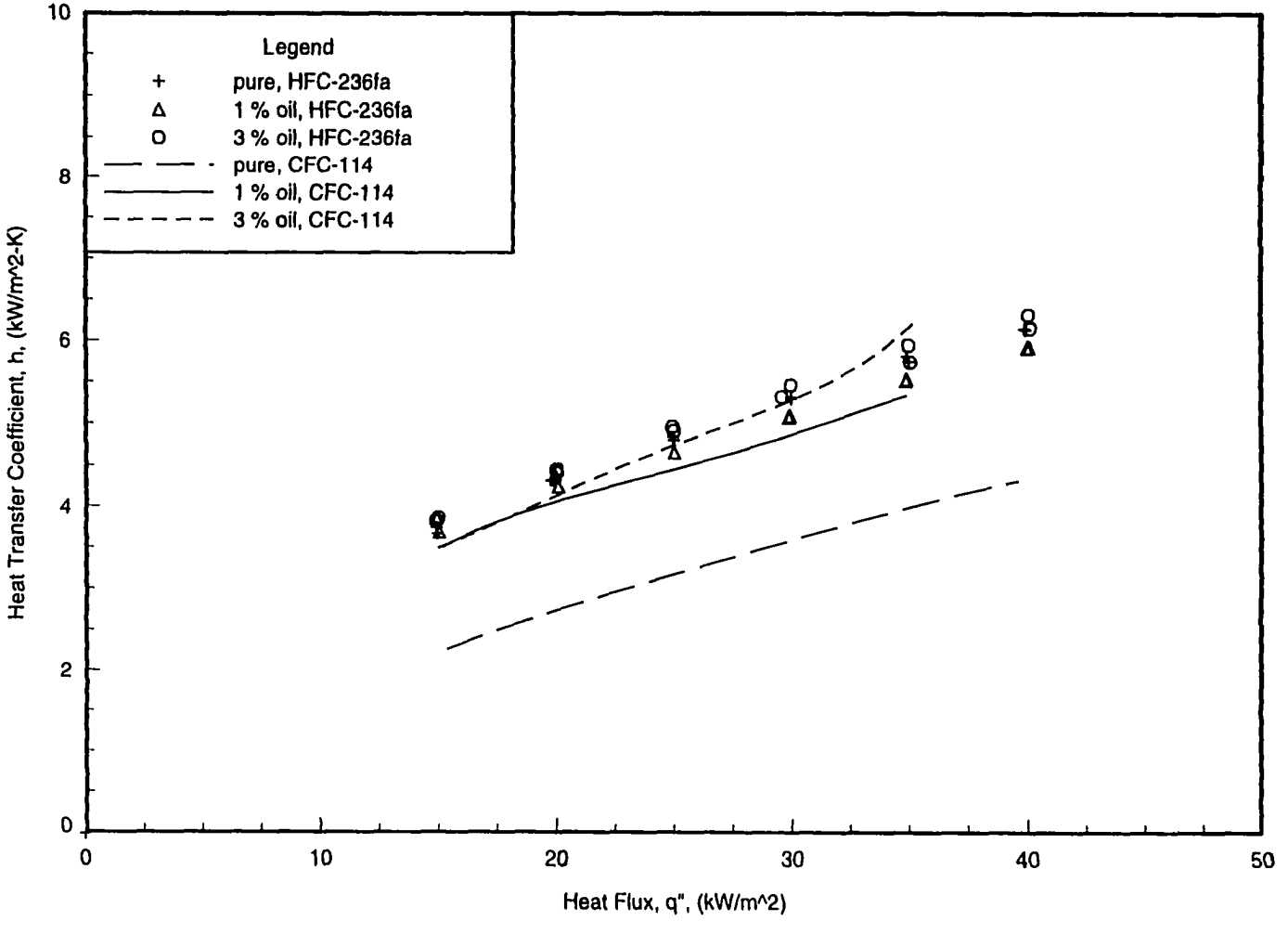

Figure 6.16 Pool boiling of HFC-236fa and CFC-114 for the 1575-fpm tube (D= 19.1 mm) at oil concentrations of 0, 1, and 3% and T_{sat}= 2°C

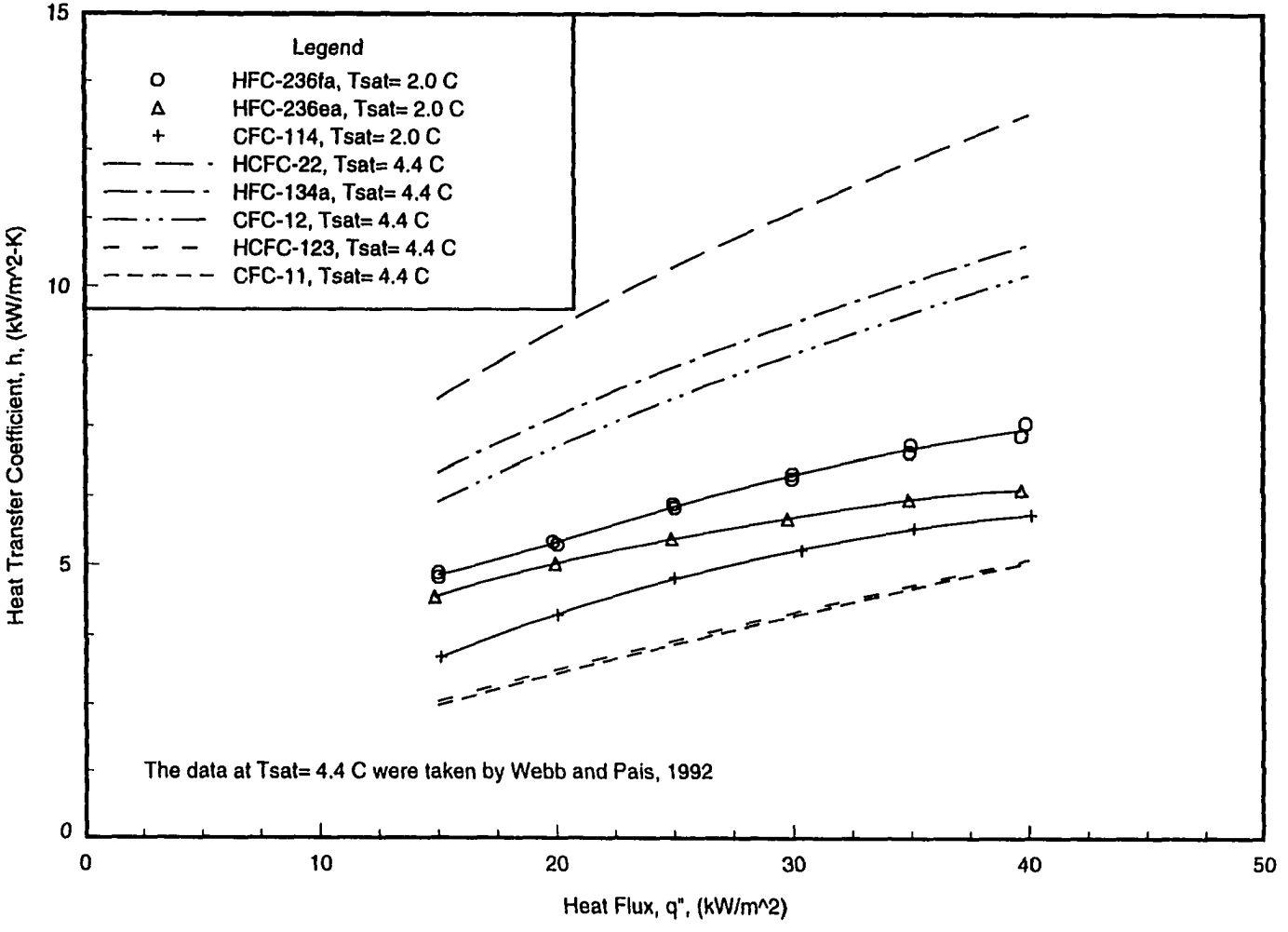

Figure 6.17 Comparison of the boiling results with Webb and Pais (1992) for the 1024-fpm tube

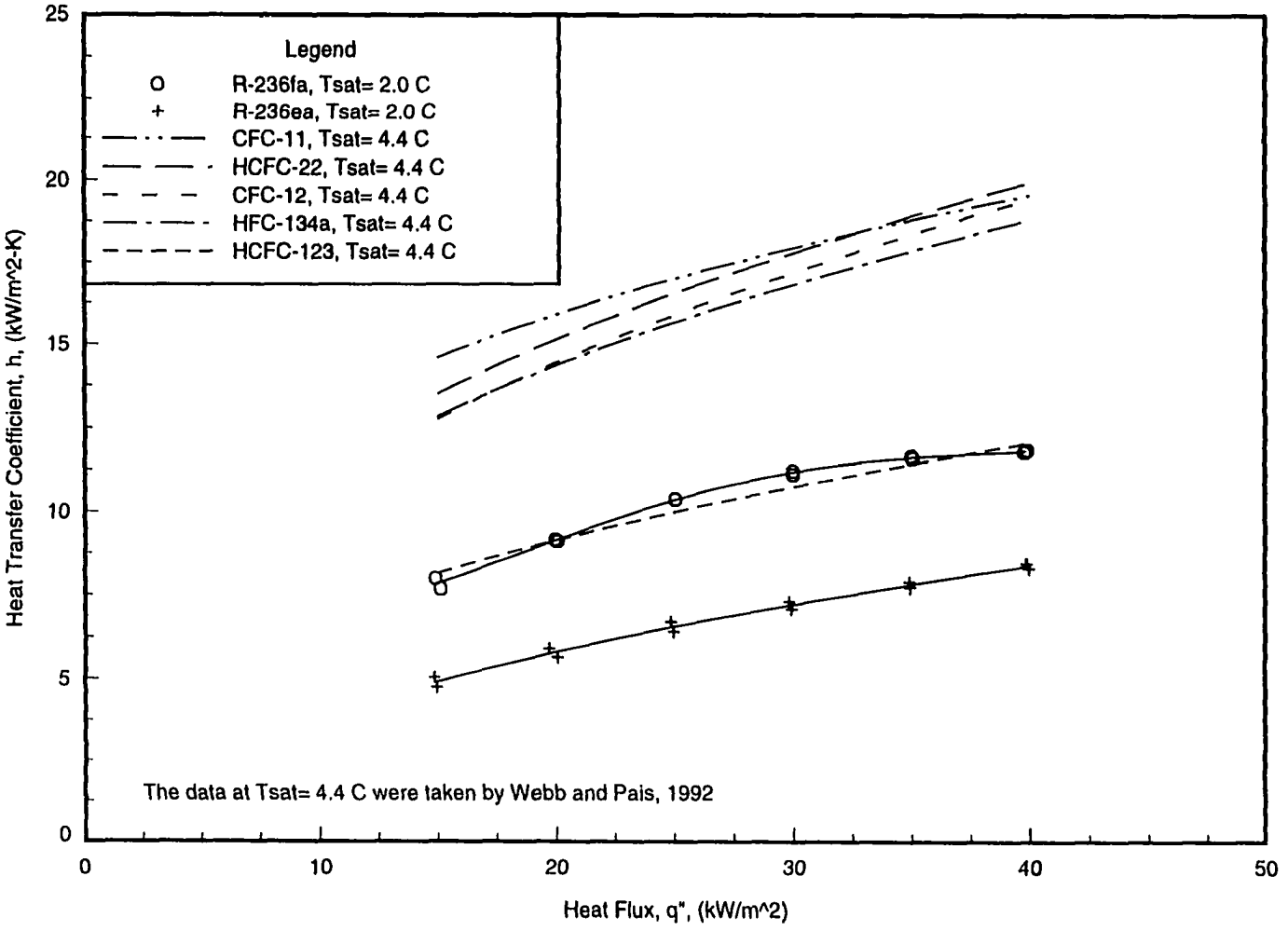

Figure 6.18 Comparison of the boiling results with Webb and Pais (1992) for the Turbo-B tube

Examination of all the data compared in Figures 6.17 and 6.18 shows a similar trend as the published results. Table 6.1 lists the saturation temperature (T_{sat}), saturation pressure (P_{sat}), reduced pressure (P_r), and critical pressure (P_{cr}) for the eight refrigerants compared here. The refrigerants are listed in order of decreasing P_{sat} or P_r. As indicated in Table 6.1, HFC-236fa, CFC-114, and HCFC-236ea have lower pressures than HFC-134a, CFC-12, and HCFC-22, but have higher pressures than CFC-11 and HCFC-123.

Table 6.1 Properties of the eight refrigerants compared in Figures 6.17 and 6.18

Refrigerant	T_{sat} (°C)	P_{sat} (Mpa)	P_r (=P_{sat}/P_{cr})	P_{cr} (Mpa)
HCFC-22	4.4	0.574	0.115	4.99
CFC-12	4.4	0.358	0.087	4.12
HFC-134a	4.4	0.345	0.085	4.06
HFC-236fa	2.0	0.118	0.037	3.20
CFC-114	2.0	0.094	0.029	3.25
HFC-236ea	2.0	0.085	0.024	3.53
CFC-11	4.4	0.049	0.011	4.41
HCFC-123	4.4	0.040	0.011	3.68

Figure 6.17 shows that for the 1024-fpm tube the heat transfer coefficients of the present data (HFC-236fa, CFC-114, and HCFC-236ea) fall below the coefficients of the high pressure refrigerants (HFC-134a, CFC-12, and HCFC-22) and are above those of the low pressure refrigerants (CFC-11 and HCFC-123). Comparison for the 1024-fpm tube shows that the heat transfer coefficients of HCFC-22 are about 65% to 75% higher than those of HFC-236fa.

If we ignore the data for the Turbo-B tube with CFC-11, which were considered to have anomalously high heat transfer performance by the authors [86], Figure 6.18 shows that for the Turbo-B tube the low pressure refrigerants (HCFC-123, HFC-236fa, CFC-114, and HCFC-236ea) has lower heat transfer coefficients than the high pressure refrigerants (HFC-134a, CFC-12, and HCFC-22). Comparison for the Turbo-B tube shows that the heat transfer coefficients of HCFC-22 are about 60% to 70% higher than those of HFC-236fa, while the coefficients of HFC-236fa are approximately equal to the HCFC-123 values.

It is not possible to compare data involving lubricant effects with any existing correlations due to the absence of property information for the refrigerant and oil mixtures.

Curve fits of the pool boiling data of HFC-236fa, CFC-114, and HCFC-236ea are developed in the same form as that proposed by Webb and Pais [86] and presented in Appendix F.

Summary

The heat transfer coefficients for four tube types (1024-fpm, 1575-fpm, Turbo-B. and Turbo-BII tubes) were determined for pool boiling of HFC-236ea, HFC-236fa, and HFC-236fa/oil. In addition, the effects of oil, tube, and refrigerant types on the boiling heat transfer performance were evaluated.

The high performance enhanced tubes performed better during nucleate boiling than the finned tubes for both HFC-236ea and HFC-236fa. The best heat transfer coefficients of HFC-236ea were provided by the high performance Turbo-BII tube with the heat transfer coefficients around 1.6~1.8, 1.9~2.4, and 1.2~1.7 times those for the 1024-fpm tube, 1575-fpm tube, and Turbo-B tube, respectively. The best heat transfer performance with HFC-236fa was also provided by the Turbo-BII tube with the heat transfer coefficients around 2~2.9, 2.4~3.8, and 1.2~1.8 times those for the 1024-fpm tube, 1575-fpm tube, and Turbo-B tube, respectively.

HFC-236fa performed better than CFC-114 and HFC-236ea during pool boiling for all the tube types tested. Maximum heat transfer increases of 80% compared with CFC-114 and 70% compared with HFC-236ea were obtained by the 1024-fpm tube and Turbo-B tube, respectively.

The presence of up to 3% oil in HFC-236fa affected the boiling performance by less than 10% from that of pure HFC-236fa for all but one of the tubes tested. The Turbo-BII tube, the only exception, showed an increase of up to 30% in boiling coefficients relative to the pure-refrigerant values for the testing with 1% oil and a variation from −10% to 15% for the 3% oil case. The Turbo-BII tube exhibited the largest changes in pool boiling performance with the addition of oil.

CHAPTER 7 SPRAY EVAPORATION RESULTS

The spray evaporation heat transfer coefficients of HFC-236ea were determined for a Turbo-B and a Turbo-CII tube as well as a 1575-fpm tube in this study. These three tubes with distinctively different surface geometries (i.e., an enhanced boiling tube, an enhanced condensation tube, and an integral-fin tube) were choosed because heat transfer coefficients were known to vary with surface geometries.

As shown in Figure 5.4, two passes of a horizontal tube were subjected to liquid refrigerant sprayed from a set of nozzles located above the tube. The nozzles used had an orifice diameter of 1.58 mm (1/16 inch) and are capable of spraying full solid cone. Tests were performed at several feed flow rates (2.6 $\sim$ 3.2 kg/min) over the heat flux range of 10 kW/m^2 to 30 kW/m^2 in order to clarify the effects of the feed rates on the spray evaporation heat transfer coefficients of HFC-236ea.

In addition, spray evaporation performance, which has been shown to provide a higher heat transfer rate with a smaller refrigerant charge than pool boiling, was compared with pool boiling performance for the Turbo-B tube and 1575-fpm tube.

Data were taken at a saturation temperature of 2°C in steps from low heat flux to high heat flux with increasing heat load, and then directly shifted in steps from high heat flux to low heat flux as the heat load decreased, therefore the hysteresis effects commonly found with high wettability fluids were exhibited. Repeat runs were also performed on different days for each tube in order to test the accuracy and repeatability of the system.

Recirculation rate

According to Equation 3.6 derived in Chapter 3, the values of recirculation rates corresponding to the heat fluxes for five spray flow rates (2.6 $\sim$ 3.2 kg/min) tested herein were calculated and listed in Table 7.1.

Recirculation rates depend on the tube arrangements as well as feed rates. The recirculation rates for air-conditioning systems are generally low; however, tests using a single tube yield higher recirculation rates than using a tube bundle, since the liquid which is not evaporated from the top tubes may fall

Table 7.1 Test-section recirculation ratios

Heat flux (kW/m^2)	Spray mass flow rate (kg/min)			
	2.6	2.8	3.0	3.2
10	14.3	15.4	16.5	17.6
15	9.5	10.2	11.0	11.8
20	7.1	7.7	8.2	8.7
25	5.7	6.1	6.6	7.0
30	4.8	5.1	5.5	5.8

onto the lower row tubes in a bundle and then be evaporated, while for a single-tube test the liquid returns directly to the pump. The large values of recirculation rates mean that most of the spray liquid was not evaporated but returned to the pump.

Multiplying the five spray flow rates (2.6 $\sim$ 3.2 kg/min) tested here by the collector test fraction (0.193) reported for the same tube diameter [53], the effective refrigerant mass flow rate hitting the tube surafce can then be estimated. The small percentage of the spray flow rates acturally reaching the tube surface was the main cause of the large recirculation rates listed in Table 7.1.

Spray evaporation coefficients of HFC-236ea for a Turbo-B, a Turbo-CII, and a 1575-fpm tube

Effects of heat fluxes

The effects of heat fluxes on the heat transfer coefficients at four liquid feed rates are exhibited in Figures 7.1 through 7.3 for the Turbo-B tube, Turbo-CII tube, and 1575-fpm tube, respectively.

These figures indicate that the heat transfer coefficient depended on the heat flux throughout the entire range of heat fluxes tested. For any tube type at any feed rate except for relatively low feed rates, the general trend revealed in these figures is that as the heat flux increased, the heat transfer coefficient increased until a critical (maximum) heat flux was reached, and then decreased beyond this critical value. This critical value was around 15 kW/m^2 for all testing conditions. In general, the critical heat flux varies with different feed rates as well as different tube types and working fluids.

At the heat fluxes below the critical heat flux, the heat transfer coefficients increased as the falling film became thinner due to evaporation with increasing heat flux. Dry-out phenomena occurred once the critical heat flux was reached and became progressively dominant beyond this critical value with increasing heat loads, and hence, resulted in decreasing heat transfer.

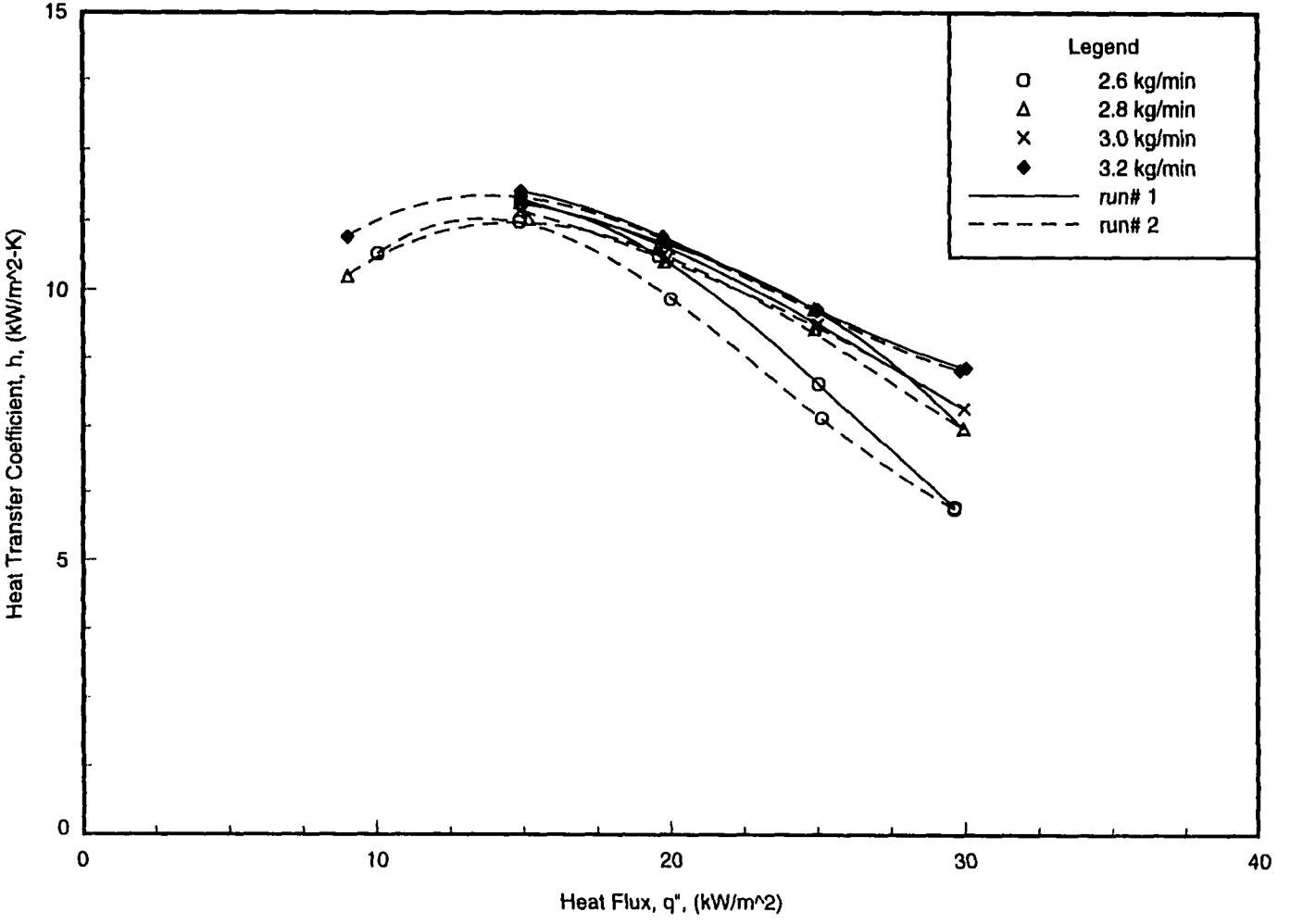

Figure 7.1 Spray evaporation heat transfer coefficients of HFC-236ea for the Turbo-B tube (D= 19.1 mm) at T_{sat}= 2°C

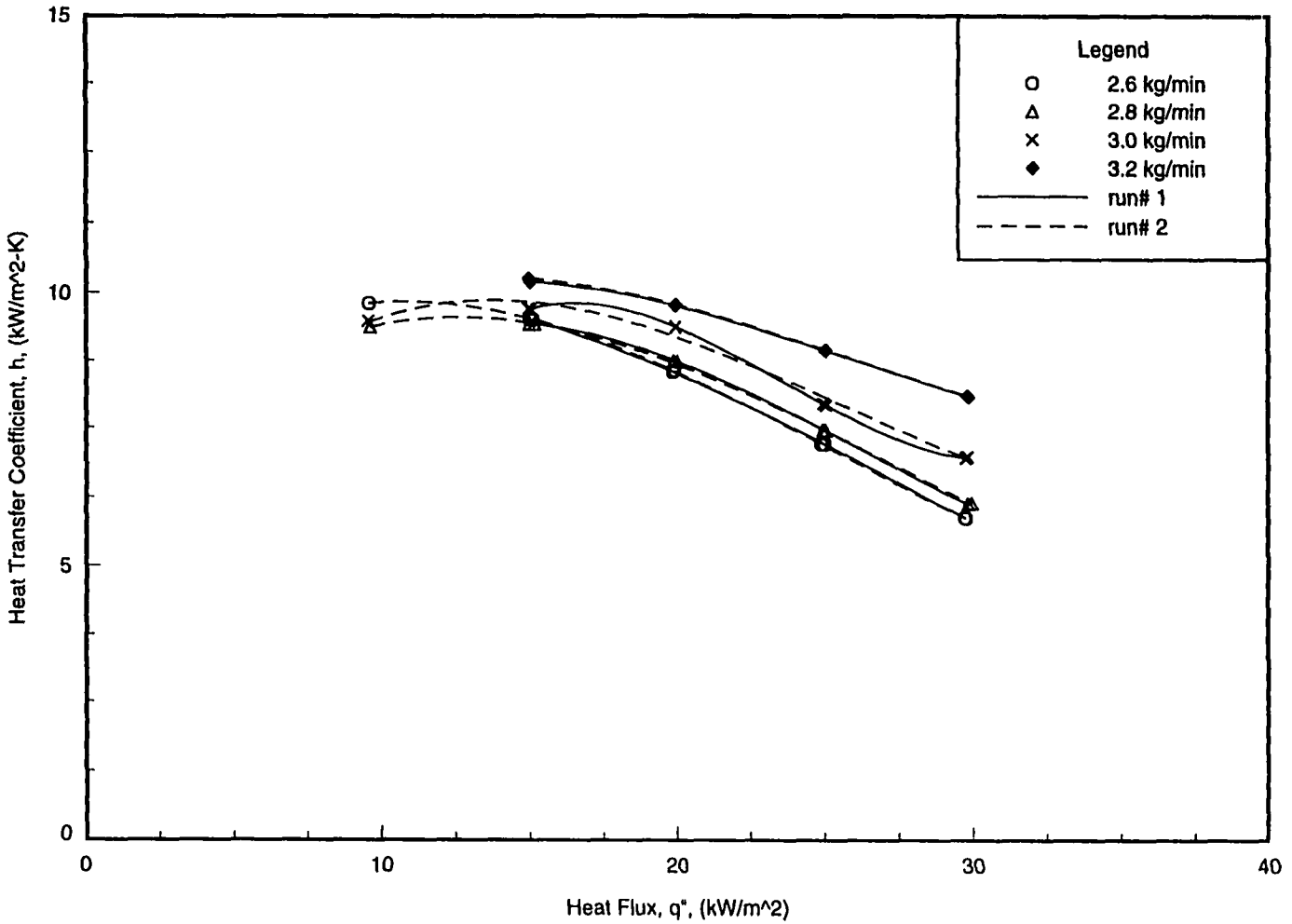

Figure 7.2 Spray evaporation heat transfer coefficients of HFC-236ea for the Turbo-CII tube (D= 19.1 mm) at T_{sat}= 2°C

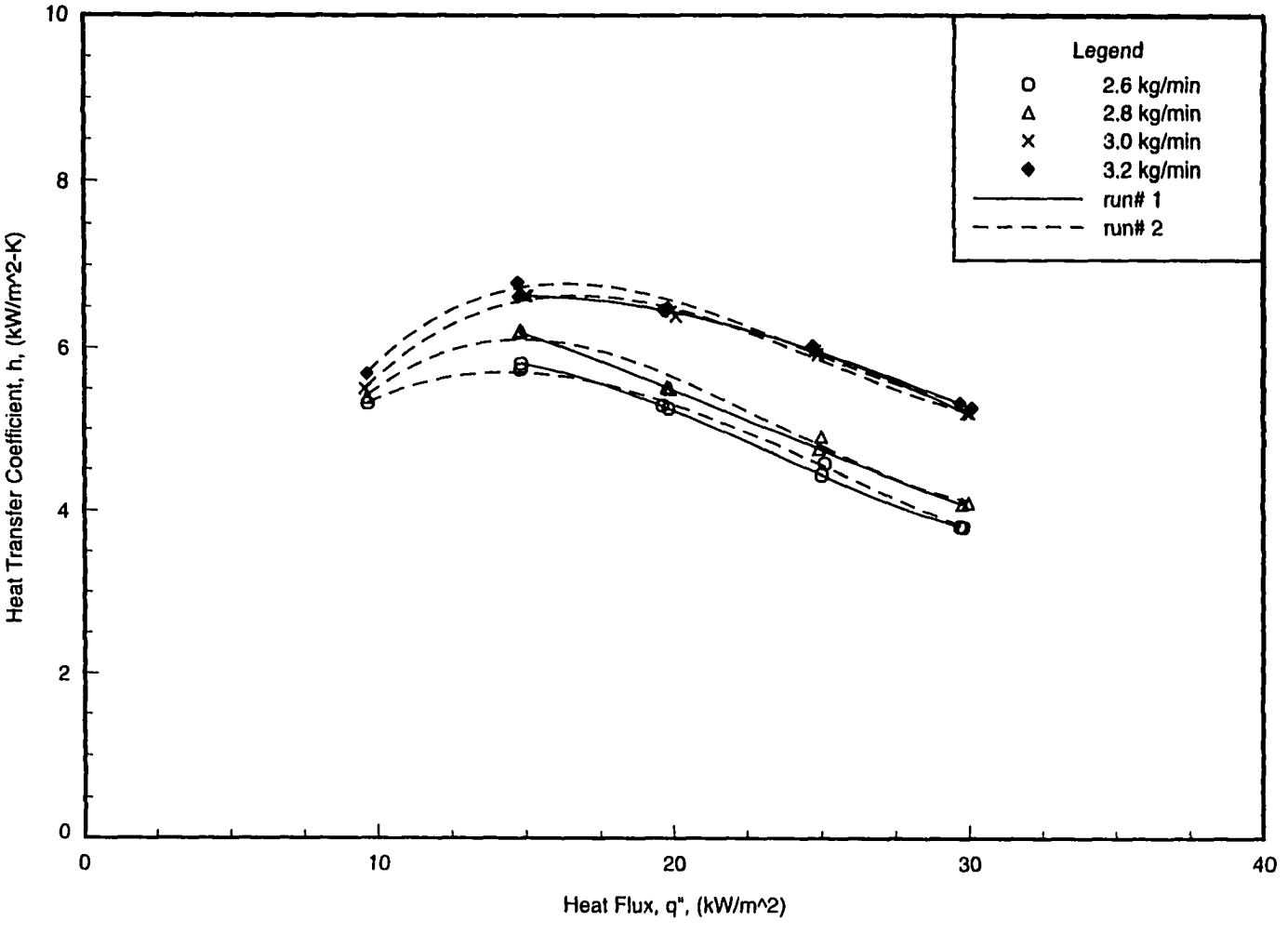

Figure 7.3 Spray evaporation heat transfer coefficients of HFC-236ea for the 1575-fpm tube (D= 19.1 mm) at T_{sat}= 2°C

It can be noted that the hysteresis effect is clearly present in the boiling curves for the Turbo-B tube at low feed rates (Figure 7.1). The increasing heat flux curve deviated from the decreasing heat flux curve since the wall superheat required for boiling with increasing heat flux was larger than that with decreasing heat flux. The hysteresis effects can be avoided by running all the experiments in order of decreasing heat loads.

Effects of feed rates

The effects of feed rates on the heat transfer behavior at various heat fluxes are shown in Figures 7.4 through 7.6 for the Turbo-B tube, Turbo-CII tube, and 1575-fpm tube, respectively.

The heat transfer coefficients for these three tubes tested were found to weakly depend on the feed rates below the heat flux of 15 kW/m^2, but strongly on them beyond this critical value. In other words, the feed rates had almost no effect on the heat transfer coefficients before dry-out phenomena occurred, but had significant influence on them afterwards.

The dry-out phenomena which began to occur at the low heat flux of 15 kW/m^2 were mainly caused by the low effective flow rates on the tube surface. Figures 7.4 through 7.6 indicate that the heat transfer coefficient generally increased as the feed rate increased when dry-out phenomena occurred on the tube. For the enhanced Turbo-B tube tested at 30 kW/m^2, a considerable increase of 45% was obtained with a raise in spray mass flow rate from 2.6 kg/min to 3.2 kg/min. Higher heat transfer coefficients were also observed at higher feed rates in the results reported by Moeykens and Pate [53]. Figure 7.6 for the 1575-fpm tube shows that there was no significant improvement in the heat transfer as the feed rate increased from 3 kg/min to 3.2 kg/min.

Effects of tube types

The effects of tube types on the heat transfer performance are demonstrated in Figure 7.7 plotted in terms of heat transfer coefficient versus heat flux at the feed rate of 3.0 kg/min.

The three tube types tested had a similar trend in the change of heat transfer coefficients with varing heat flux. The Turbo-B tube produced approximately 1.1 to 1.2 times the heat transfer coefficients of the Turbo-CII tube, and 1.5 to 2.0 times those of the 1575-fpm tube. The heat transfer enhancement of the Turbo-B tube over the Turbo-CII tube and over the 1575-fpm tube for different feed rates and heat fluxes is listed in Table 7.2. The decreased enhancement values listed in Table 7.2 with increasing heat flux indicate that the difference in tube surface geometries disappeared when dry-out phenomena became significant at higher heat fluxes.

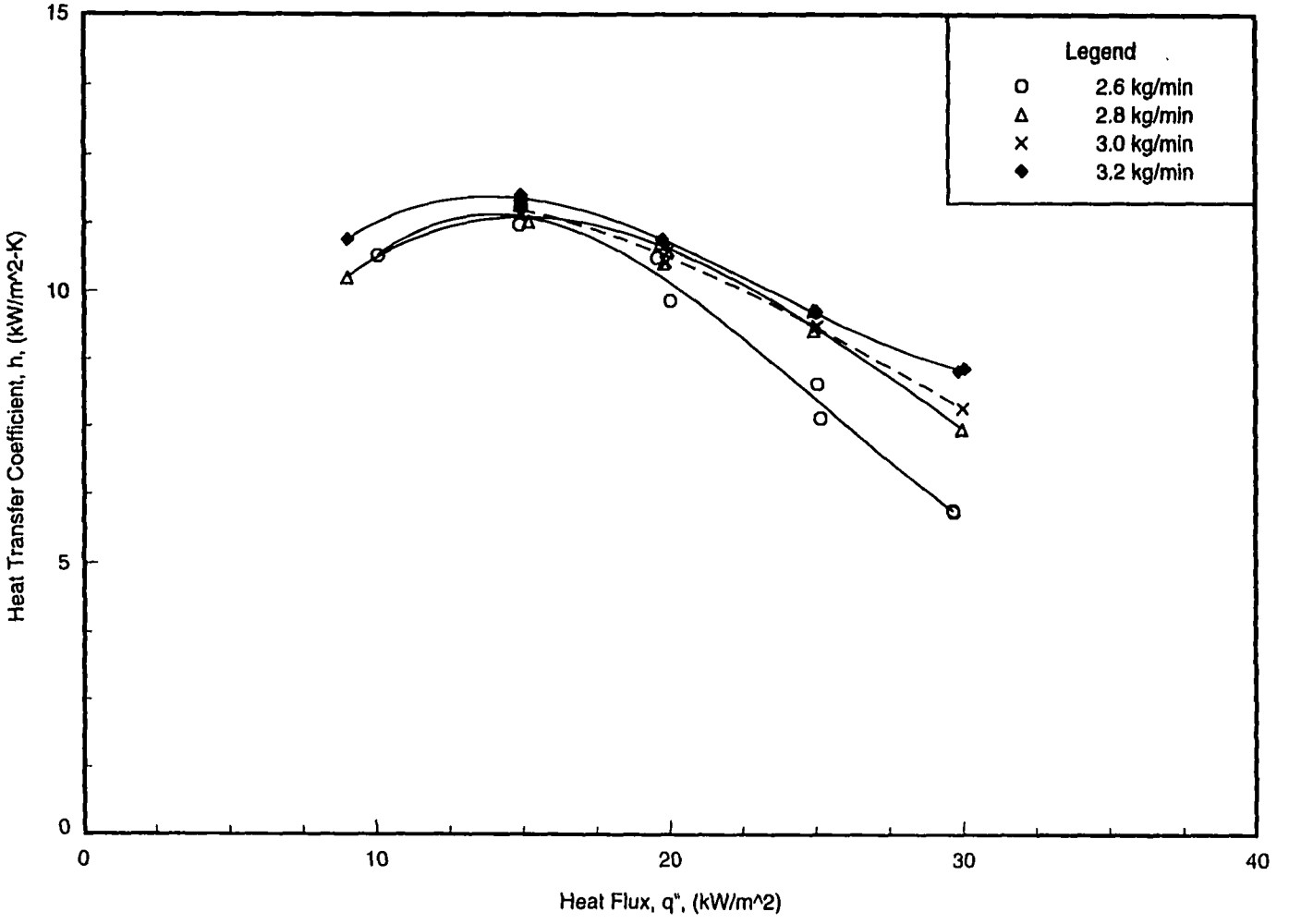

Figure 7.4 Effects of feed rates on the spray evaporation heat transfer coefficients of HFC-236ea for the Turbo-B tube (D= 19.1 mm) at T_{sat}= 2°C

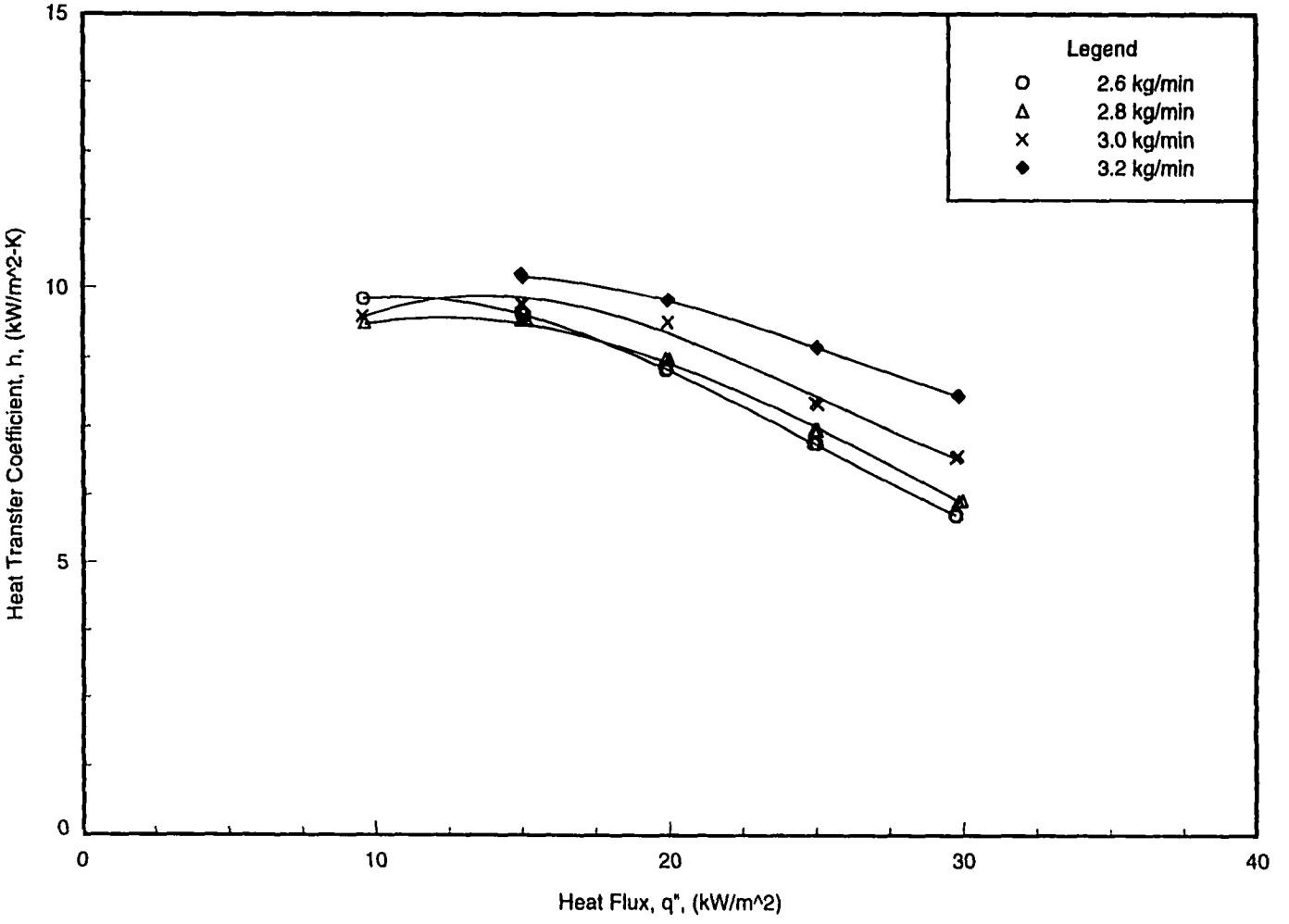

Figure 7.5 Effects of feed rates on the spray evaporation heat transfer coefficients of HFC-236ea for the Turbo-CII tube (D= 19.1 mm) at T_{sat}= 2°C

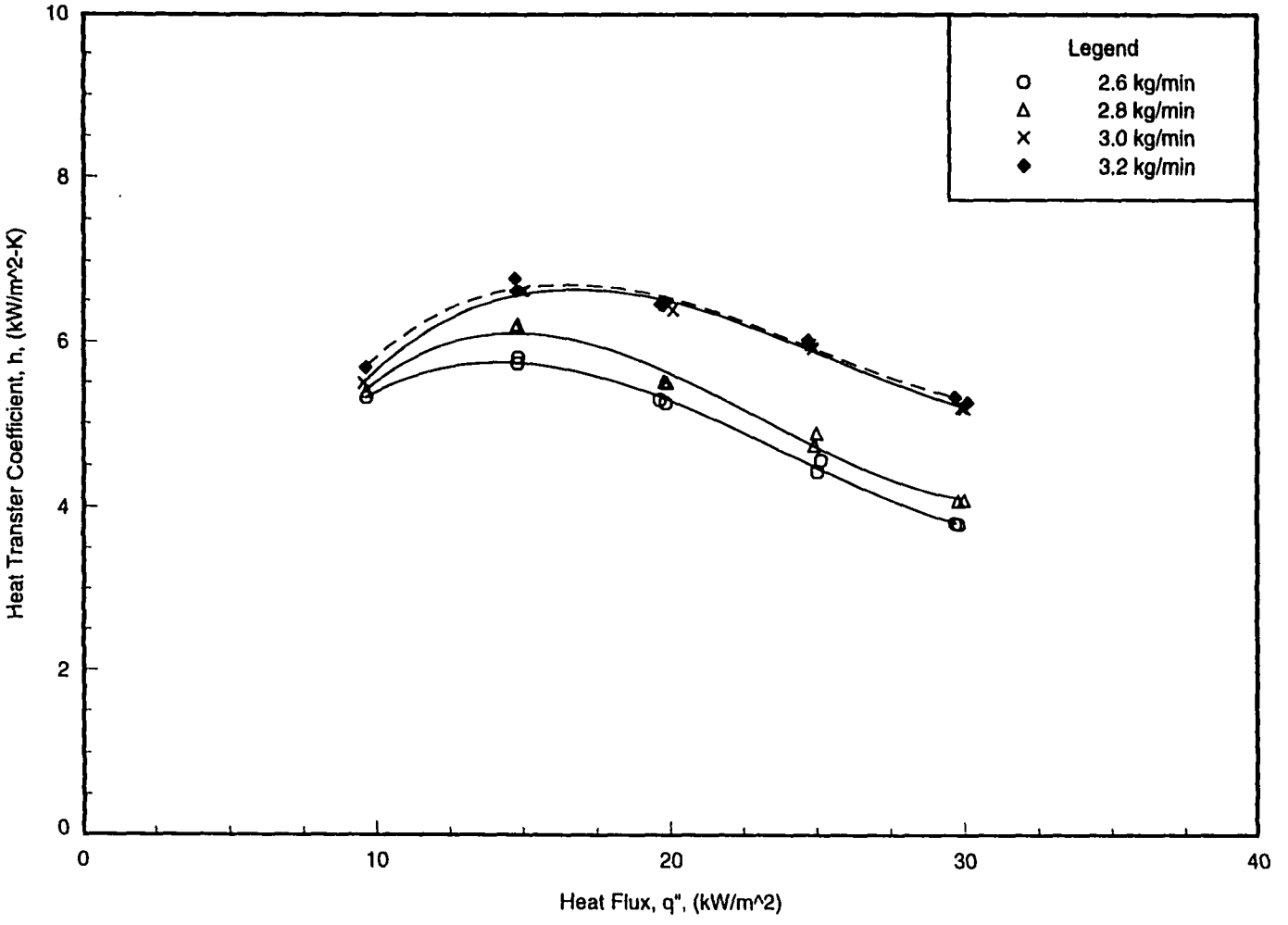

Figure 7.6 Effect of feed rates on the spray evaporation heat transfer coefficients of HFC-236ea for the 1575-fpm tube (D= 19.1 mm) at T_{sat}= 2°C

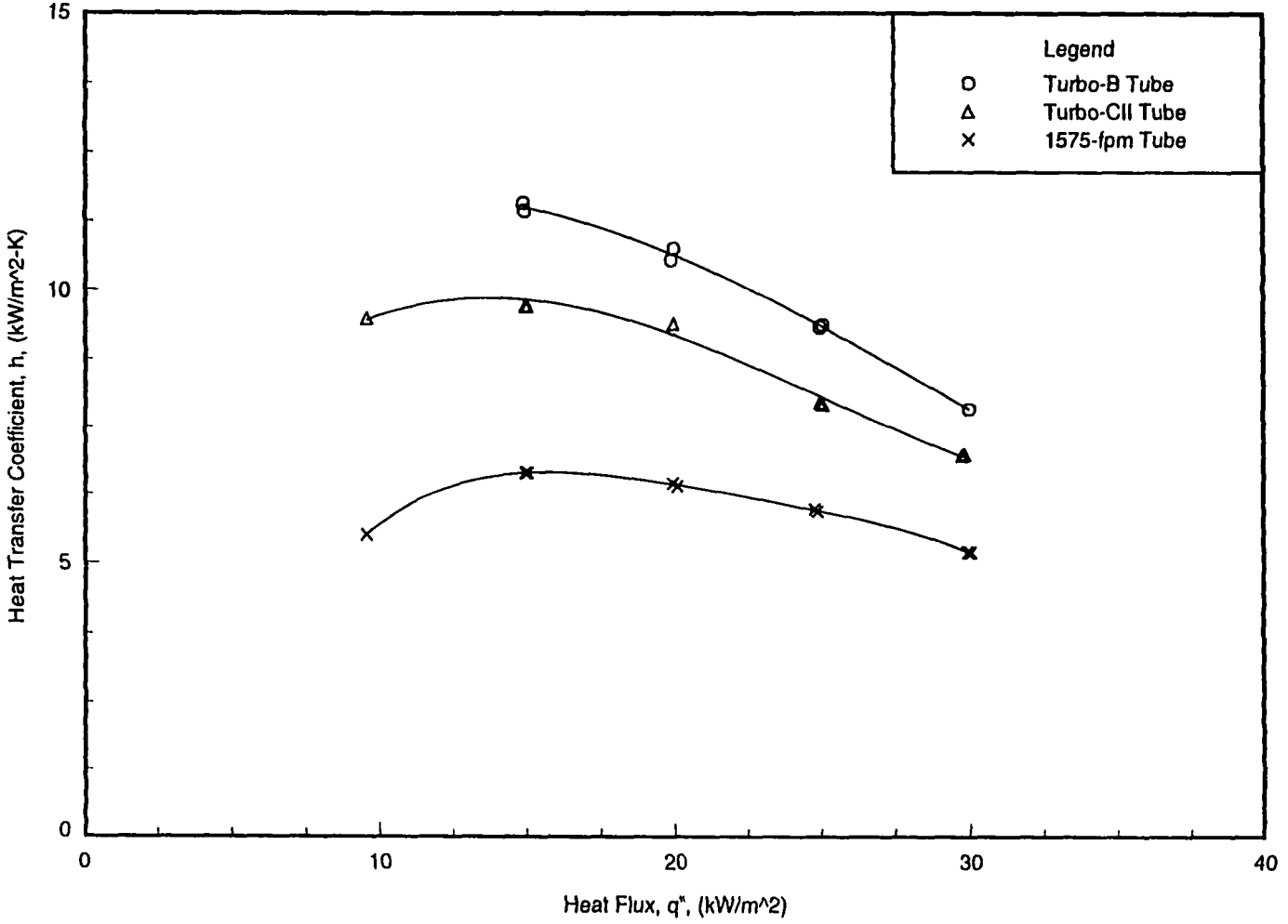

Figure 7.7 Effects of tube types on the spray evaporation heat transfer coefficients of HFC-236ca at $\dot{m}_{spr}$= 3.0 kg/min, T_{sat}= 2°C

Table 7.2 Heat tansfer enhancement for spray-evaporation testing

Spray rate (kg/min)	Heat transfer enhancement	Heat flux		
		15 kW/m^2	20 kW/m^2	30 kW/m^2
2.6	Turbo-B/Turbo-CII	1.2	1.2	1.0
	Turbo-B/1575-fpm	2.0	1.9	1.6
2.8	Turbo-B/Turbo-CII	1.2	1.2	1.2
	Turbo-B/1575-fpm	1.9	1.9	1.8
3.0	Turbo-B/Turbo-CII	1.2	1.1	1.1
	Turbo-B/1575-fpm	1.7	1.7	1.5
3.2	Turbo-B/Turbo-CII	1.2	1.1	1.1
	Turbo-B/1575-fpm	1.8	1.7	1.6

The Turbo-B tube which is designed for enhancing pool boiling provided the highest performance of spray evaporation among the tube types tested, followed by the enhanced condensation Turbo-CII tube. The 1575-fpm tube performed worst. The circular fins of the finned tube restricted the longitudinal movement of liquid and contributed to the bad performance. Film evaporation requires a mechanism to spread a thin film on the fin surface and maintain it fully wet. Repeatability runs are shown in Figures 7.8 and 7.9 for the Turbo-B tube, Figures 7.10 and 7.11 for the Turbo-CII tube, and Figure 7.12 for the 1575-fpm tube at the feed rate of 3.0 kg/min.

Effects of temerature difference

The effects of temerature difference on the heat transfer coefficient are presented in Figure 7.13 plotted in terms of heat transfer coefficient versus excess temperature at the feed rate of 3.0 kg/min.

Figure 7.13 indicates that the Turbo-B tube gave larger heat transfer coefficients than the Turbo-CII tube and 1575-fpm tube at the same excess temperature. In other words, the Turbo-B tube produced the smallest temperature difference among all the three tubes tested at a given heat flux, because it provided the highest heat transfer coefficient of all, while the 1575-fpm tube having the worst performance produced the largest temperature difference at a given heat flux.

Heat transfer performance at high heat loads

Dry patches occur when the liquid feed rate is relatively low compared to the high heat load present, and they first appear on the top surface of a tube where the film is thinnest around the tube.

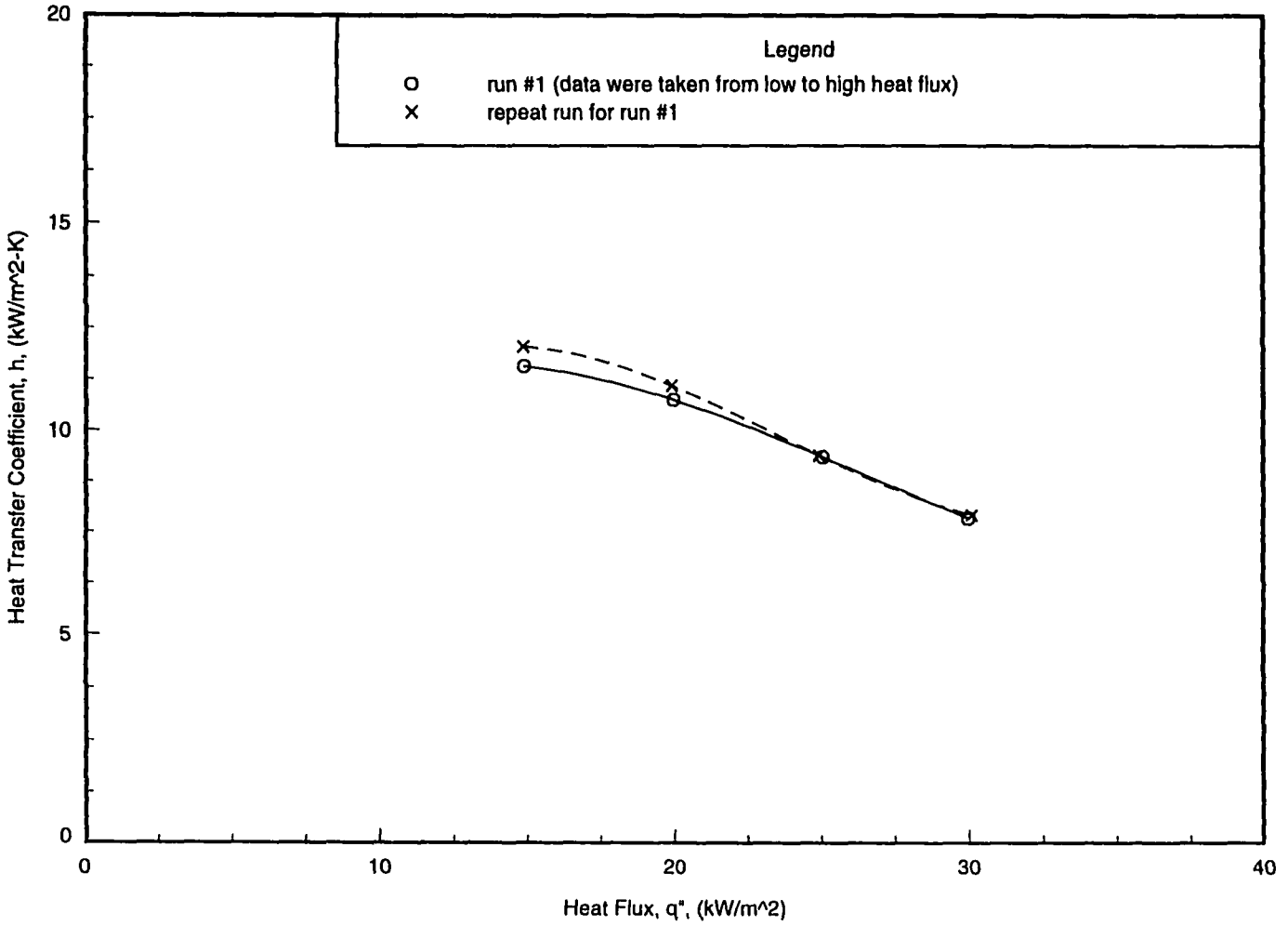

Figure 7.8 Repeatability for spray evaporation of HFC-236ea on the Turbo-B tube (D= 19.1 mm) at $\dot{m}_{spr}$= 3.0 kg/min (data were taken from low to high heat flux)

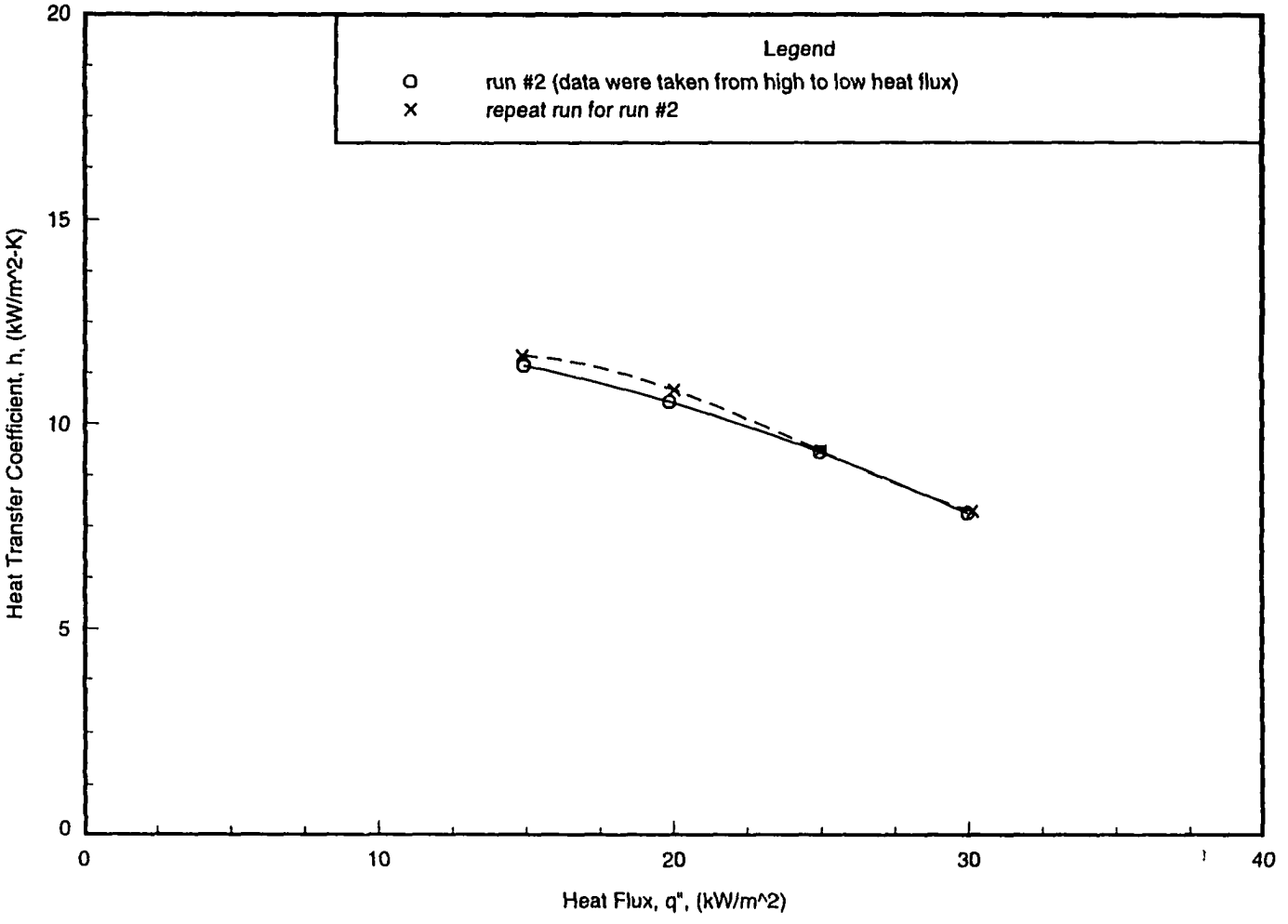

Figure 7.9 Repeatability for spray evaporation of HFC-236ea on the Turbo-B tube (D= 19.1 mm) at $\dot{m}_{spr}$= 3.0 kg/min (data were taken from high to low heat flux)

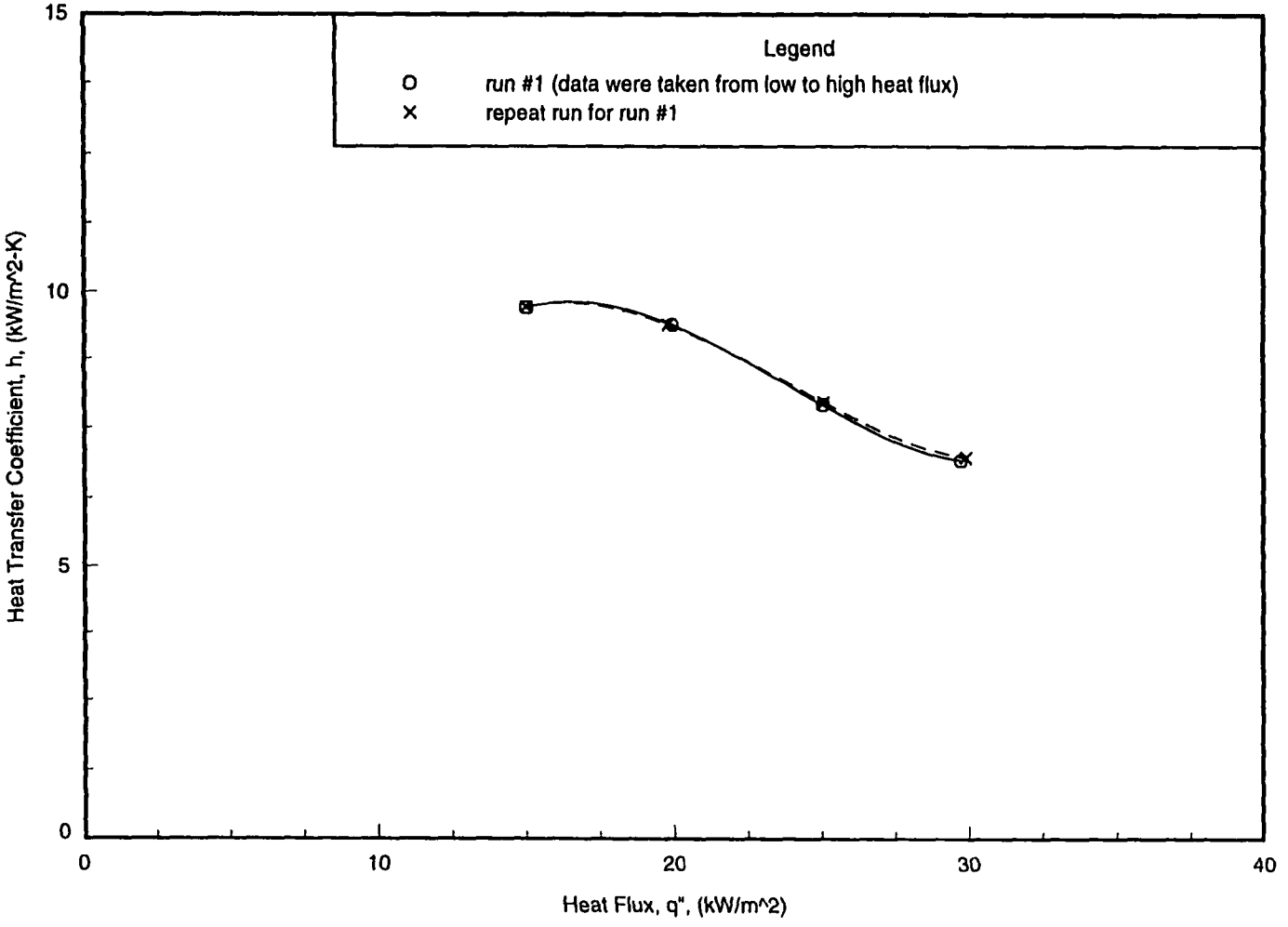

Figure 7.10 Repeatability for spray evaporation of HFC-236ea on the Turbo-CH tube (D= 19.1 mm) at $\dot{m}_{spr}$= 3.0 kg/min (data were taken from low to high heat flux)

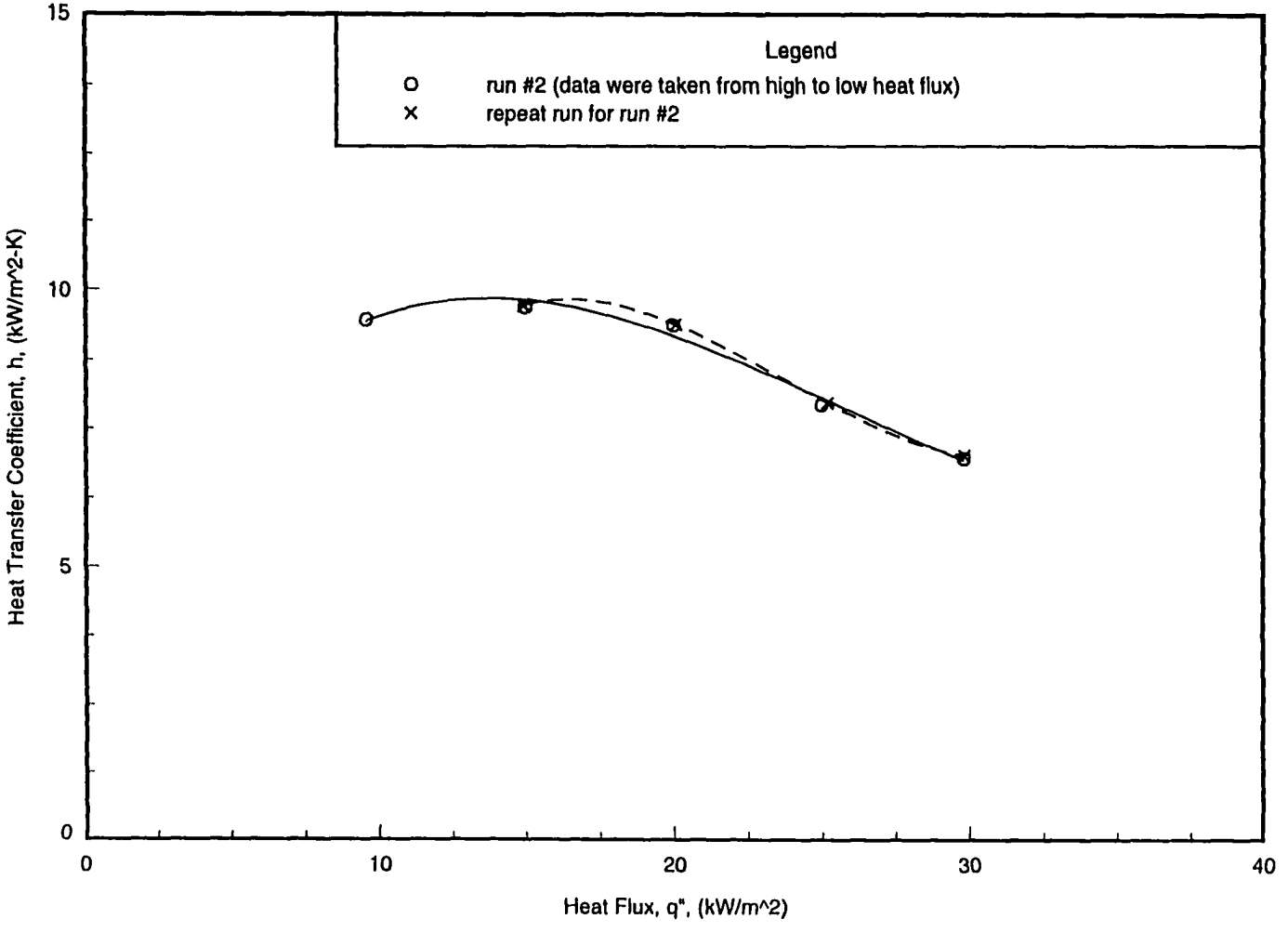

Figure 7.11 Repeatability for spray evaporation of HFC-236ea on the Turbo-CII tube (D= 19.1 mm) at $\dot{m}_{spr}$= 3.0 kg/min (data were taken from high to low heat flux)

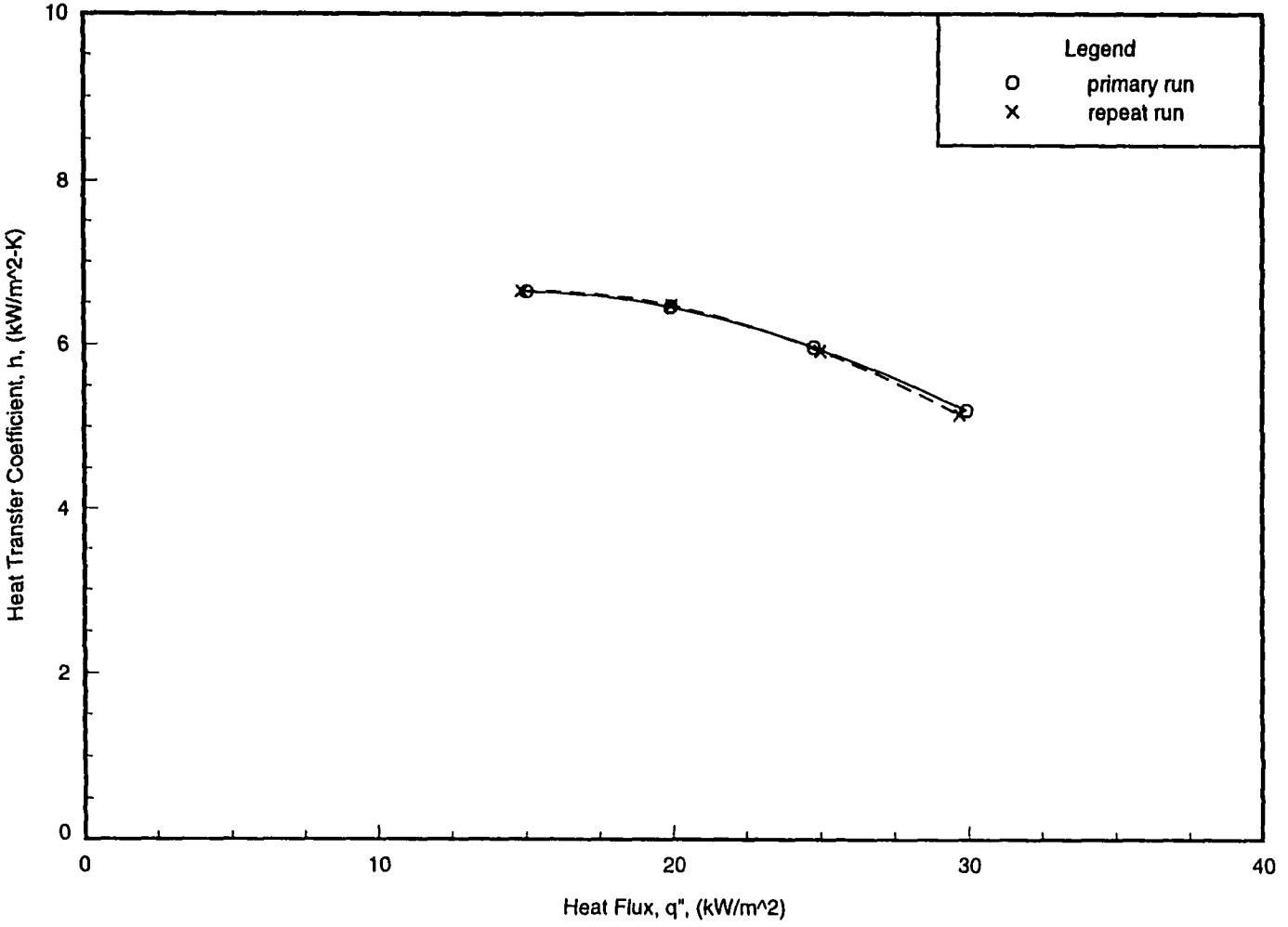

Figure 7.12 Repeatability for spray evaporation of HFC-236ea on the 1575-fpm tube (D= 19.1 mm) at $\dot{m}_{spr}$= 3.0 kg/min (data were taken from low to high heat flux)

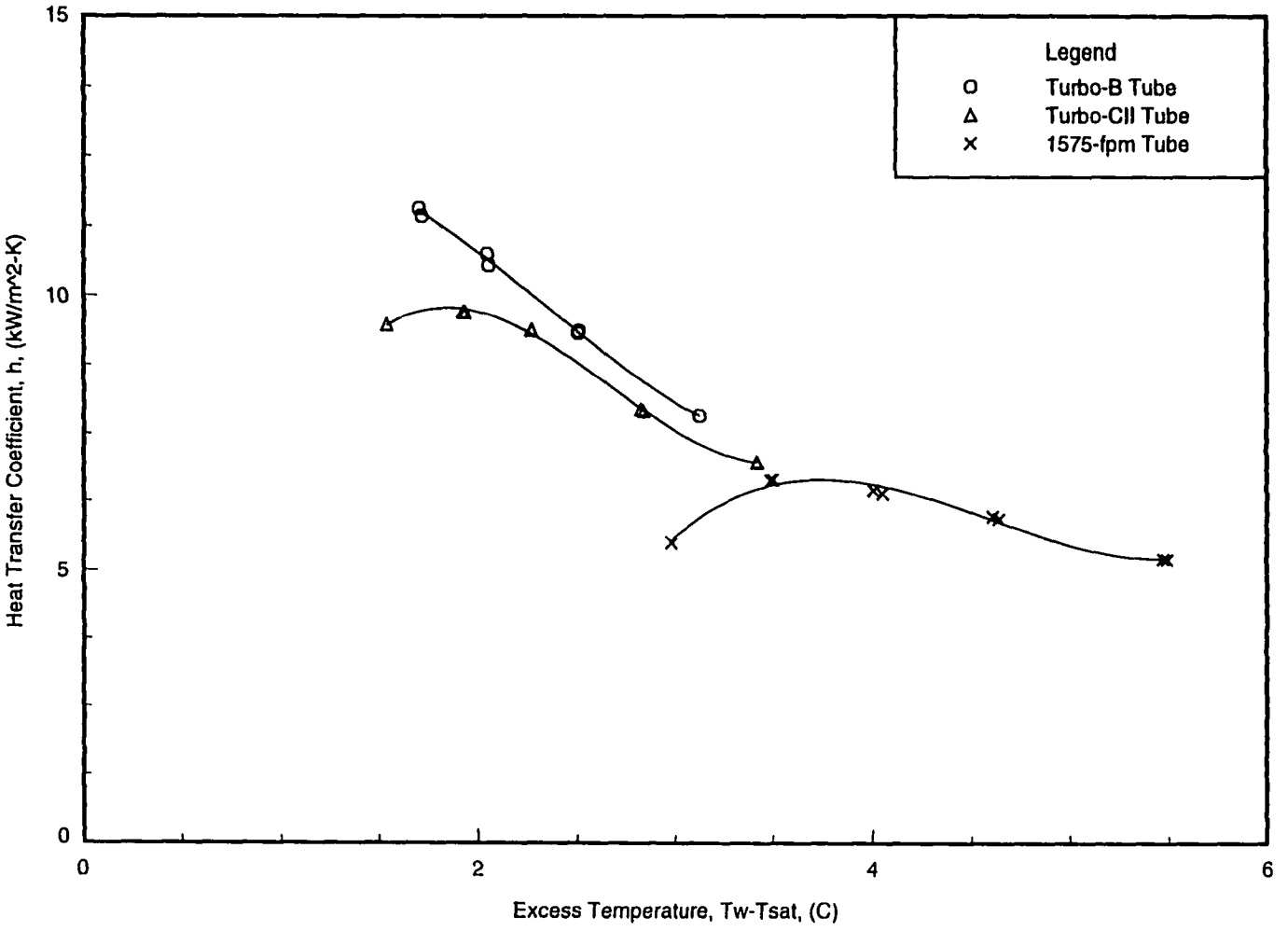

Figure 7.13 Temperature difference effects on the spray evaporation heat transfer coefficients of HFC-236ea for the Turbo-B, Turbo-CII, and 1575-fpm tubes (D= 19.1 mm) at $\dot{m}_{spr}$= 3.0 kg/min and T_{sat}= 2°C

Since the effective feed flow rate was limited by the pumping power in present study, data were not taken at high heat flux where dry-out phenomena were significant. The dry-out problem at high heat flux can be avoided by techniques which improve the effective liquid distribution onto the tube. For instance, the liquid can be distributed directly onto the tube.

Comparison of spray evaporation with pool boiling

The comparative performance of spray evaporation with pool boiling for the Turbo-B tube and 1575-fpm tube is shown in Figure 7.14 and Figure 7.15, respectively.

For both the tube types, spray-film evaporation resulted in higher heat transfer and was more efficient than pool boiling at lower heat loads. The turbulent environment generated by the spray and impingement of droplets was beneficial to the heat transfer of spray evaporation, while in pool boiling the quiescent liquid was not stirred much by low bubble density at low heat loads. Moreover, the external force of droplet impingement increased the energy of liquid molecules on the tube to overcome the binding energy within them, and thus contributed to increase the evaporation rate of spray evaporation.

However, the superiority of spray evaporation performance over pool boiling performance disappeared when nucleate boiling was completely established in pool boiling at high heat fluxes, while dry-out phenomena appeared and became significant for spray evaporation with increasing heat loads. The phenomena observed here are consistent with the results published by Moeykens and Pate [53]. Their results also indicate that the superiority in heat transfer for spray evaporation over pool boiling only existed at low heat loads.

In general, spray evaporation provided better heat transfer performance below the heat flux of 30 kW/m^2 compared with pool boiling, but tended to equal or be less beyond this heat flux. At the heat flux of 15 kW/m^2, the heat transfer performance of the Turbo-B tube in spray evaporation was approximately 2.3 times that in pool boiling and the performance of the 1575-fpm tube in spray evaporation was 1.2 times as large as the value in pool boiling. While at the heat flux of 30 kW/m^2, the boiling coefficients in these two different heat transfer forms were similar for both the Turbo-B tube and 1575-fpm tube.

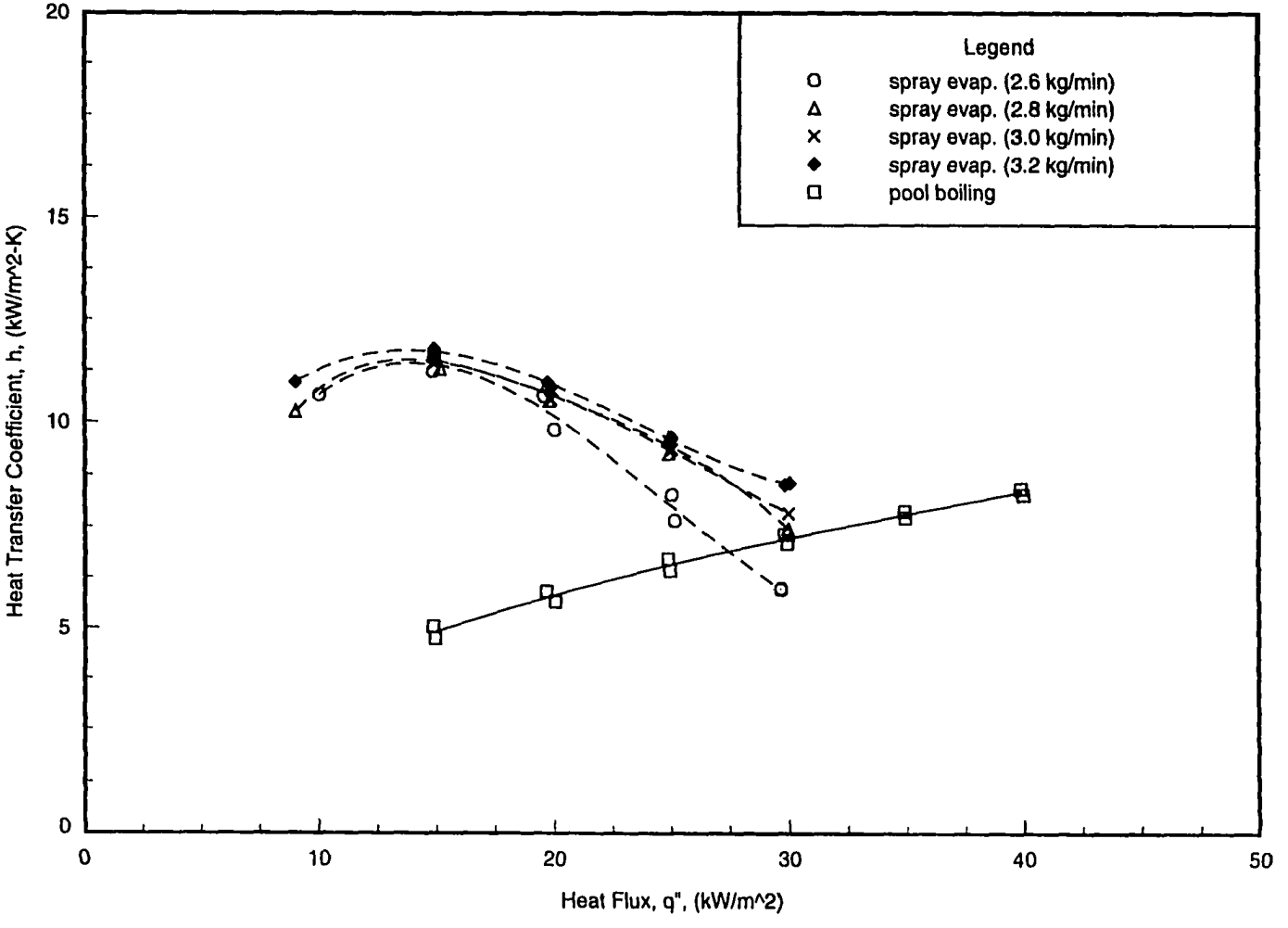

Figure 7.14 Comparison of pool boiling and spray evaporation heat transfer coefficients of HFC-236ea for the Turbo-B tube (D= 19.1 mm) at T_{sat}= 2°C

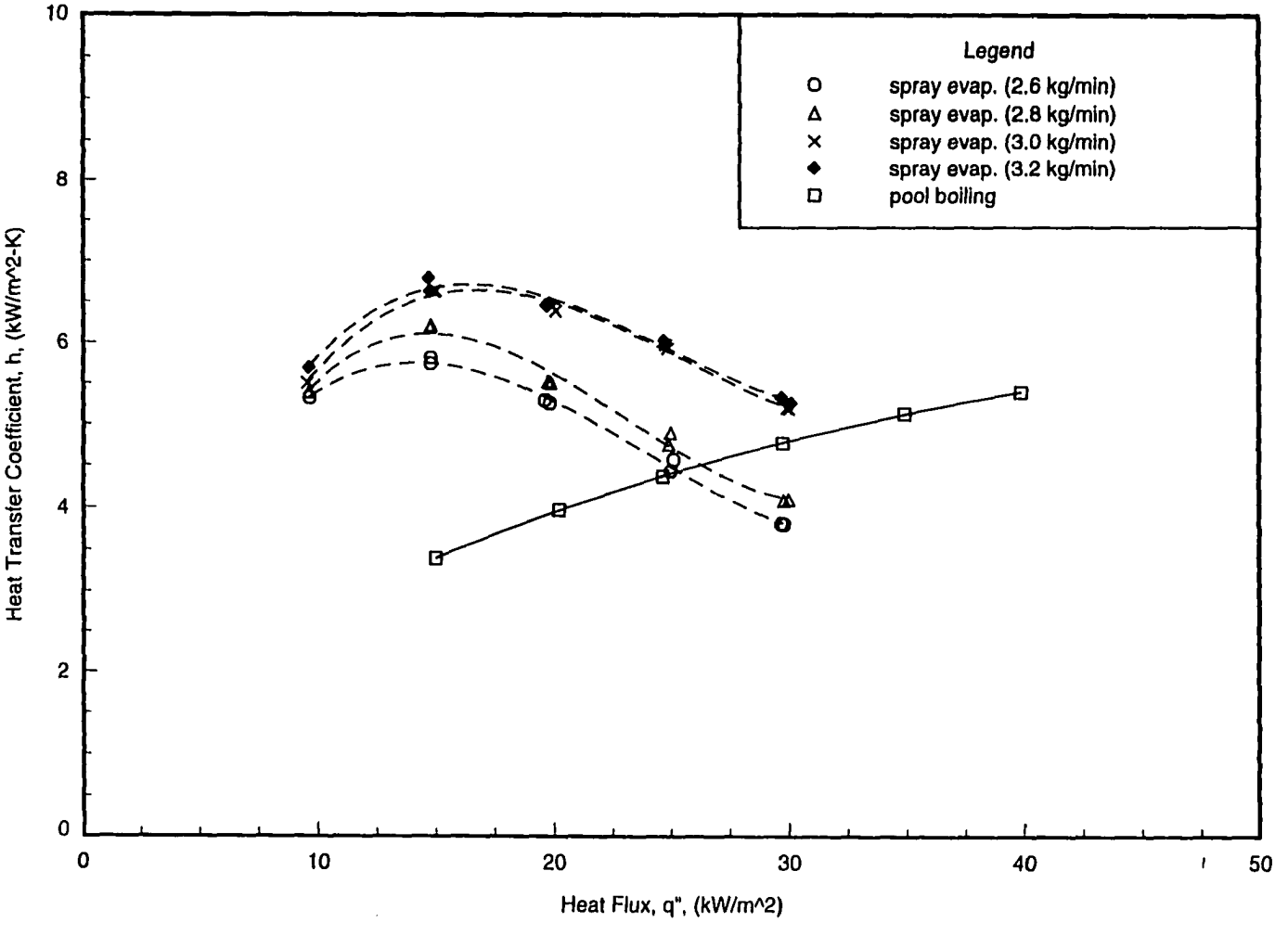

Figure 7.15 Comparison of pool boiling and spray evaporation heat transfer coefficients of HFC-236ea for the 1575-fpm tube (D= 19.1 mm) at T_{sat}= 2°C

Comparison of data with published results

The present spray evaporation data for the Turbo-B, Turbo-CII, and 1575-fpm tubes tested with HFC-236ea were compared with those with HFC-134a by Moeykens and Pate [54] in Figures 7.16 through 7.18, respectively. All the data shown in Figures 7.16 through 7.18 were taken at T_{sat}= 2°C in the same test section having the same spray system. The tubes compared had the same tube diameter and were made from the same manufacturer.

The distinguishing difference between the two data sources is that the single tube tested for HFC-134a was a single pass located in the radial center of the test section, while the single tube tested for HFC-236ea was composed of two horizonal passes arranged side by side. The detailed configuration of test section is referred to Figure 5.4. In addition, the refrigerant was heated by a cartridge heater in the tests of HFC-134a, while the energy for boiling of HFC-236ea was provided by hot water.

The effective liquid distribution onto a single-pass tube should be similar to that onto a double-pass tube if the tube is located in the same spray zone. The data for a single-pass tube should be comparable with those for a double-pass tube before dry-out phenomena became significant, since experimental results have shown that heat transfer coefficients were almost independent of feed flow rates before the tube surface dries out. The performance of single-pass tube and double-pass tube will be comparable as long as the tube is fully wetted.

Comparison of both the HFC-134a and HFC-236ea data shows that the heat transfer coefficients of HFC-134a are generally lower than those of HFC-236ea for the Turbo-B tube (Figure 7.16), while for both the Turbo-CII tube (Figure 7.17) and 1575-fpm tube (Figure 7.18) the HFC-134a coefficients are higher than the HFC-236ea values.

For the Turbo-CII and 1575-fpm tubes, the higher heat transfer coefficients gained by thin film evaporation of HFC-134a compared with HFC-236ea. These results agree with the general trend observed in the published studies in that high pressure refrigerants showed to yield higher evaporation heat transfer coefficients than low pressure refrigerants. The boiling coefficient ratios of HFC-134a to HFC-236ea for the Turbo-B tube show inconsistently low. The reason for this is probably because the Turbo-B tube performed anomalously worse than the Turbo-CII tube in the tests of HFC-134a reported by Moeykens and Pate [54]. The enhanced boiling Turbo-B tube generally performs better than the enhanced condensation Turbo-CII tube in evaporation.

Table 7.3 provides the boiling coefficient ratios of HFC-134a to HFC-236ea at the feed flow rate of 2.8 kg/min. As shown in the table, the boiling coefficient ratios for the Turbo-CII and 1575-fpm tubes are generally greater than one, while for the Turbo-B tube they are less than one.

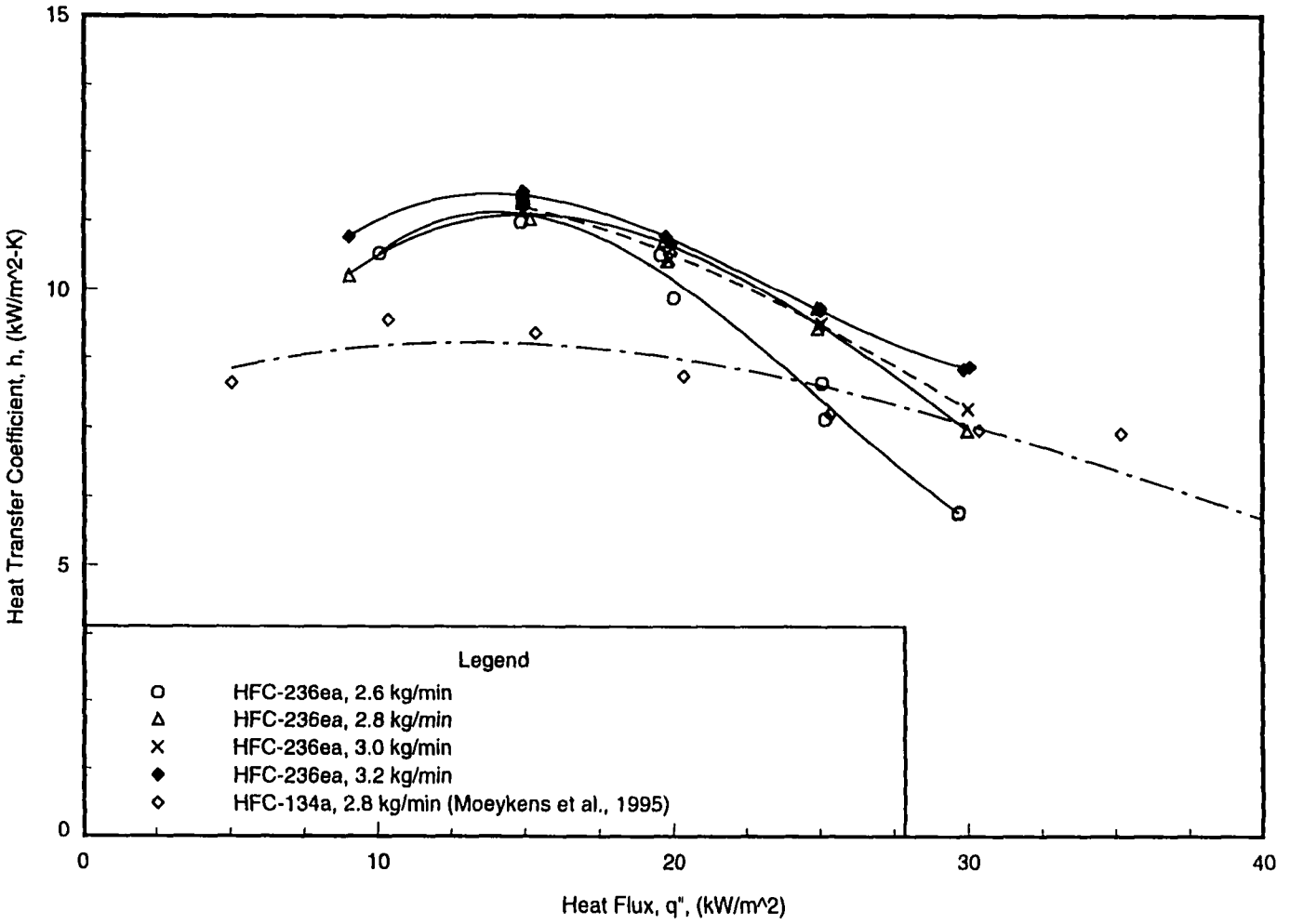

Figure 7.16 Comparison of spray evaporation data with Moeykens et al. (1995) for the Turbo-B tube (D= 19.1 mm) at T_{sat}= 2°C

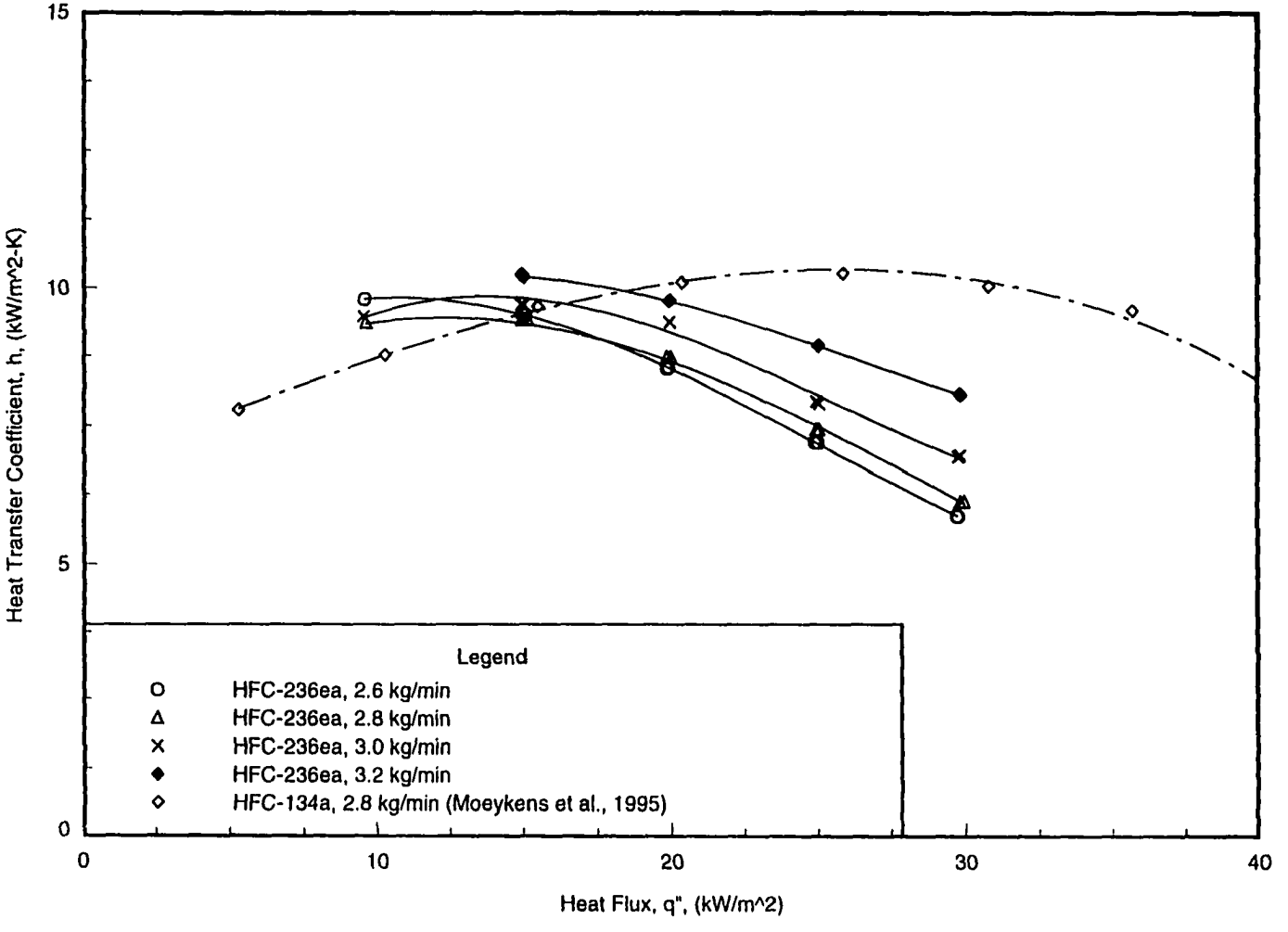

Figure 7.17 Comparison of spray evaporation data with Moeykens et al. (1995) for the Turbo-CII tube (D= 19.1 mm) at T_{sat}= 2°C

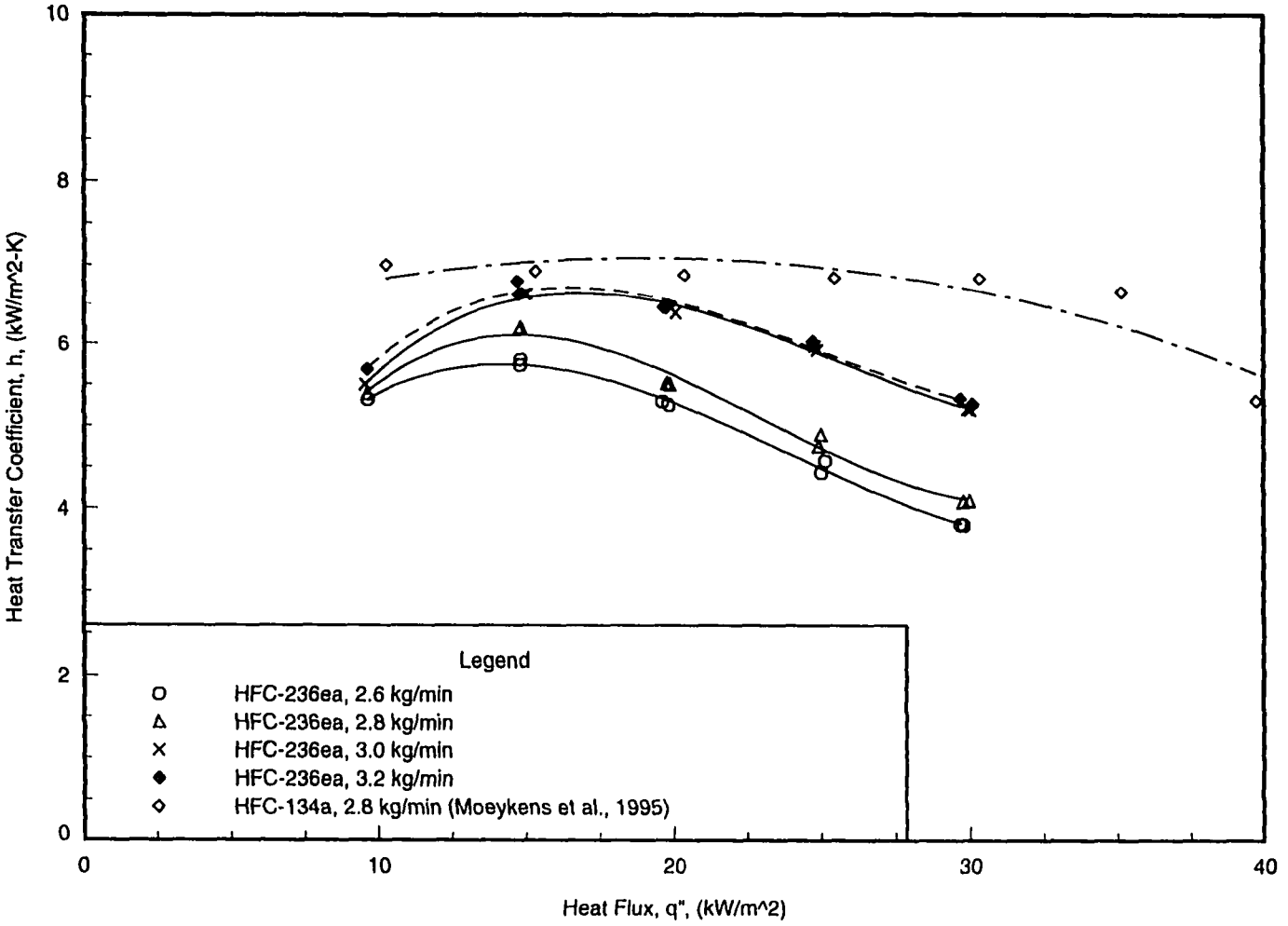

Figure 7.18 Comparison of spray evaporation data with Moeykens et al. (1995) for the 1575-fpm tube (D= 19.1 mm) at T_{sat}= 2°C

Table 7.3 Boiling coefficient ratio of HFC-134a to HFC-236ea at 2.8 kg/min

Heat flux (kW/m^2)	Boiling coefficient ratio (HFC-134a/HFC-236ea)		
	Turbo-B tube	Turbo-CII tube	1575-fpm tube
10	0.92	0.94	1.30
15	0.79	1.03	1.12
20	0.79	1.16	1.25
25	0.82	1.39	1.42
30	1.00	1.64	1.67

As shown in Figures 7.16 through 7.18, the heat transfer coefficients of HFC-236ea were relatively sensitive to the change of heat fluxes. This might due to the inherently different characteristics of the two refrigerants such as physical properties. Another possible reason is that the double-pass tube might be subjected to a lower effective refrigerant mass flow rate than the single-pass tube. Table 7.3 shows the boiling coefficient ratio of HFC-134a to HFC-236ea compared at equal feed flow rate increases with increasing heat flux, that is, the boiling coefficient of HFC-236ea decreased faster with increasing heat flux. This might indicate more significant dry-out phenomena occured due to lower effective refrigerant feed flow rates in the tests of HFC-236ea.

Collector tests were performed at the total spray rate of 2.8 kg/min by Moeykens and Pate [53] in order to estimate the percentage of the spray flow rates acturally reaching the tube surface. The fraction of liquid hitting the tube surface was 0.193 for the single-pass tube of 19.1 mm in diameter. It was not possible to measure the effective flow rate over each individual pass of the double-pass tube by using collectors due to the space limitation of test section. However, the low value (19.3%) of the collector test fraction for the single-pass tube tested indicates that the spray zone was relatively wide and most of the refrigerant supplied to the test section missed hitting the tube. Hence, the double-pass tube should be covered in a similar spray zone as the single-pass tube, the effective liquid distribution onto a single-pass tube and a double-pass tube should be similar.

Similar to the developement of the equations for spray evaporation heat transfer coefficients proposed by Moeykens [52], the spray evaporation data of HFC-236ea involving four mass flow rates for three different tubes are correlated with heat flux and total feed mass flow rate and presented in Appendix F.

Summary

The heat transfer coefficients of HFC-236ea were determined for spray evaporation on a Turbo-B, a Turbo-CII, and a 1575-fpm tube. The Turbo-B tube was the best heat transfer tube with HFC-236ea in spray evaporation and provided approximately 1.1 to 1.2 times the heat transfer coefficients of the Turbo-CII tube and 1.6 to 1.8 times the values of the 1575-fpm tube.

At the heat fluxes greater than 15 kW/m^2 where dry-out phenomena became dominant, the heat transfer coefficient dropped, but it was improved as the feed flow rate increased. However, the feed flow rate had almost no effect on the heat transfer coefficient before dry-out phenomena occurred.

The heat transfer coefficients of HFC-236ea were compared for spray evaporation and pool boiling on a 1575-fpm tube and a Turbo-B tube. The results show that these two tubes had better heat transfer performance in spray evaporation than in pool boiling at the heat fluxes less than the approximate value of 30 kW/m^2.

At the heat flux of 15 kW/m^2, the heat transfer performance of the Turbo-B tube and the 1575-fpm tube in spray evaporation was arround 2.3 times and 1.2 times, respectively, the value in pool boiling. While at the heat flux of 30 kW/m^2, the boiling coefficients in these two different heat transfer forms were similar for both of the tubes tested.

CHAPTER 8 CONDENSATION RESULTS

Three tubes with two distinctively different geometries, which include a high performance enhanced (Turbo-CII) tube and two integral-fin (1024-fpm and 1575-fpm) tubes, were tested in this study for shell-side condensation over the heat flux range of 15 kW/m^2 to 40 kW/m^2. The two finned tubes were tested for HFC-236fa and the Turbo-CII tube was tested for both HFC-236ea and HFC-236fa. Their heat transfer performance was compared with each other for the three refrigerants (HFC-236fa, HFC-236ea, and CFC-114) tested in the same test facility.

All the condensation data were collected in a single-tube apparatus at a saturation temperature of 40°C with increasing heat flux. The data for the repeatability run can be seen in all the figures of this chapter. The experiment is shown to be repeatable by comparing the data points for "primary run" and "repeat run". Both runs were taken on different days. The numerical values for all the condensation data are tabulated in Appendix C for HFC-236ea and Appendix D for HFC-236fa.

Condensing coefficients of HFC-236ea

Condensation performance of a Turbo-CII tube

The heat transfer coefficient of HFC-236ea for the Turbo-CII tube shown in Figure 8.1 increased as the heat flux increased. Condensation data published by Huber [37] and Huebsch and Pate [38] show similar trends.

As mentioned in Chapter 5, the Turbo-CII tube was tested twice with different in-tube turbulators in the two tests. In the first test, the heat transfer coefficient dropped markedly as the heat flux increased. The results are consistent with those obtained by Huber et al. [36]. However, as previously mentioned the first test had large uncertainty and therefore was considered to be erroneous. The large uncertainty accompanying the shell-side heat transfer coefficients determined from the first test is consistent with that obtained by Huber et al. [36].

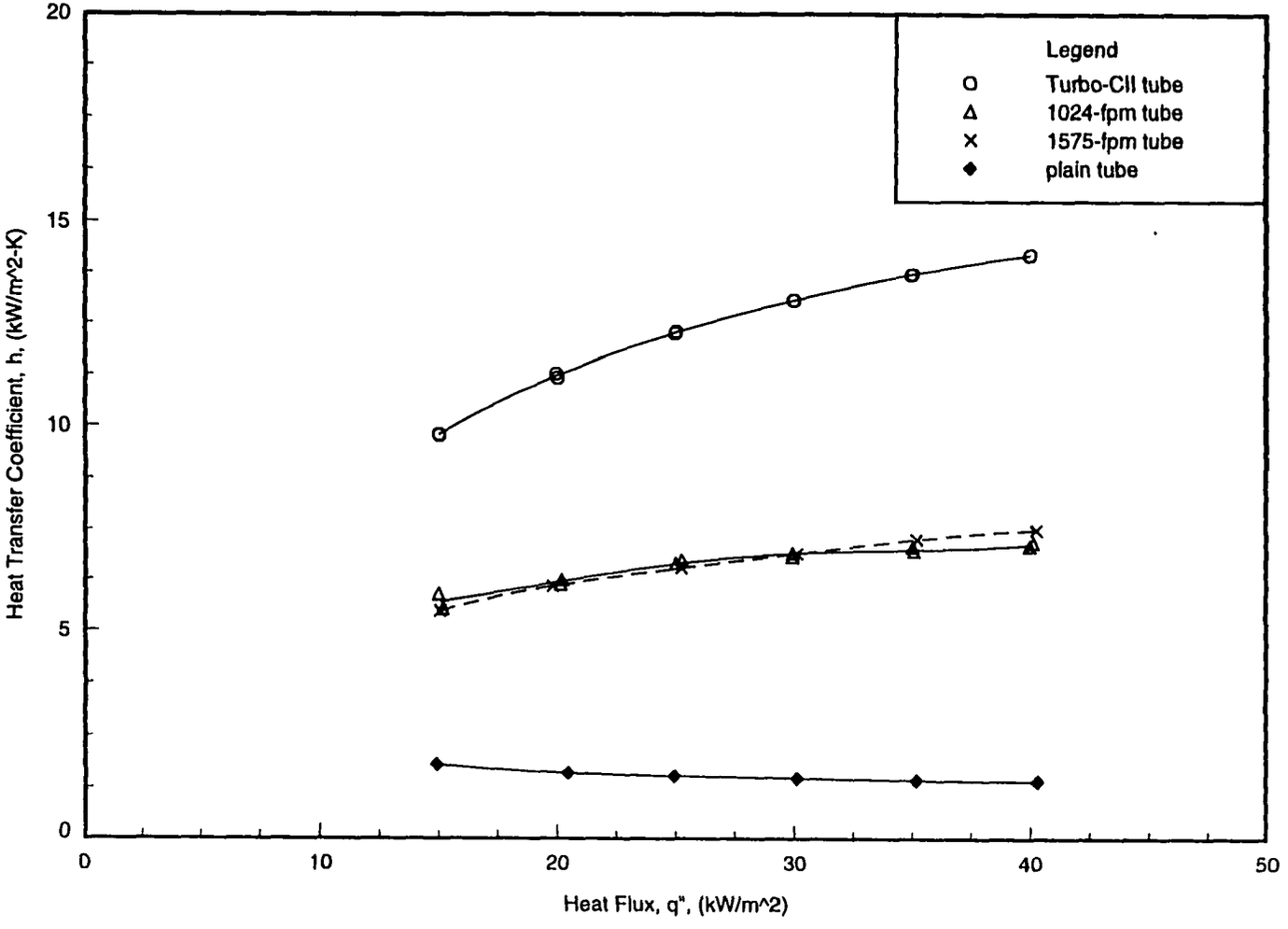

Figure 8.1 Condensation heat transfer coefficients of HFC-236ea for the Turbo-CII, 1024-fpm, 1575-fpm, and plain tubes (D= 19.1 mm) at T_{sat}= 40°C

The uncertainty in the shell-side heat transfer coefficients from the second test was substantially reduced by increasing the in-tube (tube-side) heat transfer coefficients. however, the shell-side heat transfer coefficient calculated in the second test increased as the heat flux increased.

The different in-tube turbulators caused the substantial difference between the two sets of tests. The in-tube turbulator was found to affect not only the in-tube heat transfer coefficient but also the operating temperature of water through the test section. In fact, from the heat transfer rate equation mentioned before, Equation 5.1,

$$q = U_o \cdot A_o \cdot LMTD$$

the in-tube and shell-side heat transfer coefficients (h_i and h), which are incorporated in the overall heat transfer coefficient (U_o), and the logarithmic mean temperature difference ($LMTD$) can be seen to be mutually related. The $LMTD$ is related to the operating temperature of water (see Equation 5.3). Once the in-tube heat transfer coefficient (h_i) is changed with the installation of different in-tube turbulators, the other two variables, h and $LMTD$, will follow h_i to change. It is therefore important to properly equalize the heat transfer coefficients for the two fluids (i.e., h and h_i).

Comparison of the Turbo-CII tube with 1024-fpm, 1575-fpm, and plain tubes

Figure 8.1 shows that the condensation heat transfer coefficient was a function of heat flux for the Turbo-CII tube as well as for the plain, 1024-fpm, and 1575-fpm tubes. As the heat flux increased, the heat transfer coefficient of HFC-236ea increased for the Turbo-CII tube as well as for the 1024-fpm and 1575-fpm tubes, while it decreased for the plain tube.

The Turbo-CII tube produced noticeably higher heat transfer coefficients in condensation than the 1024-fpm, 1575-fpm, and plain tubes. It was found that the two finned tubes had similar performance and the plain tube performed worst among all of the tubes tested. The Turbo-CII tube provided approximately 1.9 times the heat transfer coefficients of the 1024-fpm and 1575-fpm tubes and around 5.4 to 10.1 times the values of the plain tube.

Huber [37] reported that the Turbo-CII tubes produced around two to three times larger heat transfer coefficients of HFC-134a than the 1024-fpm and 1575-fpm tubes based on the average bundle data. The results for the Turbo-CII tubes were around four times those for the 1024-fpm tubes and three times those for the 1575-fpm tubes based on the first-row data.

Figure 8.2 shows the variation of the heat transfer coefficient with the temperature difference between the saturated refrigerant and the tube wall for the existing shell-side condensation data of HFC-236ea over the heat flux range from 15 kW/m^2 to 40 kW/m^2. As the temperature difference increased, the heat transfer coefficient increased for the Turbo-CII tube as well as for the 1024-fpm and 1575-fpm tubes, while it decreased for the plain tube.

Figure 8.2 also shows that the Turbo-CII tube produced the smallest temperature difference among the tube types tested for a given heat flux, meaning that it provided the highest heat transfer coefficient.

Condensing coefficients of HFC-236fa for a Turbo-CII, a 1024-fpm, and a 1575-fpm tube

Figure 8.3 shows that the dependence of the heat transfer coefficient on the heat flux for the tubes tested (a 1024-fpm, a 1575-fpm, and a Turbo-CII tube). The heat transfer coefficients of HFC-236fa increased with increasing heat flux for these three tubes. Condensation data published by Huber [37] and Huebsch and Pate [38] showed similar trends.

As tested with HFC-236ea, the high performance Turbo-CII tube tested with HFC-236fa performed better than the 1024-fpm and 1575-fpm tubes. In fact, the lowest condensing coefficient provided by the Turbo-CII tube was still higher than the highest values provided by the the two finned tubes. Specifically, the Turbo-CII tube provided an increase in heat transfer coefficients around 20% to 80% with respect to the 1024-fpm tube and about 40% to 70% with respect to the 1575-fpm tube.

In another investigations [35] [36] which tested these three tubes but with HFC-134a, the heat transfer coefficients produced by the Turbo-CII tube were found to be approximately two to three times larger, based on the average bundle data, than those of the 1024-fpm and 1575-fpm tubes, while for the first-row data the values were around three times larger than the 1024-fpm tube and two times larger than the 1575-fpm tube.

Figure 8.3 also reveals that the two integral-fin tubes produced similar heat transfer coefficients which were relatively insensitive to the change of heat flux. Conversely, the Turbo-CII tube yielded a sharp change in the heat transfer coefficient with increasing heat flux. These results are consistent with those reported by Huber et al. [36], which also indicated that the decrease in the heat transfer coefficient with increasing heat load was more dramatic for the Turbo-CII tube than for the two finned (1024-fpm and 1575-fpm) tubes.

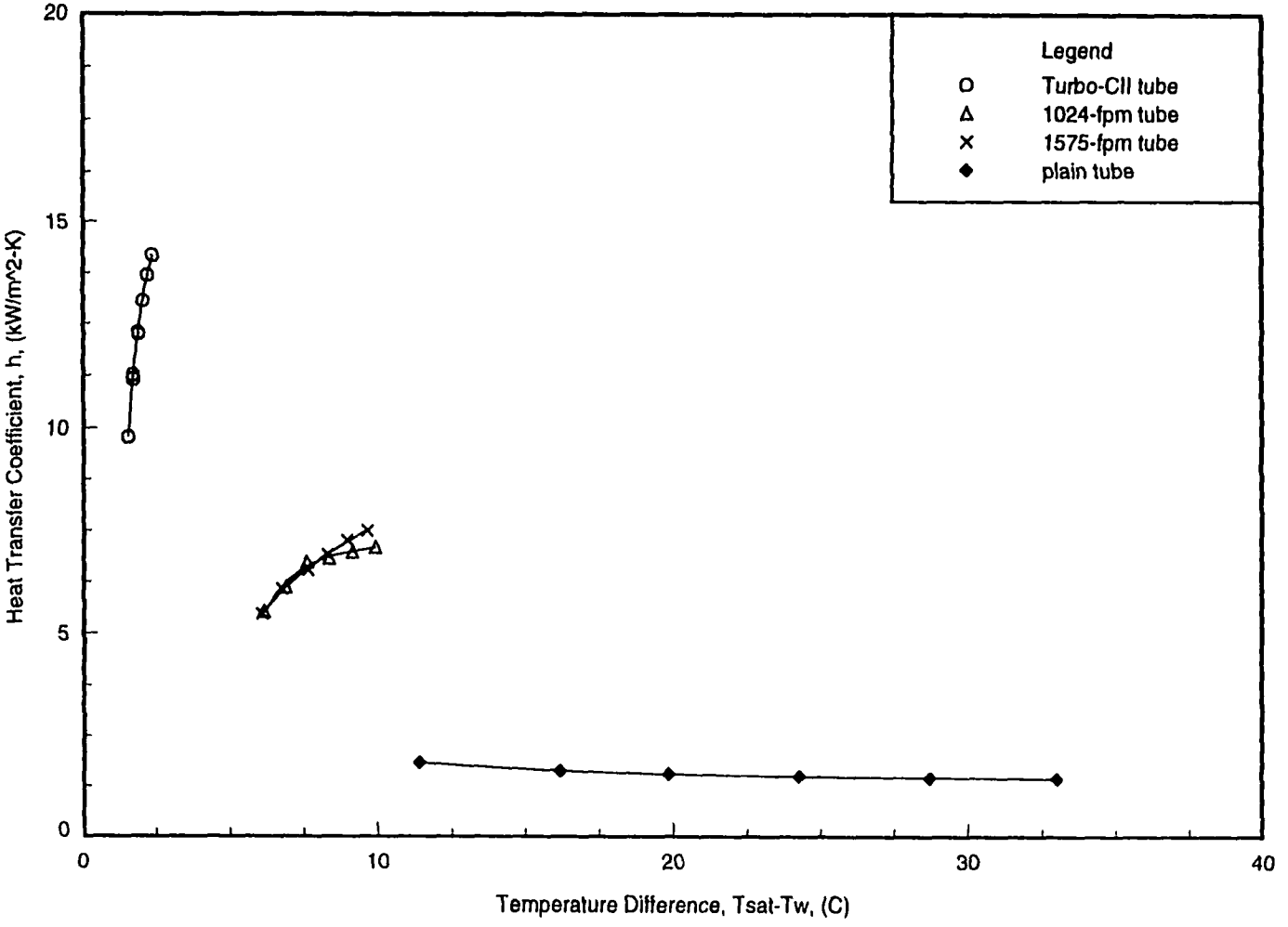

Figure 8.2 Temperature difference effects on the condensation heat transfer coefficients of HFC-236ea at T_{sat}= 40°C

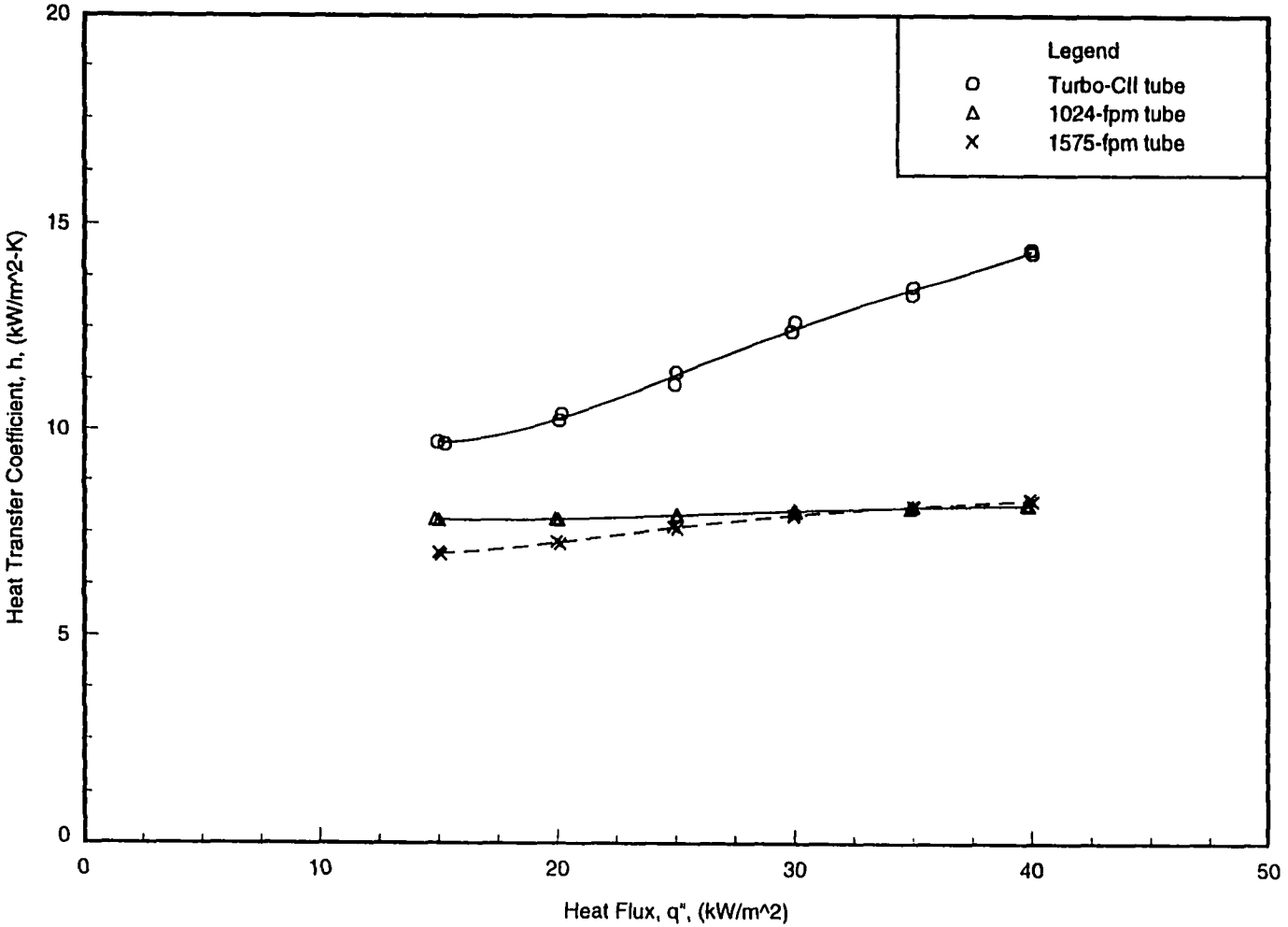

Figure 8.3 Condensation heat transfer coefficients of HFC-236fa for the 1024-fpm, 1575-fpm, and Turbo-CII tubes (D= 19.1 mm) at T_{sat}= 40°C

Figure 8.4 shows that the condensation heat transfer coefficient of HFC-236fa depended on the difference between the refrigerant saturation temperature and the tube-wall temperature. As the condensation temperature difference increased, the heat transfer coefficient increased for the Turbo-CII tube and slightly increased for the two finned tubes, the heat transfer coefficients for the finned tubes were nearly constant over the evaluated range of the condensation temperature differences. It can also be observed that for the Turbo-CII tube a small temperature difference yielded a higher heat transfer coefficient at a given heat flux.

Condensing coefficients of HFC-236fa, HFC-236ea, and CFC-114

The condensation heat transfer coefficients of HFC-236fa HFC-236ea, and CFC-114 were compared in Figures 8.5 through 8.7 for a 1024-fpm tube, a 1575-fpm tube, and a Turbo-CII tube, respectively. In general, higher heat transfer coefficients for the two finned tubes were obtained with HFC-236fa than with CFC-114 or HFC-236ea.

For the 1024-fpm tube, the heat transfer coefficients of HFC-236fa were around 30% to 40% higher than those of CFC-114 and 10% to 30% higher than those of HFC-236ea. For the 1575-fpm tube, the condensing coefficients of HFC-236fa were around 20% to 30% higher compared with CFC-114 and 10% to 30% higher compared with HFC-236ea. For the high performance Turbo-CII tube, the heat transfer coefficients of HFC-236fa were found to be similar to or slightly lower (average less than 5%) than those of HFC-236ea.

The heat transfer coefficents for HFC-236fa and HFC-236ea were reversed on the Turbo-CII tube compared with those on the finned tubes. These reversed results might indicate that the Turbo-CII tube has distinctively different surface geometry from the finned tubes. In the following section, the predicted results by the Webb-Murawski correlation show a similar trend in that the HFC-236fa coefficients are lower than the HFC-236ea values for the Turbo-CII tube. Data were not taken on the Turbo-CII tube with CFC-114.

Comparison of data with published correlations

The analytical model developed for horizontal integral-fin tubes by Beatty and Katz [4] was also used to compare the data for the two finned tubes. The Beatty and Katz model for the average condensing coefficient was given by Equation 4.8 as

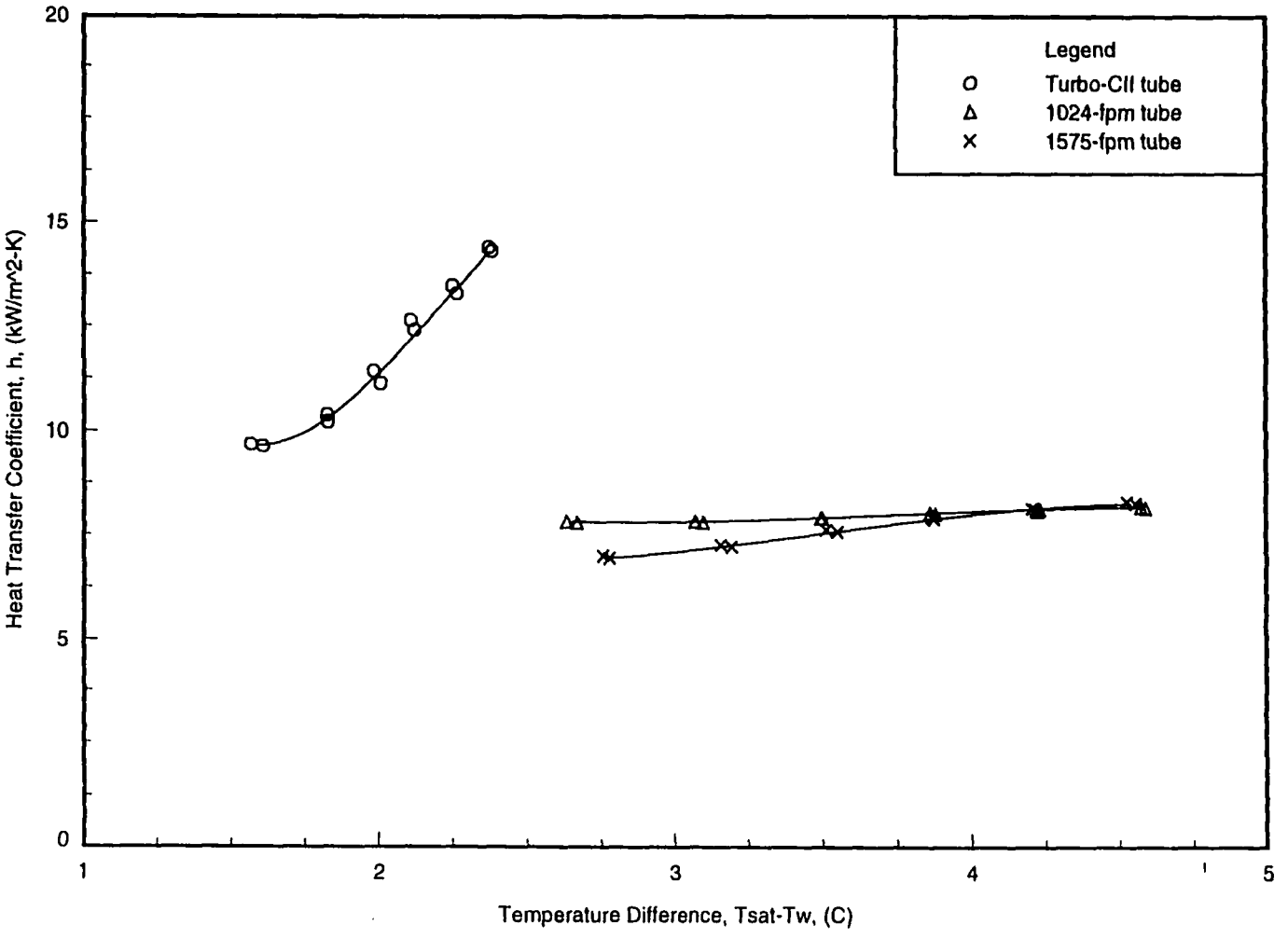

Figure 8.4 Temperature difference effects on the condensation heat transfer coefficients of HFC-236fa at T_{sat}= 40°C

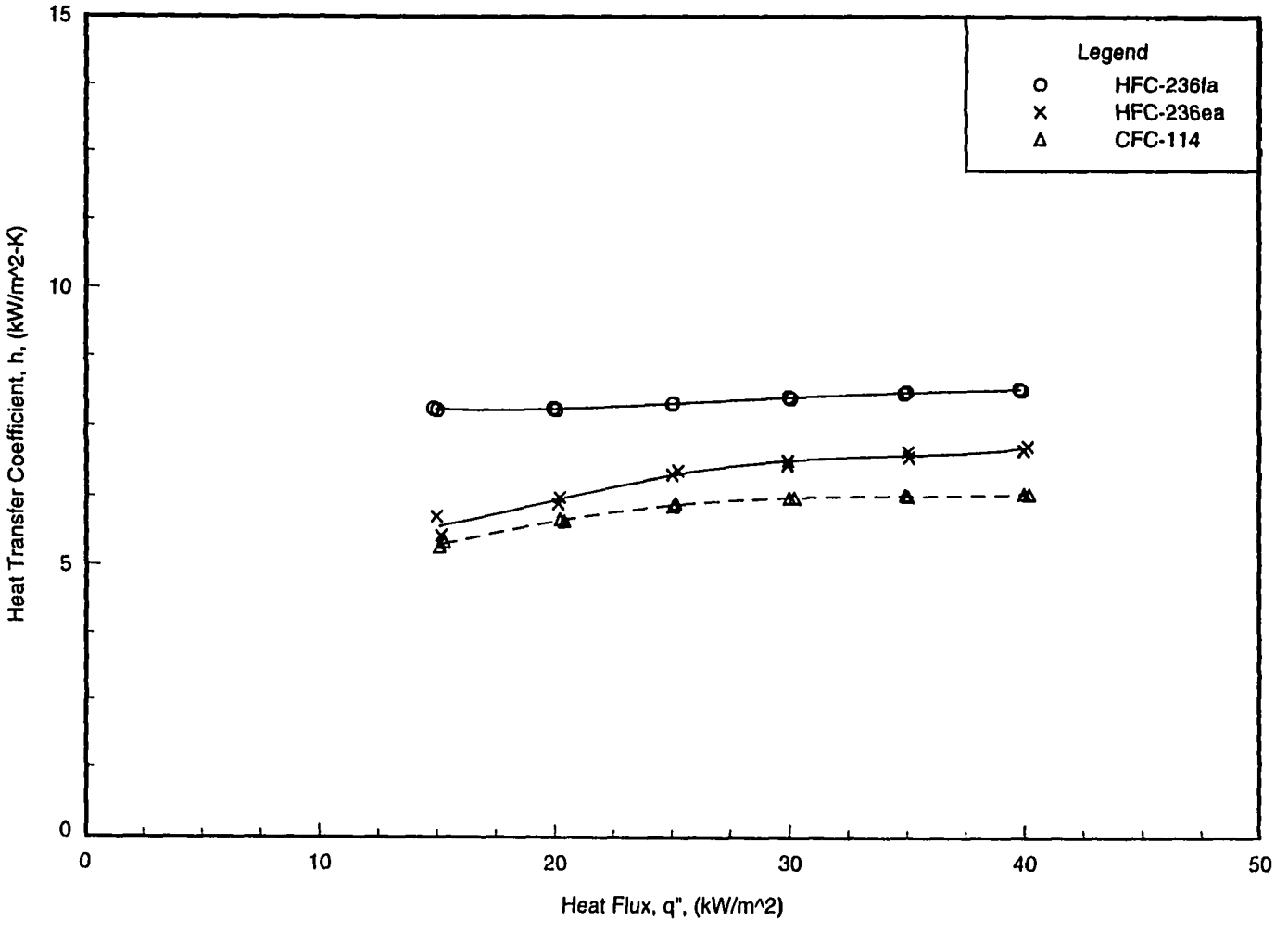

Figure 8.5 Condensation heat transfer coefficients of HFC-236fa, HFC-236ea, and CFC-114 for the 1024-fpm tube (D= 19.1 mm) at T_{sat}= 40°C

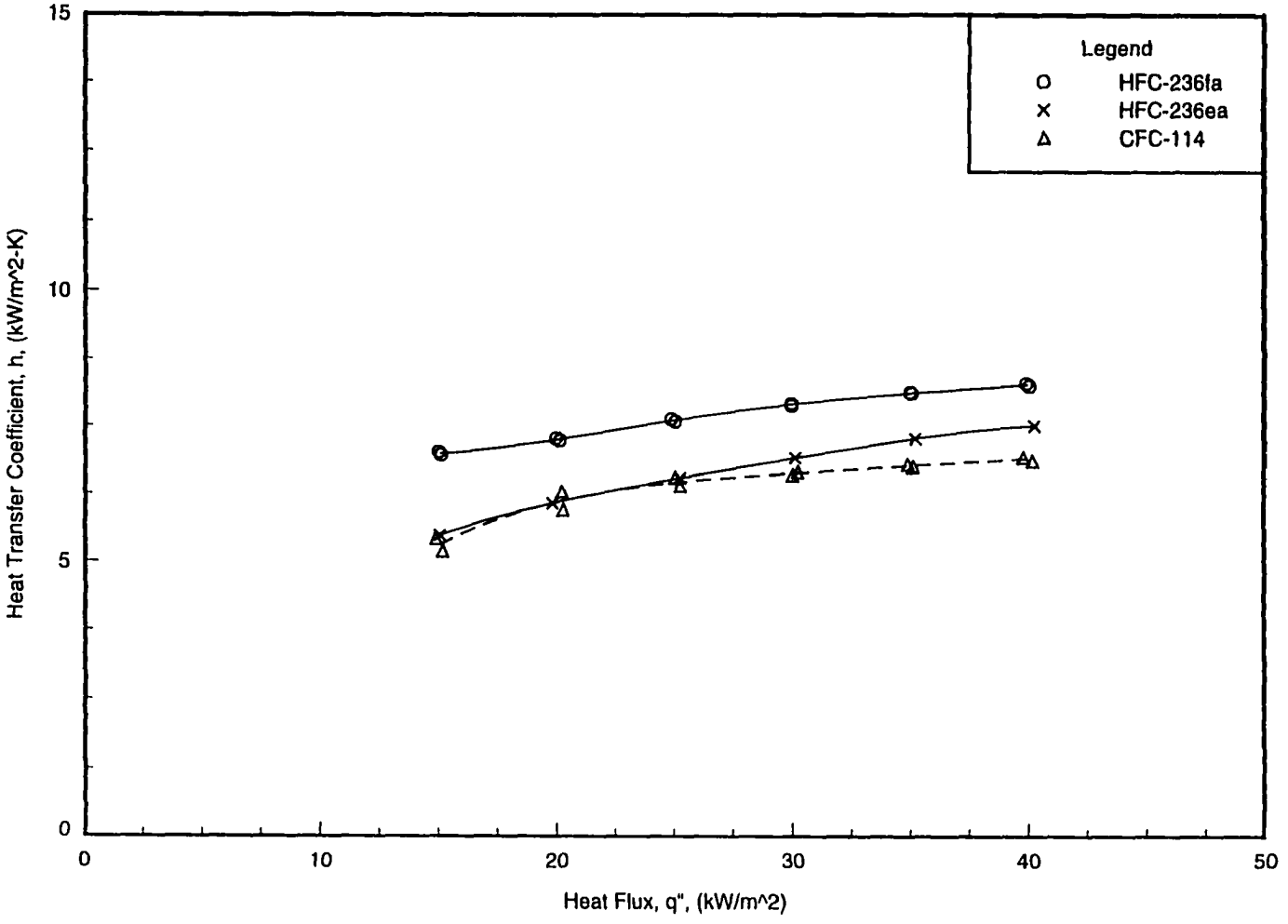

Figure 8.6 Condensation heat transfer coefficients of HFC-236fa, HFC-236ea, and CFC-114 for the 1575-fpm tube (D= 19.1 mm) at T_{sat}= 40°C

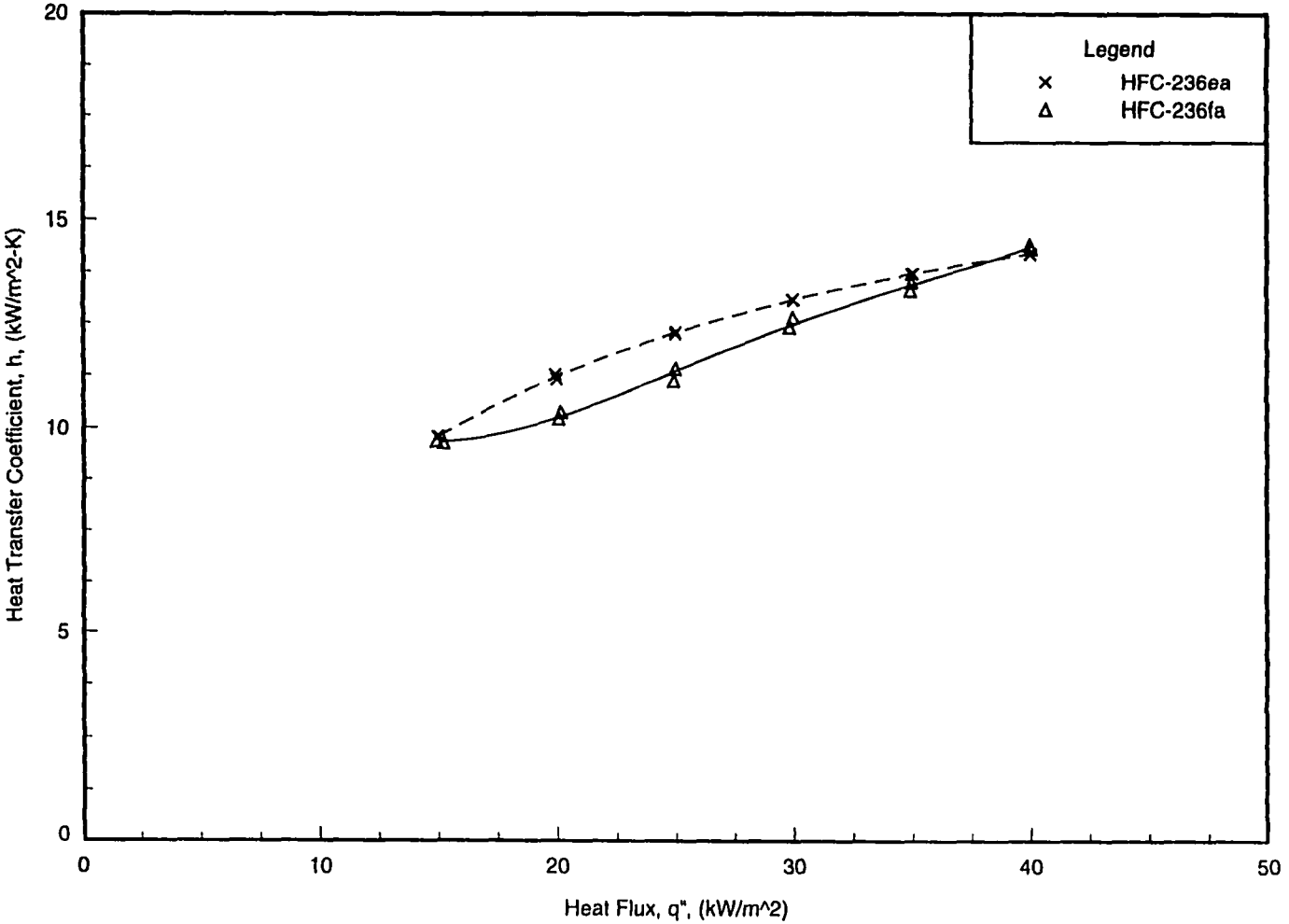

Figure 8.7 Condensation heat transfer coefficients of HFC-236ea and HFC-236fa for the Turbo-CII tube (D= 19.1 mm) at T_{sat}= 40°C

$$\bar{h} = 0.689 \left[\frac{k_l^3 \cdot \rho_l^2 \cdot g \cdot i_{fg}}{\mu_l \cdot (T_{sat} - T_w) \cdot D_{eq}} \right]^{1/4}$$

In addition to the Beatty and Katz model, the Webb and Murawski [84] correlation reviewed in Chapter 4 was used to compare the condensation data obtained in the current study for the 1024-fpm and Turbo-CII tubes, since this empirical correlation was derived for for five enhanced tube types including one integral-fin tube and four enhanced tubes with distinctly different fin profiles, while most of the existing equations were developed for condensation on the tubes with rectangular or trapezoidal cross-section fins [1] [4] [65].

The Webb-Murawski correlation for a single-tube heat transfer coefficient was given by Equation 4.12 with $N = 1$ in the form of

$$h_1 = a \cdot Re_1^{-n}$$

where the condensate Reynolds number leaving the row tested was defined by Equation 4.13 as

$$Re = \frac{4 \cdot \Gamma}{\mu_l}$$

The present data for the Turbo-CII tube and the 1024-fpm tube were compared with the Webb-Murawski correlation using the constants derived for the Turbo-C tube and for the 1024-fpm tube, respectively. The constants c and n shown in Equation 4.12 correspond to 257800 W/m^2-K and 0.507 for the Turbo-C tube, and 13900 W/m^2-K and 0. for the 1024-fpm tube. The constants for the other different tubes can be found in Table 4.1.

In general, the predicted heat transfer coefficients obtained from the Webb-Murawski correlation (i.e., Equation 4.12) are higher than the empirical results, while the theoretical values given by the Beatty and Katz model (i.e., Equation 4.8) are lower than the measured data.

Figure 8.8 compares the condensing coefficients of HFC-236fa for the 1024-fpm tube with those predicted by the correlations of Beatty and Katz [4] and Webb and Murawski [84]. The present data fall between the two correlations. The data lines for this finned tube almost parallel the correlations. The data are around 140% higher and 40% lower, respectively, than the values predicted by the Beatty-Katz and Webb-Murawski correlations.

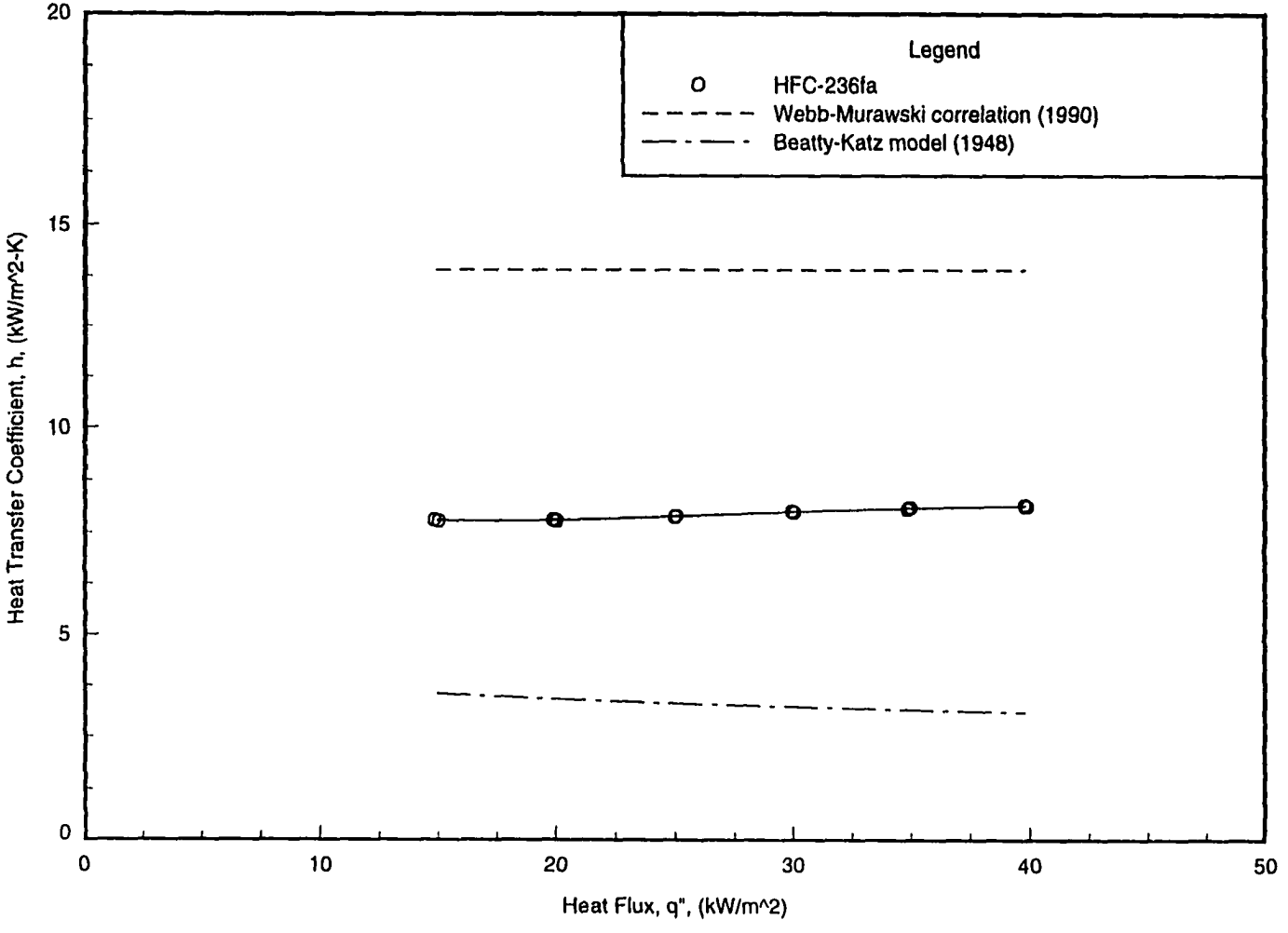

Figure 8.8 Comparison of HFC-236fa data for the 1024-fpm tube (D= 19.1 mm) with correlations of Webb and Murawski (1990) and Beatty and Katz (1948) at T_{sat}= 40°C

Figures 8.9 and 8.10 compares the HFC-236fa, HFC-236ea, and CFC-114 data with the Beatty and Katz [4] model for the 1024-fpm tube and the 1575-fpm tube, respectively. The heat transfer coefficients for the 1024-fpm tube tested with HFC-236fa, HFC-236ea, and CFC-114 are approximately 2.2 to 2.6, 1.8 to 2.5, and 1.9 to 2.5 times as large as the respective predicted coefficients, while for the 1575-fpm tube tested with HFC-236fa, HFC-236ea, and CFC-114 are approximately 1.7 to 2.3, 1.5 to 2.3, and 1.6 to 2.3 times as large as the respective predicted values. Chang et al. [9] and Cheng and Wang [11] also reported that their data were under predicted by the Beatty-Katz model.

Both the experimental and predicted results for the two finned tubes in Figures 8.9 and 8.10 show that the three refrigerants had similar trends with the order of descending heat transfer coefficients being: HFC-236fa, HFC-236ea, and CFC-114.

As shown in Figure 8.11 are the condensing coefficients of HFC-236ea and HFC-236fa measured on the Turbo-CII tube and compared with those predicted by the Webb-Murawski correlation. The Webb-Murawski correlation over predicts the HFC-236ea data by 20% to 190%, and the HFC-236fa data by up to 140%. The predicted values of both refrigerants for the Turbo-CII tube in Figure 8.11 showed an increasing deviation from the empirical values with decreasing heat flux.

In contrast to the results for the finned tubes, the experimental results for the Turbo-CII tube in Figure 8.11 show that the HFC-236fa coefficients are lower than the HFC-236ea values. This trend is in accordance with the predicted results by the Webb-Murawski correlation shown in the same figure.

Examination of Figures 8.8 through 8.11 shows that the heat transfer coefficients obtained from both the measurements and correlations for the Turbo-CII tube are relatively sensitive to the change of heat fluxes compared with the two finned tubes.

Using the Webb-Murawski correlation (Equation 4.12) and constants for the Turbo-C tube, the average heat transfer coefficients measured by Huber [37] for the Turbo-CII tube were three to four times and 20% higher than the predicted values when it was tested with HFC-134a and HCFC-123, respectively. The author attributed the poor agreement between the empirical and theoretical results to the different refrigerants tested. The Webb-Murawski correlation was developed using only one refrigerant (CFC-11) data.

All the theoretical models developed predict that the condensation heat transfer coefficient should decrease as the temperature difference or heat load increased. With an increase in these variables, the heat transfer performance drops because more vapor is condensed and a thicker liquid film is formed so that the resistance on the tube surface increases with increasing heat loads.

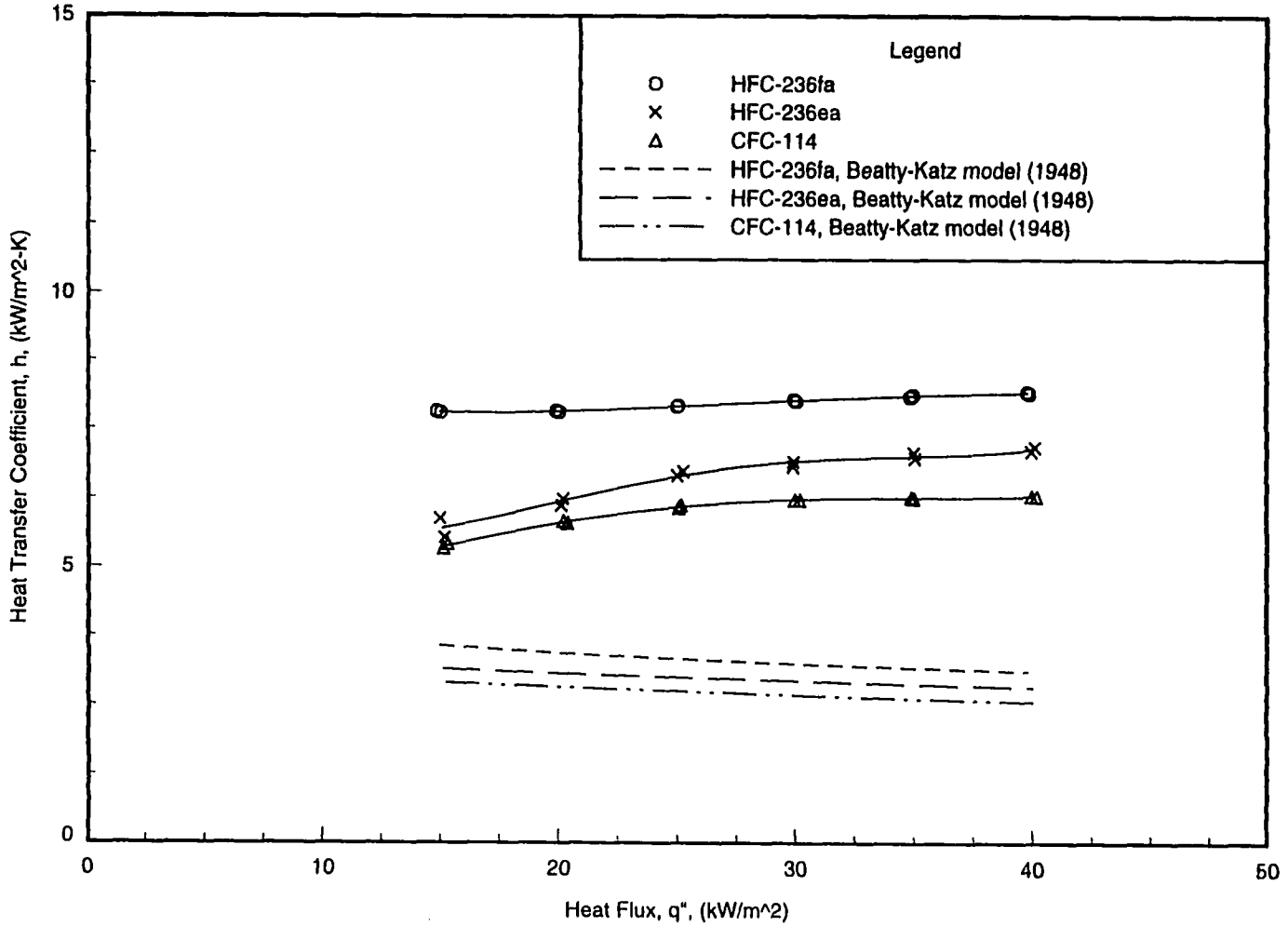

Figure 8.9 Comparison of HFC-236fa, HFC-236ea, and CFC-114 data for the 1024-fpm tube (D= 19.1 mm) with the Beatty-Katz (1948) model at T_{sat}= 40°C

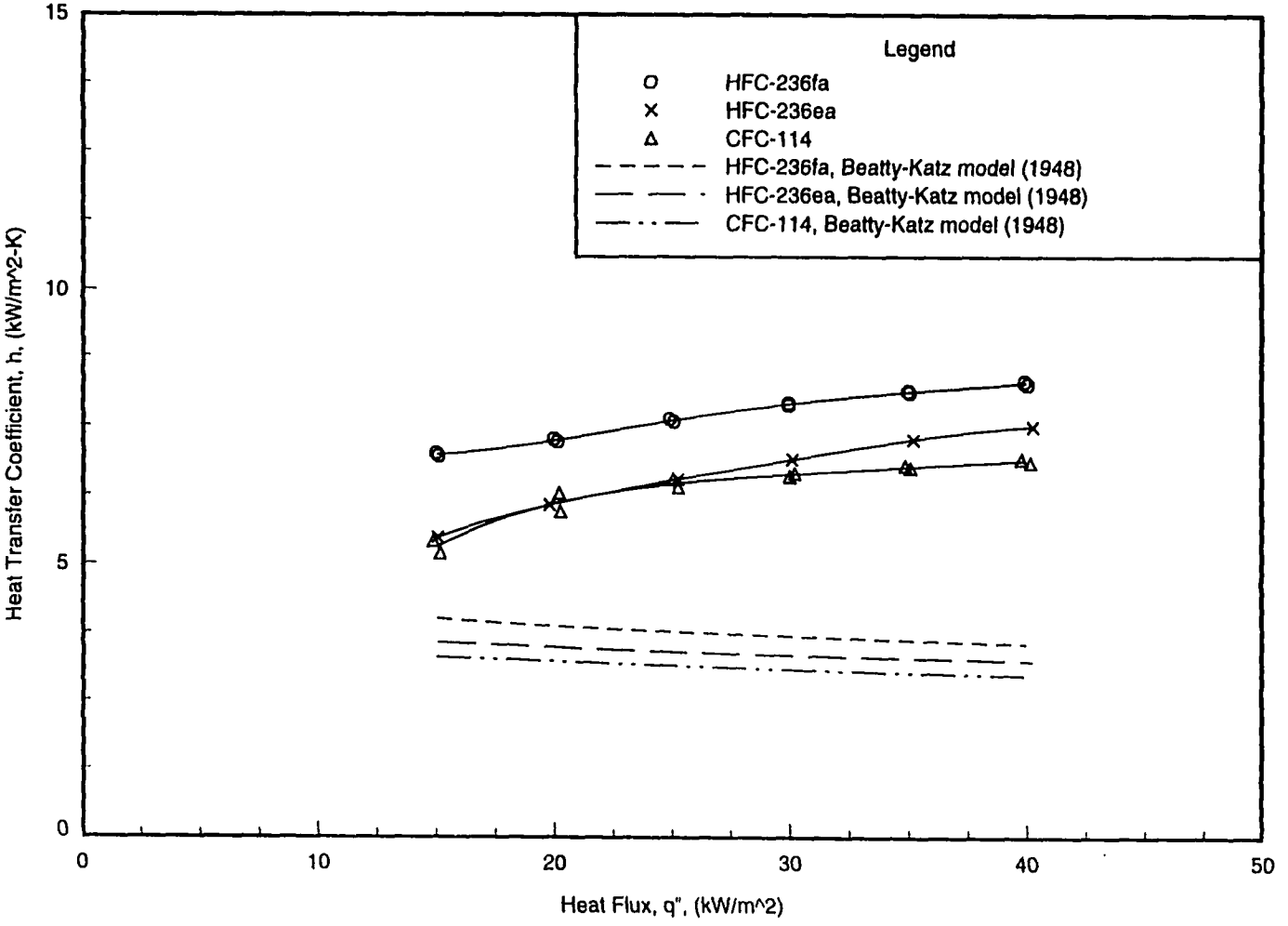

Figure 8.10 Comparison of HFC-236fa, HFC-236ea, and CFC-114 data for the 1575-fpm tube (D= 19.1 mm) with the Beatty-Katz (1948) model at T_{sat}= 40°C

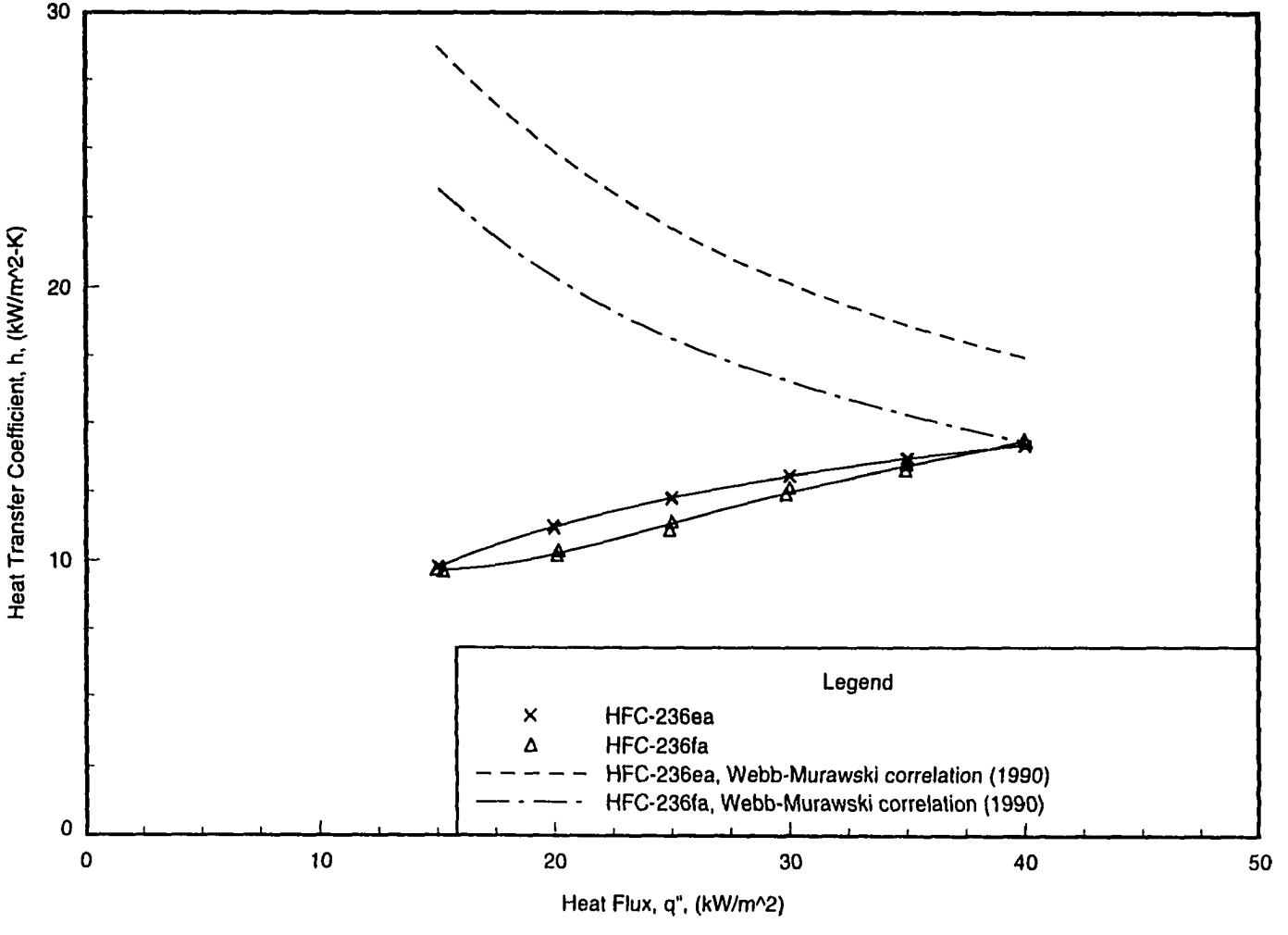

Figure 8.11 Comparison of HFC-236fa and HFC-236ea data for the Turbo-CII tube (D= 19.1 mm) with the Webb-Murawski correlation (1990) at T_{sat}= 40°C

The results of Huber [37] show that the condensing coefficients of CFC-11 for the 1024-fpm, 1575-fpm, Gewa-SC bundles also increased as the heat fluxes increased. The author suggested that the effect of vapor velocity with increasing heat flux removed the increasing condensate and thus resulted in increased heat transfer.

In this study, it is suggested that a more advanced condensation mechanism provided by the three enhanced surfaces (Turbo-CII, 1024-fpm, and 1575-fpm) with the refrigerants tested removed the increasing condensate. The improved condensation mechanism led the converse results for the three enhanced tubes relative to the plain tube and theoretical studies.

Similar to the development of the Webb-Murawski correlation [84], the condensing data of HFC-236fa, HCFC-236ea, and CFC-114 are correlated with condensate Reynolds number and presented in Appendix F.

Summary

The heat transfer performance was evaluated for both HFC-236fa and HFC-236ea condensing on a 1024-fpm, a 1575-fpm, and a Turbo-CII tube, and CFC-114 condensing on the two finned tubes.

The best heat transfer coefficients of HFC-236ea were provided by the high performance Turbo-CII tube with an increase around 90% compared with both the 1024-fpm tube and 1575-fpm tube. The best condensation heat transfer coefficients of HFC-236fa were also provided by the Turbo-CII tube with an increase in heat transfer coefficients around 20% to 80% relative to the 1024-fpm tube, and about 40% to 70% relative to the 1575-fpm tube.

All tubes tested except the Turbo-CII tube performed better in condensation of HFC-236fa than in condensation of CFC-114 and HFC-236ea. Maximum heat transfer increases of 40% compared with CFC-114 and 30% compared with HFC-236ea were obtained by the 1024-fpm tube and the 1575-fpm tube, respectively. The condensation heat transfer coefficients for both HFC-236fa and HFC-236ea tested with the Turbo-CII tube were similar. Data were not taken on the Turbo-CII tube with CFC-114.

The present condensation data fall between the predicted values of the Webb-Murawski and Beatty-Katz correlations. The analytical model developed by Beatty and Katz [4] under predicts the finned tube data, the error is up to 160% under prediction. The empirical correlation derived by Webb and Murawski [84] for the CFC-11 data over predicts the present data, the error is up to 190% over prediction.

CHAPTER 9 CONCLUSIONS AND RECOMMENDATIONS

Conclusions

The shell-side heat transfer coefficients of two alternative refrigerants (HFC-236ea and HFC-236fa) proposed as CFC-114 substitutes were evaluated for two conventional finned (1024-fpm and 1575-fpm) tubes and three high performance enhanced (Turbo-CII, Turbo-B, and Turbo-BII) tubes.

Replacing CFC-114 with HFC-236fa is desired in terms of the comparative heat transfer performance of the three refrigerants made in this study. In general, HFC-236fa was found to have higher heat transfer coefficients than CFC-114 and HFC-236ea during both shell-side condensation and pool boiling. For pool boiling, HFC-236fa provided maximum increases of 80% compared with CFC-114 and 70% compared with HFC-236ea. For condensation, HFC-236fa yielded maximum increases of 40% compared with CFC-114 and 30% compared with HFC-236ea.

The heat transfer performance of the tubes tested was compared for each individual refrigerant. The comparison results reported herein demonstrate that there were substantial increases in heat transfer performance provided by the high performance enhanced tubes compared with the plain tube and conventional finned tubes for the refrigerants tested. It was found that the Turbo-BII tube, the Turbo-B tube, and the Turbo-CII tube performed best in pool boiling, spray evaporation, and condensation, respectively. The enhanced tubes can be used to obtain smaller, lower-cost heat exchangers and systems operating with higher energy efficiency. Results tested for pool boiling, spray evaporation, and condensation are summarized as follows:

Pool boiling results

The pool boiling results for pure HFC-236ea, pure HFC-236fa, and HFC-236fa with oil show that the tube performance in descending order was Turbo-BII tube, Turbo-B tube, 1024-fpm tube, and 1575-fpm tube.

The high performance Turbo-BII and Turbo-B tubes performed better than the two integral-fin tubes during pool boiling testing at 2°C. In particular, the Turbo-BII tube outperformed the other

tubes tested and showed an increase of up to 70% and 80% in the boiling coefficients of HFC-236ea and HFC-236fa, respectively, relative to the Turbo-B tube. In turn, the Turbo-B tube tested for HFC-236ea yielded maximum heat transfer increases of 30% compared with the 1024-fpm tube and 50% compared with the 1575-fpm tube, while for HFC-236fa the Turbo-B tube provided maximum heat transfer increases of 70% compared with the 1024-fpm tube and 120% compared with the 1575-fpm tube.

Saturated pool boiling was also investigated for HFC-236fa mixed with a synthetic polyol-ester oil. The small amount of oil (1% and 3%) in HFC-236fa caused the boiling coefficients to deviate less than 10% from the pure HFC-236fa results for all the tubes tested except for the Turbo-BII tube.

Although the high performance Turbo-BII tube produced the highest heat tansfer coefficients of all the tubes tested, it showed larger changes in pool boiling performance with the addition of oil. Specifically, the Turbo-BII tube gave 10% to 30% increases at the 1% oil concentration over the pure HFC-236fa results, and a 10% decrease to a 15% increase at the 3% oil concentration.

Spray evaporation results

For spray-evaporation testing of HFC-236ea at 2°C, the Turbo-B tube performed best and provided approximately 10% to 20% higher heat transfer coefficients than the Turbo-CII tube, and 60% to 80% higher values than the 1575-fpm tube.

The heat transfer coefficient in spray evaporation was nearly independent of the feed flow rate at the heat fluxes less than 15 kW/m^2 and it increased as the feed rate increased at higher heat fluxes where dry-out phenomena became significant. For any feed rate tested, the heat transfer coefficient generally increased as the heat flux increased up to 15 kW/m^2 and then decreased beyond this value.

Comparison results of pool boiling and spray evaporation

Comparison of pool boiling and spray evaporation in heat transfer coefficients of HFC-236ea was made for the 1575-fpm and Turbo-B tubes. The results show that the superiority of spray evaporation over pool boiling for these tubes tested exists only at the heat fluxes below the approximate value of 30 kW/m^2.

At the heat flux of 15 kW/m^2, the heat transfer coefficients provided by the Turbo-B tube and the 1575-fpm tube in spray evaporation were approximately 2.3 times and 1.2 times, respectively, the values in pool boiling. At the heat flux of 30 kW/m^2, the boiling coefficients in these two different heat transfer forms were similar for both tubes tested.

Condensation results

For condensation testing of HFC-236ea at 40°C, the heat transfer coefficients provided by the Turbo-CII tube were up to 90% higher in comparison with both the 1024-fpm tube and 1575-fpm tube and up to 9 times higher compared with the plain tube, while the Turbo-CII tube showed an increase of up to 80% and 70% in the condensation heat transfer coefficients of HFC-236fa compared with the 1024-fpm tube and the 1575-fpm tube, respectively.

Recommendations

Recommendations for future research in heat transfer evaluation of alternative refrigerants for CFC-114 or other CFCs are listed as follows:

1. Establish a large database covering a wide variety of testing conditions and fluids for developing general correlations. Apply understanding of fundamentals to develope analytical models for shell-side condensation and pool boiling with complex surface geometries involved.

2. Investigate the effects on the pool boiling performance of larger oil quantity in refrigerant, and seek for a general accepted theory to explain the boiling phenomena observed in oil/refrigerant mixtures. The attraction of the high heat transfer performance offered by the high performance enhanced tubes should be in view of the oil effects with larger concentrations possibly occuring in realistic evaporators.

3. Further work for spray evaporation testing is required over a wider heat flux range. A loss of heat transfer performance existed when the tube surface was not fully wetted at high heat fluxes. The occurrence of dry-out phenomena can be avoided by improving liquid distribution on tubes and pumping power. The minimum heat flux was restricted by the lower limit of water flow rate. Data at lower heat fluxes can be taken by introducing water through a bypass back to the water pump.

This research which evaluated the heat transfer coefficients of two non-CFC candidates for CFC-114 is only a part of the conversion process from CFC-114 to a non-CFC alternative. The whole conversion process should examine the alternatives in all aspects including heat transfer performance as well as other issues, such as toxicity, energy efficiency, manufacturing feasibility (and hence cost), and so on. A suitable substitute should have not only comparable heat transfer characteristics with existing systems but also the closest comparable operating conditions.

APPENDIX A COMPARATIVE PROPERTIES OF CFC-114, HFC-236ea, AND HFC-236fa

Table A.1 Comparative properties of CFC-114, HFC-236ea, and HFC-236fa

Property		CFC-114	HFC-236ea	HFC-236fa
Molecular formula		$CClF_2CClF_2$	$CF_3CHFCHF_2$	$CF_3CH_2CF_3$
Molecular weight (kg/kmol)		1.7090E+2	1.5205E+2	1.5205E+2
Flammability		Non-flammable	Non-flammable	Non-flammable
Ozone depleting potential		8.0000E−1	0.0000E+0	0.0000E+0
Critical pressure (P_c, Pa)		3.2480E+6	3.5330E+6	3.2000E+6
Critical temperature (T_c, °C)		1.4570E+2	1.4110E+2	1.3060E+2
T_{nb} (°C) (nb: normal boiling point)		3.7800E+0	6.5000E+0	-1.1100E+0
2°C	P_{sat} (Pa)	9.4960E+4	8.5240E+4	1.1710E+5
	ρ_l (kg/m^3)	1.5250E+3	1.4970E+3	1.4340E+3
	ρ_v (kg/m^3)	7.4000E+0	5.9000E+0	8.2000E+0
	Cp_l (J/kg·K)	9.4200E+2	1.1640E+3	1.2120E+3
	h_{fg} (J/kg)	1.3237E+5	1.6520E+5	1.5570E+5
	k_l (W/m·K)	7.2200E−2	8.0300E−2	7.9300E−2
	μ_l (Pa·s)	4.6410E−4	5.3960E−4	3.9190E−4
	σ (N/m)	1.3600E−2	1.4900E−2	1.2890E−2
40°C	P_{sat} (Pa)	3.3940E+5	3.3650E+5	4.3630E+5
	ρ_l (kg/m^3)	1.4090E+3	1.3770E+3	1.3080E+3
	ρ_v (kg/m^3)	2.4950E+1	2.2190E+1	2.9300E+1
	Cp_l (J/kg·K)	1.0050E+3	1.2560E+3	1.3050E+3
	h_{fg} (J/kg)	1.1730E+5	1.4510E+5	1.3420E+5
	k_l (W/m·K)	6.1700E−2	6.6500E−2	6.9670E−2
	μ_l (Pa·s)	2.9600E−4	3.1360E−4	2.3790E−4
	σ (N/m)	9.1100E−3	1.0050E−2	7.9300E−3

APPENDIX B GEOMETRIC SPECIFICATIONS OF TUBES

Table B.1 Geometric specifications of tubes in SI units

tube	fin count (fins/m)	D_o nominal (mm)	D_i nominal (mm)	D_r (mm)	fin height (mm)	A_o/L nominal (m^2/m)	A_o/L actual (m^2/m)	A_i/L nominal (m^2/m)
1024-fpm	1024	18.80	14.40	15.90	1.45	0.0588	0.193	0.0454
1575-fpm	1575	18.80	15.70	17.10	0.86	0.0593	0.179	0.0493
Turbo-CII	~	18.90	15.54	17.07	0.91	0.0597	~	0.0488
Turbo-B	~	18.50	16.10	17.30	0.59	0.0582	~	0.0506
Turbo-BII	~	18.62	16.05	17.27	0.68	0.0585	~	0.0504

Table B.2 Geometric specifications of tubes in English units

tube	fin count (fins/in)	D_o nominal (in)	D_i nominal (in)	D_r (in)	fin height (in)	A_o/L nominal (ft^2/ft)	A_o/L actual (ft^2/ft)	A_i/L nominal (ft^2/ft)
26-fpi	26	0.739	0.568	0.625	0.057	0.193	0.634	0.149
40-fpi	40	0.743	0.622	0.675	0.034	0.195	0.586	0.163
Turbo-CII	~	0.744	0.612	0.672	0.036	0.196	~	0.160
Turbo-B	~	0.730	0.632	0.682	0.024	0.191	~	0.165
Turbo-BII	~	0.733	0.632	0.680	0.027	0.192	~	0.165

APPENDIX C TABULATED DATA OF HFC-236EA

The experimental data obtained in this study for HFC-236ea are presented in this appendix. The symbols h is shell-side heat transfer coefficient (W/m^2 K), $q"$ is heat flux (W/m^2), q is heat transfer rate (Watts), $LMTD$ is log mean temperature difference (°C), ΔT is the temperature difference between tube surface and saturation refrigerant (°C), h_i is in-tube heat transfer coefficient (W/m^2 K), Re_i is Reynolds number of water, U_o is overall heat transfer coefficient (W/m^2 K), and UN is the uncertainty of shell-side heat transfer coefficient (± %).

Table C.1 Pool boiling of HFC-236ea on the Turbo-B tube at a saturation temperature of 2°C (primary run)

h (W/m^2 K)	8.27E+03	7.72E+03	7.08E+03	6.40E+03	5.65E+03	4.74E+03
$q"$ (W/m^2)	4.00E+04	3.49E+04	2.99E+04	2.50E+04	2.01E+04	1.50E+04
q (Watts)	2.00E+03	1.75E+03	1.50E+03	1.25E+03	1.01E+03	7.50E+02
$LMTD$ (°C)	7.36E+00	6.97E+00	6.59E+00	6.17E+00	5.73E+00	5.19E+00
ΔT (°C)	3.70E+00	3.51E+00	3.32E+00	3.11E+00	2.89E+00	2.63E+00
h_i (W/m^2 K)	2.11E+04	1.89E+04	1.66E+04	1.43E+04	1.19E+04	9.40E+03
Re_i	1.43E+04	1.24E+04	1.05E+04	8.69E+03	6.86E+03	5.07E+03
U_o (W/m^2 K)	5.60E+03	5.16E+03	4.68E+03	4.17E+03	3.61E+03	2.97E+03
UN (± %)	6.46E+00	6.72E+00	7.02E+00	7.39E+00	7.87E+00	8.56E+00

Table C.2 Pool boiling of HFC-236ea on the Turbo-B tube at a saturation temperature of 2°C (repeat run)

h (W/m^2 K)	8.42E+03	7.88E+03	7.30E+03	6.70E+03	5.89E+03	5.03E+03
$q"$ (W/m^2)	3.99E+04	3.49E+04	2.98E+04	2.49E+04	1.97E+04	1.49E+04
q (Watts)	2.00E+03	1.75E+03	1.50E+03	1.25E+03	9.88E+02	7.46E+02
$LMTD$ (°C)	7.25E+00	6.87E+00	6.44E+00	5.98E+00	5.48E+00	4.98E+00
ΔT (°C)	3.65E+00	3.46E+00	3.25E+00	3.02E+00	2.77E+00	2.52E+00
h_i (W/m^2 K)	2.12E+04	1.89E+04	1.66E+04	1.43E+04	1.19E+04	9.36E+03
Re_i	1.43E+04	1.24E+04	1.05E+04	8.62E+03	6.81E+03	5.03E+03
U_o (W/m^2 K)	5.67E+03	5.23E+03	4.77E+03	4.29E+03	3.70E+03	3.08E+03
UN (± %)	6.57E+00	6.82E+00	7.20E+00	7.67E+00	8.28E+00	9.04E+00

Table C.3 Pool boiling of HFC-236ea on the Turbo-BII tube at a saturation temperature of 2°C (primary run)

h (W/m^2 K)	1.03E+04	9.94E+03	9.53E+03	9.19E+03	8.69E+03	8.02E+03
$q"$ (W/m^2)	3.98E+04	3.50E+04	2.96E+04	2.49E+04	2.01E+04	1.50E+04
q (Watts)	2.00E+03	1.76E+03	1.48E+03	1.25E+03	1.01E+03	7.53E+02
$LMTD$ (°C)	6.68E+00	6.27E+00	5.75E+00	5.28E+00	4.80E+00	4.23E+00
ΔT (°C)	3.36E+00	3.16E+00	2.90E+00	2.67E+00	2.43E+00	2.16E+00
h_i (W/m^2 K)	1.72E+04	1.54E+04	1.35E+04	1.16E+04	9.69E+03	7.61E+03
Re_i	1.41E+04	1.22E+04	1.03E+04	8.47E+03	6.70E+03	4.93E+03
U_o (W/m^2 K)	5.95E+03	5.56E+03	5.13E+03	4.69E+03	4.17E+03	3.53E+03
UN (± %)	7.96E+00	8.50E+00	9.36E+00	1.04E+01	1.18E+01	1.40E+01

Table C.4 Pool boiling of HFC-236ea on the Turbo-BII tube at a saturation temperature of 2°C (repeat run)

h (W/m^2 K)	1.03E+04	1.01E+04	9.83E+03	9.48E+03	9.05E+03	8.26E+03
$q"$ (W/m^2)	3.98E+04	3.50E+04	2.99E+04	2.50E+04	1.99E+04	1.49E+04
q (Watts)	2.00E+03	1.76E+03	1.50E+03	1.25E+03	9.98E+02	7.48E+02
$LMTD$ (°C)	6.66E+00	6.23E+00	5.72E+00	5.22E+00	4.67E+00	4.15E+00
ΔT (°C)	3.36E+00	3.14E+00	2.89E+00	2.64E+00	2.37E+00	2.11E+00
h_i (W/m^2 K)	1.72E+04	1.53E+04	1.35E+04	1.16E+04	9.66E+03	7.60E+03
Re_i	1.41E+04	1.21E+04	1.03E+04	8.44E+03	6.67E+03	4.91E+03
U_o (W/m^2 K)	5.95E+03	5.60E+03	5.22E+03	4.76E+03	4.24E+03	3.58E+03
UN (± %)	7.98E+00	8.58E+00	9.48E+00	1.06E+01	1.23E+01	1.45E+01

Table C.5 Spray evaporation of HFC-236ea on the Turbo-B tube at a saturation temperature of 2°C ($\dot{m}_{spr}$= 2.6 kg/min, run 1)

h (W/m^2 K)	1.16E+04	1.06E+04	8.28E+03	5.97E+03
q" (W/m^2)	1.50E+04	1.96E+04	2.50E+04	2.97E+04
q (Watts)	7.50E+02	9.82E+02	1.26E+03	1.49E+03
$LMTD$ (°C)	3.32E+00	3.96E+00	5.30E+00	7.32E+00
ΔT (°C)	1.71E+00	2.02E+00	2.68E+00	3.68E+00
h_i (W/m^2 K)	9.18E+03	1.17E+04	1.42E+04	1.68E+04
Re_i	4.82E+03	6.55E+03	8.48E+03	1.07E+04
U_o (W/m^2 K)	4.65E+03	5.10E+03	4.87E+03	4.18E+03
UN (± %)	1.88E+01	1.36E+01	8.98E+00	6.30E+00

Table C.6 Spray evaporation of HFC-236ea on the Turbo-B tube at a saturation temperature of 2°C ($\dot{m}_{spr}$= 2.6 kg/min, run 2)

h (W/m^2 K)	5.94E+03	7.65E+03	9.82E+03	1.12E+04	1.07E+04
q" (W/m^2)	2.97E+04	2.52E+04	2.00E+04	1.49E+04	1.01E+04
q (Watts)	1.49E+03	1.26E+03	1.00E+03	7.47E+02	5.06E+02
$LMTD$ (°C)	7.34E+00	5.57E+00	4.20E+00	3.35E+00	2.83E+00
ΔT (°C)	3.69E+00	2.82E+00	2.14E+00	1.72E+00	1.47E+00
h_i (W/m^2 K)	1.68E+04	1.42E+04	1.17E+04	9.18E+03	6.58E+03
Re_i	1.08E+04	8.54E+03	6.60E+03	4.82E+03	3.16E+03
U_o (W/m^2 K)	4.16E+03	4.65E+03	4.92E+03	4.59E+03	3.67E+03
UN (± %)	6.28E+00	8.39E+00	1.25E+01	1.84E+01	2.53E+01

Table C.7 Spray evaporation of HFC-236ea on the Turbo-B tube at a saturation temperature of 2°C ($\dot{m}_{spr}$= 2.8 kg/min, run 1)

h (W/m^2 K)	1.16E+04	1.09E+04	9.64E+03	7.44E+03
q" (W/m^2)	1.49E+04	1.97E+04	2.49E+04	3.00E+04
q (Watts)	7.49E+02	9.88E+02	1.25E+03	1.50E+03
$LMTD$ (°C)	3.31E+00	3.95E+00	4.85E+00	6.40E+00
ΔT (°C)	1.70E+00	2.01E+00	2.46E+00	3.22E+00
h_i (W/m^2 K)	9.17E+03	1.16E+04	1.40E+04	1.66E+04
Re_i	4.81E+03	6.51E+03	8.34E+03	1.04E+04
U_o (W/m^2 K)	4.65E+03	5.14E+03	5.29E+03	4.83E+03
UN (± %)	1.89E+01	1.39E+01	1.02E+01	7.26E+00

Table C.8 Spray evaporation of HFC-236ea on the Turbo-B tube at a saturation temperature of 2°C ($\dot{m}_{spr}$= 2.8 kg/min, run 2)

h (W/m^2 K)	7.43E+03	9.27E+03	1.05E+04	1.13E+04	1.03E+04
q" (W/m^2)	3.00E+04	2.49E+04	1.98E+04	1.52E+04	9.04E+03
q (Watts)	1.50E+03	1.25E+03	9.93E+02	7.63E+02	4.53E+02
$LMTD$ (°C)	6.40E+00	4.95E+00	4.02E+00	3.41E+00	2.58E+00
ΔT (°C)	3.23E+00	2.51E+00	2.05E+00	1.75E+00	1.34E+00
h_i (W/m^2 K)	1.66E+04	1.41E+04	1.17E+04	9.19E+03	6.53E+03
Re_i	1.04E+04	8.39E+03	6.55E+03	4.82E+03	3.11E+03
U_o (W/m^2 K)	4.82E+03	5.19E+03	5.07E+03	4.60E+03	3.61E+03
UN (± %)	7.25E+00	9.89E+00	1.34E+01	1.81E+01	2.71E+01

Table C.9 Spray evaporation of HFC-236ea on the Turbo-B tube at a saturation temperature of 2°C ($\dot{m}_{spr}$= 3.0 kg/min, run 1)

h (W/m^2 K)	1.16E+04	1.07E+04	9.36E+03	7.83E+03
$q"$ (W/m^2)	1.49E+04	2.00E+04	2.50E+04	3.00E+04
q (Watts)	7.48E+02	1.00E+03	1.26E+03	1.50E+03
$LMTD$ (°C)	3.31E+00	4.02E+00	4.96E+00	6.20E+00
ΔT (°C)	1.71E+00	2.05E+00	2.51E+00	3.13E+00
h_i (W/m^2 K)	9.17E+03	1.17E+04	1.41E+04	1.65E+04
Re_i	4.81E+03	6.55E+03	8.38E+03	1.04E+04
U_o (W/m^2 K)	4.64E+03	5.12E+03	5.21E+03	4.98E+03
UN (± %)	1.89E+01	1.35E+01	9.91E+00	7.52E+00

Table C.10 Spray evaporation of HFC-236ea on the Turbo-B tube at a saturation temperature of 2°C ($\dot{m}_{spr}$= 3.0 kg/min, run 2)

h (W/m^2 K)	7.83E+03	9.32E+03	1.05E+04	1.14E+04
$q"$ (W/m^2)	3.00E+04	2.50E+04	1.99E+04	1.49E+04
q (Watts)	1.50E+03	1.25E+03	9.97E+02	7.50E+02
$LMTD$ (°C)	6.20E+00	4.95E+00	4.04E+00	3.34E+00
ΔT (°C)	3.13E+00	2.51E+00	2.06E+00	1.72E+00
h_i (W/m^2 K)	1.65E+04	1.41E+04	1.16E+04	9.17E+03
Re_i	1.04E+04	8.37E+03	6.54E+03	4.81E+03
U_o (W/m^2 K)	4.98E+03	5.20E+03	5.08E+03	4.62E+03
UN (± %)	7.52E+00	9.92E+00	1.34E+01	1.86E+01

Table C.11 Spray evaporation of HFC-236ea on the Turbo-B tube at a saturation temperature of 2°C ($\dot{m}_{spr}$= 3.0 kg/min. repeat run for run 1)

h (W/m^2 K)	1.20E+04	1.11E+04	9.40E+03	7.91E+03
$q"$ (W/m^2)	1.49E+04	1.99E+04	2.49E+04	3.01E+04
q (Watts)	7.46E+02	1.00E+03	1.25E+03	1.51E+03
$LMTD$ (°C)	3.25E+00	3.95E+00	4.92E+00	6.19E+00
ΔT (°C)	1.67E+00	2.02E+00	2.49E+00	3.12E+00
h_i (W/m^2 K)	9.16E+03	1.16E+04	1.41E+04	1.65E+04
Re_i	4.80E+03	6.53E+03	8.39E+03	1.04E+04
U_o (W/m^2 K)	4.72E+03	5.20E+03	5.22E+03	5.01E+03
UN (± %)	1.96E+01	1.40E+01	1.00E+01	7.55E+00

Table C.12 Spray evaporation of HFC-236ea on the Turbo-B tube at a saturation temperature of 2°C ($\dot{m}_{spr}$= 3.0 kg/min. repeat run for run 2)

h (W/m^2 K)	7.88E+03	9.36E+03	1.08E+04	1.17E+04
$q"$ (W/m^2)	3.01E+04	2.50E+04	2.00E+04	1.49E+04
q (Watts)	1.51E+03	1.25E+03	1.01E+03	7.47E+02
$LMTD$ (°C)	6.20E+00	4.94E+00	4.01E+00	3.29E+00
ΔT (°C)	3.13E+00	2.50E+00	2.05E+00	1.70E+00
h_i (W/m^2 K)	1.66E+04	1.41E+04	1.17E+04	9.18E+03
Re_i	1.04E+04	8.38E+03	6.55E+03	4.82E+03
U_o (W/m^2 K)	5.00E+03	5.21E+03	5.15E+03	4.66E+03
UN (± %)	7.53E+00	9.93E+00	1.36E+01	1.90E+01

Table C.13 Spray evaporation of HFC-236ea on the Turbo-B tube at a saturation temperature of 2°C ($\dot{m}_{spr}$= 3.2 kg/min, run 1)

h (W/m^2 K)	1.18E+04	1.10E+04	9.63E+03	8.57E+03
q" (W/m^2)	1.49E+04	1.98E+04	2.50E+04	3.00E+04
q (Watts)	7.49E+02	9.91E+02	1.25E+03	1.51E+03
$LMTD$ (°C)	3.30E+00	3.94E+00	4.87E+00	5.87E+00
ΔT (°C)	1.70E+00	2.01E+00	2.47E+00	2.97E+00
h_i (W/m^2 K)	9.16E+03	1.16E+04	1.41E+04	1.65E+04
Re_i	4.80E+03	6.53E+03	8.35E+03	1.03E+04
U_o (W/m^2 K)	4.67E+03	5.17E+03	5.29E+03	5.27E+03
UN (± %)	1.91E+01	1.39E+01	1.02E+01	8.04E+00

Table C.14 Spray evaporation of HFC-236ea on the Turbo-B tube at a saturation temperature of 2°C ($\dot{m}_{spr}$= 3.2 kg/min, run 2)

h (W/m^2 K)	8.52E+03	9.60E+03	1.09E+04	1.17E+04	1.10E+04
q" (W/m^2)	2.98E+04	2.50E+04	1.99E+04	1.50E+04	9.05E+03
q (Watts)	1.50E+03	1.25E+03	9.96E+02	7.50E+02	4.54E+02
$LMTD$ (°C)	5.86E+00	4.88E+00	3.97E+00	3.31E+00	2.51E+00
ΔT (°C)	2.96E+00	2.47E+00	2.03E+00	1.70E+00	1.31E+00
h_i (W/m^2 K)	1.65E+04	1.41E+04	1.16E+04	9.17E+03	6.58E+03
Re_i	1.03E+04	8.35E+03	6.53E+03	4.81E+03	3.14E+03
U_o (W/m^2 K)	5.25E+03	5.28E+03	5.15E+03	4.66E+03	3.71E+03
UN (± %)	8.06E+00	1.01E+01	1.38E+01	1.90E+01	2.89E+01

Table C.15 Spray evaporation of HFC-236ea on the Turbo-CII tube at a saturation temperature of 2°C ($\dot{m}_{spr}$= 2.6 kg/min. run 1)

h (W/m^2 K)	9.50E+03	8.53E+03	7.20E+03	5.87E+03
q'' (W/m^2)	1.51E+01	1.99E+01	2.50E+01	2.97E+01
q (Watts)	7.58E+02	9.96E+02	1.25E+03	1.49E+03
$LMTD$ (°C)	3.82E+00	4.66E+00	5.92E+00	7.55E+00
ΔT (°C)	1.96E+00	2.36E+00	2.99E+00	3.80E+00
h_i (W/m^2 K)	8.51E+03	1.08E+04	1.31E+04	1.55E+04
Re_i	5.06E+03	6.89E+03	8.91E+03	1.12E+04
U_o (W/m^2 K)	4.01E+03	4.33E+03	4.29E+03	4.00E+03
UN (± %)	1.59E+01	1.14E+01	8.27E+00	6.38E+00

Table C.16 Spray evaporation of HFC-236ea on the Turbo-CII tube at a saturation temperature of 2°C ($\dot{m}_{spr}$= 2.6 kg/min. run 2)

h (W/m^2 K)	5.87E+03	7.20E+03	8.55E+03	9.51E+03	9.79E+03
q'' (W/m^2)	2.97E+01	2.49E+01	1.99E+01	1.50E+01	9.59E+00
q (Watts)	1.49E+03	1.25E+03	9.99E+02	7.54E+02	4.81E+02
$LMTD$ (°C)	7.56E+00	5.89E+00	4.67E+00	3.81E+00	2.96E+00
ΔT (°C)	3.80E+00	2.97E+00	2.37E+00	1.95E+00	1.53E+00
h_i (W/m^2 K)	1.55E+04	1.31E+04	1.08E+04	8.48E+03	6.06E+03
Re_i	1.12E+04	8.91E+03	6.89E+03	5.03E+03	3.27E+03
U_o (W/m^2 K)	3.99E+03	4.29E+03	4.33E+03	4.00E+03	3.29E+03
UN (± %)	6.37E+00	8.30E+00	1.14E+01	1.60E+01	2.49E+01

Table C.17 Spray evaporation of HFC-236ea on the Turbo-CII tube at a saturation temperature of 2°C ($\dot{m}_{spr}$= 2.8 kg/min. run 1)

h (W/m^2 K)	9.41E+03	8.73E+03	7.44E+03	6.13E+03
q" (W/m^2)	1.52E+01	2.00E+01	2.50E+01	2.98E+01
q (Watts)	7.61E+02	1.00E+03	1.26E+03	1.50E+03
$LMTD$ (°C)	3.86E+00	4.64E+00	5.81E+00	7.38E+00
ΔT (°C)	1.97E+00	2.36E+00	2.93E+00	3.71E+00
h_i (W/m^2 K)	8.50E+03	1.08E+04	1.31E+04	1.54E+04
Re_i	5.05E+03	6.88E+03	8.90E+03	1.11E+04
U_o (W/m^2 K)	3.99E+03	4.38E+03	4.37E+03	4.11E+03
UN (± %)	1.57E+01	1.15E+01	8.47E+00	6.54E+00

Table C.18 Spray evaporation of HFC-236ea on the Turbo-CII tube at a saturation temperature of 2°C ($\dot{m}_{spr}$= 2.8 kg/min, run 2)

h (W/m^2 K)	6.14E+03	7.44E+03	8.74E+03	9.42E+03	9.36E+03
q" (W/m^2)	3.00E+01	2.49E+01	1.99E+01	1.50E+01	9.64E+00
q (Watts)	1.50E+03	1.25E+03	9.97E+02	7.53E+02	4.84E+02
$LMTD$ (°C)	7.40E+00	5.79E+00	4.61E+00	3.82E+00	3.01E+00
ΔT (°C)	3.72E+00	2.92E+00	2.34E+00	1.95E+00	1.56E+00
h_i (W/m^2 K)	1.54E+04	1.31E+04	1.08E+04	8.49E+03	6.08E+03
Re_i	1.11E+04	8.87E+03	6.89E+03	5.04E+03	3.29E+03
U_o (W/m^2 K)	4.11E+03	4.37E+03	4.38E+03	3.99E+03	3.25E+03
UN (± %)	6.51E+00	8.50E+00	1.16E+01	1.59E+01	2.38E+01

Table C.19 Spray evaporation of HFC-236ea on the Turbo-CII tube at a saturation temperature of 2°C ($\dot{m}_{spr}$= 3.0 kg/min, run 1)

h (W/m^2 K)	9.71E+03	9.38E+03	7.95E+03	7.00E+03
$q"$ (W/m^2)	1.50E+01	1.98E+01	2.51E+01	2.99E+01
q (Watts)	7.54E+02	9.94E+02	1.26E+03	1.50E+03
$LMTD$ (°C)	3.78E+00	4.44E+00	5.61E+00	6.80E+00
ΔT (°C)	1.93E+00	2.26E+00	2.84E+00	3.42E+00
h_i (W/m^2 K)	8.49E+03	1.08E+04	1.30E+04	1.53E+04
Re_i	5.04E+03	6.86E+03	8.80E+03	1.09E+04
U_o (W/m^2 K)	4.04E+03	4.53E+03	4.54E+03	4.47E+03
UN (± %)	1.63E+01	1.24E+01	8.90E+00	7.14E+00

Table C.20 Spray evaporation of HFC-236ea on the Turbo-CII tube at a saturation temperature of 2°C ($\dot{m}_{spr}$= 3.0 kg/min, run 2)

h (W/m^2 K)	7.02E+03	7.98E+03	9.39E+03	9.72E+03
$q"$ (W/m^2)	2.98E+01	2.52E+01	2.01E+01	1.49E+01
q (Watts)	1.50E+03	1.26E+03	1.01E+03	7.48E+02
$LMTD$ (°C)	6.76E+00	5.62E+00	4.49E+00	3.75E+00
ΔT (°C)	3.40E+00	2.84E+00	2.28E+00	1.92E+00
h_i (W/m^2 K)	1.53E+04	1.31E+04	1.08E+04	8.48E+03
Re_i	1.09E+04	8.81E+03	6.86E+03	5.03E+03
U_o (W/m^2 K)	4.48E+03	4.55E+03	4.53E+03	4.04E+03
UN (± %)	7.19E+00	8.90E+00	1.23E+01	1.64E+01

Table C.21 Spray evaporation of HFC-236ea on the Turbo-CII tube at a saturation temperature of 2°C ($\dot{m}_{spr}$= 3.0 kg/min, repeat run for run 1)

h (W/m^2 K)	9.69E+03	9.37E+03	7.91E+03	6.95E+03
q" (W/m^2)	1.50E+01	2.00E+01	2.50E+01	2.97E+01
q (Watts)	7.54E+02	1.00E+03	1.26E+03	1.49E+03
$LMTD$ (°C)	3.79E+00	4.48E+00	5.62E+00	6.79E+00
ΔT (°C)	1.94E+00	2.28E+00	2.84E+00	3.42E+00
h_i (W/m^2 K)	8.48E+03	1.08E+04	1.31E+04	1.53E+04
Re_i	5.03E+03	6.86E+03	8.83E+03	1.09E+04
U_o (W/m^2 K)	4.03E+03	4.53E+03	4.53E+03	4.45E+03
UN (± %)	1.62E+01	1.23E+01	8.88E+00	7.15E+00

Table C.22 Spray evaporation of HFC-236ea on the Turbo-CII tube at a saturation temperature of 2°C ($\dot{m}_{spr}$= 3.0 kg/min, repeat run for run 2)

h (W/m^2 K)	6.97E+03	7.94E+03	9.37E+03	9.70E+03	9.47E+03
q" (W/m^2)	2.98E+01	2.50E+01	2.00E+01	1.50E+01	9.57E+00
q (Watts)	1.50E+03	1.25E+03	1.00E+03	7.51E+02	4.80E+02
$LMTD$ (°C)	6.79E+00	5.59E+00	4.47E+00	3.77E+00	2.98E+00
ΔT (°C)	3.42E+00	2.83E+00	2.27E+00	1.93E+00	1.54E+00
h_i (W/m^2 K)	1.53E+04	1.30E+04	1.08E+04	8.49E+03	6.06E+03
Re_i	1.09E+04	8.79E+03	6.87E+03	5.03E+03	3.27E+03
U_o (W/m^2 K)	4.46E+03	4.53E+03	4.53E+03	4.04E+03	3.25E+03
UN (± %)	7.14E+00	8.94E+00	1.23E+01	1.63E+01	2.42E+01

Table C.23 Spray evaporation of HFC-236ea on the Turbo-CII tube at a saturation temperature of 2°C ($\dot{m}_{spr}$= 3.2 kg/min, run 1)

h (W/m^2 K)	1.02E+04	9.76E+03	8.93E+03	8.06E+03
q'' (W/m^2)	1.50E+01	1.99E+01	2.50E+01	2.99E+01
q (Watts)	7.54E+02	1.00E+03	1.26E+03	1.50E+03
$LMTD$ (°C)	3.71E+00	4.39E+00	5.26E+00	6.24E+00
ΔT (°C)	1.90E+00	2.23E+00	2.66E+00	3.14E+00
h_i (W/m^2 K)	8.49E+03	1.08E+04	1.30E+04	1.52E+04
Re_i	5.03E+03	6.83E+03	8.73E+03	1.07E+04
U_o (W/m^2 K)	4.12E+03	4.61E+03	4.83E+03	4.86E+03
UN (± %)	1.70E+01	1.28E+01	9.80E+00	7.93E+00

Table C.24 Spray evaporation of HFC-236ea on the Turbo-CII tube at a saturation temperature of 2°C ($\dot{m}_{spr}$= 3.2 kg/min, run 2)

h (W/m^2 K)	8.08E+03	8.95E+03	9.78E+03	1.03E+04
q'' (W/m^2)	2.98E+01	2.50E+01	2.00E+01	1.50E+01
q (Watts)	1.50E+03	1.26E+03	1.00E+03	7.51E+02
$LMTD$ (°C)	6.21E+00	5.25E+00	4.39E+00	3.69E+00
ΔT (°C)	3.13E+00	2.66E+00	2.23E+00	1.89E+00
h_i (W/m^2 K)	1.52E+04	1.30E+04	1.08E+04	8.47E+03
Re_i	1.08E+04	8.74E+03	6.85E+03	5.01E+03
U_o (W/m^2 K)	4.88E+03	4.84E+03	4.62E+03	4.12E+03
UN (± %)	7.96E+00	9.82E+00	1.28E+01	1.72E+01

Table C.25 Spray evaporation of HFC-236ea on the 1575-fpm tube at a saturation temperature of 2°C ($\dot{m}_{spr}$= 2.6 kg/min, run 1)

h (W/m^2 K)	5.81E+03	5.25E+03	4.43E+03	3.81E+03
q'' (W/m^2)	1.48E+04	1.98E+04	2.50E+04	2.97E+04
q (Watts)	7.44E+02	9.95E+02	1.25E+03	1.49E+03
$LMTD$ (°C)	7.17E+00	8.59E+00	1.06E+01	1.28E+01
ΔT (°C)	3.61E+00	4.32E+00	5.34E+00	6.42E+00
h_i (W/m^2 K)	3.98E+03	5.12E+03	6.26E+03	7.43E+03
Re_i	5.52E+03	7.70E+03	1.01E+04	1.29E+04
U_o (W/m^2 K)	2.09E+03	2.33E+03	2.37E+03	2.34E+03
UN (± %)	1.24E+01	9.28E+00	7.05E+00	5.87E+00

Table C.26 Spray evaporation of HFC-236ea on the 1575-fpm tube at a saturation temperature of 2°C ($\dot{m}_{spr}$= 2.6 kg/min, run 2)

h (W/m^2 K)	3.80E+03	4.57E+03	5.29E+03	5.74E+03	5.32E+03
q'' (W/m^2)	2.98E+04	2.51E+04	1.96E+04	1.48E+04	9.66E+03
q (Watts)	1.49E+03	1.26E+03	9.85E+02	7.43E+02	4.85E+02
$LMTD$ (°C)	1.29E+01	1.05E+01	8.49E+00	7.19E+00	6.03E+00
ΔT (°C)	6.46E+00	5.28E+00	4.27E+00	3.62E+00	3.04E+00
h_i (W/m^2 K)	7.44E+03	6.25E+03	5.11E+03	3.99E+03	2.84E+03
Re_i	1.29E+04	1.01E+04	7.66E+03	5.54E+03	3.57E+03
U_o (W/m^2 K)	2.33E+03	2.41E+03	2.33E+03	2.08E+03	1.62E+03
UN (± %)	5.85E+00	7.16E+00	9.43E+00	1.23E+01	1.63E+01

Table C.27 Spray evaporation of HFC-236ea on the 1575-fpm tube at a saturation temperature of 2°C ($\dot{m}_{spr}$= 2.8 kg/min, run 1)

h (W/m^2 K)	6.18E+03	5.52E+03	4.75E+03	4.08E+03
q" (W/m^2)	1.48E+04	1.98E+04	2.49E+04	2.98E+04
q (Watts)	7.42E+02	9.92E+02	1.25E+03	1.49E+03
$LMTD$ (°C)	7.00E+00	8.41E+00	1.02E+01	1.24E+01
ΔT (°C)	3.52E+00	4.22E+00	5.14E+00	6.19E+00
h_i (W/m^2 K)	3.97E+03	5.10E+03	6.23E+03	7.41E+03
Re_i	5.49E+03	7.64E+03	1.00E+04	1.27E+04
U_o (W/m^2 K)	2.13E+03	2.37E+03	2.45E+03	2.43E+03
UN (± %)	1.31E+01	9.66E+00	7.41E+00	6.10E+00

Table C.28 Spray evaporation of HFC-236ea on the 1575-fpm tube at a saturation temperature of 2°C ($\dot{m}_{spr}$= 2.8 kg/min, run 2)

h (W/m^2 K)	4.09E+03	4.89E+03	5.50E+03	6.20E+03	5.39E+03
q" (W/m^2)	3.00E+04	2.50E+04	1.99E+04	1.48E+04	9.64E+03
q (Watts)	1.50E+03	1.25E+03	9.97E+02	7.44E+02	4.84E+02
$LMTD$ (°C)	1.24E+01	1.01E+01	8.46E+00	7.01E+00	5.99E+00
ΔT (°C)	6.22E+00	5.08E+00	4.25E+00	3.53E+00	3.02E+00
h_i (W/m^2 K)	7.41E+03	6.23E+03	5.11E+03	3.98E+03	2.84E+03
Re_i	1.27E+04	1.00E+04	7.65E+03	5.50E+03	3.57E+03
U_o (W/m^2 K)	2.44E+03	2.49E+03	2.37E+03	2.14E+03	1.62E+03
UN (± %)	6.07E+00	7.55E+00	9.59E+00	1.32E+01	1.65E+01

Table C.29 Spray evaporation of HFC-236ea on the 1575-fpm tube at a saturation temperature of 2°C ($\dot{m}_{spr}$= 3.0 kg/min, run 1)

h (W/m^2 K)	6.63E+03	6.44E+03	5.97E+03	5.20E+03
$q"$ (W/m^2)	1.50E+04	1.99E+04	2.48E+04	2.99E+04
q (Watts)	7.55E+02	1.00E+03	1.24E+03	1.50E+03
$LMTD$ (°C)	6.95E+00	7.97E+00	9.18E+00	1.09E+01
ΔT (°C)	3.50E+00	4.01E+00	4.61E+00	5.47E+00
h_i (W/m^2 K)	3.98E+03	5.08E+03	6.15E+03	7.28E+03
Re_i	5.50E+03	7.56E+03	9.74E+03	1.23E+04
U_o (W/m^2 K)	2.18E+03	2.52E+03	2.73E+03	2.77E+03
UN (± %)	1.37E+01	1.08E+01	8.76E+00	7.05E+00

Table C.30 Spray evaporation of HFC-236ea on the 1575-fpm tube at a saturation temperature of 2°C ($\dot{m}_{spr}$= 3.0 kg/min, repeat run for run 1)

h (W/m^2 K)	6.64E+00	6.46E+00	5.93E+00	5.15E+00
$q"$ (W/m^2)	1.49E+01	2.00E+01	2.50E+01	2.97E+01
q (Watts)	7.46E+02	1.00E+03	1.25E+03	1.49E+03
$LMTD$ (°C)	6.88E+00	7.98E+00	9.27E+00	1.09E+01
ΔT (°C)	3.46E+00	4.01E+00	4.66E+00	5.46E+00
h_i (W/m^2 K)	3.97E+03	5.08E+03	6.16E+03	7.27E+03
Re_i	5.48E+03	7.55E+03	9.77E+03	1.22E+04
U_o (W/m^2 K)	2.18E+03	2.53E+03	2.72E+03	2.75E+03
UN (± %)	1.39E+01	1.08E+01	8.64E+00	7.06E+00

Table C.31 Spray evaporation of HFC-236ea on the 1575-fpm tube at a saturation temperature of 2°C ($\dot{m}_{spr}$= 3.0 kg/min, run 2)

h (W/m^2 K)	5.19E+03	5.93E+03	6.38E+03	6.63E+03	5.50E+03
$q"$ (W/m^2)	3.00E+04	2.49E+04	2.01E+04	1.50E+04	9.57E+03
q (Watts)	1.51E+03	1.25E+03	1.01E+03	7.51E+02	4.80E+02
$LMTD$ (°C)	1.10E+01	9.24E+00	8.06E+00	6.93E+00	5.91E+00
ΔT (°C)	5.49E+00	4.64E+00	4.05E+00	3.49E+00	2.98E+00
h_i (W/m^2 K)	7.28E+03	6.15E+03	5.09E+03	3.97E+03	2.84E+03
Re_i	1.23E+04	9.75E+03	7.58E+03	5.49E+03	3.56E+03
U_o (W/m^2 K)	2.77E+03	2.72E+03	2.52E+03	2.18E+03	1.64E+03
UN (± %)	7.02E+00	8.68E+00	1.06E+01	1.38E+01	1.70E+01

Table C.32 Spray evaporation of HFC-236ea on the 1575-fpm tube at a saturation temperature of 2°C ($\dot{m}_{spr}$= 3.2 kg/min, run 1)

h (W/m^2 K)	6.63E+03	6.45E+03	5.97E+03	5.26E+03
q'' (W/m^2)	1.48E+04	1.97E+04	2.48E+04	3.01E+04
q (Watts)	7.42E+02	9.87E+02	1.24E+03	1.51E+03
$LMTD$ (°C)	6.86E+00	7.87E+00	9.17E+00	1.09E+01
ΔT (°C)	3.45E+00	3.96E+00	4.60E+00	5.48E+00
h_i (W/m^2 K)	3.96E+03	5.07E+03	6.16E+03	7.26E+03
Re_i	5.47E+03	7.53E+03	9.75E+03	1.22E+04
U_o (W/m^2 K)	2.18E+03	2.52E+03	2.73E+03	2.78E+03
UN (± %)	1.39E+01	1.10E+01	8.76E+00	7.05E+00

Table C.33 Spray evaporation of HFC-236ea on the 1575-fpm tube at a saturation temperature of 2°C ($\dot{m}_{spr}$= 3.2 kg/min, run 2)

h (W/m^2 K)	5.33E+03	6.02E+03	6.48E+03	6.79E+03	5.69E+03
q'' (W/m^2)	2.97E+04	2.47E+04	1.98E+04	1.47E+04	9.64E+03
q (Watts)	1.49E+03	1.24E+03	9.95E+02	7.39E+02	4.83E+02
$LMTD$ (°C)	1.07E+01	9.11E+00	7.93E+00	6.77E+00	5.91E+00
ΔT (°C)	5.36E+00	4.57E+00	3.99E+00	3.41E+00	2.98E+00
h_i (W/m^2 K)	7.25E+03	6.15E+03	5.06E+03	3.96E+03	2.82E+03
Re_i	1.22E+04	9.72E+03	7.52E+03	5.46E+03	3.54E+03
U_o (W/m^2 K)	2.80E+03	2.74E+03	2.53E+03	2.19E+03	1.65E+03
UN (± %)	7.22E+00	8.85E+00	1.09E+01	1.43E+01	1.74E+01

Table C.34 Condensation of HFC-236ea on the Turbo-CII tube at a saturation temperature of 40°C (primary run)

h (W/m^2 K)	9.79E+03	1.13E+04	1.23E+04	1.31E+04	1.37E+04	1.42E+04
$q"$ (W/m^2)	1.50E+04	2.00E+04	2.50E+04	3.00E+04	3.50E+04	4.00E+04
q (Watts)	7.54E+02	1.00E+03	1.26E+03	1.51E+03	1.76E+03	2.01E+03
$LMTD$ (°C)	3.02E+00	3.35E+00	3.71E+00	4.06E+00	4.38E+00	4.72E+00
ΔT (°C)	1.57E+00	1.72E+00	1.90E+00	2.07E+00	2.23E+00	2.39E+00
h_i (W/m^2 K)	1.29E+04	1.63E+04	1.93E+04	2.22E+04	2.51E+04	2.78E+04
Re_i	1.08E+04	1.44E+04	1.77E+04	2.10E+04	2.45E+04	2.77E+04
U_o (W/m^2 K)	5.05E+03	6.05E+03	6.84E+03	7.51E+03	8.12E+03	8.61E+03
UN (± %)	7.63E+00	7.00E+00	6.46E+00	6.10E+00	5.78E+00	5.51E+00

Table C.35 Condensation of HFC-236ea on the Turbo-CII tube at a saturation temperature of 40°C (repeat run)

h (W/m^2 K)	9.77E+03	1.12E+04	1.22E+04	1.31E+04	1.37E+04	1.42E+04
$q"$ (W/m^2)	1.50E+04	2.00E+04	2.50E+04	3.00E+04	3.50E+04	4.00E+04
q (Watts)	7.54E+02	1.00E+03	1.25E+03	1.50E+03	1.75E+03	2.01E+03
$LMTD$ (°C)	3.03E+00	3.38E+00	3.73E+00	4.05E+00	4.38E+00	4.71E+00
ΔT (°C)	1.57E+00	1.74E+00	1.91E+00	2.07E+00	2.23E+00	2.39E+00
h_i (W/m^2 K)	1.29E+04	1.62E+04	1.92E+04	2.22E+04	2.51E+04	2.78E+04
Re_i	1.08E+04	1.43E+04	1.76E+04	2.11E+04	2.44E+04	2.77E+04
U_o (W/m^2 K)	5.05E+03	6.02E+03	6.81E+03	7.52E+03	8.11E+03	8.61E+03
UN (± %)	7.63E+00	6.92E+00	6.43E+00	6.07E+00	5.77E+00	5.52E+00

APPENDIX D TABULATED DATA OF HFC-236FA

The experimental data obtained in this study for HFC-236fa are presented in this appendix. The symbols h is shell-side heat transfer coefficient (W/m^2 K), $q"$ is heat flux (W/m^2), q is heat transfer rate (Watts), $LMTD$ is log mean temperature difference (°C), ΔT is the temperature difference between tube surface and saturation refrigerant (°C), h_i is in-tube heat transfer coefficient (W/m^2 K), Re_i is Reynolds number of water, U_o is overall heat transfer coefficient (W/m^2 K), and UN is the uncertainty of shell-side heat transfer coefficient (± %).

Table D.1 Pool boiling of HFC-236fa on the 1024-fpm tube at a saturation temperature of 2°C (primary run)

h (W/m^2 K)	7.55E+03	7.16E+03	6.64E+03	6.09E+03	5.42E+03	4.86E+03
$q"$ (W/m^2)	3.99E+04	3.50E+04	3.00E+04	2.50E+04	1.99E+04	1.50E+04
q (Watts)	2.00E+03	1.76E+03	1.50E+03	1.25E+03	9.96E+02	7.53E+02
$LMTD$ (°C)	1.08E+01	1.03E+01	9.79E+00	9.20E+00	8.53E+00	7.77E+00
ΔT (°C)	5.42E+00	5.17E+00	4.91E+00	4.62E+00	4.28E+00	3.91E+00
h_i (W/m^2 K)	9.79E+03	8.74E+03	7.67E+03	6.60E+03	5.50E+03	4.31E+03
Re_i	1.78E+04	1.53E+04	1.30E+04	1.06E+04	8.41E+03	6.15E+03
U_o (W/m^2 K)	3.69E+03	3.40E+03	3.06E+03	2.71E+03	2.33E+03	1.93E+03
UN (± %)	7.25E+00	7.53E+00	7.87E+00	8.30E+00	8.86E+00	9.81E+00

Table D.2 Pool boiling of HFC-236fa on the 1024-fpm tube at a saturation temperature of 2°C (repeat run)

h (W/m^2 K)	7.32E+03	7.02E+03	6.56E+03	6.03E+03	5.36E+03	4.78E+03
$q"$ (W/m^2)	3.97E+04	3.49E+04	3.00E+04	2.50E+04	2.00E+04	1.50E+04
q (Watts)	1.99E+03	1.75E+03	1.50E+03	1.26E+03	1.01E+03	7.54E+02
$LMTD$ (°C)	1.09E+01	1.04E+01	9.83E+00	9.28E+00	8.64E+00	7.83E+00
ΔT (°C)	5.47E+00	5.21E+00	4.93E+00	4.66E+00	4.34E+00	3.94E+00
h_i (W/m^2 K)	9.79E+03	8.73E+03	7.69E+03	6.58E+03	5.50E+03	4.31E+03
Re_i	1.78E+04	1.53E+04	1.30E+04	1.06E+04	8.42E+03	6.16E+03
U_o (W/m^2 K)	3.64E+03	3.36E+03	3.05E+03	2.70E+03	2.32E+03	1.92E+03
UN (± %)	7.15E+00	7.44E+00	7.80E+00	8.21E+00	8.72E+00	9.68E+00

Table D.3 Pool boiling of HFC-236fa on the 1575-fpm tube at a saturation temperature of 2°C (primary run)

h (W/m^2 K)	6.14E+03	5.81E+03	5.32E+03	4.80E+03	4.31E+03	3.74E+03
$q"$ (W/m^2)	3.99E+04	3.49E+04	3.00E+04	2.50E+04	1.99E+04	1.50E+04
q (Watts)	2.00E+03	1.75E+03	1.50E+03	1.25E+03	9.98E+02	7.51E+02
$LMTD$ (°C)	1.19E+01	1.13E+01	1.08E+01	1.02E+01	9.39E+00	8.59E+00
ΔT (°C)	5.96E+00	5.67E+00	5.42E+00	5.12E+00	4.71E+00	4.32E+00
h_i (W/m^2 K)	9.29E+03	8.28E+03	7.27E+03	6.24E+03	5.19E+03	4.05E+03
Re_i	1.68E+04	1.45E+04	1.22E+04	1.00E+04	7.91E+03	5.75E+03
U_o (W/m^2 K)	3.38E+03	3.12E+03	2.80E+03	2.47E+03	2.14E+03	1.76E+03
UN (± %)	6.32E+00	6.54E+00	6.72E+00	6.97E+00	7.46E+00	8.02E+00

Table D.4 Pool boiling of HFC-236fa on the 1575-fpm tube at a saturation temperature of 2°C (repeat run)

h (W/m^2 K)	6.13E+03	5.75E+03	5.30E+03	4.84E+03	4.31E+03	3.66E+03
$q"$ (W/m^2)	3.99E+04	3.50E+04	3.00E+04	2.50E+04	1.98E+04	1.50E+04
q (Watts)	2.00E+03	1.75E+03	1.50E+03	1.25E+03	9.94E+02	7.52E+02
$LMTD$ (°C)	1.19E+01	1.14E+01	1.08E+01	1.02E+01	9.36E+00	8.68E+00
ΔT (°C)	5.98E+00	5.71E+00	5.43E+00	5.10E+00	4.70E+00	4.36E+00
h_i (W/m^2 K)	9.29E+03	8.27E+03	7.27E+03	6.24E+03	5.18E+03	4.07E+03
Re_i	1.68E+04	1.45E+04	1.22E+04	1.00E+04	7.88E+03	5.79E+03
U_o (W/m^2 K)	3.38E+03	3.10E+03	2.80E+03	2.48E+03	2.14E+03	1.74E+03
UN (± %)	6.29E+00	6.48E+00	6.71E+00	7.02E+00	7.49E+00	7.90E+00

Table D.5 Pool boiling of HFC-236fa on the Turbo-B tube at a saturation temperature of 2°C (primary run)

h (W/m^2 K)	1.18E+04	1.16E+04	1.12E+04	1.04E+04	9.14E+03	7.97E+03
$q"$ (W/m^2)	3.98E+04	3.50E+04	3.00E+04	2.50E+04	2.00E+04	1.49E+04
q (Watts)	2.00E+03	1.76E+03	1.50E+03	1.26E+03	1.00E+03	7.48E+02
$LMTD$ (°C)	5.88E+00	5.47E+00	5.03E+00	4.69E+00	4.33E+00	3.89E+00
ΔT (°C)	2.97E+00	2.76E+00	2.55E+00	2.38E+00	2.20E+00	1.98E+00
h_i (W/m^2 K)	2.08E+04	1.86E+04	1.64E+04	1.40E+04	1.18E+04	9.26E+03
Re_i	1.38E+04	1.20E+04	1.01E+04	8.32E+03	6.64E+03	4.90E+03
U_o (W/m^2 K)	6.97E+03	6.60E+03	6.14E+03	5.50E+03	4.75E+03	3.95E+03
UN (± %)	7.38E+00	7.93E+00	8.63E+00	9.26E+00	9.98E+00	1.12E+01

Table D.6 Pool boiling of HFC-236fa on the Turbo-B tube at a saturation temperature of 2°C (repeat run)

h (W/m^2 K)	1.18E+04	1.17E+04	1.11E+04	1.04E+04	9.09E+03	7.67E+03
$q"$ (W/m^2)	3.99E+04	3.50E+04	3.00E+04	2.50E+04	2.01E+04	1.51E+04
q (Watts)	2.00E+03	1.75E+03	1.50E+03	1.26E+03	1.01E+03	7.58E+02
$LMTD$ (°C)	5.88E+00	5.44E+00	5.06E+00	4.69E+00	4.37E+00	4.02E+00
ΔT (°C)	2.97E+00	2.75E+00	2.56E+00	2.38E+00	2.22E+00	2.05E+00
h_i (W/m^2 K)	2.08E+04	1.86E+04	1.63E+04	1.40E+04	1.17E+04	9.28E+03
Re_i	1.38E+04	1.19E+04	1.01E+04	8.34E+03	6.64E+03	4.92E+03
U_o (W/m^2 K)	6.98E+03	6.62E+03	6.10E+03	5.50E+03	4.73E+03	3.88E+03
UN (± %)	7.38E+00	7.97E+00	8.56E+00	9.25E+00	9.89E+00	1.07E+01

Table D.7 Pool boiling of HFC-236fa on the Turbo-BII tube at a saturation temperature of 2°C (primary run)

h (W/m^2 K)	1.45E+04	1.45E+04	1.45E+04	1.46E+04	1.45E+04	1.39E+04
$q"$ (W/m^2)	4.00E+04	3.50E+04	3.00E+04	2.50E+04	2.00E+04	1.50E+04
q (Watts)	2.01E+03	1.76E+03	1.50E+03	1.26E+03	1.01E+03	7.55E+02
$LMTD$ (°C)	5.61E+00	5.21E+00	4.77E+00	4.34E+00	3.89E+00	3.46E+00
ΔT (°C)	2.83E+00	2.64E+00	2.42E+00	2.21E+00	1.99E+00	1.78E+00
h_i (W/m^2 K)	1.70E+04	1.52E+04	1.34E+04	1.15E+04	9.59E+03	7.58E+03
Re_i	1.37E+04	1.18E+04	1.00E+04	8.26E+03	6.55E+03	4.86E+03
U_o (W/m^2 K)	7.10E+03	6.70E+03	6.25E+03	5.74E+03	5.12E+03	4.32E+03
UN (± %)	9.08E+00	9.99E+00	1.13E+01	1.31E+01	1.57E+01	1.94E+01

Table D.8 Pool boiling of HFC-236fa on the Turbo-BII tube at a saturation temperature of 2°C (repeat run)

h (W/m^2 K)	1.45E+04	1.45E+04	1.45E+04	1.47E+04	1.45E+04	1.39E+04
$q"$ (W/m^2)	4.00E+04	3.50E+04	3.00E+04	2.49E+04	2.00E+04	1.50E+04
q (Watts)	2.01E+03	1.76E+03	1.51E+03	1.25E+03	1.01E+03	7.55E+02
$LMTD$ (°C)	5.61E+00	5.20E+00	4.79E+00	4.30E+00	3.90E+00	3.47E+00
ΔT (°C)	2.83E+00	2.63E+00	2.43E+00	2.19E+00	1.99E+00	1.78E+00
h_i (W/m^2 K)	1.70E+04	1.52E+04	1.33E+04	1.15E+04	9.58E+03	7.55E+03
Re_i	1.37E+04	1.19E+04	1.00E+04	8.25E+03	6.55E+03	4.83E+03
U_o (W/m^2 K)	7.11E+03	6.71E+03	6.25E+03	5.76E+03	5.12E+03	4.32E+03
UN (± %)	9.10E+00	1.00E+01	1.13E+01	1.33E+01	1.57E+01	1.94E+01

Table D.9 Pool boiling of HFC-236fa with 1% oil on the 1024-fpm tube at a saturation temperature of 2°C (primary run)

h (W/m^2 K)	6.72E+03	6.43E+03	6.02E+03	5.57E+03	5.00E+03	4.28E+03
q" (W/m^2)	3.99E+04	3.50E+04	3.00E+04	2.50E+04	2.00E+04	1.50E+04
q (Watts)	2.00E+03	1.76E+03	1.51E+03	1.25E+03	1.00E+03	7.55E+02
$LMTD$ (°C)	1.14E+01	1.08E+01	1.02E+01	9.58E+00	8.87E+00	8.20E+00
ΔT (°C)	5.73E+00	5.43E+00	5.14E+00	4.81E+00	4.46E+00	4.12E+00
h_i (W/m^2 K)	9.87E+03	8.81E+03	7.71E+03	6.62E+03	5.50E+03	4.32E+03
Re_i	1.81E+04	1.56E+04	1.31E+04	1.07E+04	8.45E+03	6.20E+03
U_o (W/m^2 K)	3.49E+03	3.23E+03	2.93E+03	2.61E+03	2.25E+03	1.84E+03
UN (± %)	6.73E+00	7.03E+00	7.34E+00	7.78E+00	8.32E+00	8.89E+00

Table D.10 Pool boiling of HFC-236fa with 1% oil on the 1024-fpm tube at a saturation temperature of 2°C (repeat run)

h (W/m^2 K)	6.76E+03	6.46E+03	6.03E+03	5.59E+03	5.06E+03	4.29E+03
q" (W/m^2)	4.00E+04	3.50E+04	3.01E+04	2.50E+04	1.99E+04	1.50E+04
q (Watts)	2.01E+03	1.76E+03	1.51E+03	1.26E+03	1.00E+03	7.51E+02
$LMTD$ (°C)	1.14E+01	1.08E+01	1.03E+01	9.58E+00	8.82E+00	8.15E+00
ΔT (°C)	5.72E+00	5.42E+00	5.15E+00	4.81E+00	4.43E+00	4.09E+00
h_i (W/m^2 K)	9.86E+03	8.79E+03	7.71E+03	6.62E+03	5.50E+03	4.32E+03
Re_i	1.81E+04	1.55E+04	1.31E+04	1.07E+04	8.45E+03	6.19E+03
U_o (W/m^2 K)	3.50E+03	3.24E+03	2.93E+03	2.61E+03	2.26E+03	1.84E+03
UN (± %)	6.75E+00	7.05E+00	7.33E+00	7.79E+00	8.38E+00	8.96E+00

Table D.11 Pool boiling of HFC-236fa with 1% oil on the 1575-fpm tube at a saturation temperature of 2°C (primary run)

h (W/m^2 K)	5.92E+03	5.53E+03	5.09E+03	4.65E+03	4.38E+03	3.85E+03
q" (W/m^2)	4.00E+04	3.49E+04	2.99E+04	2.50E+04	2.00E+04	1.50E+04
q (Watts)	2.01E+03	1.75E+03	1.50E+03	1.26E+03	1.00E+03	7.51E+02
$LMTD$ (°C)	1.22E+01	1.16E+01	1.10E+01	1.04E+01	9.35E+00	8.49E+00
ΔT (°C)	6.10E+00	5.81E+00	5.53E+00	5.21E+00	4.69E+00	4.26E+00
h_i (W/m^2 K)	9.30E+03	8.29E+03	7.30E+03	6.24E+03	5.20E+03	4.05E+03
Re_i	1.69E+04	1.45E+04	1.23E+04	1.01E+04	7.91E+03	5.73E+03
U_o (W/m^2 K)	3.32E+03	3.04E+03	2.74E+03	2.43E+03	2.16E+03	1.78E+03
UN (± %)	6.15E+00	6.35E+00	6.56E+00	6.82E+00	7.51E+00	8.18E+00

Table D.12 Pool boiling of HFC-236fa with 1% oil on the 1575-fpm tube at a saturation temperature of 2°C (repeat run)

h (W/m^2 K)	5.91E+03	5.51E+03	5.08E+03	4.65E+03	4.24E+03	3.68E+03
q" (W/m^2)	4.01E+04	3.49E+04	2.99E+04	2.50E+04	2.01E+04	1.51E+04
q (Watts)	2.01E+03	1.75E+03	1.50E+03	1.26E+03	1.01E+03	7.56E+02
$LMTD$ (°C)	1.22E+01	1.16E+01	1.10E+01	1.04E+01	9.57E+00	8.71E+00
ΔT (°C)	6.11E+00	5.81E+00	5.53E+00	5.21E+00	4.80E+00	4.37E+00
h_i (W/m^2 K)	9.31E+03	8.31E+03	7.29E+03	6.26E+03	5.19E+03	4.06E+03
Re_i	1.69E+04	1.46E+04	1.23E+04	1.01E+04	7.92E+03	5.76E+03
U_o (W/m^2 K)	3.32E+03	3.03E+03	2.74E+03	2.43E+03	2.12E+03	1.75E+03
UN (± %)	6.14E+00	6.34E+00	6.56E+00	6.83E+00	7.29E+00	7.88E+00

Table D.13 Pool boiling of HFC-236fa with 1% oil on the Turbo-B tube at a saturation temperature of 2°C (primary run)

h (W/m^2 K)	1.32E+04	1.26E+04	1.19E+04	1.10E+04	9.98E+03	8.60E+03
$q"$ (W/m^2)	4.00E+04	3.50E+04	2.99E+04	2.49E+04	2.00E+04	1.50E+04
q (Watts)	2.01E+03	1.75E+03	1.50E+03	1.25E+03	1.00E+03	7.55E+02
$LMTD$ (°C)	5.56E+00	5.23E+00	4.87E+00	4.53E+00	4.15E+00	3.78E+00
ΔT (°C)	2.81E+00	2.65E+00	2.47E+00	2.30E+00	2.11E+00	1.93E+00
h_i (W/m^2 K)	2.07E+04	1.85E+04	1.63E+04	1.40E+04	1.17E+04	9.25E+03
Re_i	1.37E+04	1.19E+04	1.00E+04	8.30E+03	6.60E+03	4.89E+03
U_o (W/m^2 K)	7.41E+03	6.89E+03	6.33E+03	5.66E+03	4.96E+03	4.10E+03
UN (± %)	7.93E+00	8.42E+00	9.05E+00	9.73E+00	1.07E+01	1.19E+01

Table D.14 Pool boiling of HFC-236fa with 1% oil on the Turbo-B tube at a saturation temperature of 2°C (repeat run)

h (W/m^2 K)	1.31E+04	1.26E+04	1.19E+04	1.10E+04	9.96E+03	8.65E+03
$q"$ (W/m^2)	4.00E+04	3.50E+04	3.00E+04	2.50E+04	2.00E+04	1.50E+04
q (Watts)	2.01E+03	1.76E+03	1.51E+03	1.26E+03	1.00E+03	7.50E+02
$LMTD$ (°C)	5.56E+00	5.23E+00	4.89E+00	4.56E+00	4.15E+00	3.76E+00
ΔT (°C)	2.81E+00	2.65E+00	2.48E+00	2.31E+00	2.12E+00	1.92E+00
h_i (W/m^2 K)	2.07E+04	1.85E+04	1.63E+04	1.40E+04	1.17E+04	9.21E+03
Re_i	1.37E+04	1.18E+04	1.00E+04	8.33E+03	6.61E+03	4.86E+03
U_o (W/m^2 K)	7.41E+03	6.90E+03	6.33E+03	5.66E+03	4.95E+03	4.10E+03
UN (± %)	7.93E+00	8.42E+00	9.01E+00	9.67E+00	1.07E+01	1.20E+01

Table D.15 Pool boiling of HFC-236fa with 1% oil on the Turbo-BII tube at a saturation temperature of 2°C (primary run)

h (W/m^2 K)	1.90E+04	1.90E+04	1.88E+04	1.85E+04	1.77E+04	1.55E+04
q" (W/m^2)	3.99E+04	3.50E+04	3.00E+04	2.51E+04	2.01E+04	1.52E+04
q (Watts)	2.00E+03	1.76E+03	1.50E+03	1.26E+03	1.01E+03	7.61E+02
$LMTD$ (°C)	4.96E+00	4.65E+00	4.32E+00	4.00E+00	3.65E+00	3.38E+00
ΔT (°C)	2.51E+00	2.36E+00	2.20E+00	2.04E+00	1.87E+00	1.74E+00
h_i (W/m^2 K)	1.69E+04	1.51E+04	1.33E+04	1.14E+04	9.56E+03	7.56E+03
Re_i	1.35E+04	1.16E+04	9.91E+03	8.19E+03	6.52E+03	4.84E+03
U_o (W/m^2 K)	8.01E+03	7.48E+03	6.91E+03	6.25E+03	5.47E+03	4.47E+03
UN (± %)	1.13E+01	1.25E+01	1.41E+01	1.61E+01	1.88E+01	2.13E+01

Table D.16 Pool boiling of HFC-236fa with 1% oil on the Turbo-BII tube at a saturation temperature of 2°C (repeat run)

h (W/m^2 K)	1.93E+04	1.92E+04	1.92E+04	1.88E+04	1.80E+04	1.56E+04
q" (W/m^2)	4.00E+04	3.49E+04	3.00E+04	2.51E+04	2.00E+04	1.51E+04
q (Watts)	2.01E+03	1.75E+03	1.50E+03	1.26E+03	1.00E+03	7.60E+02
$LMTD$ (°C)	4.94E+00	4.62E+00	4.29E+00	3.98E+00	3.62E+00	3.37E+00
ΔT (°C)	2.50E+00	2.35E+00	2.18E+00	2.03E+00	1.85E+00	1.73E+00
h_i (W/m^2 K)	1.69E+04	1.51E+04	1.33E+04	1.14E+04	9.57E+03	7.57E+03
Re_i	1.35E+04	1.16E+04	9.90E+03	8.17E+03	6.52E+03	4.85E+03
U_o (W/m^2 K)	8.06E+03	7.53E+03	6.97E+03	6.28E+03	5.50E+03	4.48E+03
UN (± %)	1.15E+01	1.27E+01	1.43E+01	1.63E+01	1.92E+01	2.15E+01

Table D.17 Pool boiling of HFC-236fa with 3% oil on the 1024-fpm tube at a saturation temperature of 2°C (primary run)

h (W/m^2 K)	6.87E+03	6.49E+03	6.09E+03	5.58E+03	5.06E+03	4.34E+03
$q"$ (W/m^2)	4.00E+04	3.50E+04	3.00E+04	2.50E+04	2.01E+04	1.50E+04
q (Watts)	2.00E+03	1.76E+03	1.50E+03	1.25E+03	1.01E+03	7.55E+02
$LMTD$ (°C)	1.13E+01	1.08E+01	1.02E+01	9.58E+00	8.88E+00	8.15E+00
ΔT (°C)	5.68E+00	5.41E+00	5.11E+00	4.81E+00	4.46E+00	4.09E+00
h_i (W/m^2 K)	9.85E+03	8.79E+03	7.72E+03	6.61E+03	5.50E+03	4.32E+03
Re_i	1.80E+04	1.55E+04	1.31E+04	1.07E+04	8.46E+03	6.19E+03
U_o (W/m^2 K)	3.53E+03	3.25E+03	2.95E+03	2.61E+03	2.26E+03	1.85E+03
UN (± %)	6.81E+00	7.07E+00	7.40E+00	7.78E+00	8.33E+00	9.00E+00

Table D.18 Pool boiling of HFC-236fa with 3% oil on the 1024-fpm tube at a saturation temperature of 2°C (repeat run)

h (W/m^2 K)	6.89E+03	6.54E+03	6.11E+03	5.61E+03	5.08E+03	4.36E+03
$q"$ (W/m^2)	4.00E+04	3.50E+04	3.00E+04	2.51E+04	2.00E+04	1.51E+04
q (Watts)	2.01E+03	1.76E+03	1.51E+03	1.26E+03	1.01E+03	7.55E+02
$LMTD$ (°C)	1.13E+01	1.07E+01	1.02E+01	9.60E+00	8.84E+00	8.14E+00
ΔT (°C)	5.67E+00	5.38E+00	5.10E+00	4.82E+00	4.44E+00	4.09E+00
h_i (W/m^2 K)	9.84E+03	8.79E+03	7.70E+03	6.61E+03	5.50E+03	4.32E+03
Re_i	1.80E+04	1.55E+04	1.31E+04	1.07E+04	8.46E+03	6.20E+03
U_o (W/m^2 K)	3.53E+03	3.26E+03	2.95E+03	2.62E+03	2.27E+03	1.85E+03
UN (± %)	6.82E+00	7.11E+00	7.42E+00	7.77E+00	8.38E+00	9.01E+00

Table D.19 Pool boiling of HFC-236fa with 3% oil on the 1575-fpm tube at a saturation temperature of 2°C (primary run)

h (W/m^2 K)	6.14E+03	5.74E+03	5.32E+03	4.91E+03	4.41E+03	3.83E+03
$q"$ (W/m^2)	4.01E+04	3.50E+04	2.96E+04	2.50E+04	2.00E+04	1.49E+04
q (Watts)	2.01E+03	1.76E+03	1.48E+03	1.26E+03	1.01E+03	7.50E+02
$LMTD$ (°C)	1.20E+01	1.14E+01	1.07E+01	1.01E+01	9.37E+00	8.49E+00
ΔT (°C)	6.00E+00	5.72E+00	5.35E+00	5.07E+00	4.70E+00	4.26E+00
h_i (W/m^2 K)	9.29E+03	8.29E+03	7.25E+03	6.22E+03	5.17E+03	4.05E+03
Re_i	1.68E+04	1.45E+04	1.22E+04	9.99E+03	7.87E+03	5.74E+03
U_o (W/m^2 K)	3.38E+03	3.10E+03	2.80E+03	2.50E+03	2.16E+03	1.78E+03
UN (± %)	6.27E+00	6.46E+00	6.81E+00	7.07E+00	7.50E+00	8.16E+00

Table D.20 Pool boiling of HFC-236fa with 3% oil on the 1575-fpm tube at a saturation temperature of 2°C (repeat run)

h (W/m^2 K)	6.31E+03	5.94E+03	5.46E+03	4.96E+03	4.45E+03	3.86E+03
$q"$ (W/m^2)	4.00E+04	3.50E+04	3.00E+04	2.50E+04	2.00E+04	1.50E+04
q (Watts)	2.01E+03	1.75E+03	1.50E+03	1.25E+03	1.01E+03	7.55E+02
$LMTD$ (°C)	1.18E+01	1.12E+01	1.07E+01	1.00E+01	9.34E+00	8.50E+00
ΔT (°C)	5.91E+00	5.61E+00	5.35E+00	5.04E+00	4.69E+00	4.27E+00
h_i (W/m^2 K)	9.24E+03	8.26E+03	7.25E+03	6.22E+03	5.17E+03	4.06E+03
Re_i	1.67E+04	1.44E+04	1.22E+04	9.98E+03	7.86E+03	5.75E+03
U_o (W/m^2 K)	3.43E+03	3.15E+03	2.84E+03	2.51E+03	2.17E+03	1.79E+03
UN (± %)	6.37E+00	6.62E+00	6.84E+00	7.13E+00	7.54E+00	8.16E+00

Table D.21 Pool boiling of HFC-236fa with 3% oil on the Turbo-B tube at a saturation temperature of 2°C (primary run)

h (W/m^2 K)	1.25E+04	1.21E+04	1.14E+04	1.04E+04	9.36E+03	8.23E+03
q" (W/m^2)	4.00E+04	3.50E+04	3.00E+04	2.50E+04	2.00E+04	1.50E+04
q (Watts)	2.00E+03	1.76E+03	1.51E+03	1.26E+03	1.00E+03	7.54E+02
$LMTD$ (°C)	5.73E+00	5.34E+00	5.00E+00	4.69E+00	4.29E+00	3.86E+00
ΔT (°C)	2.89E+00	2.70E+00	2.53E+00	2.38E+00	2.19E+00	1.97E+00
h_i (W/m^2 K)	2.07E+04	1.86E+04	1.63E+04	1.40E+04	1.17E+04	9.23E+03
Re_i	1.37E+04	1.19E+04	1.01E+04	8.32E+03	6.64E+03	4.88E+03
U_o (W/m^2 K)	7.19E+03	6.75E+03	6.18E+03	5.50E+03	4.80E+03	4.01E+03
UN (± %)	7.63E+00	8.17E+00	8.70E+00	9.25E+00	1.01E+01	1.15E+01

Table D.22 Pool boiling of HFC-236fa with 3% oil on the Turbo-B tube at a saturation temperature of 2°C (repeat run)

h (W/m^2 K)	1.25E+04	1.20E+04	1.13E+04	1.03E+04	9.36E+03	8.17E+03
q" (W/m^2)	4.00E+04	3.50E+04	3.00E+04	2.50E+04	2.00E+04	1.50E+04
q (Watts)	2.01E+03	1.76E+03	1.51E+03	1.26E+03	1.00E+03	7.54E+02
$LMTD$ (°C)	5.73E+00	5.37E+00	5.03E+00	4.70E+00	4.29E+00	3.88E+00
ΔT (°C)	2.89E+00	2.72E+00	2.55E+00	2.38E+00	2.18E+00	1.98E+00
h_i (W/m^2 K)	2.07E+04	1.86E+04	1.63E+04	1.40E+04	1.17E+04	9.23E+03
Re_i	1.37E+04	1.19E+04	1.01E+04	8.32E+03	6.62E+03	4.89E+03
U_o (W/m^2 K)	7.19E+03	6.72E+03	6.14E+03	5.49E+03	4.80E+03	3.99E+03
UN (± %)	7.64E+00	8.11E+00	8.63E+00	9.23E+00	1.02E+01	1.14E+01

Table D.23 Pool boiling of HFC-236fa with 3% oil on the Turbo-BII tube at a saturation temperature of 2°C (primary run)

h (W/m^2 K)	1.68E+04	1.66E+04	1.62E+04	1.54E+04	1.42E+04	1.22E+04
$q"$ (W/m^2)	3.99E+04	3.50E+04	3.00E+04	2.50E+04	2.00E+04	1.50E+04
q (Watts)	2.00E+03	1.76E+03	1.51E+03	1.26E+03	1.00E+03	7.53E+02
$LMTD$ (°C)	5.23E+00	4.91E+00	4.57E+00	4.26E+00	3.91E+00	3.61E+00
ΔT (°C)	2.65E+00	2.49E+00	2.32E+00	2.17E+00	2.00E+00	1.85E+00
h_i (W/m^2 K)	1.69E+04	1.51E+04	1.33E+04	1.14E+04	9.58E+03	7.56E+03
Re_i	1.36E+04	1.17E+04	9.98E+03	8.22E+03	6.55E+03	4.85E+03
U_o (W/m^2 K)	7.59E+03	7.11E+03	6.54E+03	5.86E+03	5.09E+03	4.15E+03
UN (± %)	1.02E+01	1.12E+01	1.24E+01	1.37E+01	1.55E+01	1.73E+01

Table D.24 Pool boiling of HFC-236fa with 3% oil on the Turbo-BII tube at a saturation temperature of 2°C (repeat run)

h (W/m^2 K)	1.68E+04	1.65E+04	1.61E+04	1.53E+04	1.39E+04	1.18E+04
$q"$ (W/m^2)	4.00E+04	3.50E+04	3.00E+04	2.51E+04	2.00E+04	1.50E+04
q (Watts)	2.01E+03	1.76E+03	1.51E+03	1.26E+03	1.01E+03	7.55E+02
$LMTD$ (°C)	5.25E+00	4.92E+00	4.58E+00	4.28E+00	3.95E+00	3.66E+00
ΔT (°C)	2.66E+00	2.49E+00	2.33E+00	2.18E+00	2.02E+00	1.87E+00
h_i (W/m^2 K)	1.69E+04	1.51E+04	1.33E+04	1.15E+04	9.58E+03	7.56E+03
Re_i	1.36E+04	1.17E+04	9.98E+03	8.22E+03	6.55E+03	4.85E+03
U_o (W/m^2 K)	7.60E+03	7.09E+03	6.53E+03	5.84E+03	5.05E+03	4.09E+03
UN (± %)	1.02E+01	1.11E+01	1.23E+01	1.36E+01	1.51E+01	1.67E+01

Table D.25 Condensation of HFC-236fa on the 1024-fpm tube at a saturation temperature of 40°C (primary run)

h (W/m^2 K)	7.78E+03	7.79E+03	7.89E+03	7.99E+03	8.08E+03	8.14E+03
$q"$ (W/m^2)	1.50E+04	2.01E+04	2.50E+04	3.00E+04	3.49E+04	3.99E+04
q (Watts)	7.54E+02	1.01E+03	1.25E+03	1.51E+03	1.75E+03	2.00E+03
$LMTD$ (°C)	5.27E+00	6.14E+00	6.94E+00	7.71E+00	8.41E+00	9.14E+00
ΔT (°C)	2.67E+00	3.10E+00	3.49E+00	3.88E+00	4.22E+00	4.59E+00
h_i (W/m^2 K)	6.05E+03	7.59E+03	8.98E+03	1.03E+04	1.16E+04	1.28E+04
Re_i	1.12E+04	1.47E+04	1.80E+04	2.13E+04	2.45E+04	2.76E+04
U_o (W/m^2 K)	2.85E+03	3.26E+03	3.60E+03	3.90E+03	4.15E+03	4.36E+03
UN (± %)	8.77E+00	7.50E+00	6.80E+00	6.34E+00	6.01E+00	5.73E+00

Table D.26 Condensation of HFC-236fa on the 1024-fpm tube at a saturation temperature of 40°C (repeat run)

h (W/m^2 K)	7.81E+03	7.82E+03	7.91E+03	8.02E+03	8.11E+03	8.16E+03
$q"$ (W/m^2)	1.49E+04	1.99E+04	2.51E+04	3.00E+04	3.50E+04	3.98E+04
q (Watts)	7.45E+02	1.00E+03	1.26E+03	1.50E+03	1.75E+03	2.00E+03
$LMTD$ (°C)	5.20E+00	6.09E+00	6.95E+00	7.68E+00	8.42E+00	9.11E+00
ΔT (°C)	2.63E+00	3.07E+00	3.50E+00	3.86E+00	4.23E+00	4.57E+00
h_i (W/m^2 K)	6.06E+03	7.61E+03	8.98E+03	1.03E+04	1.16E+04	1.28E+04
Re_i	1.12E+04	1.48E+04	1.80E+04	2.13E+04	2.45E+04	2.75E+04
U_o (W/m^2 K)	2.85E+03	3.27E+03	3.61E+03	3.90E+03	4.15E+03	4.37E+03
UN (± %)	8.92E+00	7.55E+00	6.80E+00	6.37E+00	6.00E+00	5.75E+00

Table D.27 Condensation of HFC-236fa on the 1575-fpm tube at a saturation temperature of 40°C (primary run)

h (W/m^2 K)	7.00E+03	7.26E+03	7.62E+03	7.92E+03	8.13E+03	8.29E+03
q" (W/m^2)	1.50E+04	2.00E+04	2.49E+04	3.00E+04	3.50E+04	3.99E+04
q (Watts)	7.53E+02	1.00E+03	1.25E+03	1.50E+03	1.75E+03	2.00E+03
$LMTD$ (°C)	5.45E+00	6.26E+00	6.98E+00	7.69E+00	8.37E+00	9.02E+00
ΔT (°C)	2.76E+00	3.16E+00	3.51E+00	3.87E+00	4.21E+00	4.53E+00
h_i (W/m^2 K)	5.65E+03	7.10E+03	8.41E+03	9.64E+03	1.08E+04	1.20E+04
Re_i	1.02E+04	1.35E+04	1.66E+04	1.95E+04	2.25E+04	2.54E+04
U_o (W/m^2 K)	2.78E+03	3.22E+03	3.60E+03	3.93E+03	4.22E+03	4.47E+03
UN (± %)	8.05E+00	7.12E+00	6.61E+00	6.21E+00	5.92E+00	5.70E+00

Table D.28 Condensation of HFC-236fa on the 1575-fpm tube at a saturation temperature of 40°C (repeat run)

h (W/m^2 K)	6.95E+03	7.21E+03	7.58E+03	7.88E+03	8.11E+03	8.25E+03
q" (W/m^2)	1.51E+04	2.01E+04	2.51E+04	3.00E+04	3.50E+04	4.00E+04
q (Watts)	7.58E+02	1.01E+03	1.26E+03	1.50E+03	1.76E+03	2.01E+03
$LMTD$ (°C)	5.49E+00	6.34E+00	7.05E+00	7.70E+00	8.39E+00	9.07E+00
ΔT (°C)	2.78E+00	3.19E+00	3.55E+00	3.87E+00	4.22E+00	4.56E+00
h_i (W/m^2 K)	5.67E+03	7.09E+03	8.39E+03	9.65E+03	1.08E+04	1.20E+04
Re_i	1.02E+04	1.35E+04	1.65E+04	1.95E+04	2.25E+04	2.54E+04
U_o (W/m^2 K)	2.78E+03	3.21E+03	3.59E+03	3.92E+03	4.21E+03	4.45E+03
UN (± %)	7.95E+00	7.04E+00	6.54E+00	6.20E+00	5.91E+00	5.67E+00

Table D.29 Condensation of HFC-236fa on the Turbo-CII tube at a saturation temperature of 40°C (primary run)

h (W/m^2 K)	9.68E+03	1.02E+04	1.14E+04	1.26E+04	1.35E+04	1.44E+04
q" (W/m^2)	1.50E+04	2.01E+04	2.50E+04	3.00E+04	3.50E+04	4.00E+04
q (Watts)	7.50E+02	1.01E+03	1.25E+03	1.50E+03	1.75E+03	2.01E+03
$LMTD$ (°C)	3.02E+00	3.56E+00	3.88E+00	4.14E+00	4.42E+00	4.67E+00
ΔT (°C)	1.57E+00	1.83E+00	1.98E+00	2.11E+00	2.25E+00	2.37E+00
h_i (W/m^2 K)	1.29E+04	1.62E+04	1.92E+04	2.22E+04	2.50E+04	2.78E+04
Re_i	1.08E+04	1.42E+04	1.76E+04	2.10E+04	2.44E+04	2.78E+04
U_o (W/m^2 K)	5.03E+03	5.73E+03	6.55E+03	7.36E+03	8.03E+03	8.70E+03
UN (± %)	7.08E+00	6.19E+00	5.88E+00	5.75E+00	5.50E+00	5.37E+00

Table D.30 Condensation of HFC-236fa on the Turbo-CII tube at a saturation temperature of 40°C (repeat run)

h (W/m^2 K)	9.63E+03	1.04E+04	1.11E+04	1.24E+04	1.33E+04	1.43E+04
q" (W/m^2)	1.53E+04	2.02E+04	2.49E+04	2.98E+04	3.49E+04	4.00E+04
q (Watts)	7.66E+02	1.01E+03	1.25E+03	1.50E+03	1.75E+03	2.01E+03
$LMTD$ (°C)	3.10E+00	3.55E+00	3.93E+00	4.16E+00	4.46E+00	4.69E+00
ΔT (°C)	1.61E+00	1.82E+00	2.01E+00	2.12E+00	2.26E+00	2.38E+00
h_i (W/m^2 K)	1.28E+04	1.62E+04	1.92E+04	2.21E+04	2.51E+04	2.78E+04
Re_i	1.07E+04	1.42E+04	1.75E+04	2.09E+04	2.44E+04	2.77E+04
U_o (W/m^2 K)	5.00E+03	5.77E+03	6.45E+03	7.28E+03	7.96E+03	8.66E+03
UN (± %)	6.89E+00	6.32E+00	5.78E+00	5.64E+00	5.51E+00	5.39E+00

APPENDIX E DERIVATION OF UNCERTAINTY ANALYSIS EQUATIONS

This appendix presents the derivation of uncertainty analysis equations for the shell-side heat transfer coefficients calculated in this study.

Substituting Equation 5.2 and 5.3 into Equation 5.4 and replacing U_o and R_w in Equation 5.5 by those given in Equation 5.4 and Equation 5.6, respectively, results in the following equation for the shell-side heat transfer coefficient (h),

$$h = \left[\frac{A_o}{\dot{m}_i \cdot Cp_i \cdot ln\left(\frac{T_{sat}-T_{i,in}}{T_{sat}-T_{i,out}}\right)} - \frac{A_o}{h_i \cdot A_i} - \frac{A_o \cdot ln(D_o/D_i)}{2\pi k_w L} \right]^{-1} \tag{E.1}$$

Equation E.1 shows that the uncertainty of h depends on the six variables: $\dot{m}_i$, Cp_i, h_i, T_{sat}, $T_{i,out}$, and $T_{i,in}$. The other terms in Equation E.1 are constants for a given test tube. Therefore, the uncertainty in the calculated shell-side heat transfer coefficients according to the propagation of error approach described in [27] is defined as

$$\delta h = (\delta hsq)^{1/2} \tag{E.2}$$

with

$$\begin{aligned} \delta hsq = & \left(\frac{\partial h}{\partial \dot{m}_i}\delta \dot{m}_i\right)^2 + \left(\frac{\partial h}{\partial Cp_i}\delta Cp_i\right)^2 + \left(\frac{\partial h}{\partial h_i}\delta h_i\right)^2 + \\ & \left(\frac{\partial h}{\partial T_{sat}}\delta T_{sat}\right)^2 + \left(\frac{\partial h}{\partial T_{i,out}}\delta T_{i,out}\right)^2 + \left(\frac{\partial h}{\partial T_{i,in}}\delta T_{i,in}\right)^2 \end{aligned} \tag{E.3}$$

where $\delta \dot{m}_i$ is the uncertainty of the water mass flow rate, δCp_i is the uncertainty of the water's specific heat, and δh_i is the uncertainty of the in-tube heat transfer coefficient. δCp_i was calculated based on

the bulk water temperature ($T_{i,bulk} = (T_{i,in}+T_{i,out})/2$. °C). The remaining three terms: ∂T_{sat}. $\partial T_{i,out}$. and $\partial T_{i,in}$. are referred to the uncertainty due to the temperature measurements of the refrigerant saturation temperature, water outlet, and water inlet temperatures, respectively. The uncertainty in the shell-side heat transfer coefficient was caused by the existing uncertainty in the measurements. The instrumentation accuracy of the test facility is summarized in Chapter 5.

The following equations which are the partial derivatives of Equation E.1 with respect to the six independent variables are required in the determination of the uncertainty in the calculated shell-side heat transfer coefficients (i.e., Equation E.2).

$$\frac{\partial h}{\partial \dot{m}_i} = -h^{-2} \cdot \frac{-A_o}{\dot{m}_i^2 \cdot Cp_i \cdot ln\left(\frac{T_{sat}-T_{i,in}}{T_{sat}-T_{i,out}}\right)} \tag{E.4}$$

$$\frac{\partial h}{\partial Cp_i} = -h^{-2} \cdot \frac{-A_o}{\dot{m}_i \cdot Cp_i^2 \cdot ln\left(\frac{T_{sat}-T_{i,in}}{T_{sat}-T_{i,out}}\right)} \tag{E.5}$$

$$\frac{\partial h}{\partial h_i} = -h^{-2} \cdot \frac{A_o}{h_i^2 \cdot A_i} \tag{E.6}$$

$$\frac{\partial h}{\partial T_{sat}} = -h^{-2} \cdot \frac{A_o}{\dot{m}_i \cdot Cp_i} \cdot \frac{-1}{\left[ln\left(\frac{T_{sat}-T_{i,in}}{T_{sat}-T_{i,out}}\right)\right]^2} \cdot \left(\frac{1}{T_{sat}-T_{i,in}} - \frac{1}{T_{sat}-T_{i,out}}\right) \tag{E.7}$$

For the calculation of the uncertainty in condensation,

$$\frac{\partial h}{\partial T_{i,out}} = -h^{-2} \cdot \frac{A_o}{\dot{m}_i \cdot Cp_i} \cdot \frac{-1}{\left[ln\left(\frac{T_{sat}-T_{i,in}}{T_{sat}-T_{i,out}}\right)\right]^2} \cdot \left(\frac{1}{T_{sat}-T_{i,out}}\right) \tag{E.8}$$

$$\frac{\partial h}{\partial T_{i,in}} = -h^{-2} \cdot \frac{A_o}{\dot{m}_i \cdot Cp_i} \cdot \frac{-1}{\left[ln\left(\frac{T_{sat}-T_{i,in}}{T_{sat}-T_{i,out}}\right)\right]^2} \cdot \left(\frac{-1}{T_{sat}-T_{i,in}}\right) \tag{E.9}$$

While for the calculation of the uncertainty in evaporation, Equation E.1 becomes

$$h = \left[\frac{A_o}{\dot{m}_i \cdot Cp_i \cdot ln\left(\frac{T_{i,in}-T_{sat}}{T_{i,out}-T_{sat}}\right)} - \frac{A_o}{h_i \cdot A_i} - \frac{A_o \cdot ln(D_o/D_i)}{2\pi k_w L}\right]^{-1} \tag{E.10}$$

The partial derivatives of Equation E.10 with respect to the six independent variables are the same as those of Equation E.1, i.e., Equations E.4 through E.9 can also be used to determine the uncertainty in evaporation.

The estimate of uncertainty is listed in Tables 5.1 through 5.3 and Appendixes C and D and is presented as a percentage of the calculated heat transfer coefficient, i.e., $(\delta h/h)\times 100$.

APPENDIX F PREDICTION CORRELATIONS FOR HEAT TRANSFER COEFFICIENTS

Empirical correlations to reproduce the present data with sufficient accuracy were developed in order to provide designers more feasible access to these data. An unique model was derived for each separate type of heat transfer forms (i.e., pool boiling, spray evaporation, condensation). Different empirical coefficients were given for each specific tube and refrigerant. In addition, agreement of the correlations developed with the experimental data is confirmed by means of figures where both experimental and predicted heat transfer coefficients are present.

Pool boiling

Curve fits of the pool boiling data were developed in the same form as that proposed by Webb and Pais [86]. According to the heat flux (q'', W/m^2) dependence of the boiling coefficients (h, W/m^2-K), the correlation is expressed as

$$h = b \cdot (q'')^m \tag{F.1}$$

Table F.1 provides the values of the coefficients (b) and the exponent (m) in Equation F.1. It can be noted from the table that all the coefficients of determination except for the Turbo-BII tube with HFC-236fa are greater than 0.96. The coefficient of determination (R-square= 0.4634) is small for the Turbo-BII tube tested with HFC-236fa, the following polynomial equation was provided for this special case with the R-square value of 0.9889.

$$\frac{h}{\bar{h}} = 0.5281 + 1.3869\left(\frac{q''}{\bar{q}''}\right) - 1.2870\left(\frac{q''}{\bar{q}''}\right)^2 + 0.3847\left(\frac{q''}{\bar{q}''}\right)^3 \tag{F.2}$$

Table F.1 Coefficient b and exponent m in the boiling correlation (Equation F.1)

Tube	Refrigerant	b	m	R-square
1024-fpm	HFC-236fa	5.8902E1	4.5737E-1	9.9460E-1
	HFC-236ea	1.2343E2	3.7362E-1	9.9460E-1
	CFC-114	7.3601E0	6.1379E-1	9.9880E-1
1575-fpm	HFC-236fa	2.5624E1	5.1747E-1	9.9850E-1
	HFC-236ea	3.5549E1	4.7504E-1	9.9800E-1
	CFC-114	3.4147E0	6.7454E-1	9.9930E-1
Turbo-B	HFC-236fa	1.2231E2	4.3508E-1	9.6390E-1
	HFC-236ea	2.6642E1	5.4298E-1	9.8550E-1
Turbo-BII	HFC-236fa	1.0189E4	3.4049E-2	4.6340E-1
	HFC-236ea	8.6278E2	2.3446E-1	9.6160E-1

where the average heat transfer coefficient ($\bar{h}$) is 14409.6 W/m^2-K and the average heat flux ($\bar{q}''$) is 27513.1 W/m^2.

Figures F.1 through F.4 present both experimental and predicted heat transfer coefficients for the 1024-fpm, 1575-fpm, Turbo-B, and Turbo-BII tubes, respectively. These figures indicate that Equation F.1 generally predicts the pool boiling data well.

Spray evaporation

Similar to the development of the equations for spray evaporation heat transfer coefficients proposed by Moeykens [52], the spray evaporation data of HFC-236ea involving four mass flow rates for three different tubes were correlated in the following form

$$\begin{aligned} h = {} & s_0 + s_1 \cdot (q'' - \bar{q}'') + s_2 \cdot (\dot{m}_{spr} - \bar{\dot{m}}_{spr}) + s_3 \cdot (q'' - \bar{q}'')^2 + s_4 \cdot (\dot{m}_{spr} - \bar{\dot{m}}_{spr})^2 + \\ & s_5 \cdot (q'' - \bar{q}'') \cdot (\dot{m}_{spr} - \bar{\dot{m}}_{spr}) + s_6 \cdot [(q'' - \bar{q}'') \cdot (\dot{m}_{spr} - \bar{\dot{m}}_{spr})^2] + \\ & s_7 \cdot [(q'' - \bar{q}'')^2 \cdot (\dot{m}_{spr} - \bar{\dot{m}}_{spr})] + s_8 \cdot [(q'' - \bar{q}'')^2 \cdot (\dot{m}_{spr} - \bar{\dot{m}}_{spr})^2] \end{aligned} \quad \text{(F.3)}$$

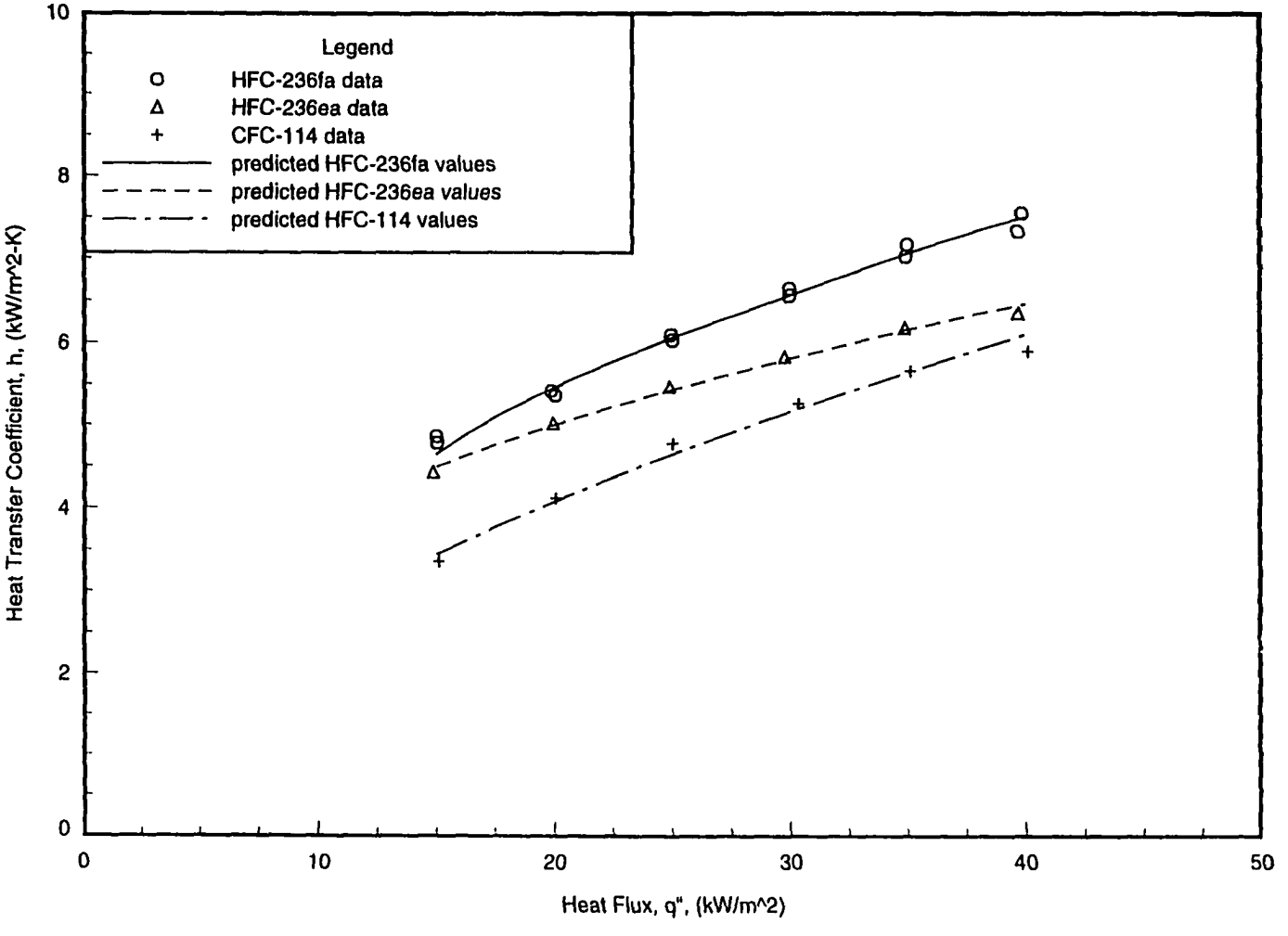

Figure F.1 Comparison of pool boiling data for the 1024-fpm tube (D= 19.1 mm) with predicted values at T_{sat}= 2°C

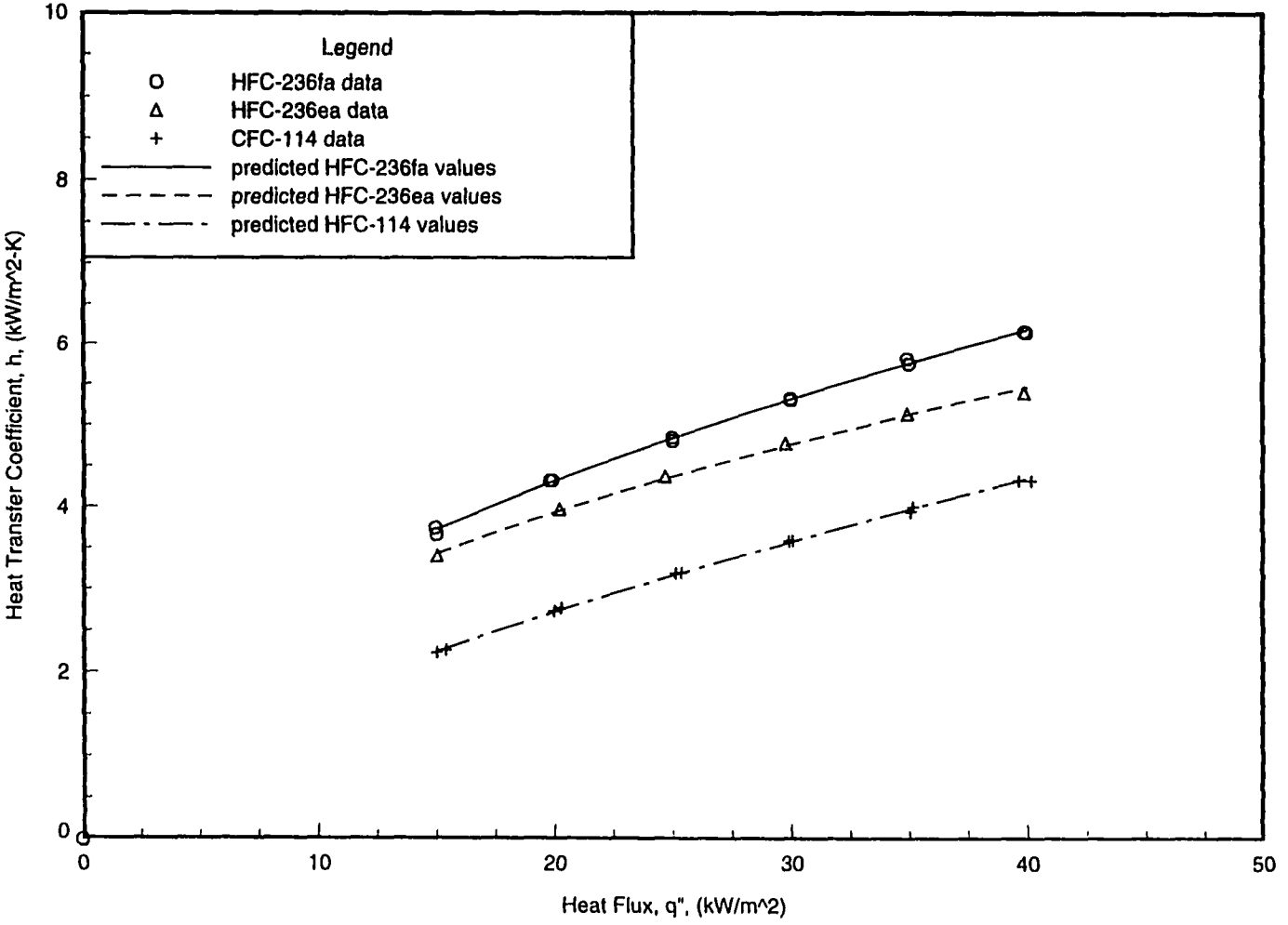

Figure F.2 Comparison of pool boiling data for the 1575-fpm tube (D= 19.1 mm) with predicted values at T_{sat}= 2°C

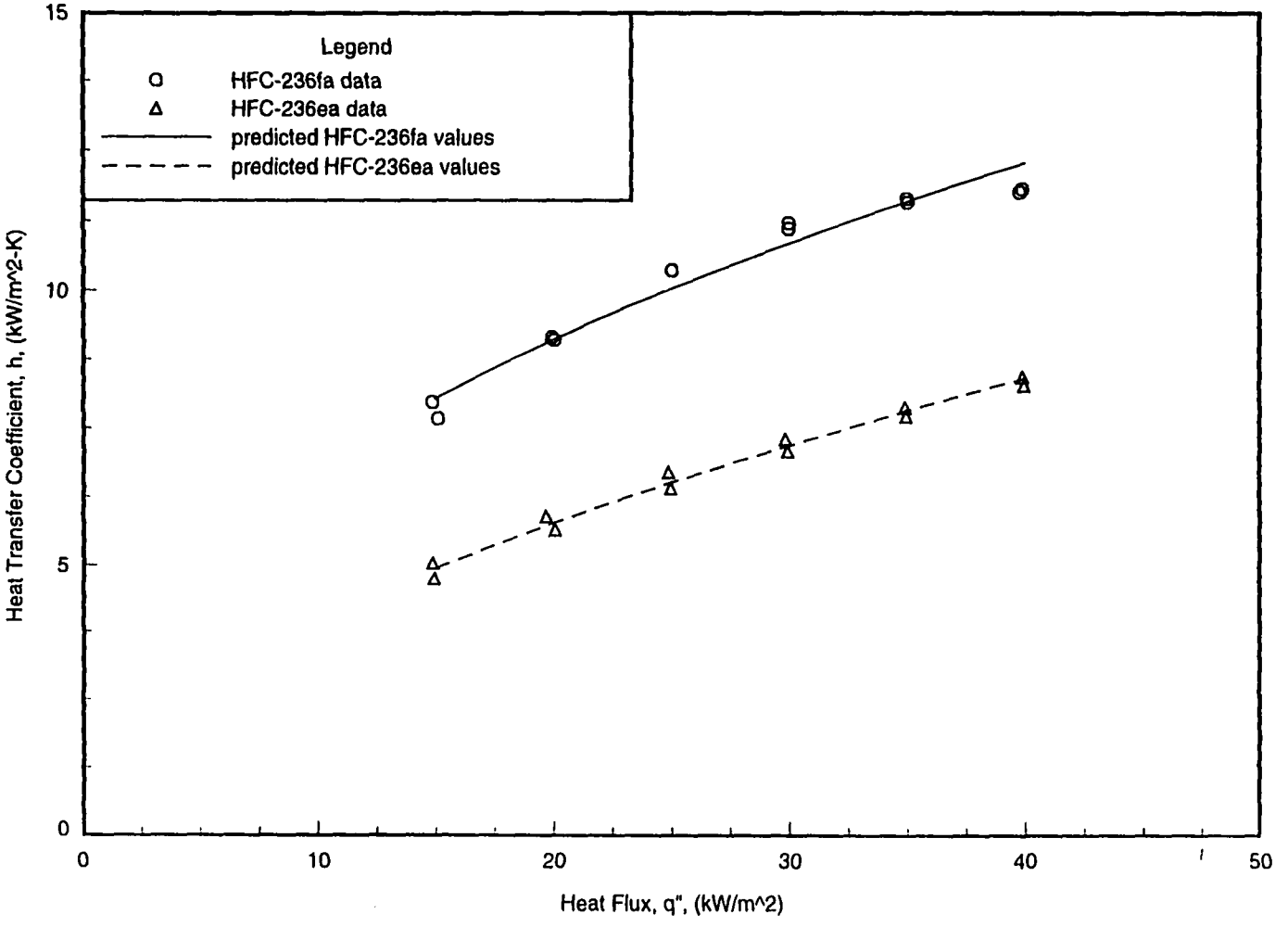

Figure F.3 Comparison of pool boiling data for the Turbo-B tube (D= 19.1 mm) with predicted values at T_{sat}= 2°C

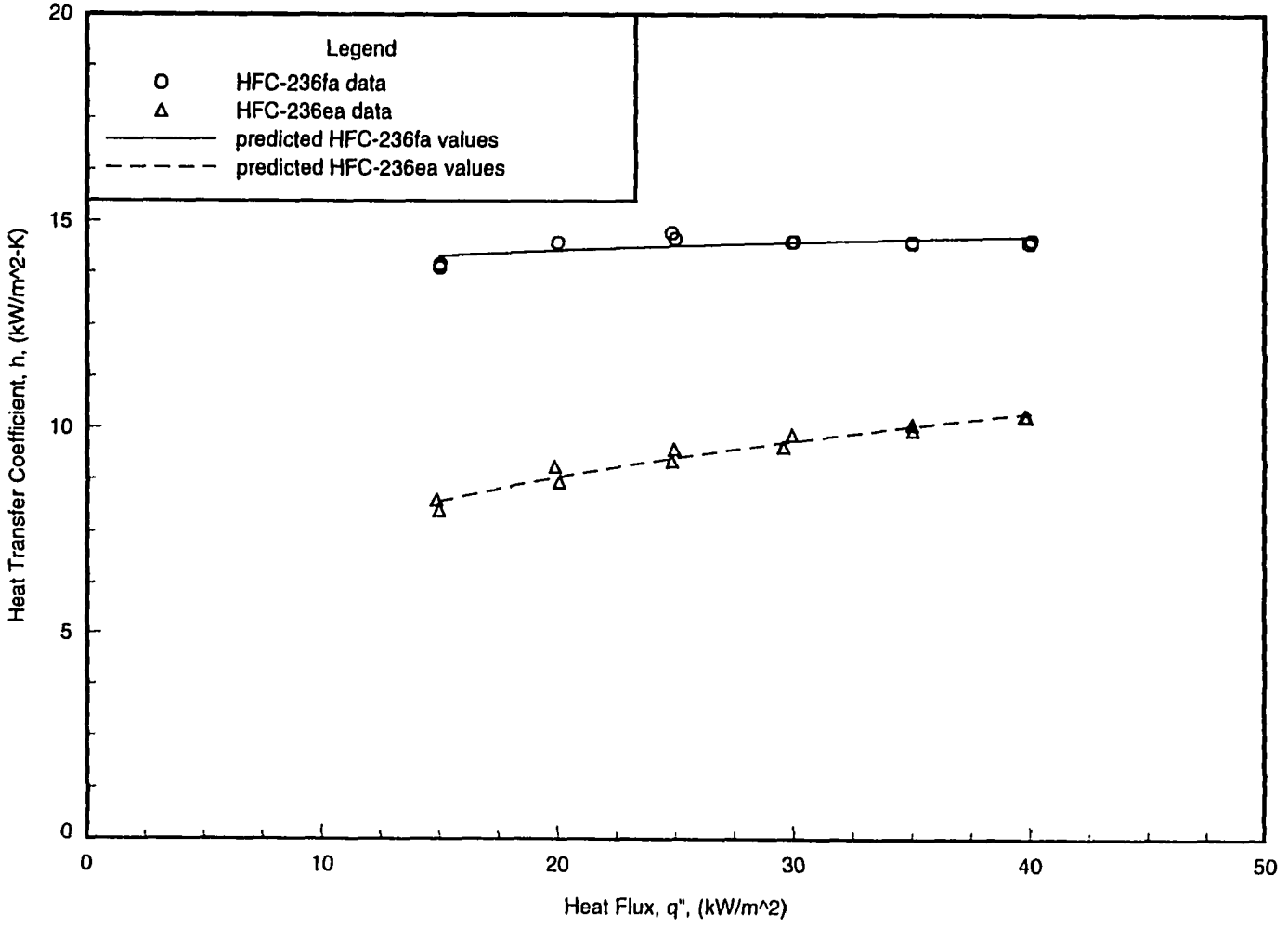

Figure F.4 Comparison of pool boiling data for the Turbo-BII tube (D= 19.1 mm) with predicted values at T_{sat}= 2°C

The bundle heat flux and the bundle overfeed ratio were the two independent variables in the Moeykens correlations [52], while the correlation developed here for the heat transfer coefficients (h, W/m^2-K) is a function of heat flux ($q"$, W/m^2) and total feed mass flow rate ($\dot{m}_{spr}$, kg/min). Because the overfeed ratio can not be estimated in this study due to the unknown effective refrigerant mass flow rate hitting the tube surafce, the total feed mass flow rate instead of the overfeed ratio is correlated. The overfeed ratio is defined by Moeykens as the ratio of the amount of refrigerant contacting the tube to the amount of refrigerant being evaporated on the tube. In addition, the correlation is reproduced from the average values of the data taken with increasing and decreasing heat fluxes.

Table F.2 gives the values of the nine constants (s_0 through s_8) required in Equation F.3. In addition, the values of the R-square along with the average heat flux ($\bar{q}"$, W/m^2) and the average feed mass flow rate ($\bar{\dot{m}}_{spr}$, kg/min) are also presented in the table. The R-square values shown in Table F.2 are all greater than 0.91.

Table F.2 Constants in the spray evaporation correlation (Equation F.3)

	Turbo-B tube	Turbo-CII tube	1575-fpm tube
s_0	1.0730E+4	8.8213E+3	6.0955E+3
s_1	-1.6995E−1	-1.6074E−1	-5.1627E−2
s_2	1.1779E+3	2.0012E+3	2.2724E+3
s_3	-1.6536E−5	-1.0354E−5	-1.0055E−5
s_4	-2.6721E+3	2.5166E+3	-1.7985E+3
s_5	1.9777E−1	1.4675E−1	1.1074E−1
s_6	-5.1183E−1	-9.6721E−2	-7.7342E−2
s_7	1.4900E−5	2.0750E−6	-5.0460E−6
s_8	5.8190E−6	4.4527E−5	1.3022E−5
$\bar{q}"$	2.0361E+4	2.0272E+4	1.9815E+4
$\bar{\dot{m}}_{spr}$	2.8947E+0	2.8842E+0	2.9000E+0
R-square	9.7190E−1	9.9190E−1	9.1590E−1

Figures F.5 through F.7 compare both experimental and predicted heat transfer coefficients for the Turbo-B, Turbo-CII, and 1575-fpm tubes, respectively. These figures indicate that Equation F.3 generally predicts the spray evaporation data with adequate accuracy, although wider dispersions of data were observed for the 1575-fpm tube.

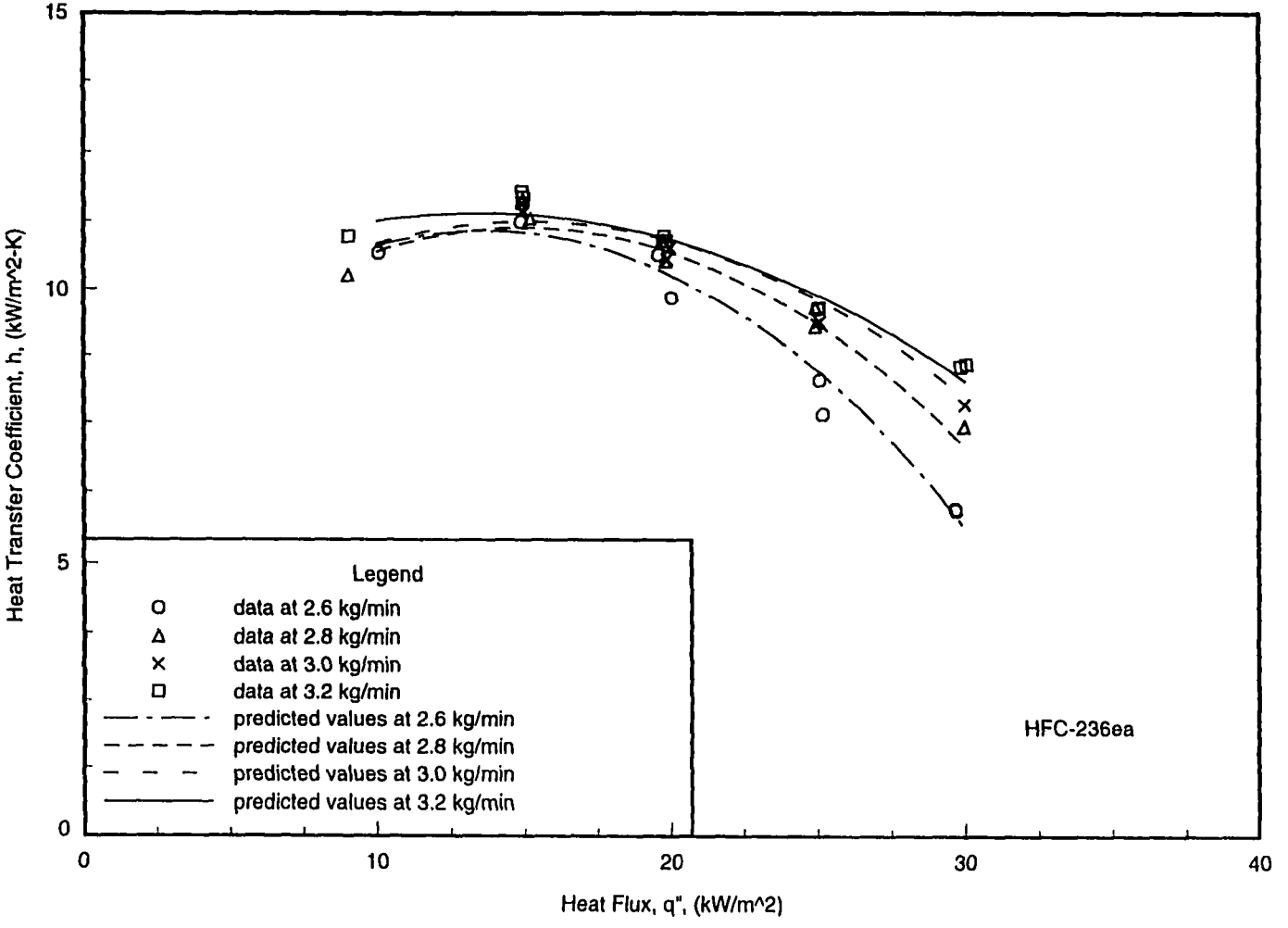

Figure F.5 Comparison of spray evaporation data for the Turbo-B tube (D= 19.1 mm) with predicted values at T_{sat}= 2°C

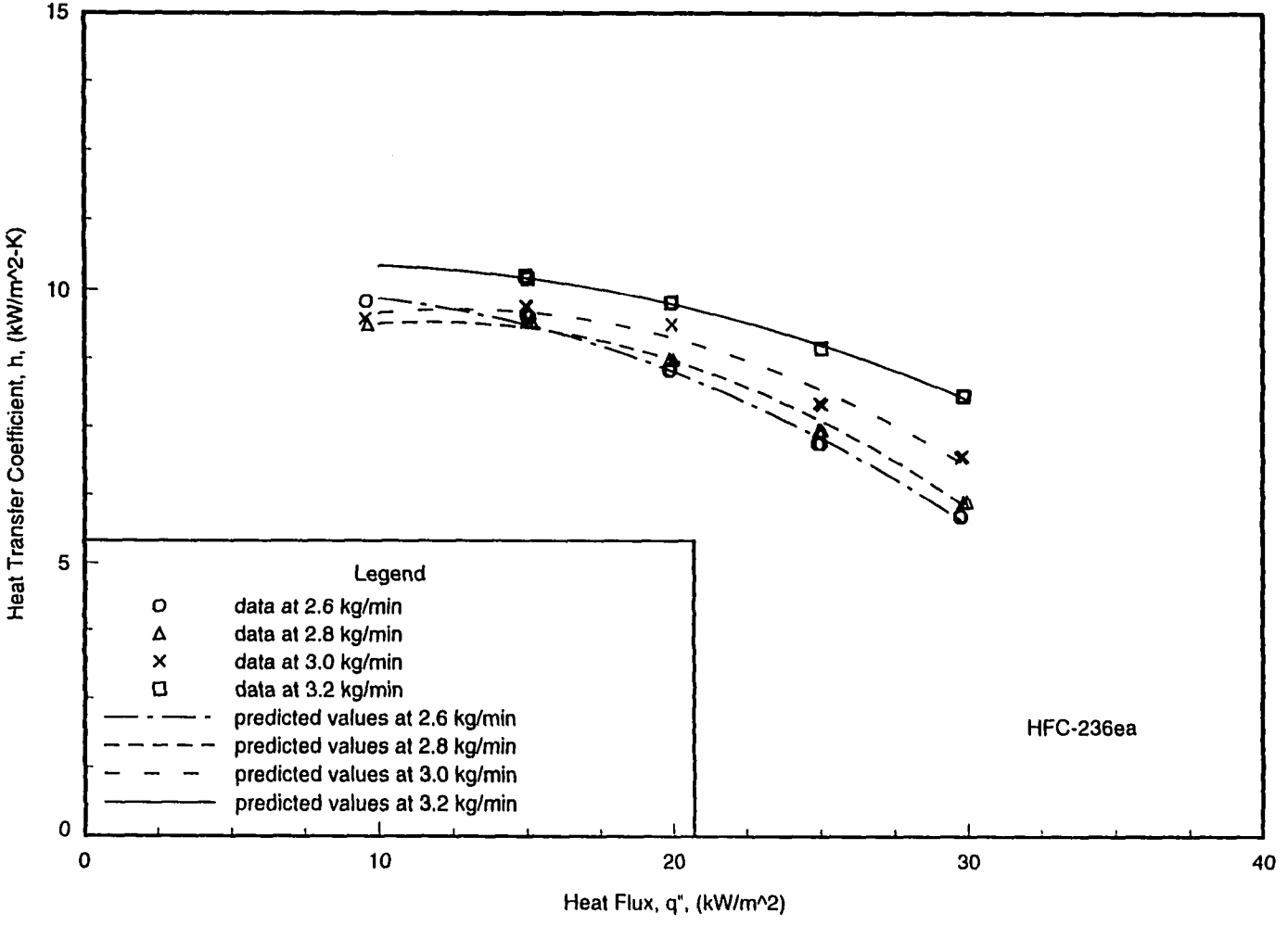

Figure F.6 Comparison of spray evaporation data for the Turbo-CII tube (D= 19.1 mm) with predicted values at T_{sat}= 2°C

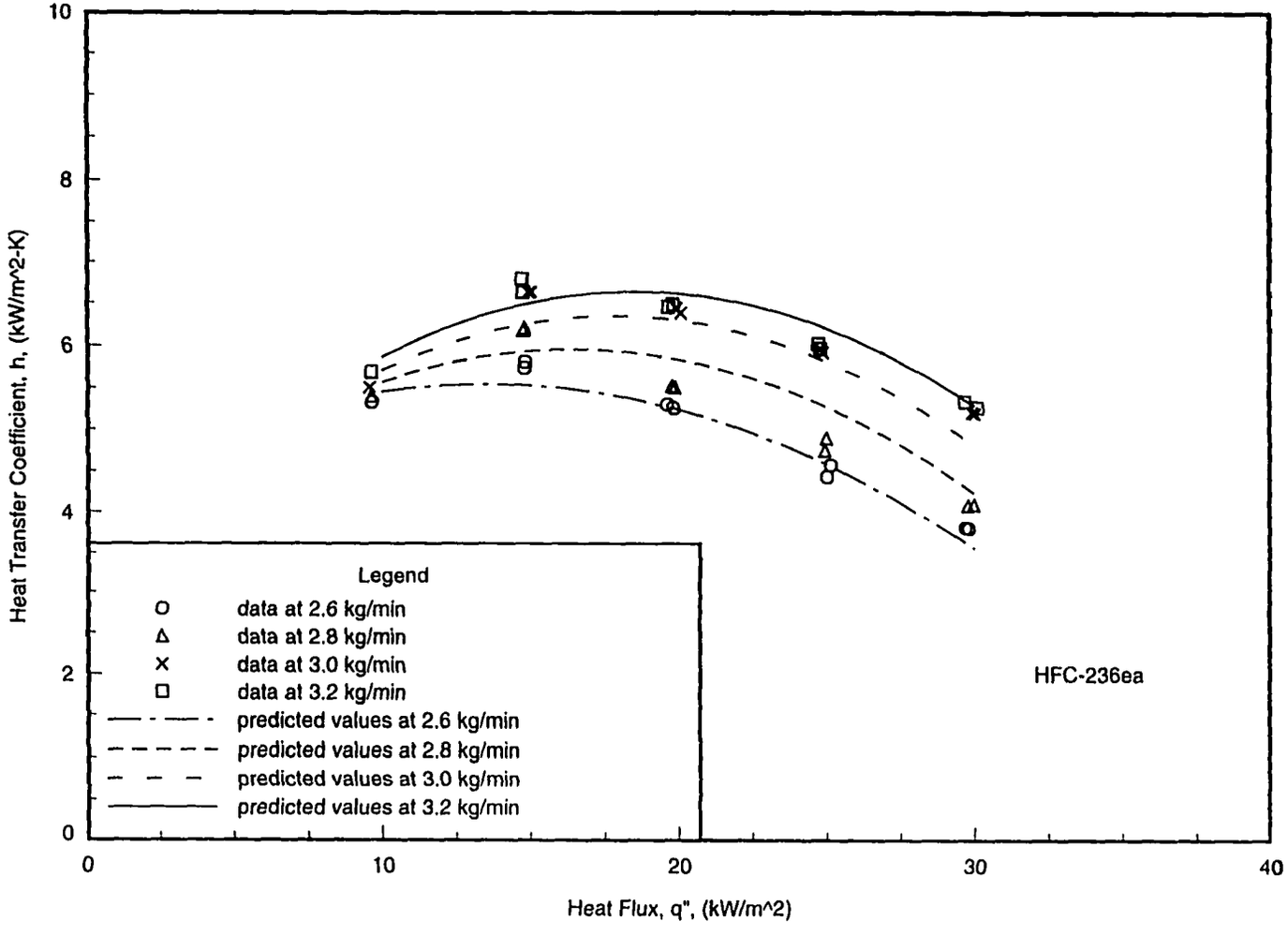

Figure F.7 Comparison of spray evaporation data for the 1575-fpm tube (D= 19.1 mm) with predicted values at T_{sat}= 2°C

Shell-side condensation

The condensing data are correlated in the same form as that developed by Webb and Murawski [84]. That is, the condensing coefficients (h, W/m^2-K) are correlated with condensate Reynolds number (Re) in the following form

$$h = c \cdot Re^n \tag{F.4}$$

The values of the coefficients (c) and the exponent (n) in Equation F.4 are presented in Table F.3. It can be seen from the table that all the coefficients of determination are greater than 0.90.

Table F.3 Coefficient c and exponent n in the condensation correlation (Equation F.4)

Tube	Refrigerant	c	n	R-square
1024-fpm	HFC-236fa	5.3054E3	4.9039E-2	9.2200E-1
	HFC-236ea	1.0469E3	2.3200E-1	9.6260E-1
	CFC-114	1.5896E3	1.6205E-1	9.0580E-1
1575-fpm	HFC-236fa	1.6881E3	1.8303E-1	9.9290E-1
	HFC-236ea	5.2681E2	3.1896E-1	9.9670E-1
	CFC-114	7.9659E2	2.5313E-1	9.1210E-1
Turbo-CII	HFC-236fa	3.6262E2	4.2104E-1	9.7740E-1
	HFC-236ea	6.1311E2	3.7858E-1	9.8920E-1

As shown in Figures F.8 through F.10 are the condensing coefficients measured on the 1024-fpm, 1575-fpm, and Turbo-CII tubes, respectively, and compared with those predicted by Equation F.4. The relatively small dispersion observed in the experimental data from the correlation is indicative of its adequency.

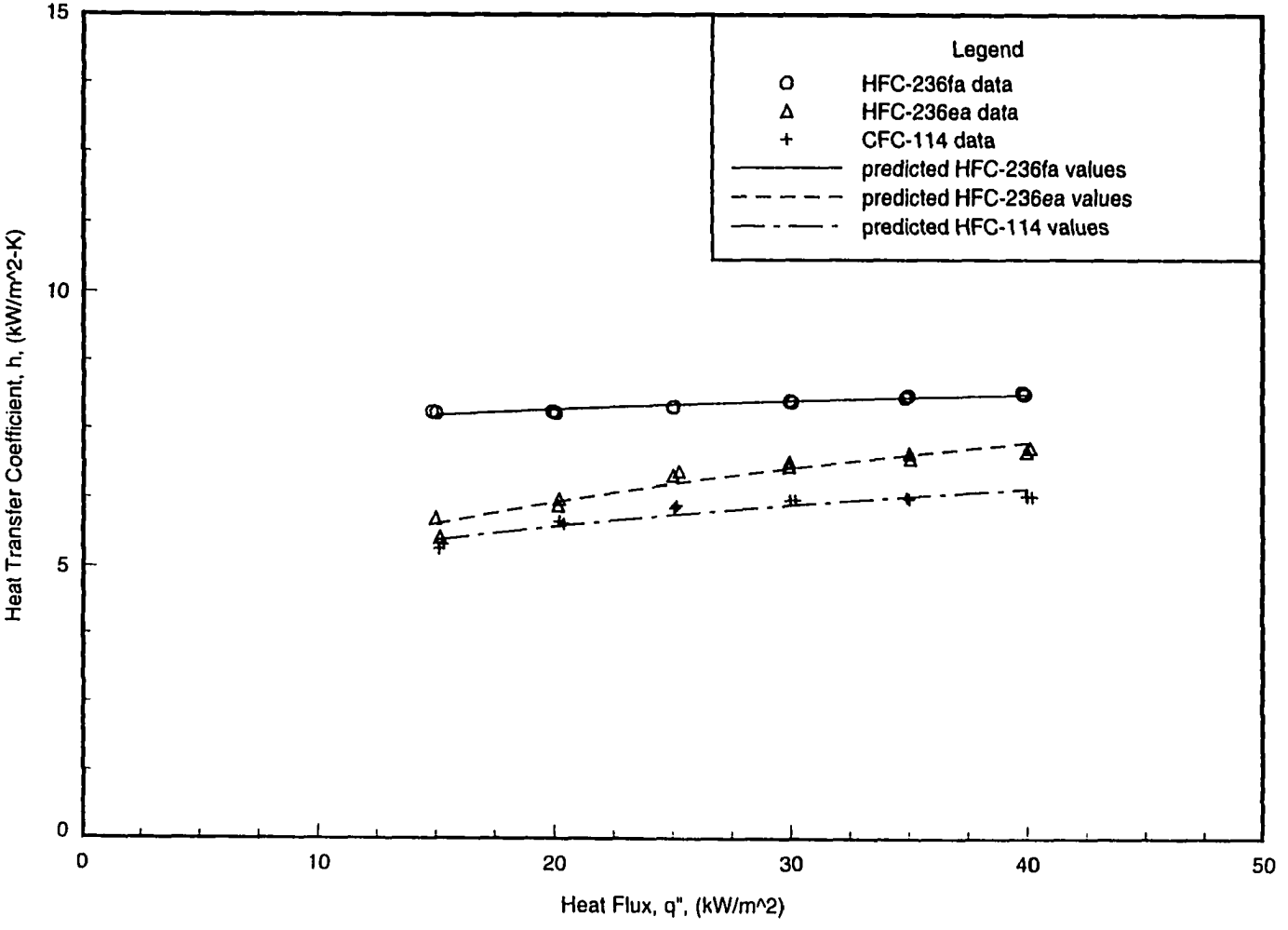

Figure F.8 Comparison of condensation data for the 1024-fpm tube (D= 19.1 mm) with predicted values at T_{sat}= 40°C

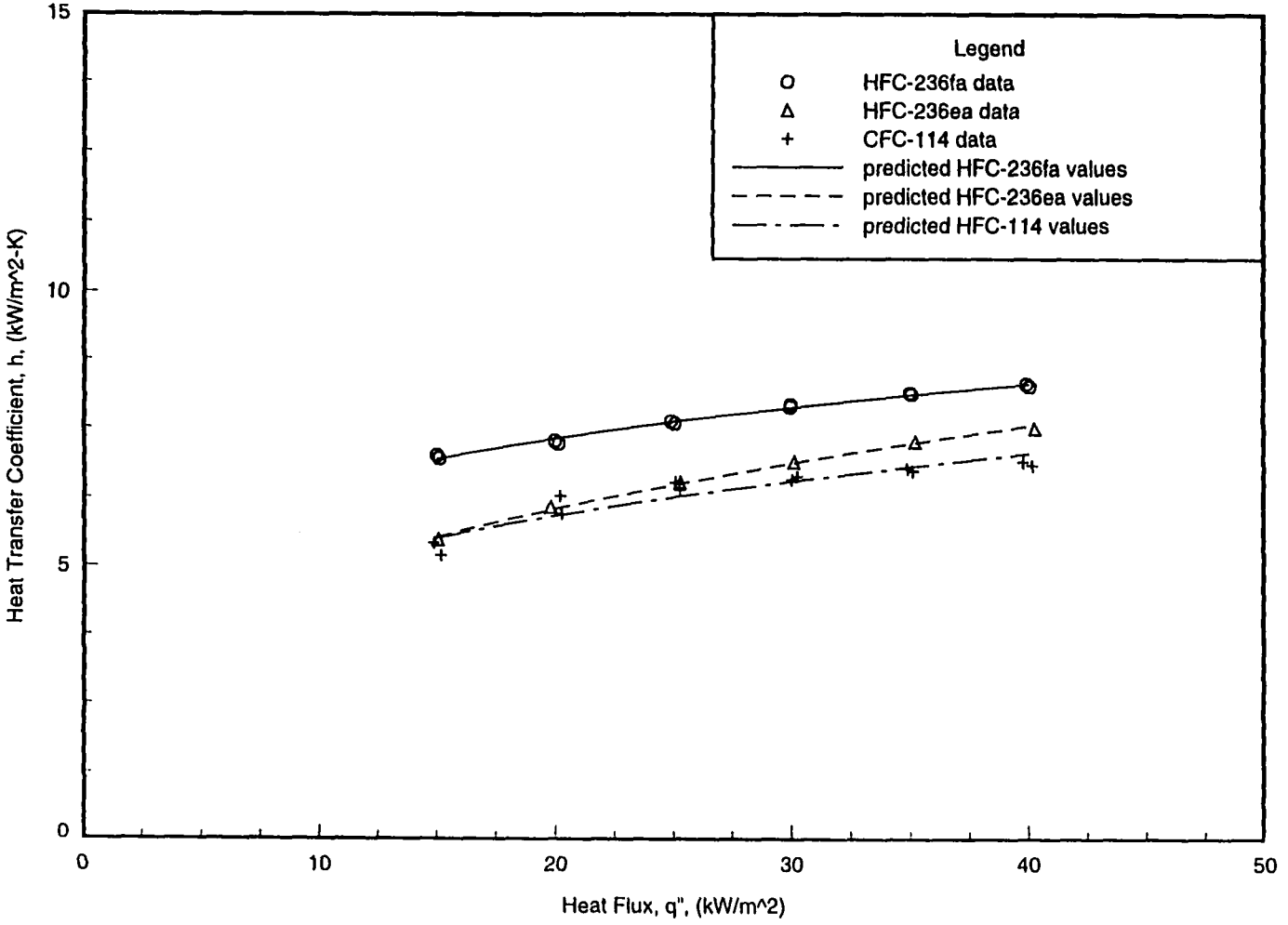

Figure F.9 Comparison of condensation data for the 1575-fpm tube (D= 19.1 mm) with predicted values at T_{sat}= 40°C

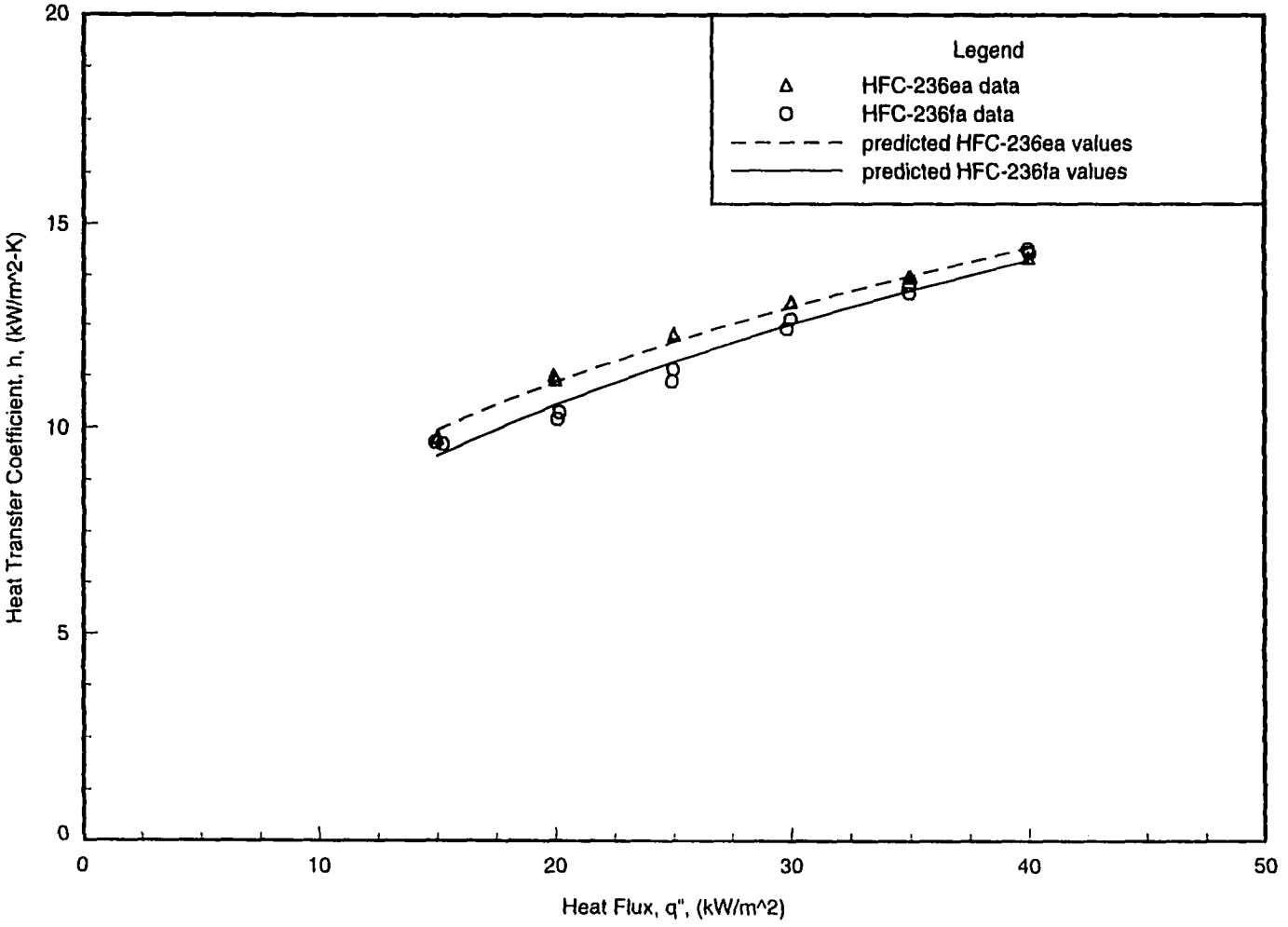

Figure F.10 Comparison of condensation data for the Turbo-CII tube (D= 19.1 mm) with predicted values at T_{sat}= 40°C

BIBLIOGRAPHY

[1] Adamek, T. and Webb, R. L. 1990. Prediction of film condensation on horizontal integral fin tubes. *International Journal of Heat and Mass Transfer*, Vol. 33, pp. 1721-1735.

[2] Adamek, T. and Webb, R. L. 1990. Prediction of film condensation on vertical finned plates and tubes— A model for the drainage channel. *International Journal of Heat and Mass Transfer*, Vol. 33, pp. 1736-1749.

[3] Barthau, G. 1992. Active nucleation site density and pool boiling heat transfer—an experimental study. *International Journal of Heat and Mass Transfer*, Vol. 35, pp. 271-278.

[4] Beatty, K. O., Jr. and Katz, D. L. 1948. Condensation of vapors on outside of finned tubes. *Chemical Engineering Progress*, Vol. 44(1), pp. 908-914.

[5] Bella, B., Cavallini, A., Longo, G. A., and Rossetto, L. 1993. Pure vapour condensation of refrigerants 11 and 113 on a horizontal integral finned tube at high vapour velocity. *Journal of Enhanced Heat Transfer*, Vol. 1, No. 1, pp. 77-86.

[6] Briggs, A., Baichoo, S., and Rose, J. W. 1994. Condensation of steam and CFC113 on commercially available integral-fin tubes. *Fundamentals of Phase Change: Boiling and Condensation*, American Society of Mechanical Engineers, Heat Transfer Division, (Publication) HTD Vol. 273, pp. 41-47.

[7] Briggs, A. and Rose, J. W. 1994. Effect of fin efficiency on a model for condensation heat transfer on horizontal integral-fin tube. *International Journal of Heat and Mass Transfer*, Vol. 35, pp. 271-278.

[8] Cavallini, A., Bella, B., Longo, G. A., and Rossetto, L. 1995. Experimental heat transfer coefficients during condensation of halogenated refrigerants on enhanced tubes. *Journal of Enhanced Heat Transfer*, Vol. 2, Nos. 1-2, pp. 115-125.

[9] Chang, Y.-J., Hsu, C.T., Wang, C.-C. 1996. Single-tube performance of condensation of R-134a on horizontal enhanced tubes. *ASHRAE Transactions*, Vol. 102(1), pp. 821-829.

[10] Chen, J. C. 1963. A correlation for boiling heat transfer to saturated fluids in convective flow. *6th National Heat Transfer Conference*, ASME Paper 63-HT-34, Boston, MA.

[11] Cheng, W. Y. and Wang, C. C. 1994. Condensation of R-134a on enhanced tubes. *ASHRAE Transactions*, Vol. 100(2), pp. 809-817.

[12] Cheng, W. Y., Wang, C. C., Hu, Y. Z. Robert, and Huang, L. W. 1996. Film condensation of HCFC-22 on horizontal enhanced tubes. *International Communications of Heat and Mass Transfer*, Vol. 23, pp. 79-90.

[13] Chongrungreong, S. and Sauer, H. J. Jr. 1980. Nucleate boiling performance of refrigerants and refrigerant/oil mixtures. *Journal of Heat Transfer*, Vol. 102, pp. 701-705.

[14] Chu, C. M. and McNaught, J. M. 1992. Condensation on bundles of plain and low-finned tubes: effect of vapor shear and condensate inundation. *Institution of Chemical Engineers. Symposium Series*, Vol. 129, pp. 225-229.

[15] Chyu, M. C. and Bergles, A. E. 1987. An analytical and experimental study of falling-film evaporation on a horizontal tube. *Journal of Heat Transfer*, Vol. 109, pp. 983-990.

[16] Chyu, M. C. and Bergles, A. E. 1989. Horizontal-tube falling-film evaporation with structured surfaces. *Journal of Heat Transfer*, Vol. 111, pp. 518-524.

[17] Chyu, M. C., Zeng, X., and Ayub, Z. H. 1995. Nozzle-sprayed flow rate distribution on a horizontal tube bundle. *ASHRAE Transactions*, Vol. 101(2), pp. 443-453.

[18] Collier, J. G. and Thome, J. R. 1994. *Convective Boiling and Condensation*, 3rd ed. New York: Oxford University Press, Inc., pp. 430.

[19] Cooper, M. G. 1984. Saturation nucleate pool boiling— A simple correlation. *Institution of Chemical Engineers. Symposium Series*, Vol. 86, pp. 785-792.

[20] Cornwell, K. and Houston, S. D. 1994. Nucleate pool boiling on horizontal tubes: A convection-based correlation. *International Journal of Heat and Mass Transfer*, Vol. 37, pp. 303-309.

[21] Danilova, G. N., Burkin, V. G., and Dyundin, V. A. 1976. Heat transfer spray-type refrigerator evaporators. *Heat Transfer-Soviet Research*, Vol. 8, No. 6, pp. 105-113.

[22] Fujita, Y. and Tsutsui, M. 1995. Evaporation heat transfer of falling films on horizontal tube— Part 1, Analytical study. *Heat Transfer-Japanese Research*, Vol. 24, No. 1, pp. 1-16.

[23] Fujita, Y. and Tsutsui, M. 1995. Evaporation heat transfer of falling films on horizontal tube— Part 2, Experimental study. *Heat Transfer-Japanese Research*, Vol. 24, No. 1, pp. 17-31.

[24] Gorenflo, D., Sokol, P., and Caplanis, S. 1991. Pool boiling heat transfer from single tubes to new refrigerants. *XVIIIth International Congress of Refrigeration*, Vol. 2, pp. 423-428.

[25] Hahne, E., Chen, Q., and Windisch, R. 1991. Pool boiling heat transfer on finned tubes— an experimental and theoretical study. *International Journal of Heat and Mass Transfer*, Vol. 34, pp. 2071-2079.

[26] Hahne, E. and Müller, J. 1983. Boiling on a finned tube and finned tube bundle. *International Journal of Heat and Mass Transfer*, Vol. 26, pp. 849-859.

[27] Holman, J. P. 1984. *Experimental methods for engineers*, 4th ed. New York: McGraw-Hill.

[28] Honda, H. and Nozu, S. 1987. A prediction method for heat transfer during film condensation on horizontal low integral-fin tubes. *Journal of Heat Transfer*, Vol. 109, pp. 218-225.

[29] Honda, H., Uchima, B., Nozu, S., Nakada, H., and Torigoe, E. 1991. Film condensation of R-113 on in line bundles of horizontal finned tubes. *Journal of Heat Transfer*, Vol. 113, pp. 479-486.

[30] Honda, H., Uchima, B., Nozu, S., Torigoe, E. and Imai, S. 1992. Film condensation of R-113 on staggered bundles of horizontal finned tubes. *Journal of Heat Transfer*, Vol. 114, pp. 442-449.

[31] Honda, H., Takamatsu, H., and Kim, K. 1994. Condensation of CFC-11 and HCFC-123 in in-line bundles of horizontal finned tubes: effects of fin geometry. *Journal of Enhanced Heat Transfer*, Vol. 1, pp. 197-209.

[32] Honda, H., Takamatsu, H., Takada, N., and Makishi, O. 1996. Condensation of HCFC-123 in bundles of horizontal finned tubes: effects of fin geometry and tube arrangement. *International Journal of Refrigeration*, Vol. 19, No. 1 ?, pp. 1-9.

[33] Houston, S. D. and Cornwell, K. 1996. Heat transfer to sliding bubbles on a tube under evaporating and non-evaporating conditions. *International Journal of Heat and Mass Transfer*, Vol. 39, No. 1, pp. 211-214.

[34] Hsu. Y. Y. and Graham. R. W. 1986. In Chapter 2: Nucleate boiling mechanism. *Transport processes in boiling and two-phase systems*. 2nd ed. La Grange Park. Illinois: American Nuclear Society.

[35] Huber. J. B.. Rewerts. L. E.. and Pate. M. B. 1994. Shell-side condensation heat transfer of R-134a—Part I: Finned tube performance. *ASHRAE Transactions*. Vol. 100(2). pp. 239-247.

[36] Huber. J. B.. Rewerts. L. E.. and Pate. M. B. 1994. Shell-side condensation heat transfer of R-134a—Part II: Enhanced tube performance. *ASHRAE Transactions*. Vol. 100(2). pp. 248-256.

[37] Huber. J. B. 1994. Shell-side condensation of HFC-134a and HCFC-123 on enhanced-tube bundles. Ph.D. Dissertation. Iowa State University.

[38] Huebsch. W. W. and Pate. M. B. 1994. Heat transfer evaluation of R-236ea and R-114 in condensation and pool boiling. *EPA-600/R-96-070. U. S. Environmental Protection Agency*. Research Triangle Park. NC.

[39] Incropera. F. P. and DeWitt. D. P. 1990. *Fundamentals of Heat and Mass Transfer*. 3rd ed. New York: Wiley.

[40] Jabardo. M. S. and da Silva. C. L. 1991. Modeling of the nucleate boiling of refrigerant-oil mixtures. *XVIIIth International Congress of Refrigeration*. Vol. 2. pp. 514-518.

[41] Jensen. M. K. and Jackman. D. L. 1984. Prediction of nucleate boiling heat transfer coefficients of refrigerant-oil mixtures. *Journal of Heat Transfer*. Vol. 106. No. 1. pp. 184-190.

[42] Karkhu. V. A. and Borovkov. V. P. 1971. Film condensation of vapor at finely-finned horizontal tubes. *Heat Transfer-Soviet Research*. Vol. 3. No. 2. pp. 183-191.

[43] Kern. K. Q. 1958. Mathematical development of loading in horizontal condenser. *AIChE Journal*. Vol. 4. pp. 157-160.

[44] Kocamustafaogullari. G. and Chen. I. Y. 1989. Horizontal tube evaporators: Part II— Experimental overall heat transfer performance. *International Communications of Heat and Mass Transfer*. Vol. 16. pp. 621-632.

[45] Lorenz. J. J. and Yung. D. 1982. Film breakdown and bundle-depth effects in horizontal-tube. falling-film evaporators. *Journal of Heat Transfer*. Vol. 104. pp. 569-571.

[46] Leiner. W. and Gorenflo. D. 1992. Methods of predicting the boiling curve and a new equation based on thermodynamic similarity. *Pool and External Flow Boiling*. Eds. Dhir V. and Bergles. A. E. ASME. pp. 99-103.

[47] Marto. P. J. 1988. An evaluation of film condensation on horizontal integral-fin tubes. *Journal of Heat Transfer*. Vol. 110. pp. 1287-1305.

[48] McNaught. J. M. and Chu. C. M. 1993. Heat transfer measurements in condensation on bundles of low-finned tubes: effect of fin frequency. *ASME Condensation Condenser Design*. pp. 367-376.

[49] Memory. S. B. and Marto P. J. 1992. The influence of oil on boiling hysteresis of R-114 from enhanced surfaces. *Pool and External Flow Boiling*. ASME. New York. pp. 63-71.

[50] Memory. S. B.. Bertsch. G.. and Marto P. J. 1993. Pool boiling of HCFC-124/oil mixtures from smooth and enhanced tubes. *Heat Transfer with Alternate Refrigerants*. ASME. HTD Vol. 243. pp. 9-18.

[51] Mikic. B. B. and Rohsenow. W. M. 1969. A new correlation of pool-boiling data including the effect of heating surface characteristics. *Journal of Heat Transfer*. Vol. 91. pp. 245-250.

[52] Moeykens, S. A. 1994. Heat transfer and fluid flow in spray evaporators with application to reducing refrigerant inventory. Ph.D. Dissertation, Iowa State University.

[53] Moeykens, S. A. and Pate, M. B. 1994. Spray evaporation heat transfer of R-134a on plain tubes. *ASHRAE Transactions*, Vol. 100(2), pp. 173-184.

[54] Moeykens, S. A. and Pate, M. B. 1995. Heat transfer of R-134a in single-tube spray evaporation including lubricant effects and enhanced surface results. *ASHRAE Transactions*, Vol. 101(1), pp. 111-123.

[55] Moeykens, S. A. and Pate, M. B. 1996. Effect of lubricant on spray evaporation heat transfer performance of R-134a and R-22 in tube bundles. *ASHRAE Transactions*, Vol. 102(1), pp. 410-426.

[56] Moeykens, S. A. and Pate, M. B. 1996. Spray evaporation heat transfer performance of R-123 in tube bundles. *ASHRAE Transactions*, Vol. 102(2), pp. 259-272.

[57] Morrison, G., McLinden, M., Gallagher, J., Huber, M., and Ely, J. 1991. REFPROP. *NIST Thermodynamic Properties of Refrigerant Mixtures Database*, Gnithersburg, MD.

[58] Mostinski, I. L. 1963. Calculation of heat transfer and critical heat flux in boiling liquids based on the law of corresponding states. *Teploenergetika*, 10(4), pp. 66-71.

[59] Murata, K. and Hashizzume, K. 1992. Prediction of condensation heat transfer coefficient in horizontal integral-fin tube bundles. *Experimental Heat Transfer*, Vol. 5, pp. 115-130.

[60] Nguyen, T.-N. and Orozco, J. A. 1994. Condensation of R-113 on enhanced surfaces. *ASHRAE Transactions*, Vol. 100(1), pp. 736-743.

[61] Nusselt, W. 1916. Die Oberflachenkondensation des Wasserdampfes. *Z. Ver. Deut. Ing.*, Vol. 60, pp. 541-569.

[62] Pais, C. and Webb, R. L. 1991. Literature survey of pool boiling on enhanced surfaces. *ASHRAE Transactions*, Vol. 97(1), pp. 79-89.

[63] Parken, W. H., Fletcher, L. S., Sernas, V., and Han, J. C. 1990. Heat transfer through falling film evaporation and boiling on horizontal tubes. *Journal of Heat Transfer*, Vol. 112, pp. 744-750.

[64] Rohsenow, W. M. 1952. A method of correlating heat-transfer data for surface boiling of liquids. *Journal of Heat Transfer*, Vol. 74, pp. 969-975.

[65] Rose, J. W. 1994. An approximate equation for the vapor-side heat-transfer coefficient for condensation on low-finned tubes. *International Journal of Heat and Mass Transfer*, Vol. 37, pp. 865-875.

[66] Rudy, T. M. and Webb, R. L. 1983. Theoretical model for condensation on horizontal, integral-fin tubes. *Heat Transfer, Seattle, AIChE Symposium Series*, Vol. 79, No. 225, pp. 11-18.

[67] Rudy, T. M. and Webb, R. L. 1985. An analytical model to predict condensate retention on horizontal integral-fin tubes. *Journal of Heat Transfer*, Vol. 107, pp. 361-368.

[68] Stephan, K. 1995. Two-phase heat exchange for new refrigerants and their mixtures. *International Journal of Refrigeration*, Vol. 18, No. 3, pp. 198-209.

[69] Stephan, K. and Abdelsalam, M. 1980. Heat transfer correlations for natural convection boiling. *International Journal of Heat and Mass Transfer*, Vol. 23, pp. 73-87.

[70] Snyder, J. E. and Sprouse, A. M. 1980. Design of 1MWe ocean thermal energy conversion (OTEC) heat exchangers for ocean testing. *Heat Transfer in Ocean Thermal Energy Conversion (OTEC) Systems*, ASME HTD Vol. 12, pp. 17-26.

[71] Sukhatme, S. P., Jagadish. B. S., and Prabhakaran, P. 1990. Film condensation of R-11 vapor on single horizontal enhanced condenser tubes. *Journal of Heat Transfer*, Vol. 112, pp. 229-234.

[72] Thome, J. R. 1994. Two-phase heat transfer to new refrigerants. *Proceedings of International Heat Transfer Conference*, Brighton, England, Vol. 1, pp. 19-41.

[73] Thome, J. R. 1990. *Enhanced Boiling Heat Transfer*, New York: Hemisphere Publishing Co.

[74] Ullmann, A. and Letan, R. 1989. Effect of noncondensibles on condensation and evaporation of bubbles. *Journal of Heat Transfer*, Vol. 111, pp. 1060-1067.

[75] Vachon, R. I., Nix, G. H., and Tanger, G. E. 1968. Evaluation of constants for the Rohsenow pool-boiling correlation. *Journal of Heat Transfer*, Vol. 90, pp. 239-245.

[76] Wanniarachchi, A. S., Marto, P. J., and Reilly, J. T. 1986. The effect of oil contamination on the the nucleate pool-boiling performance of R-114 from a porous-coated surface. *ASHRAE Transactions*, Vol. 92(2B), pp. 525-538.

[77] Wanniarachchi, A. S., Sawyer L. M., and Marto, P. J. 1987. Effect of oil on pool boiling performance of R-114 from enhanced surfaces. *Procedure 2nd ASME/JSME Thermal Engineering Conference*, Vol. 1, Honolulu, Hawaii, pp. 531-537.

[78] Webb, R. L. 1981. The evolution of enhanced surface geometries for nucleate boiling. *Heat Transfer Engineering*, Vol. 2, pp. 46-69.

[79] Webb, R. L., Keswani, S. T., and Rudy, T. M. 1982. Investigation of surface tension and gravity effects in film condensation. *Proceedings of the Seventh International Heat Transfer Conference*, Vol. 5, pp. 175-181. New York: Hemisphere Publishing Co.

[80] Webb, R. L. 1983. Nucleate boiling on porous coated surfaces. *Heat Transfer Engineering*, Vol. 4, pp. 71-82.

[81] Webb, R. L., Rudy, T. M., and Kedzierski, M. A. 1985. Prediction of the condensation coefficient on horizontal integral-fin tubes. *Journal of Heat Transfer*, Vol. 107, pp. 369-376.

[82] Webb, R. L. 1988. Enhancement of film condensation. *International Communications of Heat and Mass Transfer*, Vol. 15, pp. 475-507.

[83] Webb, R. L., Choi, K. D. and Apparao, T. R. 1989. Prediction of the heat duty in flooded refrigerant evaporators. *ASHRAE Transactions*, Vol. 95(1), pp. 339-348.

[84] Webb, R. L. and Murawski, C. G. 1990. Row effect for R-11 condensation on enhanced tubes. *Journal of Heat Transfer*, Vol. 112, pp. 768-776.

[85] Webb, R. L. and Pais, C. 1991. Pool boiling data for five refrigerants on three tube geometries. *ASHRAE Transactions*, Vol. 97(1), pp. 72-78.

[86] Webb, R. L. and Pais, C. 1992. Nucleate pool boiling data on plain, integral-fin, and enhanced tube geometries. *International Journal of Heat and Mass Transfer*, Vol. 35, pp. 1893-1904.

[87] Webb, R. L. and McQuade, W. F. 1993. Pool boiling of R-11 and R-123 oil-refrigerant mixtures on plain and enhanced tube geometries. *ASHRAE Transactions*, Vol. 99(1), pp. 1225-1236.

[88] Webb, R. L. 1994. *Principles of Enhanced Heat Transfer*, New York: Wiley Interscience.

[89] Webb, R. L.; Chien, L.-H.; McQuade, W. F.; and Imadojemu, H. E. 1995. Pool boiling of oil-refrigerant mixtures on enhanced tubes. *Proceedings of ASME/JSME Thermal Engineering Joint Conference*, Vol. 2, pp. 247-255.

[90] Xin, M. and Chao, Y. 1985. Analysis and experiment of boiling heat transfer on T-shaped finned surfaces. *23rd National Heat Transfer Conference*, August 4-7, Denver.

[91] Zuber, N. 1959. Hydrodynamic aspects of boiling heat transfer. *U.S. AEC Rep.*, AECU 4439.

[92] Zeng, X., Chyu, M. C. and Ayub, Z. H. 1994. Characteristic study of sprayed fluid flow in a tube bundle. *ASHRAE Transactions*, Vol. 100(1), pp. 63-72.

[93] Zeng, X., Chyu, M. C. and Ayub, Z. H. 1995. Evaporation heat transfer performance of nozzle-sprayed ammonia on a horizontal tube. *ASHRAE Transactions*, Vol. 101(1), pp. 136-149.